Improvement of Scratch Resistance of PMMA by Reinforcing with Nano SiO_2 Particles

A THESIS

SUBMITTED TO THE COLLEGE OF ENGINEERING

UNIVERSITY OF BASRAH

IN PARTIAL FULFILLMENT

OF

THE REQUIREMENTS FOR THE DEGREE

OF DOCTOR OF PHILOSOPHY

IN

MECHANICAL ENGINEERING

(APPLIED MECHANICS)

BY

Mushtaq Abdul Kareem Hussein Al Bahrani

(M.Sc. Mech. Eng.)

September 2020

بِسْمِ اللهِ الرَّحْمنِ الرَّحِيمِ

يَرْفَعِ اللَّهُ الَّذِينَ آمَنُوا مِنكُمْ
وَالَّذِينَ أُوتُوا الْعِلْمَ دَرَجَاتٍ

صدق الله ألعلي العظيم

سورة المجادلة, آية (11)

الأهداء

الى رمز التضحية والعطاء.....والدي الغالي

الى نبع العاطفة والحنان .....والدتي العزيزة

الى سندي وذخري.....اخوتي واخواتي الاحبة

الى نصفي الآخر.....زوجتي الحبيبة

الى جنات ومسرات وملاك....بناتي العزيزات

حفظكم الله جميعا

اهدي هذا العمل المتواضع

مشتاق

Acknowledgements

First of all, I would like to thank Allah the great creator of the universe for continuous helping, supporting and blessing.

I would like to thank my supervisors, Prof. Dr. Abdul Kareem F. Hassan and Prof. Dr. Najim Abdul Ameer Saad for their much valued advises assistance, support, friendship, and tuition during the period of this study.

Also, I would like to thank the Dean of College of Engineering Assist. Prof. Dr. Ramzy S. Ali and special thank for the head of Department of Mechanical Engineering Dr. Hassanein Ibraheem Khalaf for supporting and facilitating the achievement of this work.

I present my thanks and appreciation to Assist. Prof. Dr. Abdul Baqi K. Ali, Assist. Prof. Dr. Jaafar Khalaf Ali and Engineer Ahmed Alloush for their helping during this study.

I would like to express my sincere gratitude to the staff of the laboratories in Materials Engineering College in the Babylon University.

Finally, I would like to thank my family for their support, encouragement and patience throughout the achievement of this study.

Certification

We certify that this thesis titled "**Improvement of Scratch Resistance of PMMA by Reinforcing with Nano SiO_2 Particles**" which is being submitted by **Mushtaq Abdul Kareem Hussein** was prepared under our supervision at the University of Basrah as a partial fulfilment of the requirements for the degree of Doctor of Philosophy in Mechanical Engineering.

Signature:

Name: Prof. Dr. Abdul Kareem F. Hassan

(Supervisor)

Date: 29 / 9 / 2020

Signature:

Name: Prof. Dr. Najim Abdul Ameer Saad

(Supervisor)

Date: 28 / 9 / 2020

In view of the available recommendation, I forward this thesis for debate by the examining committee.

Signature:

Name: Dr. Hassanein Ibraheem Khalaf

(Head of Mech. Eng. Dept.)

Date: / /

Examining Committee's Report

We certify that we have read this titled "**Improvement of Scratch Resistance of PMMA by Reinforcing with Nano SiO_2 Particles**" which is being submitted by **Mushtaq Abdul Kareem Hussein** and as examining committee, examined the student in its contents. In our opinion, the thesis is adequate for award of degree of Doctor of Philosophy in Science of Mechanical Engineering.

Signature**:**
Name: **Prof. Dr.**
Abdul Kareem F. Hassan
(Member, Supervisor)

Signature**:**
Name: **Prof. Dr.**
Najim Abdul Ameer Saad
(Member, Supervisor)

Signature**:**
Name: **Prof. Dr.**
Adnan S. Jabur
(Member)

Signature**:**
Name: **Prof. Dr.**
Ameen Ahmed Nassar
(Member)

Signature**:**
Name: **Assist. Prof. Dr.**
Haider Maath Mohammad
(Member)

Signature**:**
Name: **Assist. Prof. Dr.**
Abdul Baki K. Ali
(Member)

Signature:
Name: **Prof. Dr.**
Ali A. A. Mukeef Al-Zubiedy
(Chairman)

Approval of the College of Engineering

Signature**:**
Name: **Prof. Dr.**
Ramzy S. Ali
Dean of Engineering College
University of Basrah

ABSTRACT

PMMA material is used in many engineering industries and applications such as cars, airplanes, traffic lights, light advertisements, lenses, eyeglasses, solar cells, dental industry, many electrical appliances and construction applications such as decorations , commodity displays, sports swimming pools, and golf courses, as well as in many agricultural fields. The PMMA material is characterized by abundance, cheap price, low density, good relative durability, ease of forming and cutting to desire sizes and shapes required, non-toxicity, electrical insulation and chemical resistance, but its resistance to scratch is weak.

Getting high-quality surfaces of PMMA has become a priority for both the manufacturers and the researchers alike for two reasons, one functional and the other aesthetic, because the scratches on the PMMA surface reduce their use in the optical industry and many engineering applications, as the presence of scratches leads to increase stress during tensile, impact and fatigue loading that undermines the longevity of PMMA during use. In the current study, silicon oxide nanoparticles (SiO_2) was added in two groups of ratios, the first (1, 2, 3 and 4wt %) and the second (0.1, 0.2, 0.3, 0.4 and 0.5wt %) in order to study the effect of SiO_2 on the scratch resistance and the other properties of PMMA.

The pure and reinforced PMMA specimens were prepared in three methods in current work, which are dissolving, pressing and casting method. An automated scratch device was designed and constructed to perform scratch tests in the current study. The device consists of three parts, namely mechanical parts, scratch mechanism and electrical and electronic parts, as well as the program for operating and controlling the device.

Results obtained from tests conducted on pure and reinforced PMMA in current study were an improvement of tensile strength of PMMA/SiO_2 composites compared to pure PMMA, the best improvement occurred for specimens with nanoparticles of 1wt% compared to other ratios of SiO_2. Decreasing in elongation of PMMA/SiO_2 composites compared to pure PMMA, the lowest elongation occurs for specimens with nanoparticles ratio 1wt%. An improvement of the hardness for reinforced PMMA compared with pure PMMA, the hardness increases with increasing the nanoparticles (SiO_2) ratio. The results also showed that an improvement of scratch resistance where the applied normal load required for scratching the reinforced PMMA was greater than that for the pure PMMA, and increases with increasing nanoparticles ratio, also the applied loads used with the spherical indenter were greater than those used with a conical indenter. Friction coefficient for reinforced PMMA was lower compared to pure PMMA and decreases when the ratio of nanoparticles increases. The glass transition temperature (T_g) of the reinforced specimens was higher than that of the pure specimens and increases with increasing ratio of nanoparticles (SiO_2).

Finally, the study proved the ability of the designed device to measure the tangential force required for scratching accurately and quickly and in simple steps as well as the possibility of calculating the friction coefficient directly from the inputs and outputs of the device, also demonstrated the effectiveness of the program designed to control the device in terms of ease of entering variables and the accuracy of outputs.

Contents

Nomenclature

Symbol	Description	Unit
A	Cross section area	mm^2
Al_2O_3	Aluminium oxide (alumina)	
$CaCO_3$	Calcium carbonate	
F	Applied force	N
F_n	Applied normal load	N
F_t	Measured tangential force	N
L	Length of sample	mm
L_0	Original length of sample	mm
Ra	Surface roughness coefficient	μm
SiO_2	Silicon oxide (silica)	
T_g	Glass transition temperature	^oC
TiO_2	Titanium dioxide (titania)	
T_m	Melting temperature	^oC
V_{tip}	Sliding speed of tip	mm/s
w	Scratch groove width	mm
ZrO_2	Zirconium dioxide (zirconia)	

Greek Symbols

Symbol	Description	Unit
μ	Friction coefficient	
$\mu_{ad.}$	Adhesive friction coefficient	
$\mu_{app.}$	Apparent friction coefficient	
$\mu_{def.}$	Geometrical friction coefficient	
$\mu_{loc.}$	True local friction coefficient	
$\mu_{plast.}$	Friction coefficient of plasticity	
$\mu_{visco.}$	Friction coefficient of viscosity	
ΔL	Length difference	mm
σ	Stress	N/m^2
ε	Strain	
$\dot{\varepsilon}$	Strain rate	s^{-1}

Abbreviations

Symbol	Description
1-VID	1-Vinylimidazole ($C_5H_6N_2$)
AFM	Atomic Force Microscopy
APS	Ammonium Persulfate $(NH_4)_2S_2O_8$
ASTM	American Society for Testing and Materials
BPA	Bisphenol-A
CR39	Diethylene glycol-bis allyl carbonate $(C_{12}H_{18}O_7)_n$
DSC	Differential Scanning Calorimetry
EP	Ethylene - Propylene
FTIR	Fourier Transform Infrared
GC	Gas Chromatography
ICI	Imperial Chemical Industries
LCD	Liquid Crystal Display
L.T.D.S	Laboratory of Tribology and Dynamics System
MMA	Methyl Methacrylate
MTS	Mechanical Testing and Sensing
NBR	Nitrile Butadiene Rubber
PBO	Benzoyl Peroxide ($C_{14}H_{10}O_4$)
PC	Polycarbonate
PETG	Polyethylene Terephthalate Glycol
PMMA	Polymethyl Methacrylate
PP	Polypropylene $(C_3H_6)_n$
PWM	Pulse Width Modulated
SEM	Scanning Electron Microscope
TGA	Thermal Gravimetric Analysis
THF	Tetrahydrofuran (C_4H_8O)
Y-TSZ	Yttrium Stabilizer Zirconia

Chapter One
Introduction

Chapter One

Introduction

1.1 Background

The polymer is a term containing two sections: poly which means multi or many, and mer which means part or binary unit. Polymer is a chemical compound that contains large molecules made of many smaller molecules of the same type called monomers; some polymers are naturally present and others are produced in laboratories and factories in a way called the polymerization process. The polymers can be binary (i.e. the ability to connect to two mono molecules), triangular and multi-bonded. Most polymers are organic (i.e. depended on a carbon chain) however there are also non-organic polymers whose chains are depended on the silicon origin. The polymers are formed as a long chains, and human has discovered the polymeric materials in nature in the past, such as starch, fibers, rubber and gum, and in the 19th century, scientists carried out imitating nature to produce industrial polymers. In the 20th century, when the need for rubber increased, German scientists managed produce artificial rubber with the same composition of polymer which is characterized by the chain length. The polymer industry has grown and developed so far that it has become bigger than the iron, copper and aluminum industries, and even bigger than all industries [1].

The polymer industry has expanded in all applications of human life, surpassing any other type of material, they used in the manufacture of adhesive materials, foam materials, paints, packaging materials, textiles, artificial fibers, composite materials, as well as electronic, biomedical, and optical devices, and many high precision technology products [2].Two important properties determine the most important characteristics of polymer which are the temperature of glass transition and the average of molecular weight.

The temperature of the glass transition is defined as the temperature at which the mechanical properties of the polymer change significantly. If the temperature of the glass transition is less than the temperature of the room, the polymers act as an elastic matter (thermoplastic). While the temperature of the glass transition is higher than the temperature of the room, the polymers act as a rigid matter (thermoset). A second important characteristic of polymers is the molecular weight since the chemical and mechanical properties of a polymer such as its viscosity, resistance to creep, resistance to abrasion, etc. are determined by the weight of molecular of the polymer.

Polymers can be classified depending on the source origin, structure, forces of molecular and type of polymerization, the chart in figure (1-1) shows this classification. Polymers can be classified depending on structural composition into linear, branched, and crosslink polymers, figure (1-2) shows this classification. When the polymer is composed of one type of repetitive unit (monomer), the polymer is called the homopolymer. When the resulting compound is composed of two types of repetitive units, the polymer is called the copolymer; either when the resulting composite consists of three repetitive units the polymer is called a terpolymer, as shown in figure (1-3). Technological classification of polymers includes thermoplastic and thermoset polymers [6]. Thermoplastic category includes polymers that are affected by heat becomes in the molten- state when the temperature rises and the polymers will return to its solid state when the temperature is lowered. Thermoset polymers undergo chemical changes when they are heated their chains are intertwined and the polymers become poor conductivity of the electric and heat when they are heat-treated [7].

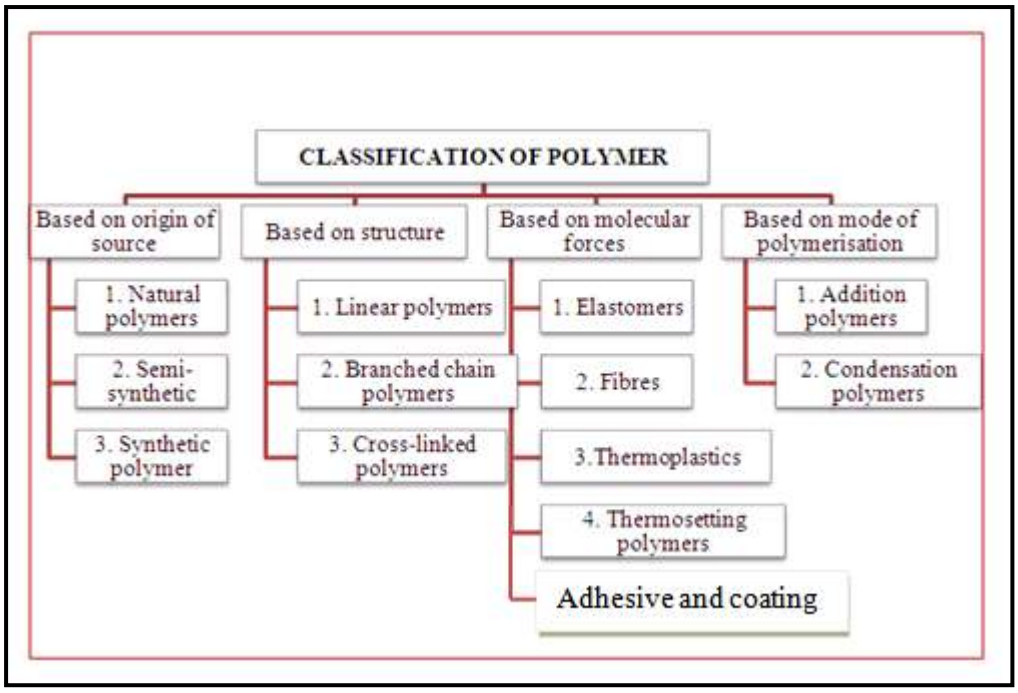

Figure (1-1) General classification of polymers [3].

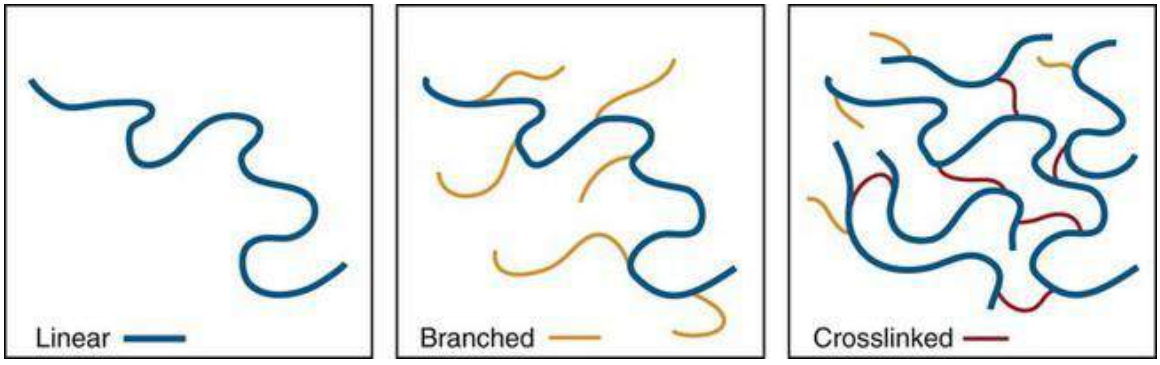

Figure (1-2) Polymers classification depending on structural composition [4].

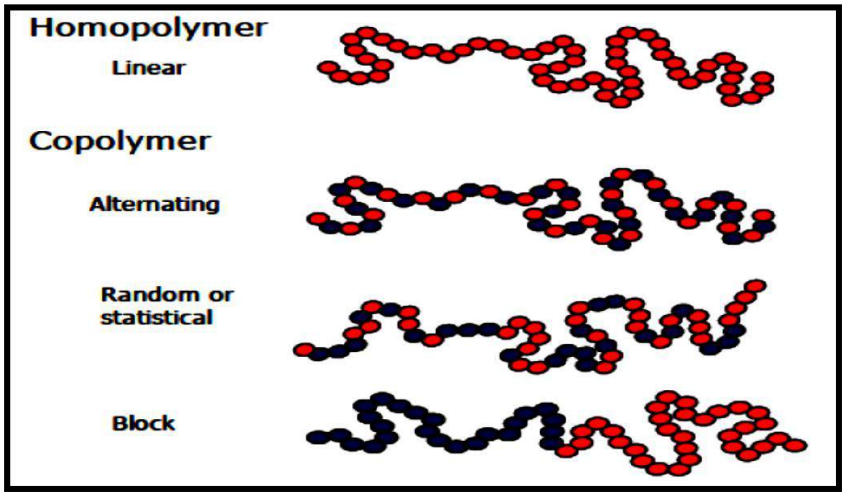

Figure (1-3) Classification of the polymers depending on homogenization [5].

1.2 Polymerization

The simple molecules from which the polymer molecules are built are called monomers. Binding these simple molecules together is called the polymerization process. The monomers are simple chemical compounds that have small molecular weights. The molecules of these compounds are characterized by special structures that enable interaction with other molecules of the same type or molecules of another compound under the appropriate conditions to form the polymer chains. So, the polymerization can be defined as a chemical union for two-part or more of one or more substances with a small molecular composition to form a compound with a great molecular mass and different in its chemical and physical properties from its constituent compounds. Polymerization reactions are classified into two types which are illustrated in the figure (1-4).

1. Polymerization by addition.
2. Polymerization by condensation.

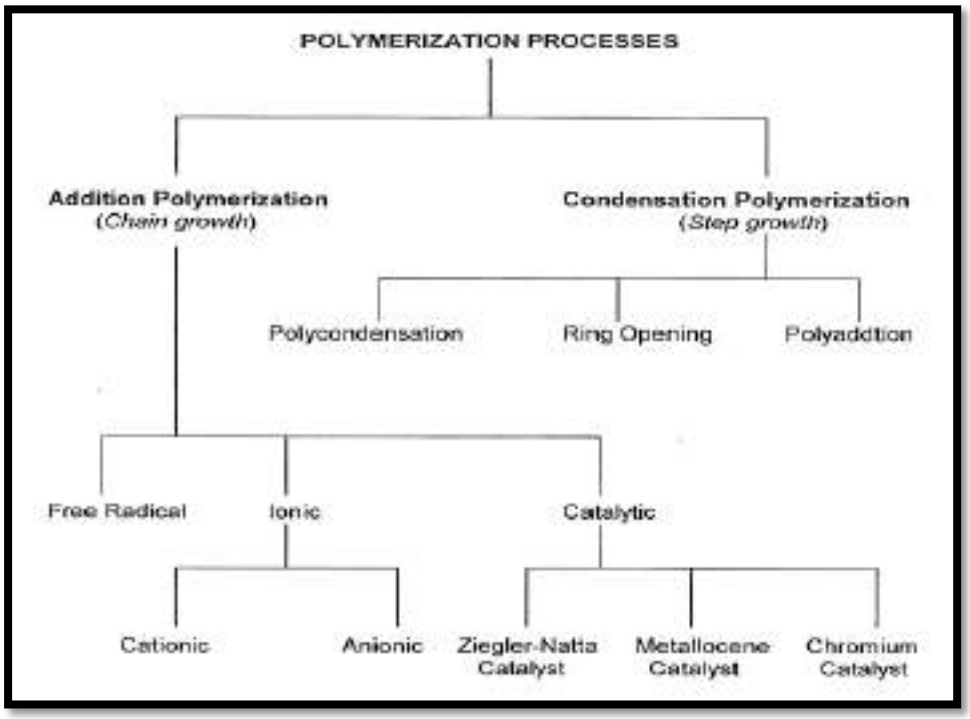

Figure (1-4) Classification diagram of polymerization process [8].

The process in which polymers are produced as a result of adding monomers to each other rapidly and sequentially is called addition polymerization. Passing every moment, a new active center bond is formed that enhances the interaction of additional monomers. The end result of this polymerization is a long polymer chain with a high molecular weight and containing the same number of primary "monomer" atoms. Thus, the molecular formula of the repeated unit in the polymer molecule is similar to that of the monomer. All methods of addition polymerization consist of three stages are:

1. Initiation step: where active stations are formed.
2. Propagation or diffusion step: where the polymers with a high molecular weights are formed.
3. Termination step: where the reaction ends with the disappearance of the active centers by interactions whose nature depends on the kind of active center and the conditions of reaction.

The process in which polymers are produced as a result of the interaction of functional groups in the structure of two molecules of monomers is called condensation polymerization. The final hull is a long polymer chain with a high molecular weight, containing fewer atoms than interacting monomers, with secondary products being made up of small molecules such as water molecules, hydrogen chloride, methanol, etc. The molecular formula of the unit repeated polymer molecules are smaller than the total of two monomer formulations united in the condensation process [8].

The polymerization method was not used in the preparation of PMMA specimens in the current work due to the difficulty of this method, shortage of time and the lack of necessary equipment, but the pure and composite specimens were prepared in three ways are dissolving, pressing, and casting method, each method is explained in detail in chapter four.

1.3 Organic solvents

Organic solvents are chemical substances with evaporation and volatilization characteristics such as benzene, chloroform, acetone and some cleaning fluids. Organic solvents are organic liquids that have the ability to dissolve other organic and inorganic substances, without changing their chemical properties. This characteristic has led to the use of solvents in many important industries. When selecting the appropriate solvent for organic compounds, follow the rule (like dissolves like) this rule requires knowledge of some characteristics of organic compounds for dissolved in an appropriate solvent chemical reactions, for example, non-proton polar solvents are suitable to dissolve non-proton polar substances, and proton solvents are very important in their ability to form hydrogen bonds between molecules to dissolve proton materials in chemical reactions. Solvents generally have a low boiling point, evaporate easily or can be isolated by distillation, leaving dissolved solids behind. In order to prevent the dangers of organic solvents, the following points should be considered [1]:

1. The hazardous organic solvent must be replaced with other solvents that are less hazardous to the life of the worker or manufacturer.
2. Ventilation factors should be provided where organic solvents are used.
3. Explain the risks of organic solvents to their users and teach them ways to prevent these risks.
4. Warning signs should be placed in factories that produce hazardous materials.

The solvents used in this work were tetrahydrofuran, acetone, and isopropanol, the specifications of which will be explained in detail in chapter four.

1.4 Polymethyl methacrylate (PMMA)

Polymethyl methacrylate is a thermoplastic transparent plastic notable a lot of unremarkably by the brand "Plexiglass, Lucite, Acrylic, Polycast, Optix, and PMMA". When the large impact resistance is not required of polycarbonate (PC) the acrylic is more suitable to use as alternate to the glass because of the acrylic is analogous to PC in this case. It had been initially made in 1928 and was placed on the market in 1933 by Hass and Rohm. Usually, in the market may be PMMA one amongst more evident plastics types. The primary application of PMMA was in World War II, it had been used for airplanes windows, periscopes of submarine, canopies, and turrets. The eyes of the pilots, who were harmed by acrylic shrapnel, were better than those of the pilots who were harmed by glass shrapnel because the PMMA is breaks into large pieces instead of small shrapnel [9]. Acrylics are used at present for a set of applications that usually benefit from their natural transparency and resistance to the influence of some variables. Common uses include furniture, LCD screens, security barriers, paint, lenses, and medical devices. Because of their clarity, they are oftentimes used for attachments around the exhibits and windows.

PMMA is defined as "thermoplastic" (as against "thermosetting"), and the name depends on the method that the plastic responds to heat. At the melting point the thermoplastic material converts to liquid, the foremost advantage of thermoplastic is maybe liquefying, refrigerated, and reheated without significant disintegration. This feature allows the thermoplastic to be injected into the molds and then recycled instead of burned. On the contrary, thermosetting can only be heated once (usually during casting in molds or injection). The result of the first heating leads to an irreversible change in the chemical properties of the material, if the material is heated again, it will simply be burn. This feature makes thermosetting material a weak candidate for recycling [7].

The PMMA raw material allows for internal light movement with approximately the same glass capacity, making it a great alternative, and this is exactly the same for polycarbonate. PMMA is available in a set of colors (possibly transparent and possibly opaqueness). The major differences include that acrylic does not contain potentially hurtful Bisphenol-A (BPA), while polycarbonate has greater impact resistance also acrylic is cheap and readily available. If impact resistance is an unimportant factor so PMMA can be used as an alternative to polycarbonate. In order to obtain a double performance combining the impact resistance of polycarbonate and scratch resistance of acrylic, a layer of acrylic is added to the surface of polycarbonate. Several bullet-proof glass is made in this manner. The PMMA on the surface used for scratch resistance throughout daily use, the Polycarbonate stops a bullet [9].

When high impact resistance is not a problem for applications requiring transparency, the acrylic is suitable plastic. Acrylic is very scratch resistant compared to other evident plastics. In applications, if strength is not a decisive operator, acrylic is a suitable alternative to the glass and an economical alternative to (PC) polycarbonate. Using laser cutting technology it can be cut into very precise forms because the material evaporates when energized using concentrated laser energy. Polyethylene terephthalate (PETG) and Polycarbonate (PC) may not be as clear as PMMA, but they are "sufficiently clear". Acrylic must be used when optical clarity is very important. The parts require polished to tear out tool effect and return transparency after machining.

The most important advantage of acrylic is that it does not release or contain Bisphenol throughout contact with water, while polycarbonate contains Bisphenol, so the toxicity of Bisphenol is not a problem with acrylic. Most government-funded studies have shown that (BPA) is a health hazard, while many industrialists with industrial finance have shown less or no medical hazards. Acrylic is another BPA-free alternative to polycarbonate and is not

poisoned in a solid format. However, vapors should not be inhaled from three-dimensional printing acrylic or molten media used during injection molding. These manufacturing operations must perform in the well ventilated facility to avoid potential gaseous polymer dangerous effects. Table (1-1) represents the PMMA properties; figure (1-5) shows the molecular structure of PMMA.

Table (1-1) Properties of PMMA [1].

Properties	Values
Technical Name	Acrylic (PMMA)
Chemical Formula	$(C_5H_8O_2)_n$
Melt Temperature	130°C (266°F)
Typical Injection Mold Temperature	79-107°C (175-225°F)
Heat Deflection Temperature (HDT)	95°C (203°F) at 0.46 MPa (66 PSI)
Tensile Strength	65 MPa (9400 PSI)
Flexural Strength	90 MPa (13000 PSI)
Specific Gravity	1.18 g cm^{-3}
Shrink Rate	0.2 - 1% (0.002 - 0.01 in/in)

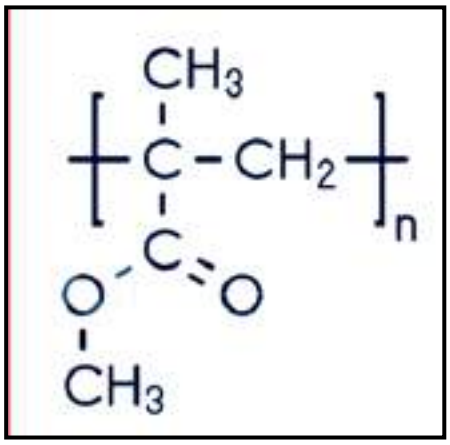

Figure (1-5) Molecular Structure of PMMA [1].

1.5 Polymer Scratch Importance

Obtaining quality surfaces of polymeric materials from an aesthetic and functional point of view has become one of the most important characteristics that determine the choice of these materials in many industries and engineering applications. Producing a desired layer for the polymer surface is a very difficult process, as the difficulty lies in the ability to maintain the surface quality throughout the polymer life cycle during service. One of the main reasons that lead to a decrease in the surface quality of polymeric materials is scratches that are a form of surface deformations. Surface quality characteristics can be categorized based on the applications of polymer into aesthetics of surface, structural integrity of surface, surface durability [10, 11].

Aesthetics of surface, such as the interior and exterior parts of automotive (car dashboards and lighting lamps), covers (housing) for electronic and electrical products and telecommunications devices (cellular phones) , are very important because the scratches of surface may reduce the value of these products although their intended functions are still generally unaffected. In applications of coating, the presence of scratches on the surface of the polymeric coating causes damage to the wooden substrate or corrosion of the metal. Therefore, the coating layers must maintain their mechanical integrity throughout their expected service life. For applications such as the use of polymeric materials in food packaging, the structural integrity of the packaging membranes is a matter of great concern and important for maintaining food quality and safety. The scratches formed on the food packaging membranes may lead to rupture them and thus spoilage the food inside. In the industry of data storage, surface durability is necessary as scratches can cause permanent data loss from optical storage devices and hard drives. From the point of view of structural integrity, another concern could be added that scratches act as

concentration points for stresses. These points lead to a decrease in load bearing capacity that ultimately causes early fracture and structural component failure. Also, scratch damage can extend to nanotechnology devices and precision mechanical devices, as the scratches formation in these devices can lead to completely lose their functions because of the small scale of this type of devices.

From the above it is clear that the scratch study is a very important issue for many industries and engineering applications. Attention to the scratch and surface quality of polymers has emerged only in the past few decades and has increased in recent years as a result of advances in science and technology of polymers. Research interest in the study of scratch and surface quality of polymers can be represented by the number of research publications related to this topic over previous years as shown in figure (1-6).

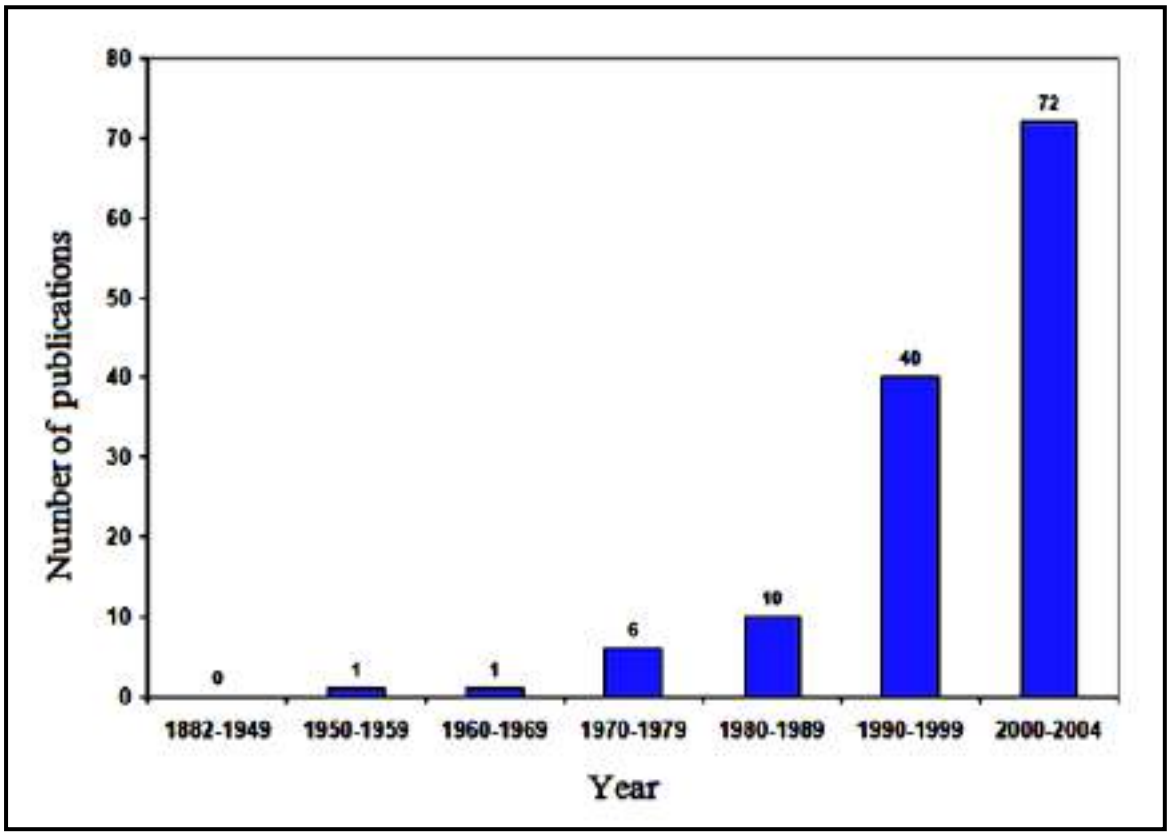

Figure (1-6) Progress of scratch research over past few decades [11].

1.6 Scratch resistance of PMMA

Advantages such as abundance, cheap price, low density, relatively good durability and ease of cutting to desired shapes and sizes are reasons for increasing the use of polymethyl methacrylate PMMA, especially transparent ones, in the medical, construction, automotive and aircraft industries [12, 13]. Getting high-quality surfaces of PMMA has become a priority for both the manufacturer and the researchers alike for two reasons, one of which is functional and the other aesthetic. When a solid object moves on a surface it will cause grooves scratched on the surface as shown in figure (1-7), such process was simply called scratching which was a part of the tribology science which concerned with studying friction, wear and lubrication of interacting surfaces in relative motion [15].The most important disadvantages of polymethyl methacrylate are abrasion and poor scratch resistance [16, 17]. Scratches on the surface of polymethyl methacrylate reduce their use in the optical industry and many engineering applications, as the presence of scratches leads to increase stress during tensile, impact and fatigue loading that undermines the longevity of PMMA during use.

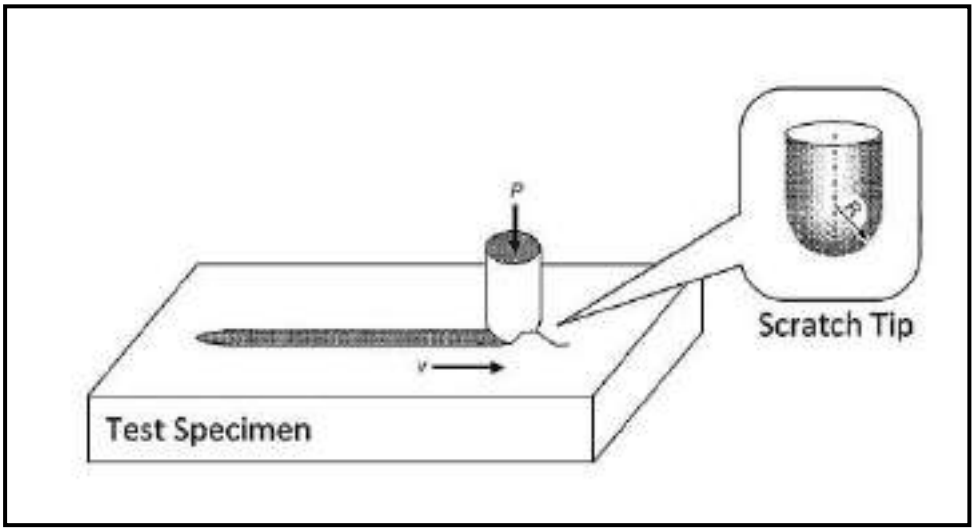

Figure (1-7) Schematic of a scratching process [14].

Although most scratch tests had been developed for metals and ceramics, those tests cannot be carried out to polymers without a few modifications. This is mainly due to the differences in mechanical behaviors among metals, ceramics, and polymers, wherein viscoelastic results are significant. All researchers in the scratch field of polymers have developed scratch testing equipment for their research because of the lack of standardized test methods for scratch. The knowledge gained by these researchers will be specific to the testing equipment they developed as well as the experimental conditions and materials they used. Methods for evaluating scratches also differ with researchers, some of whom use human eyesight for evaluation and the other uses scanners. All these constraints make it difficult for researchers in the field of scratching polymers to compare and verify their experimental results. In this work, a scratch test device, which was used to test all PMMA samples with different ratios of SiO_2, was manufactured. It will be explained in detail in chapter five.

1.7 Factors affecting scratch behavior

Scratch resistance behavior for polymers depends on some factors such as material type, fillers, preparation techniques, indenter geometry, applied load, and sliding velocity. Height of the accumulation on both sides of the scratching and the strain hardening are increased with increasing the indenter attack angle [18]. The value of applied normal load required to start scratching on the surface of the polymeric material is greatly influenced by the geometry of the indenter; this value does not mean anything without accurate description of the tip used [19]. The wear volume resulting from the scratching is proportional to the applied load [18, 20]. The true contact radius decreases and the mean strain in the contact region increase with increasing sliding speed [21]. The scratching

resulting from various contact conditions provides an appropriate and reliable method for studying the mechanical properties of polymers [17, 22, and 23].

Scratching occurs as a result of friction between the polymeric material surface and the hard bodies in contact with it. The ratio between the tangential force that causes the movement of the scratching tip and the vertical force due to the load applied on the scratching tip is called the apparent friction coefficient

$$\mu_{app} = F_t / F_n \quad \ldots\ldots (1.1)$$

The apparent friction coefficient includes two friction coefficients types, one of which is the result of separation at the region between scratched surface and tip is called coefficient of true local friction ($\mu_{loc.}$), the other is a result of plowing the material formed in front of the moving tip is called geometrical friction coefficient($\mu_{def.}$), the apparent friction coefficient becomes

$$\mu_{app} = \mu_{loc.} + \mu_{def.} \quad \ldots\ldots (1.2)$$

The apparent friction can be divided into adhesive friction and plowing friction and the second term may include two terms, one for viscosity and the other for plasticity.

$$\mu_{app} = \mu_{ad.} + \mu_{visco.} + \mu_{plast} \quad \ldots\ldots (1.3)$$

Factors such as sliding speed, material kind, indenter geometry, and lubrication have a significant impact on the coefficient of total friction of polymers when performing a scratch test [15]. The level of the strain in contact region and the senility of polymer are factors on which the true local friction depends [24, 25]. The gradient of plastic strain under the moving tip is heavily dependent on the true friction and surface smoothness of PMMA [26].

Several published papers focused on improving the scratch resistance of PMMA by adding nanoparticles fillers, also, study the correlation of scratching with other properties of PMMA, the researchers also dealt with the method of dispersing the nanoparticles fillers and the method of preparing the composite specimens. Fracture strain during scratch test can be associated with the fracture

strain during tensile test, and polymeric material begins fracturing when the value of tensile stress generated behind the indenter reaches the value of ultimate tensile strength [16].

1.8 Methods of incorporating of reinforcement phase in matrix phase

Polymeric composites (filler/polymer nanocomposites) have received much attention in recent times due to their exciting and beneficial characteristics such as mechanical properties, thermal resistance and chemical resistance. Polymeric composites are manufactured by adding fillers to the polymer. The purpose of adding fillers with different types and ratios is to improve the desired property in the original polymer. The difficulty of this process lies in dispersing the inorganic filler in the organic polymer matrix and finding the appropriate method for dispersion in order to obtain the required nanocomposite. The methods used to produce nanocomposites (for example PMMA/SiO_2 nanocomposites) can be classified into the following methods [27]:

1. Interpolating (intercalation) method
2. Local (in situ) polymerization method
3. In situ formation method for both the nanofillers and polymerization.
4. The direct mechanical mixing method of the polymer and the nanofillers.

Some of these methods require the modification of nano-filler surfaces and/or complex polymerization reactions, which makes them unsuitable for the industrial production of nanocomposites. The procedures for producing SiO_2 / PMMA nanocomposites used in the current work according to the above methods are illustrated as follows:

The first method is based on the principle of reducing the size of the filler used to nanoscale dimensions. The silicate layers used as inorganic filler is

peeled by inserting organic compound between the silicate layers, which converts the filler into nanoscale dimensions (or disassemble nanosilica agglomerates) as well as the uniform dispersion of the resulting nanofillers such as plates[28]. Silicate layers must be modified organically by organic substance which tends to reduce the surface tension like phosphonium salts, imidazolium and amino acids to provide enough hydrophobicity to be mixed with organic compounds, where the silicates are hydrophilic, while organic compounds are hydrophobic [29]. The polymeric material is inserted into the silica layers that have undergone organic modification as well as the next peeling of silicate layers are performed using chemical or mechanical methods. The chemical methods are in situ polymerization of monomers inside the layers of silica [30].

The second method, in addition to in situ interpolative polymerization method are depends on the reactions of polymerization [31]. Inorganic nanofillers are dispersed either inside the monomer or in the solution of monomer. The resulting mixture after dispersion process is polymerized using the standard methods of polymerization. The difficulty of this method is to find the appropriate method for dispersing the filler in the monomer, this requires modified organically of the surface of the filler particles in order to enhance the wettability.

The third method relies mainly on the sol-gel technique in its work. Many molecular hybrid material (organic/inorganic) are produced in this method using metallic alkoxides reactions [32].

$$Si(OR)_4 + 4\ H_2O \rightarrow [Si(OH)_x(OR)_{4-x} + xROH] \rightarrow SiO_2 + 4\ ROH + 2\ H_2O \quad \ldots\ldots\ldots (1.4)$$

Equation (1.4) shows the reactions of polycondensation and hydrolysis of tetraalkoxysilane as a reaction of sol-gel technique used for producing SiO_2/polymer molecular hybrid materials. Using the sol-gel technique, it became

possible to dissipate the filler with dimensions shorter than the length of the molecular chain of the polymer matrix.

The fourth method is based on the breaking of the filler agglomerates resulting from the direct mixing process of both the nanofillers and polymer matrix. This method is more suitable for producing filler/polymer composites that contain a nano or micron - scale fillers. In general, two ways are used to mix fillers and polymer. The first is without using any solvents called (powder mixing method) [33, 34]. The second uses solvents to mix the fillers and polymer as a solution called (solution mixing method) [35, 36].

From the above it is clear that the first three methods used to produce filler/polymer composites require the modification of nanofillers surfaces and / or complex polymerization reactions, which makes them unsuitable for the production of SiO_2/PMMA composites for the current work. The fourth method was adopted in the current work to produce the SiO_2 / PMMA composites for several reasons, including the simplicity of this method, availability of required equipment, and SiO_2 used is nano-filler. Another reason for adopting the fourth method is the current work focuses on the effect of SiO_2 dispersion methods and samples preparation methods on scratch resistance behavior of PMMA, these two important parameters can be performed using the fourth method.

1.9 The aim of the present work

The current work aims to improve the scratch resistance of PMMA by adding SiO_2 nanoparticles and study the factors affecting the scratch resistance such as preparation techniques, SiO_2 ratios, indenter geometry, sliding speed, and applied normal load.

The main aim of the present study is achieved by performing the following objectives

1. Preparing new PMMA/SiO_2 composite materials to improve the scratch resistance of PMMA.
2. Study the tribological and mechanical properties of composite materials prepared using tribological and mechanical tests.
3. Study the parameters affecting the scratch resistance such as preparation techniques of PMMA/SiO_2 composites, SiO_2 ratios, indenter geometry, sliding speed and applied load.
4. Design and construction an automated scratch test device in order to conduct scratch tests, as well as manufacture all the necessary equipments for the current work such as glassy and metallic molds, glassy containers, horizontal leveling platforms, and nanoparticles dispersing device.

1.10 Layout of the Thesis

The present study is divided into seven chapters as well as relevant appendix:

Chapter one describes the introduction and the objectives of the study.

In **chapter two** a literature review in the field of scratch resistance of PMMA has been presented.

Scratch theory, mechanisms of scratch formation, scratch test methods and scratch analysis techniques are explained in **chapter three**.

Chapter four describes the methods for preparing PMMA samples, tools and materials used in the preparation, and mechanical and tribological tests of PMMA samples.

Chapter five of this thesis describes in detail the scratch device and the manufactured equipment in current work.

The results and discussion of the experimental results of the hardness, tensile, transparent and scratch tests of PMMA samples at different ratio of SiO_2 are presented in **chapter six**.

Conclusions of the current work and recommendations for future are listed in the **chapter seven**.

The references and necessary appendix are listed at the end of this thesis.

Chapter Two
Literature Review

Chapter Two

Literature Review

2.1 Introduction

A review of published researches dealing with the development of scratch behavior and the mechanical and tribological properties as a result of adding nanoparticles of PMMA provides a basis for understanding the scratch behavior of this substance in the current study. In this chapter, published research papers dealing with mechanical and tribological tests of pure and reinforced PMMA by adding nanoparticles in different ratios and research dealing with PMMA scratch behavior and the different devices used to perform the scratch test were presented. Some of these researches dealt with testing the tensile strength, impact strength, transverse force, hardness, water absorption, abrasion resistance and radiation of nanoparticles dispersed in the polymer matrix. While other researches dealt with the effect of heat treatment on transparency, the effect of the annealing process on the surface hardness, the effect of temperature on the behavior of fracture toughness, the relationship between scratching properties and mechanical properties and the factors affecting the preparation of nanocomposites for PMMA. other Researches dealing with the scratch behavior of PMMA and influencing factors such as sliding speed, applied normal load, and indenter geometry in addition to the friction coefficient and the types of devices used in scratch resistance tests.

In 1991, M. Balzano and K. Ravi-Chandar [37] studied the effects of temperature on the fracture toughness behavior of polymethyl methacrylate. The softening temperatures of the polymeric material were close to the ambient temperatures and therefore its mechanical behavior was very sensitive at temperatures near the ambient temperatures. Also, the fracture behavior of polymeric materials can undergo tremendous changes from brittle failures with low energy dispersion to ductile rupture with significant energy dispersion. These kinds of transition with the associated increase of fracture energy leads to

substantial applications in the polymeric materials, especially thermoplastic polymers. The type of samples used was SEN (single-edge notched), the 200 μm wide cracks were laser made in the sample and a sharp crack tip was obtained by the hammer impact with a razor blade attached to the slit. To break the samples were pulled by the tensile testing machine at speeds ranging from 0.25 mm/min to 500 mm/min; the temperature used ranged from 20°C to 95°C. The results showed different mechanisms of cracking as a function of temperature. At temperatures below 20°C, the growth of brittle cracking begins. The second cracking began to form a craze at the tip of the cracking and it was observed at temperature ranged from 20°C to the critical temperature (T_c). At temperatures higher than T_c and due to large deformations the blunting dominates on the breakage process. Finally, at temperatures above 95°C a fracture does not occur due to cracking tip operations; significant deformation of the sample with crazing distribution prevails.

In 1993, V. Jardret et al. [23] studied understanding and estimating the effect of elastic and plastic deformations on metals and polymers during scratch testing. A scratch test device developed in the Laboratory of Tribology and Dynamics Systems (L.T.D.S.), in the Central School of Lyon in France was used to perform scratching experiments on three metals: aluminum, brass, and bearing steel, and two types of polymers: Delrin acetal polymer and Hytrel (thermoplastic elastomer) from DuPont, using the Berkovich indenter with semi-angle of 65.3°. The depth used in the experiments was 50μm and the scratching speed was 500μm/s. The results showed the formation of two pile-up pads on both sides of the groove due to the plastic flow around the indenter in both polymers and metals, grooves were sharper for metal than polymers this indicates that the amount of elastic deformation was more for polymers than for metals. Discrimination between three types of deformities, firstly an elastic deformation occurs within the groove resulting elastic recovery, secondarily the

elastic deflection of the surface occurs around the contact zone, and thirdly the plastic deformation occurs in the remaining groove and pile-up bads.

C. Gauthier and R. Schirrer (2000) [48] studied the scratching properties of the PMMA surfaces based on temperature and time. A high-performance device was built to study the scratching properties of polymers with the ability to control the velocity of the tip ranging from 1 µm/s to 10^4µm/s, as well as temperature control from -70°C to 120°C. The principle of the machine depends on the moving cross head of the tensile machine type Instron, the whole mechanism has been placed in the Instron environmental chamber. The tests were carried out on the PMMA at a constant load of 1.4 N, the velocity of the tip ranging from 1µm/s to 10^4µm/s, and temperature ranging from -10°C to 100°C. Cross-section grooves on the surface were recorded using a mechanical tactile recording device, while scratches of transparent polymers were displayed using a microscope during the scratching process. To calculate scratch hardness, normal and tangential loads and groove size were used. The results show that the numerical values of scratch hardness were identical to those in other measurements. The results also showed that the scratching behavior was similar to the indentation behavior and this was inferred from examining the geometry of the remaining grooves on the surface as a function of the temperature and speed of the tip.

Vincentd D. Jardret and Warren C. Oliver (2000) [19] investigated the effect of indenter tip geometry on the measurement of the critical loads of scratch test robustness for thin films. The scratch test has demonstrated the ability to identify mechanisms of damage and characterize the critical load for thin film failure. However, it is not possible to compare the results of the scratch test of the same material for several researchers. The main reason for that is the great influence of the tip geometry on the results of the critical loads and the

unrepeatability of the conical indenter geometry. The two authors presented a new method to characterize the indenter geometry, depending on the technique of penetration. Four pyramidal indenters have different radii were used with different semi- angles, two of which are congruent, the third with an acute angle, and the fourth with an obtuse angle. The effect of indenter tip geometry on the results of critical loads for thin films using the four indenters was compared with the results conducted using only one indenter. The results showed that the value of the critical load required to fail the polymer surface is meaningless without a full description of the geometry of the indenter used. Also, the results proved that it is possible to obtain the same critical load measurement by using different tips of the similar indenter geometry.

In 2001, S. Lafaye et al. [49] provided an analysis of the experimental results of the elastic recovery of poly (methyl methacrylate) scratches. The experimental data was obtained using a new scratching device with an integrated microscope, which allows for local analysis of the contact area and the remaining groove on the surface. The scratching device relies on a commercial servo mechanism that carries a small transparent environmental chamber containing the sample and movement tip. Tip velocity and temperature within the device can be controlled, in order to cover many types of polymers; the velocity of the tip also can be changed gradually within a single groove. The range of loads that can be applied to the tip from 0.05 – 2 N. The tip was a diamond ball of 100 µm radius in case of viscous plastic scratches. A 200 µm radius diamond ball was used in case of transition from viscous plastic scratches to viscous elastic grooves and a 1500µm radius steel ball was used for viscous elastic contacts. The results of the analysis of the experiments showed that during the process of scratching when the deformation was completely plastic there was no recovery while there was a partial recovery in the case of elastic-plastic materials after deformation. Also, the recovery process depends

on the temperature, tip shape, speed, nature of materials and width of the contact area under load.

In 2001, Michael J. Adams et al. [18] performed a study of the behavior of nano-scratch of PMMA in order to study the possibility to form of wear particles by reacting various scratches in conditions of tillage-plastic .The samples used for the scratch test were cut from transparent, non-reinforced PMMA sheets. The diamond Berkovich indenter has spherical tip with radius of 290 nm was used in the scratch test, the sliding speed was 10μm/s and the normal load was 10mN. The results show that crossed, perpendicular scratches produce lumpy protrusions that can serve as a portent for wear particles. While scratches that were parallel in close proximity have resulted in the mechanism of self-protection due to the capacity of load carrying of adjacent scratches.

Maurizio Avella et al. (2001) [38] studied the improvement abrasion resistance of the PMMA material by the addition of ($CaCO_3$) calcium carbonate nanoparticles. SOCAL brand calcium carbonate ($CaCO_3$) was used as filler with varies ratio (2wt%, 3 wt%, 4wt%, and 6wt% $CaCO_3$) and PMMA as a matrix for the preparation of PMMA/$CaCO_3$ nanoparticles by the in situ polymerization process. The thermal differential scanner (DSC) was used to analyze the temperature of glass transition of pure PMMA samples and reinforced with calcium carbonate ($CaCO_3$) PMMA samples. Abrasion tests were carried out using a tapir model where abrasive paper containing 80 grains was installed on a Teflon roller in the machine and a load of 1000 g and a speed of 500 RPM was applied to all samples. Micrographs of samples after abrasion testing were done using a Philips SEM 501(scanning electron microscope). The results showed a significant improvement in the abrasion resistance of samples reinforced with calcium carbonate ($CaCO_3$) compared to non-reinforced samples. Also,

a significant increase in the flexural modulus reaches 50% when adding 3wt % $CaCO_3$ and up to 67% when adding 6wt % $CaCO_3$.

In 2003, Vincent Jardret and Pierre Morel [17] investigated the relationship between scratching properties and mechanical properties at different temperatures and the effect of viscoelastic on scratch resistance of PMMA. The development of dynamic mechanical parameters obtained from penetration tests and uniaxial tensile tests of poly (methyl methacrylate) (PMMA) compared with the development of scratch resistance parameters as a function of strain rate and temperature helped determine association between toughness of scratch fracture and the tensile stress-strain behavior. This type of association was essentially a new understanding of the mechanisms of fracture during the scratching process. Scratch and penetration tests were performed by using XP Nano indenter. For temperature control and preservation during the test the instrument was placed in an isothermal chamber, also for measure the dynamic response of the material a small oscillation in addition to the load was applied. The temperature range at which the penetration test was conducted ranges from 5 to 90° C, while the frequency value used to measure the viscoelastic properties was 45 Hz. The results show that the behavior of PMMA changes from brittle at low temperatures to ductile behavior at high temperatures when loaded in a tensile state. Under uniaxial tension conditions, the strain at fracture can be associated with maximum strain for fracture during scratching, the strain value of the fracture depends only on the temperature and the strain rate, not on the state of the scratch test and the indenter geometry.

Hesham Afifi and Ebtisam Hasan (2003) [39] studied the effect of the annealing process on the hardness of the PMMA using two methods, the first using mechanical tests and the second using the ultrasonic pulse echo method. The PMMA material was especially used in the manufacture of CD discs and

DVD discs. The hardness was measured with the same annealing conditions for both methods, and a good convention was found between the two measurement methods. All test samples were annealed at the range of temperatures from the temperature of room to about 95°C and for about 24 hours. The annealed samples are cooled to room temperature by leaving them inside the oven. Longitudinal modulus, rigidity and Young's modulus were derived from experimental data. The results showed that the hardness was very sensitive to annealing temperature and was increased by increasing the temperature of annealing from the temperature of room to about 80°C while observed a reduction at about 90°C for both methods.

In 2004, Min Chen et al. [40] studied the factors affecting the preparation of nanocomposite particles (PMMA/SiO_2) by using the free radical addition polymerization of methyl methacrylate (MMA) with 1-vinylimidazole ($C_5H_6N_2$) as well as the existence of (SiO_2) aqueous silica. Materials used in synthesis PMMA/SiO_2 nanocomposite particles were methyl methacrylate (MMA), 1-Vinylimidazole (1-VID) and ammonium persulfate (APS). From the results it can be noted that the mean particle size decreases when initial charge of silica increased, the increase in reaction temperature also leads to decrease the content of silica and a slight increase in the average size of particle. When the pH value increases the content of silica in the (PMMA/SiO_2) nanocomposite particles decreases, a long-stable synthesis of nanocomposite particles with a high content of silica can also be obtained at 10 mol% of (1-VID).

In 2004, R.D.K. Misra et al. [50] investigated the effect of reinforcement with mineral materials on surface damage behavior of polymeric composites during scratch deformation. The scratching device was a conventional type machine consisting of a lever attached to its arm a diamond conical indenter with a tip radius of 5 μm and an apex angle of 120°. The specimens

were fixed on a leveling platform which was provided with scratching speeds range of 0.001 mm/s to 40 mm/s, the scratch friction force was recorded by using a piezoelectric transducer which connected to the indenter holder. The conditions of scratch test for all four polymeric materials were the normal load of 7 N and the scratch velocity of 2 mm/s. By using of scratching deformation parameters and local crystalline properties deduced from the atomic force microscope (AFM) in addition to using scanning electron microscopy (SEM) the behavior of surface damage during scratch deformation of pure and wollastonite reinforced polypropylene (PP) and ethylene-propylene (EP) polymeric materials was studied. The results show that the increasing of tensile modulus and reduction of plastic deformation of reinforced polymeric materials due to the effective reinforcement of wollastonite particles. Also, pure ethylene-propylene (EP) exhibited parabolic scratch paths, while polypropylene (PP) displayed the zigzag nature of the scratch paths. The SEM micrographs also indicate that the plastic plowing deformation process was severe in pure polymers compared to reinforced polymers.

J. L. Bucaille et al. (2004) [51] presented an experimental and numerical study of the scratch test at large deformation of polymeric materials. Scratches near the surface of three polymers were polycarbonate (PC) and CR39 (diethylene glycol-bis allyl carbonate) and sol-gel coating had been experimentally and numerically studied. By injection molding polycarbonate (thermoplastic polymer) was obtained while CR39 (thermosetting polymer) was obtained by casting and heating at a temperature of 80°C for 24 hours. The sol-gel hard coating (or called oa 10 varnish) consists of a hybrid matrix (mineral - thermoset polymer) reinforced with silica nanoparticles, the varnish was deposited by dip coating process on the CR 39. The experiential scratch tests for the three types of polymers were performed using the nanoindenter from MTS (Mechanical Testing and Sensing corporation) having a conical diamond tip

with 30° of include angle and 60 nm of the spherical radius. The numerical simulation was done using 3D modeling of finite- elements (FEM) using the Forge3 implicit code, scratch tests were modeled using an automatic remeshing procedure. The simulation results and scratching experiments of the three types of polymers showed that by increasing penetration depth both the scratch hardness and the friction coefficient increased. Also, the results show that the apparent coefficient of friction is higher for polycarbonates and smaller for CR39 and finally for oa10, and the hardest material is oa10 followed by CR39 and then polycarbonate for both simulation and scratching experiments.

M. Bonne et al. (2005) [52] presented an experimental study to determine the nano- indentation hardness profiles of different depths of scratches produced upon the poly(methyl methacrylate) surface. The black PMMA (PERSPEX CS Black 962) was used in experimental tests. The indenter used to create scratches on the PMMA surface was made of hardened steel cone having a diameter of 4 mm with an included angle of 90° was produced by AW Precision Limited Company in the UK. The experiments of nano-indentation were obtained with a compliant indentation device that allows loads to be applied for a few micrograms; also it had a method of operation called constant stiffness that allows the imposition of a small volatile load on the gradually changing imposed load. The nano-indenter with a three-sided diamond pyramid tip supplied by Nano-Instruments, Oak Ridge in the USA was used in nano-indentation experiments. All data and images of scratched surfaces were obtained by using the techniques of the scanning electron microscope (SEM), laser profilometer and optical microscope. The results of experiments showed that the nano-indentation technique can be used to obtain the subsurface morphological properties generated during the scratch deformation of the polymer surface. This technique also provides useful information for subsurface damage in plastic

polymers where the traditional methods of sectioning and imaging were often impractical.

In 2005, S. Lafaye et al. [24] developed a model of surface flow line to determine the true and geometric friction coefficients between the material surface and the moving scratching tip from the apparent friction coefficient. The simulation model to test three types of surface flow lines to estimate the coefficient of apparent friction of spherical tip and conical tip that scratch the PMMA surface was designed. The simulation model requires input of some data such as the coefficient of true local friction, the effective pressure on the contact surface and the true contact area. Simulation results were for horizontal lines model that the apparent friction was less than the actual friction of the low values of the contact radius. For vertical flow lines, the apparent friction of the lower cone angles was estimated significantly in relation to the Tabor and Bowden calculations. Secant lines model tends to horizontal lines model for low angles of the cone while tends to vertical lines model for large angles of the cone.

R. Schirrer et al. (2006) [25] studied the apparent friction analysis of polymeric surfaces to determine local friction. The scratch device used in the experiments was a commercial servo mechanism that carries an environmental chamber containing the scratch tip and the sample, a microscope was also installed to measure the dimensions of the remaining groove on the scratched surface. Scratch tests were performed for a range of speeds from 1μm/s to 15mm/s and a temperature range from -70°C to +120°C and the normal load range applied to the tip from 0.05N to 5N. A computer was used to control the moving tip and record the load, temperature and speed during the experiment. Poly (methylmethacrylate) (PMMA) and CR39 (allyl diglycol carbonate)) were used in the tests. A conical tip with radius of 110 μm and apex angle of 90^{o} was

used in the scratch test of CR39, while a conical tip with radius of 30 μm and apex angle of 120° was used in the scratch test of PMMA. The results show that the parameters which act on the coefficient of true local friction were temperature, sliding speed, and strain level in the contact interface.

R.D.K. Misra et al. (2007) [53] investigated the effect of the indenter geometry on the surface deformation of pure polyethylene (PE) and $CaCO_3$ - polyethylene composite during the scratch. All the samples used in tensile and impact tests of pure polyethylene and $CaCO_3$ / polyethylene composites depending on American Society for Testing and Materials (ASTM) D-638 and D-256 respectively and prepared by injection molded. The scratch device used in the experiments can control the temperature and velocity of the moving tip and record the normal and tangential loads using the computer. The dimensions of the left groove on the surface can be determined in situ by (AFM) atomic force microscope built into a scratch apparatus. Three types of indenters were used in scratching experiments included Hoffman with a radius of 0.5 mm, a needle with a radius of 1.66 mm and a loop with a radius of 3.49 mm. For direct comparative evaluation, the conditions of scratch test were similar for all polymeric samples being investigated. The results showed that the greatest increase in the resistance to scratching was in the scratch caused by the use of the loop followed by scratching from the use of needle while the smallest was in the Hoffman scratching. Also, the relationship between scratch resistance and the indenter radius was not linear and it depended on the geometry of indenter.

In 2008, Pelletier et al. [54] carried out analysis of the residual groove after contact between a spherical indenter and PMMA surface during scratching using experimental and simulation results. Scratch device called the microvisioscratch to determine precise parameters related to the viscoelastic and viscoplastic behavior of the scratch of the PMMA material was used. The speed

of scratch, temperature and moving tip as well as the recording of normal and tangential loads in the scratch device was controlled by computer, the integrated microscope allows for on-site monitoring and measurement of the remaining groove on the surface. The scratch experiments were conducted at 30 °C and a fixed speed of 0.03 mm /s with a normal load applied to the moving tip ranging from 5 N to 35 N, diamond conical tip with spherical extremity with apex angle of 60^{o} and a tip radius of 200 μm. Scratch tests were simulated for the different radius of spherical indenter and different penetration depths were tested using a specific 3D element code, all calculations were performed using the implicit FEM package MSC Marc. The results of the analysis showed that the FEM results indicate that the residual groove shape in the elastic - plastic contact was directly related to the plastic strain field in the deformation below the indenter during scratch. Also, analysis of optical micrographs of the left groove on the surface of polymer allows determining the true geometry shape of the contact area and the recovery at the rear part of the contact. All the geometrical parameters provided to describe the residual groove recovery were related to the friction coefficient and mean contact strain imposed during scratch.

H. Pelletier et al. (2008) [26] carried out experimental and finite-element analysis of the effect of polymeric materials properties on the scratch resistance. Two types of polymers were studied; the PMMA and the allyl diglycol carbonate (CR39). Scratch experiments were carried out using a scratch device that can control temperatures ranging from - 70°C to +120°C and a scratch velocity ranging from 1 μm/s to 10μm/s. The device also allows for on-site monitoring during depth sensor measurements on the polymer surface, this equipment was characterized by the ability to distinguish the contact area during loading through the groove remaining on the surface. Scratch experiments were conducted at room temperature and at a fixed scratch speed of about 0.1 mm /s with a variable normal load within a single groove. The specifications of the

indenter were diamond tip with cone shaped having an apex angle of 60° and radius of 116 μm. Results of analysis show that the increase in the coefficient of friction leads to an increase of the maximum plastic strain and an important adjustment of the size and the shape of the gradient of plastic strain at the rear part of the indenter for both PMMA and CR39. Also, with the increasing of the friction coefficient, the inversion with the case of tensile plastic strain was more important than the case of compressive plastic strain at the front part of the contact. The results obtained by FEM were well correlated with experimental observations and show that the gradient of plastic strain below the indenter clearly depends on the coefficient of true friction as well as the rheological parameters of the materials which tested.

In 2010, N.Aleks et al. [55] studied numerically the mechanical origin of the PMMA healing phenomenon. The scratch tests were conducted using fixed normal load of 150 mN, fixed tip speed of 10μm/s, scratch path length of 300 μm, and nanoindenter XP has spherical tip with radius of 35μm. The mechanical model used in numerical simulation consists of three elements connected together. Behavior in small strains was represented by the first spring, which represents linear elasticity. Viscoelastic element represented by the dashpot which represents the yield stress depends on the time and the softening of strain. The non-linear strain was represented by the second spring which refers to the behavior of hyperelastic materials. The results show that increased temperature if may be controlled, allows to reduce plastic deformation caused by scratch on an amorphous polymer, also show that the healing phenomenon depends on the activation of the strain hardening and the sensitivity of material temperature. Finally, improving or characterizing the mechanical properties of PMMA for better recovery potential was a motivating possibility.

M. Manshaa et al. (2011) [21] investigated the effect of plasticization on the scratch resistance of poly (methyl methacrylate) using fatty acid amides. Three types of fatty acid amides (Stearamide, Erucamide, and Behenamide) to study the effect on the mechanical properties of the PMMA surface at a wide range of temperatures were used. The scratching device relies on a commercial servo mechanism having a little transparent environmental box containing the sample and movement tip. Temperature and tip velocity within the device can be controlled, the velocity of the tip ranging from 10^{-3}mm/s to 15 mm/s, the range of temperature from -70°C to +120°C. The rang of loads that can be applied to the tip from 0.05 N to 35 N. The scratching device was equipped with an integrated microscope, which allows for local analysis of the contact and the left groove on the scratched surface. Temperature, normal load, the geometry of tip, and speed of sliding were represented the input parameters; while real contact area, the geometry of groove and tangential force were represented the output parameters. A computer was used to control the moving tip and record the load, temperature and speed during the experiment. All samples were scratched by indenter with conical tip which has a radius of 116 µm and apex angle of 60°. The results show that the PMMA friction coefficient can be reduced by the use of suitable plasticizers. In smaller amounts than being in large quantities, fatty acid amides were more successful for decreasing the coefficient of friction in the PMMA. The maximum limit of the reduction in friction coefficient of the PMMA occurs with the weight ratios 0.1 %, 0.05 % and 0.1 % of Behenamide, Erucamide, and Stearamide, respectively.

Jyothi Atla et al. (2013) [41] carried out the effect of aluminium oxide powder (Al_2O_3) addition on thermal diffusivity of heat-activated acrylic resins (PMMA). In 1937, Dr. Walter Wright introduced PMMA as the best dental base material, but it has low mechanical properties, especially in terms of thermal diffusivity. To determine the thermal diffusivity of acrylic resin (PMMA) in

the temperature range from 0°C to 700°C, modified acrylic resin samples were prepared by mixing pure acrylic with different ratios of Al_2O_3 (5wt%, 10wt%, 15wt% and 20wt%), which were then mixed with monomer and packaged in the dough stage in the molds and placed under a hydraulic press. By means of thermocouples incorporated in cylindrical specimens and using a new technology developed by Watts and Smith that allows rapid and accurate determination of thermal diffusion, the thermal diffusion of acrylic resin was measured. The results showed that samples containing alumina (Al_2O_3) had high thermal diffusion compared to samples without alumina. Also, the samples containing 20wt% of alumina had the highest thermal diffusion value, followed by samples containing 15wt% and then containing 10wt% and finally samples containing 5wt% were the lowest thermal diffusion value.

In 2014, Onur Coban [42] investigated the effect of heat treatment on the optical transmittance of samples of polymethyl methacrylate (PMMA) exposed to solid particle abrasion. The mechanical, thermal, physical and chemical properties of PMMA samples resulting from the heat treatment effect were studied by TGA, FTIR, DSC and Vickers hardness measurement methods. The PMMA sheets were used in the manufacture of Fresnel lenses by hot-stamping, extruding, and injection method, where these lenses were widely used in concentrating sunlight on cells used in solar energy applications. The optical transmittance efficiency of Fresnel lenses was affected by several factors such as soil elements raised by the wind, eruptions of volcanic, movement of the vehicles, and pollution. Improving both surface hardness and impact strength for Fresnel lenses has become an important necessity to reduce scratching. The results showed that heat treatment improved the surface hardness and increased the glass transition temperature of the PMMA sheets from 116.24° C to 119.22°C. The maximum abrasion occurred at the 30° collision angle of the solid particles with the PMMA surface while the minimum abrasion occurred at

the 90 ° collision angle. Also, the results showed that 5% of the PMMA optical transmittance lost during lens manufacturing can be restored after 3 hours of heat treatment at 85°C.

Saeed Shirkavand and Elnaz Moslehifard (2014)[43] studied the effect of titanium dioxide (TiO_2) nanoparticles addition on tensile strength of polymethyl methacrylate (PMMA) resin used in the dental industry. The PMMA resins were widely used in the manufacture of temporary base materials used in the manufacture of dental and prosthetic alternatives due to their optical, aesthetic and bio-compatibility properties. According to standard ISO 1567, the 36 samples of the tensile tests were prepared, 9 samples of pure PMMA resin and 9 samples for each ratio of TiO_2-reinforced PMMA resin (0.5, 1, and 2 wt% TiO_2). Using a testing universal machine type Zwick Z100, Germany, the tensile test was obtained of samples under the load of 10 kN and speed of 5mm/min. The results of the tensile test showed a significant increase in tensile strength values of the reinforced PMMA resin specimens by 1wt% TiO_2 nanoparticles comparison with the pure and reinforced by another ratio of TiO_2 for the PMMA resin. Also, any another increase in TiO_2 nanoparticles content above 1wt% imposes an adverse effect by reducing the tensile strength due to the particles agglomeration that act as tense defects and concentration points.

Ehsan Moghbelli et al. (2014) [56] studied the effect of exposure to moisture on PMMA scratch resistance. Three categories of black PMMA plates injection-molded were used with dimensions of 150mm × 150 mm × 3mm were two impact-modified categories (PMMA-1) and (PMMA-2) and a scratch-resistant category (PMMA-3) supplied by Arkema Inc., among the PMMA categories, the number 3 category has the highest polarity, followed by category 2 and category 1 . The PMMA plates were placed in a vacuum oven at a temperature of 80 ° C and pressure about 30 mmHg for one full day in order to

dry the PMMA plates. After drying, the plates were weighed using a high-precision digital balance, then the PMMA plates were placed in a controlled relative humidity chamber at a relative humidity of 75% and a temperature of 23° C for a period of 28 days , the PMMA plates were removed and weighed after the end of the period. Scratch tests were performed according to ASTMD7027 / ISO 19252 using a gradient loading range from 1N to100N at a constant sliding speed of 100mm / s for a scratch path length of 100mm. A stainless steel indenter with spherical tip has diameter of 1 mm was used for scratching all samples. The results showed that depending on the PMMA polarity and the exposure period to moisture, the accumulation of water molecules leads to a beneficial effect on the PMMA surface and adds a degree of lubrication and thus improves the scratch resistance.

In 2015, Vipul Asopa et al. [44] carried out evaluation and comparison of mechanical properties of high impact PMMA resin with and without zirconia addition. Test samples were prepared using high-impact acrylic resin (Trevalon high impact powder) as a control element and zirconium oxide (ZrO_2) as filler with two mixing ratio 10 wt% and 20wt% to reinforce acrylic resin. Mechanical tests included testing for impact and transverse strength, water sorption and surface hardness. The transverse strength test was done using a Universal Testing Machine of type STS 248, the pendulum impact test machine was used to test the impact strength of the samples. The water sorption test was carried out by placing samples in a desiccator of type Mahavir at 37°C for 23 hours and then placed at ambient temperature for one hour and each sample weighed, these samples were placed in distilled water for 7 days at a temperature of 37°C and then taken out and each sample weighed, the weight difference between the two cases for each sample represents the water sorption. The surface hardness test was performed using a digital Vickers microhardness tester. The results showed an increase in the transverse strength and water sorption of the reinforced acrylic

resin in both ratios (10 % and 20 %) compared with the non-reinforced acrylic resin. Also, decrease in surface hardness and impact strength of reinforced acrylic resin in both ratios compared to non-reinforced acrylic resin.

A. O. Alhareb et al. **(2016) [45]** investigated the radiopacity of Al_2O_3 and Y-TSZ (alumina and zirconia) particles with NBR (nitrile butadiene rubber) dissipated in PMMA used in the manufacture of dental bases. The PMMA mixture was prepared without filling by mixing 0.5% PBO (benzoyl peroxide) as a control material with PMMA powder. A similar PMMA mixture was prepared from mixing of Al_2O_3 (alumina) and Y-TSZ (yttrium zirconia) 1:1 with NBR (nitrile butadiene rubber) particles as a reinforcing material. Alumina and zirconia quantities changed from 1 to 10 wt% while the amount of nitrile butadiene rubber was limited at 7.5 wt %. The results showed that for the reinforced PMMA mixture with 10 wt% of the Y-TSZ /Al_2O_3 mixture the radiopacity increased by 25% higher than that the non-reinforced PMMA mixture. The results also showed that increasing fill rates to PMMA lead to undesirable effects such as reductions in some mechanical properties.

Ahmed Omran Alhareb et al. (2017) [46] studied toughness of fracture, the strength of impact, and improvement of the hardness of PMMA denture bases via the addition of NBR (nitrile rubber) with 2-types of ceramic paddings. One of the prerequisites for good performance of PMMA used in the dental industry was its sufficient strength for impact and hardness of fracture. Another crucial feature was surface hardness which helps ease the finishing/polishing process easily and also provides good scratch resistance while cleaning dental prostheses. The results showed a significant improvement in scratch resistance, fracture toughness, and impact strength of PMMA resins after reinforcement with NBR and ceramic paddings although there was no apparent improvement in hardness. Also, the results showed that the optimal mixture of fillers in

PMMA resins was 7.5 wt% of NBR with 2.5 wt% of Al_2O_3 and 2.5 wt% of YSZ.

In 2017, Z Hasratiningsih et al. [47] investigated the improvement of the hardness of polymethyl methacrylate (PMMA) by adding the filler system of ZrO_2-Al_2O_3- SiO_2 at two different calcification temperatures. A comparison between pure and reinforced PMMA hardness with a filler system (ZrO_2-Al_2O_3-SiO_2) was performed at two different calcification temperatures firstly by heated at 550°C for one hour and then increased to 700°C and secondly by directly heated to 700°C. The filler (zirconia ZrO_2 - Alumina Al_2O_3 - silica SiO_2) was added to the PMMA in different ratios starting from 7 wt% to 15 wt%. Tests on the surface of each sample were done by MicroVickers using a Vickers hardness tester device (LECO-Japan M-400-H1/H2/H3) for 15 seconds with a load of 200g. Using a scanning electron microscope (SEM) all images and observations in -site of the indentation was obtained. Test results showed that the PMMA hardness improved significantly when added filler system of (ZrO_2 - Al_2O_3 - SiO_2). The (ZrO_2-Al_2O_3-SiO_2) filler system reinforced by 13% at 700°C shows approximately 25% higher hardness compared to the calcification temperature of 550 - 700°C.

2.2 Summary

After reviewing the previous works, the following remarks can be reported:

1. Improving the PMMA scratch resistance by adding nanoparticles needs further studies; the current study is a new contribution for improving the PMMA scratch resistance by adding SiO_2 in new ratios.
2. In the previous studies, SiO_2 was added at high ratios sometimes reaching greater than 10wt%. In the current study, SiO_2 was added with two groups of ratios, the first ranging from 1wt% to 4wt% and the second ranging from 0.1wt% to 0.5wt% in order to make a comparison of the evolution of PMMA scratch resistance for the two groups and choose the best of them.
3. The pure and reinforced PMMA samples were prepared in previous studies using the polymerization, extrusion and injection method. In the present study pure and reinforced PMMA samples were prepared using the pressing, dissolving and casting method.
4. The large majority of previous studies on the evolution of scratch resistance for PMMA have been conducted using non transparent (opaque) PMMA, in the current study transparent PMMA was used due to the wide uses of this type.
5. The scratch resistance test of PMMA in previous studies was done by using nanoscale indenters to scratch small samples with thickness in micrometer, in the current study; scratch tests were performed on large samples with a thickness of 4 mm using conical and spherical indenters with radii in millimeter.
6. In previous studies, the parameters affecting the scratch behavior of PMMA were studied and the number of parameters was not more than two in each study. In the present work, the effect of five simultaneous parameters on the scratch behavior of PMMA was studied which are the preparation method of specimens, SiO_2 content, indenter geometry, applied normal load and sliding speed.

7. In previous studies, the scratch test was performed using devices modified from other devices such as a modified tensile tester. In the current work, a new automated device for testing the scratch resistance was completely designed and manufactured, and it is the first device in the College of Engineering, University of Basrah, and the College of Materials Engineering, University of Babylon.

Chapter Three
Theoretical Background

Chapter Three

Theoretical Background

3.1 Introduction

Due to its low cost, ease of manufacture and high strength relative to weight, polymers are widely used for durable goods applications. However, the scratch resistance of polymeric materials is considerably lower than that of metals and ceramic materials. As a result, the scratch resistance of polymers has received much attention in academia and industry. This chapter represents a theoretical background for polymer scratch, in which the origins of polymer scratch, scratch theory, scratch testing methods, polymer scratch analysis techniques, and mechanisms of scratch formation will be covered in detail.

3.2 Polymer Scratch Origins

Tribology dated back to the experiments of Leonardo da Vinci in the fifteenth century that studied two contact surfaces in a state of relative motion. After hundreds of years, the first basic laws of friction were established by Charles de Coulomb. The hardness scale of minerals based on the harder metal can scratch the softer metal was developed in 1812 by Frederic Mohs. Also, during this time period, important progress was made in tribology by establishing friction laws by Amontons and Coulomb.

Tribology includes three main branches are friction, wear, and lubrication. Wear can occur due to adhesion, abrasion, corrosion and surface fatigue. Abrasive wear can result from a single-path or multi-path confrontation between two surfaces. The type of contact between two surfaces can be either single asperity contact (e.g. nail on a surface) or multi-asperity contact (e.g. sandpaper

on a surface). In the present work, the scratch that falls under the abrasive wear category is defined as a single path process with single asperity contact; it was performed using a constant applied load and a constant sliding speed for each stage of the scratch test. Tribology developed by Professor Friedrich can be illustrated as a scheme in figure (3-1),while figure (3-2) illustrates a diagram for the definition of scratch in current work (indicated by a black lines).

Figure (3-3) represents a single path case, a single asperity scratch deformation where a spherical tip passes across the polymer surface using a constant or variable normal load at a specific sliding speed. The ability of the polymeric material to resist deformation of the surface resulting from a sliding penetration of an asperity during the application of a specific normal load is a measure of the scratch resistance of this material.

Maintaining the surface quality of polymeric materials requires a lot of attention due to their ability to surface deformation and damage when exposed to low loads compared to ceramics and minerals, however, significant progress has been made in basic knowledge of scratch behavior in polymers only recently. Before that, there was a lack of standardized test methodologies and equipment required for conducting scratch tests on polymers where the researchers resorted to manufacturing and developing their own scratch devices to perform experiments [62].This lead to, the acquired knowledge of polymer scratch behavior is only for experimental conditions, materials, and testing equipment. Scratch test standards such as ISO [59, 60] and ASTM [61] only appeared in 1997 and 2003, respectively, these standards more suitable for ceramic and mar study. The methods of evaluating scratches also differed, as some researchers used optical devices such as SEM, while others relied on the subjective human eyesight. As a result of incorrect limitations used in the scratch test and evaluation, which resulted in researchers being unable to compare and verify experimental results, this impeded progress in polymer

scratch research. However, the level of complexity implicated in studying the polymer scratch behavior is perhaps the most important factor. The diagram shown in figure (3-4) lists the most important factors and considerations involved in studying the polymers scratch [11].

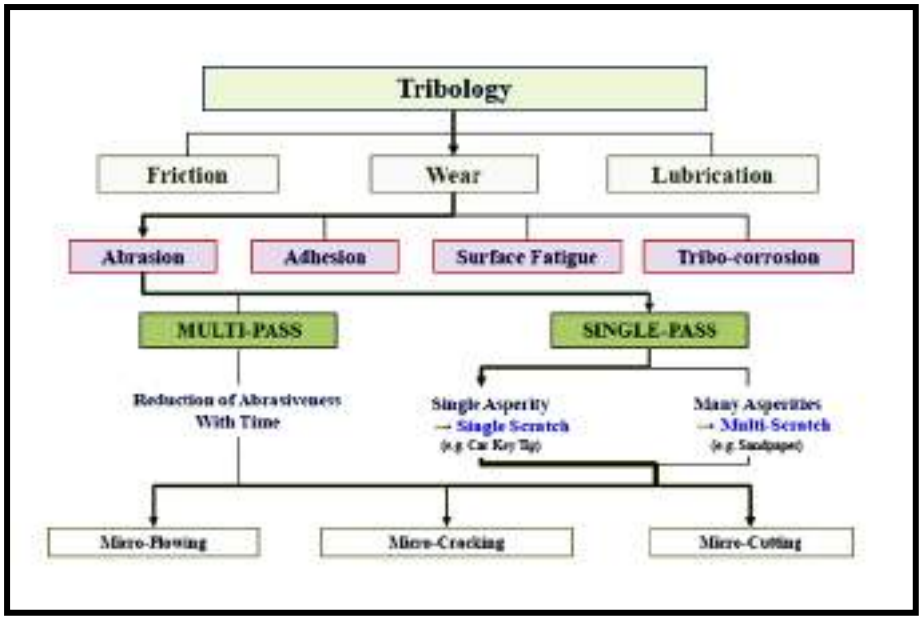

Figure (3-1) Classification schematic of Tribology [57].

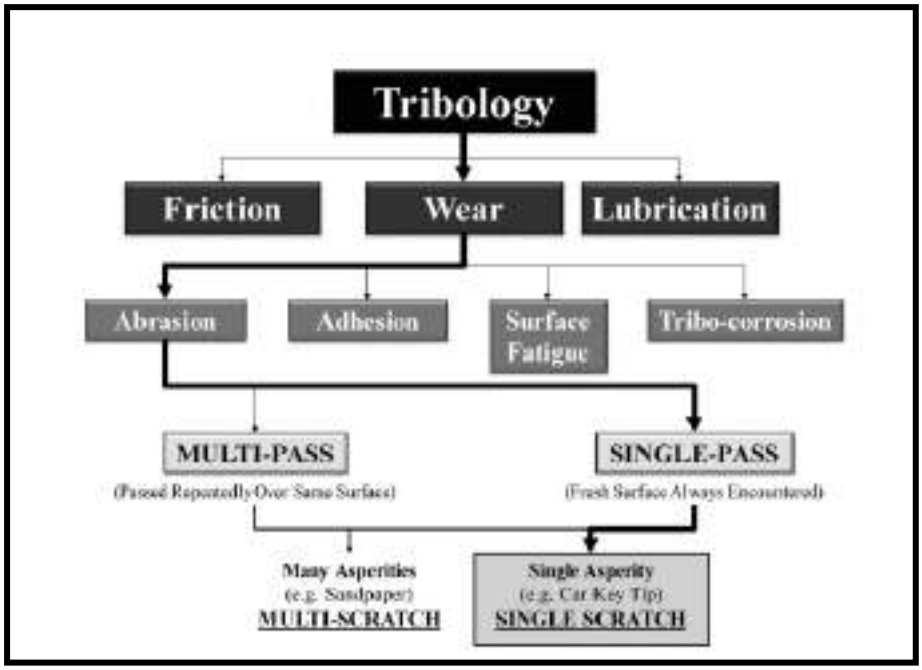

Figure (3-2) Definition of scratch in present work [57].

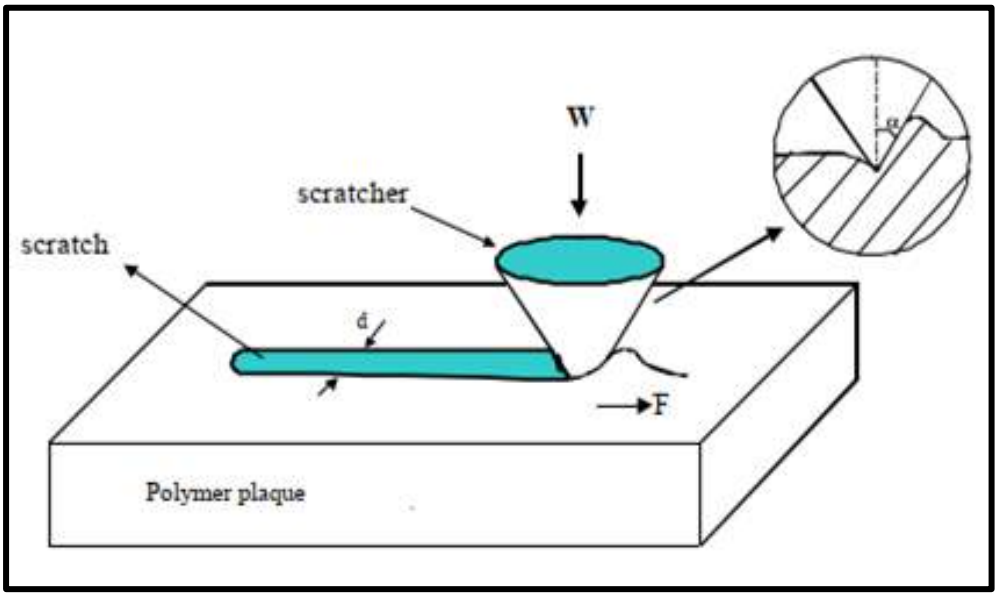

Figure (3-3) Schematic representation of a scratch [58].

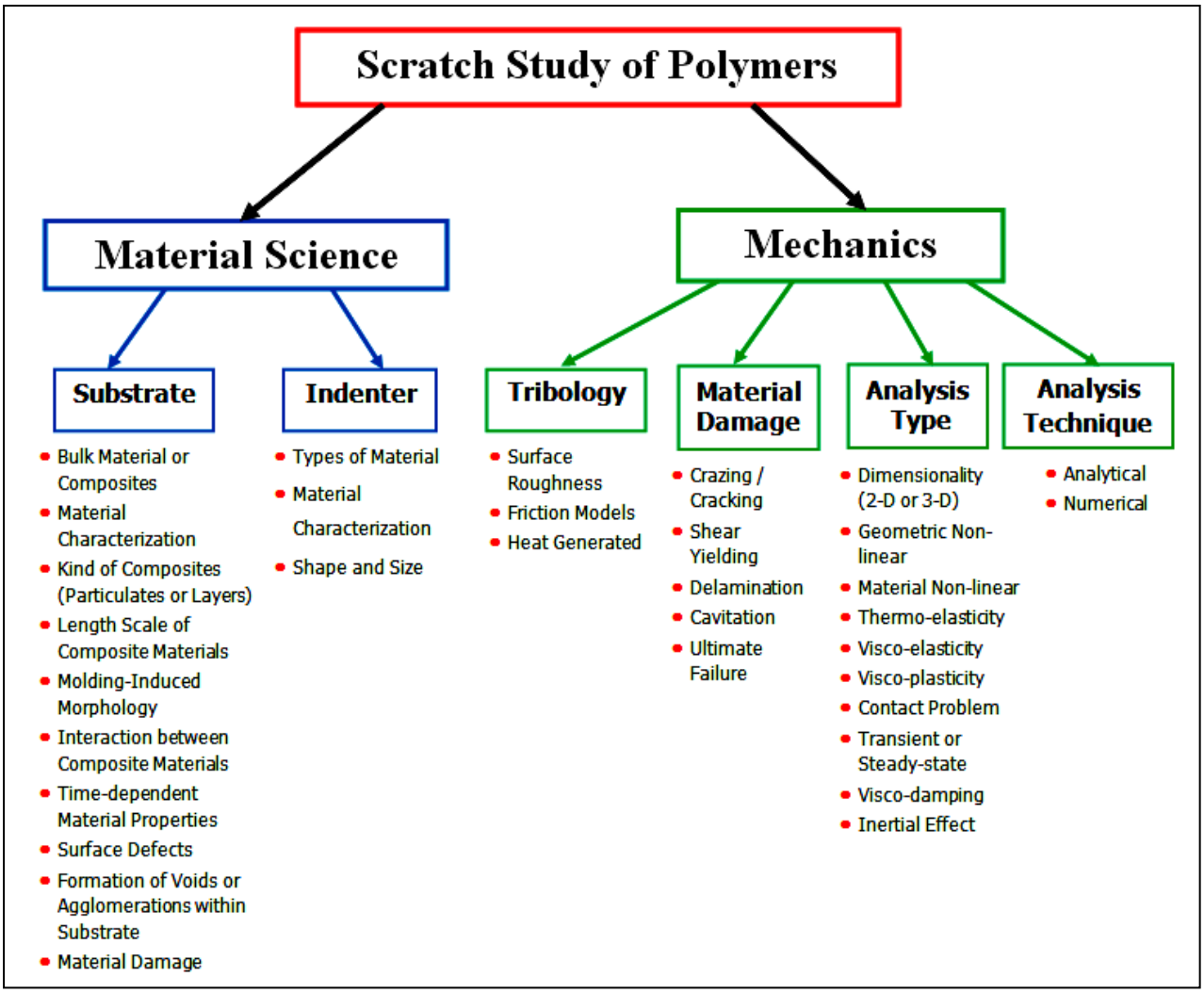

Figure (3-4) Considerations and factors for the scratch study of polymers [11].

3.3 Scratch Theory

Scratch is the process of creating a groove on a surface when a hard object placed in contact with it moves across that surface as shown in the previous figure (3-3). Scratch is part of the science that studies wear, lubrication and friction for surfaces in relative motion, known as tribology [63]. Two quantities closely related to scratch are friction and hardness. Friction is defined as the resistance that can be generated when one body moves over another, while hardness is the surface resistance to penetration. During the sliding friction process, the sliding friction coefficient also called apparent friction coefficient can be defined as follows

$$\mu_{app} = \frac{F_t}{F_n} \qquad \ldots\ldots (3.1)$$

Where:

F_t : the tangential force required for moving the body on the opposite surface, and F_n: the applied normal load. In polymers, the value of μ_{app} can range from 0.06 for polytetrafluoroethylene (PTFE) to greater than 2 for rubber [64].

The apparent friction coefficient includes two friction coefficients types, one of which is the result of separation at the region between scratched surface and tip is called coefficient of true local friction $\mu_{loc.}$ (or called adhesive friction coefficient $\mu_{ad.}$), the other is a result of plowing the material formed in front of the moving tip is called geometrical friction coefficient μ_{def} (or called coefficient of plowing friction μ_{plough}). In general, contributions to friction can be classified into two categories: friction due to adhesion $F_{ad.}$ and friction due to deformation $F_{def.}$, and accordingly friction can be rewritten as follows:

$$\mu_{app} = \mu_{loc.} + \mu_{def} \quad \text{OR} \quad \mu_{app} = \mu_{ad.} + \mu_{plough} \qquad \ldots\ldots (3.2)$$

The adhesion contribution is generated by the molecular attractive forces between the asperities on each surface of the sliding surfaces on each other. The smallest points that provide actual contact between surfaces are called asperities. For polymers, the adhesion strength mainly depends on the asperities size and the type of chemical groups in the polymer chain. Another factor that contributes to the adhesion of polymers is the secondary bonds formed through hydrogen bonding and Van der Waals forces. Depending on the polymeric chemical structure, the strength of the bonds formed will vary. The deformation term means any distortion process that occurs on the surface and dissipates energy while slipping over it. Deformation in polymers comes from two major contributions: viscoelastic deformation and plastic deformation, the coefficient of friction becomes

$$\mu_{app} = \mu_{ad..} + \mu_{visco.} + \mu_{plast.} \quad \text{..... (3.3)}$$

Friction can be considered one of the physical parameters that lead to energy dissipation, and it is originally wear phenomenon that occurs between two moving surfaces. The apparent friction components can be analyzed by means of tests that allow a separate evaluation of each preliminary friction coefficient. Tabor and Bowden [65] analysis of plastic contact allows linking between adhesive friction and adhesive shear. When the angle between the substrate surface and the frontal face of the scratch tip is small (attack angle), adhesive force and applied normal load are

$$F_{ad.} = \tau_{ad} S_n \quad \text{...... (3.4)}$$

$$F_n = p S_n \quad \text{..... (3.5)}$$

Where, τ_{ad} : the shear stress due to adhesion in the contact area, p: interfacial pressure in contact region, and S_n : the actual contact area.

From the above two equations, the adhesive friction coefficient is

$\mu_{ad..} = F_{ad.} / F_n = \tau_{ad} / p$ ……. (3.6)

The apparent shear stress consists of shear stress resulting from adhesion and shear stress resulting from the ploughing. Briscoe and Tabor [66] calculated the apparent shear stress in the polymeric material by the product of dividing the tangential force by the normal contact area.

$\tau_{app} = F_t / S_n$ ….. (3.7)

Thus, the plowing shear stress can be written as

$\tau_{plough} = \tau_{app} - \tau_{ad}$ ….. (3.8)

The μ_{plast} term (plastic friction coefficient) is used to evaluate plastic deformation in polymers due to asymmetric contact of moving scratch tip during the scratch process based on plastic deformation model provided by Bowden and Tabor [65]. This model is shown in figure (3-5), where a conical tip with apex angle θ was used, and the projections of the front and horizontal contact areas were used to calculate the coefficient of plastic friction.

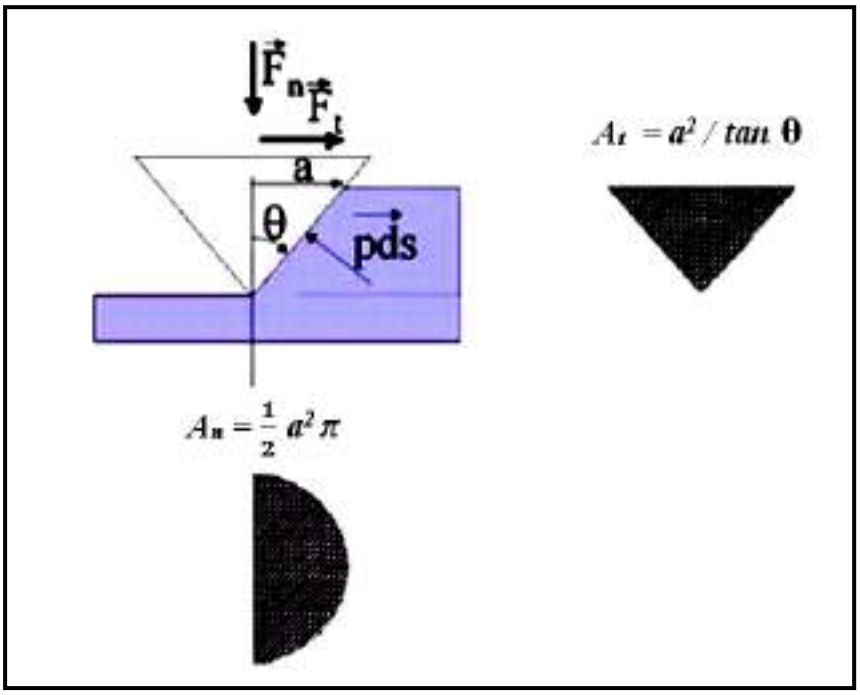

Figure (3-5) Model of plastic friction using conical tip with apex angle θ [65].

From figure (3-5), the tangential force and normal load can by calculated as follow

$F_t = p / A_t = a^2 p / tan\ \theta$ …… (3.9)

$F_n = p / A_n = = \frac{1}{2} a^2 p/\pi$ ……(3.10)

Where, A_t : frontal projected contact area, A_n : horizontal projected contact area and p as known.

From the above two equations, the plastic friction coefficient is

$\mu_{plast.} = \frac{2}{\pi} cot\ \theta$ ..… (3.11)

It is clear from equation (3.11) that the μ_{plast} is only affected by the geometry of the tip. The perfectly elastic behavior, elastic-plastic behavior in polymers and the shape of contact after elastic recovery which partially restores the rear contact with the tip, all of them were not taken into account. In order to take into account the rear contact region that occurs after the partial recovery process of the plastic deformation behavior in the polymers, Bucaille et al. [67] generalized the Tabor model as shown in figure (3-6) where the rear contact area is defined by the angle ω, the plowing friction coefficient becomes

$$\mu_{plough} = \frac{2}{\pi}\cot\theta\left(\frac{\pi \sin(\omega + \pi/2)}{\pi + 2\omega}\right)$$ ….. (3.12)

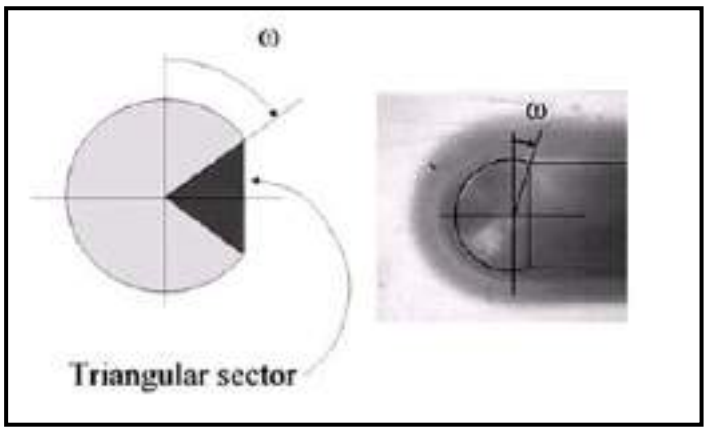

Figure (3-6) Contact area model showing angle ω and triangular sector [67].

The model presented by Bucaille et al. allows for the calculation of the plowing friction coefficient for specific values of angle ω but does not take into account the triangular sector located within the dorsal angle. To overcome this problem, they put an approximate relationship to estimate the cross section as a triangle section whose height is equal to the height of the hyperbola and its base is equal to the width of rear contact region as shown in figure (3-7). The plowing friction coefficient after approximation becomes

$$\mu_{\text{plough}} = \frac{2}{\pi}\cot\theta\left(\frac{\pi\cos\omega(1-\sin\omega)}{\pi+2\omega+\sin 2\omega}\right) \qquad \text{.....(3.13)}$$

When ω = 0 the plowing friction coefficient from equation (3.13) is equal to friction coefficient calculated by Tabor and Bowden, equation (3.11) , when ω = π/2 the plowing friction coefficient is null.

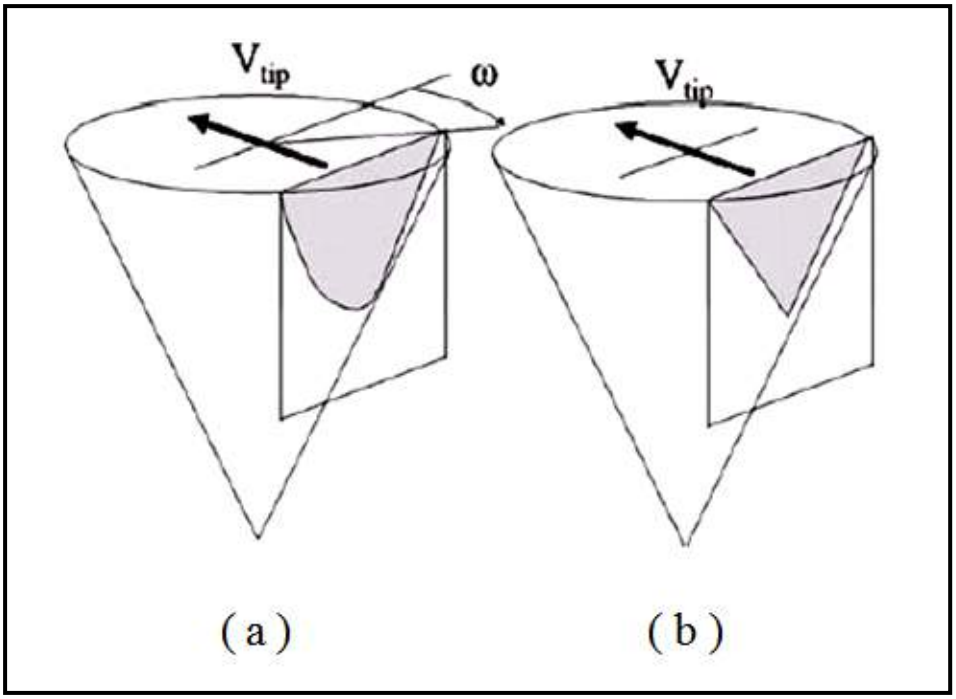

Figure (3-7) Rear contact region of Bucaille model, (a) exact solution and (b) triangular solution [67].

Another attempt to generalize a Tabor model by Lafaye et al. [24] using a conical scratch tip with apex angle θ, as shown in figure (3-8). Assuming that the contact pressure on the front face and rear face of the scratch tip is the same, and ratio between half the width of the rear contact (b) to half the width of the front contact (a) is $x = b/a$, from force equilibrium the following equations can be obtained

$$F_n = p(S_f + S_d)\sin\theta + \tau_{app}(S_d - S_f)\cos\theta \quad \ldots\ldots (3.14)$$

$$F_t = p(S_f - S_d)\cos\theta + \tau_{app}(S_d + S_f)\sin\theta \quad \ldots\ldots (3.15)$$

where S_f : frontal contact area, S_d : rear contact area.

After substituting $S_d = x\, S_f$ and $\tau_{app} = \mu_{ad.}p$ in the above two equations, the apparent friction coefficient is

$$\mu_{app} = \frac{F_t}{F_n} = \frac{(1-x)+\mu_{ad.}(1+x)tan\theta}{(1+x)tan\theta+\mu_{ad.}(x-1)} \quad \ldots\ldots (3.16)$$

Using equation (3.16), the polymer scratch behavior can be evaluated by the friction coefficient as follows:

1. When $x=1$ (i.e. a=b) this leads to $\mu_{app} = \mu_{ad.}$ and the behavior is perfectly elastic contact.
2. When $x=0$ (i.e. b=0) this leads to $\mu_{app} = \frac{(1+\mu_{ad.}tan\theta)}{(tan\theta-\mu_{ad.})}$ and the behavior is perfectly plastic contact.
3. When $\mu_{ad.}=0$ (i.e. there is no adhesive friction coefficient) this leads to $\mu_{app} = \mu_{plough} = \frac{(1-x)}{(1+x)tan\theta}$ and the behavior is elastic - plastic contact.

The reader can refer to the papers [68] and [69] to find out more friction coefficient relationships when using a spherical or pyramidal indenter during the scratch process.

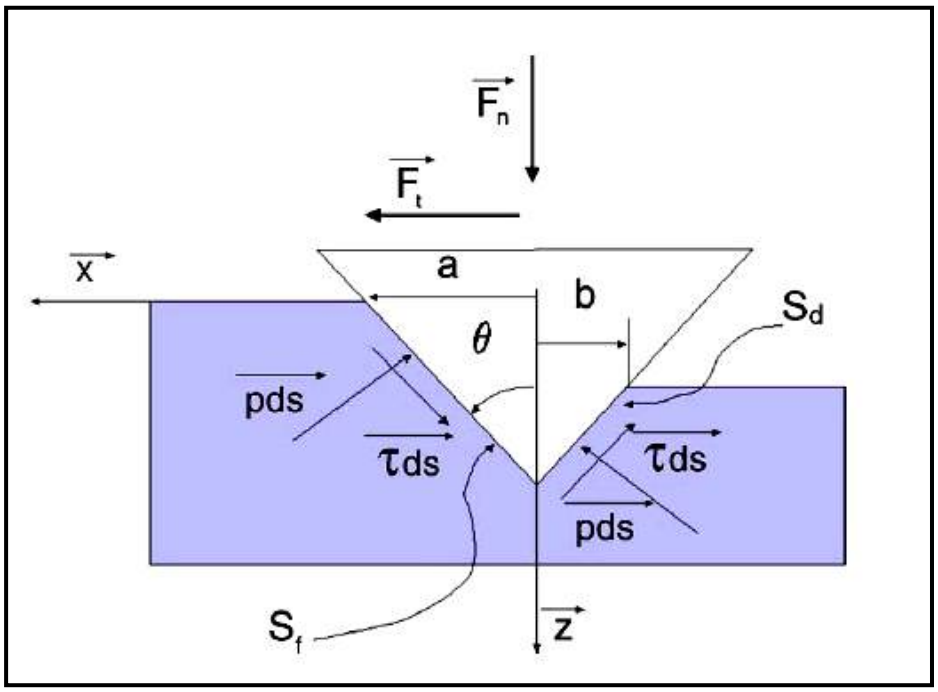

Figure (3-8) Describe the stresses influencing the Lafaye model[24].

The second quantity associated with scratching is hardness, as mentioned earlier. In penetration hardness testing using a spherical indenter, Meyer's hardness for a perfectly plastic material is defined as the ratio of the applied load on the indenter to the projected penetration area [58]. If the applied load on the indenter is F_n and the diameter of the depression left on the material surface after the lifting of the indenter is d, Mayer's hardness is given as

$$H_M = 4\,F_n / \pi d^2 \qquad \text{…….. (3.17)}$$

The equation (3.17) is also valid in the case of using a conical or pyramidal indenter. The only difference is in calculating the projected area of the pyramidal indenter. The ratio of applied normal load on the indenter to the load bearing area is called the scratch hardness. It is always equivalent to the penetration average pressure exerted on the polymer during the scratch process. When using a conical or spherical indenter in the scratching process of the viscoelastic-plastic polymers, because the elastic recovery occurs almost immediately, load bearing area can be considered as the circle has diameter

equal to scratch width remaining on the surface. If the applied normal load is F_n and the remaining scratch width is d, the scratch hardness can be given as

$$H_{sc} = 4\,F_n / \pi d^2 \qquad \text{…….. (3.18)}$$

For the plastic materials, it can be seen that the scratch hardness is similar to the Meyer's hardness; a dimensionless parameter (q) is added to above equation in order to take into account the effect of elastic recovery during scratching **[70]**, the scratch hardness becomes

$$H_{sc} = 4\,q\,F_n / \pi d^2 \qquad \text{…... (3.19)}$$

Where q: dimensionless parameter has values ($1 < q < 2$) depending on the amount of elastic recovery during the scratch process, q = 1 for full elastic recovery (perfectly elastic deformation), and q = 2 no recovery (perfectly plastic deformation).

In the current study, the scratch device used to perform scratch tests for PMMA samples was designed on the basis of equation (3.1), where the dead weights represent the applied normal load F_n while the device reading represents the corresponding measured tangential force F_t . Equation (3.16) is used to calculate the coefficient of friction for PMMA samples depending on the resulting scratch behavior. Equation (3.19) can be used to calculate the scratch hardness.

3.4 Scratch Testing Methods

Scratch, which is a branch of abrasion in the tribology, can be defined as a process includes two actions performed simultaneously by a rigid tip on the polymer surface are indenting and traversing [71, 72]. Over many years, experimental techniques and methods have been developed to measure scratch resistance in polymeric materials, but with limited success [73 - 77]. In the last few years, a standardized methodology of test has been adopted, which classified as ASTM D7027-05 / ISO 19252 standards [78, 79]. These standards have been widely used for quantitative evaluation of the polymers scratch resistance and conduct investigations of the relationship between structure and property [80- 85]. Several methods have been used to evaluate the polymers scratch resistance, ranging from simple test methods such as pencil hardness tests and Mohs hardness test to complex methods such as test of Taber, pin on disk, Ford five-finger and single-pass pendulum. Below is an explanation of each test method.

- **Pencil hardness test**

Coating and paint manufacturers use this test to evaluate the scratch resistance of coatings. The mechanism of this test is based on pushing a group of different hardness pencils across the surface of the coating samples at an angle of 45°. The pencil that does not break and leaves no scratch mark on the surface gives an estimate of the scratch resistance of that sample [74, 86].

- **Mohs hardness test**

Since 1822 the Mohs hardness test has been used to evaluate the hardness of minerals. Mohs hardness scale consists of 10 metals arranged in descending order, starting with diamonds that take sequence 10 as the hardest and ending with talc that take sequence 1 as the softest as shown in table(3-1). This test is depending on principle that hard material that can scratch the surface of a Mohs mineral will have the same hardness as that of the mineral. The Mohs hardness

test is not suitable for polymers because the gradients of hardness between the metals in the Mohs scale are not equal, leading to the polymers occupying the lower range [87, 88].

Table (3-1) Table of Mohs hardness scale [57].

Mineral	Mohs' Hardness Scale
Diamond	10
Corundum	9
Topaz	8
Quartz	7
Orthoclase (Feldspar)	6
Apatite	5
Fluorite	4
Calcite	3
Gypsum	2
Talc	1

- **Taber test and Pin-on- disc test**

The sample to be scratched is placed on a rotating base that can control its rotational speed. Samples are scratched by a diamond indenter with a conical tip installed at the end of the cantilever arm; the normal load applied on the tip can be controlled. Both Kody and Martin [75] used the Taber test to investigate the scratch deformation of talc / polypropylene composite in their study using a conical tip with diameter of 152 μm and an apex angle of 90°, the applied load ranging (0 - 10 N) and scratch velocity of 1.8 mm / s. Chanda et al. used a pin-on-disc test in their study with scratch rates ranging from 1.04 to 2.08 m/s and applied load from 10 N to 40 N [89].

- **Ford five-finger test**

This test is mainly used in the automotive industry [76]. In this test, surface damage due to scratch is evaluated on a scale of 1 to 5 and higher values may be used to indicate further surface damage. The number of spherical tips used for testing may reach 5 with diameters ranging from 1 mm to 7 mm. The dead load applied in this test ranges from 0.6 N to 20 N, where it is controlled by adding weight plates, the scratch speed of 100 mm / s is controlled by a compressed air

pump. This test gives a relative arrangement of the damage formed on the polymer surface during the scratch process, but does not quantity nor identifies any critical values [90].

- **Single-pass pendulum test**

The test device consists of a rigid bar that swings around one end while a disc blade or indenter is connected with dead weights at the other end. Scratches are made on the surface of the test samples by releasing the end containing the indenter and the dead weights (the free end) from a certain height, the scratch will be made at the lowest point of the swing path. The test sample is installed on a platform in the device through which the scratch depth can be adjusted on the surface of the sample as well as the length of the scratch path. In this test, conical tips with different apex angles and diameters or disc blades with constant diameter (30 mm) and different apex angles are used. The shape of the scratch groove formed on the sample surface in this test is different from the tests mentioned above; also, the process of calculating the applied normal load is more complicated [91- 93].

Finally, the main reason for the significant progress made in understanding the basic nature of scratch behavior in polymers is the recently establishment of a scratch test standard ISO/ASTM. In this test the load is applied on a spherical tip with 1 mm diameter made from stainless steel. Also, the test uses normal load that increases linearly for generating a continuous progression of damage and deformation along the scratch path. With this test it became possible to conduct a direct analysis of the scratch resistance behavior of the polymers as well as the possibility of establishing a relationship between the structure and the property. This test has been used for conducting all scratch resistance tests of SiO_2 / PMMA composites samples in the current work and according to ASTM D7027 standard.

3.5 Scratch Formation Mechanisms

During the polymer scratch process, the scratching tip plows the material in front of it; this material is either pushed forward or stacked on both sides of the scratch groove [11]. This phenomenon is most often observed in relatively ductile polymers where the plastic deformation and ironing process occur easily. In addition to the presence of friction between the scratch tip and the substrate, accumulated material in front of the scratch tip also provides resistance against the movement of the tip [94]. The increase in applied normal load lead to deeper penetration of the tip into the substrate, which causes increasing in the friction force, as shown in figure (3-9-a). When the tip moves forward during the scratch process will pull the substrate material along with it. If the magnitude of induced stress during scratch becomes greater than the value of yield stress, the pattern of fish-scale damage will be formed as a result of the plastic pull of the material, as shown in figure (3-9-b). Ultimately, the transition to the next stage of scratch damage, which is the removal of the material, will take place when the exerted tensile stress becomes high enough.

The phenomenon of "slip-stick" happens when the indenter encounters periodic changes in resistance during the movement of the tip [96- 99]. In the scratch process, the scratching tip is designed to move on the polymer surface at a constant speed. Nevertheless, the actual speed of the tip movement relative to the substrate surface fluctuates due to the physical nature of the surface contact between the substrate and the tip where formation and breaking of the local adhesion between the material and the tip occurs repeatedly. The sticking phenomenon occurs when there is a decrease in the tip speed relative to the substrate surface, this phenomenon becomes more important when the penetration depth of the tip in the substrate increases, thus providing an additional resistance force to the tip movement.

The strain energy continues to accumulate due to increase both the inertia exerted from constant testing rate and applied normal load, as shown in figure (3-9-a). When the exerted stress value on the material surface is lower than the ultimate strength value, the scratching tip will pull the material with it along the scratch path, as in figure (3-9-b) and will slip over the peaks of the accumulation region, as in figure (3-9-c). The scratch tip may be losing its entire contact with the substrate surface through this slip. As a result of the decrease in resistance for the movement of tip, the tip can be move forward at full speed again. Scratching tip restores the contact with the material surface by the effect of applied normal load and begins again to compress the surface of the substrate, where the stick stage happens again, and then the next slip stage repeats itself again, and so on.

The stick -slip step includes two possible mechanisms. Repeated surface contact and compression of the substrate surface by the scratch tip after each stick-slip step lead to formation of the observed periodic damage in ductile and weak polymers. In brittle and strong polymers, an accumulation of strain energy also occurs during the stick stage as a result of the increase in applied normal load and the inertia resulting from the constant test rate, as shown in figure (3-10-a). The magnitude of tensile stress in the zone behind the tip may reach to its ultimate strength value before the scratch tip loses its entire contact with the material surface and begins to slip. Then, a brittle fracture occurs, which releases the accumulated strain energy. The scratch tip begins to slip over and move again when the material resistance to the tip movement decreases, as in figure (3-10-b and c). The repeated process of releasing the accumulated strain energy through brittle damages behind the scratch tip leads to the formation of the parabolic crack region. In brittle and weak polymers, due to the ease of forming brittle damage in the region behind the scratch tip, a fish-scale pattern cannot be developed before the slip. Rather of that, many micro cracks, voids,

and /or crazes will be formed. When using high applied normal loads, the resulting large tensile stresses will cause brittle damage, which can be considered a predominant damage feature. Due to the brittle damage, moving the scratch tip forward through accumulation leads to remove the material by a process similar to plowing.

The patterns of periodic scratch damage resulting from the stick-slip phenomenon depend not only on the adhesive forces between the substrate and the indenter, but also on other factors like applied normal load, type of material, scratch speed and tip shape. For example, when low normal loads are applied, there is little accumulation of material in front of the scratching tip; in this case the stick-slip phenomenon stages are easily overcome by the inertia resulting from the tip movement and by the low friction resistance of the substrate surface. When large normal loads are applied, the depth of the scratch increases and more material accumulates in front of the scratch tip; in this case the stick-slip phenomenon becomes more dominant. It is clear that the properties of the material, the state of stress, and the magnitude of stress are important factors that influence the formation mechanisms of scratch damage in polymers, where it has become possible to curb or enhance some of the damage mechanisms resulting from scratch. Depending on the type of material used and scratch load, it can be expected the material properties required to prevent the formation of unwanted scratch damage mechanisms.

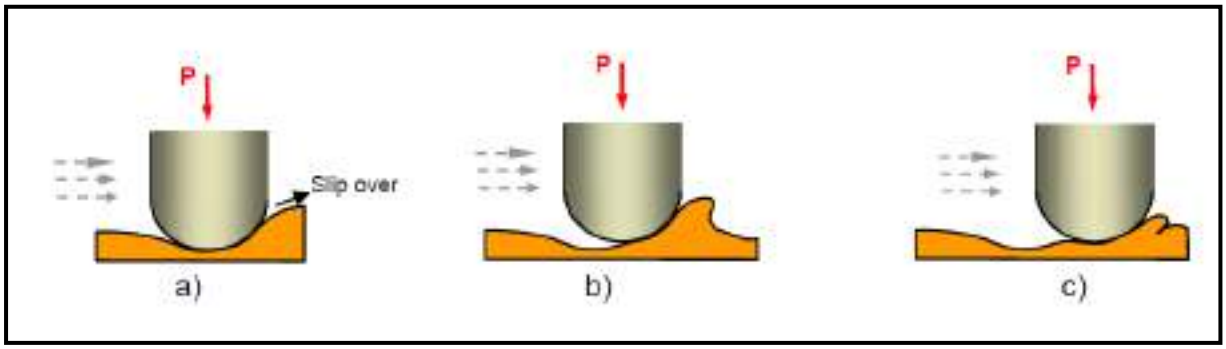

Figure (3-9) Formation mechanisms of fish-scale pattern: (a) slipping step, (b) drawing step and (c) compression of substrate [95].

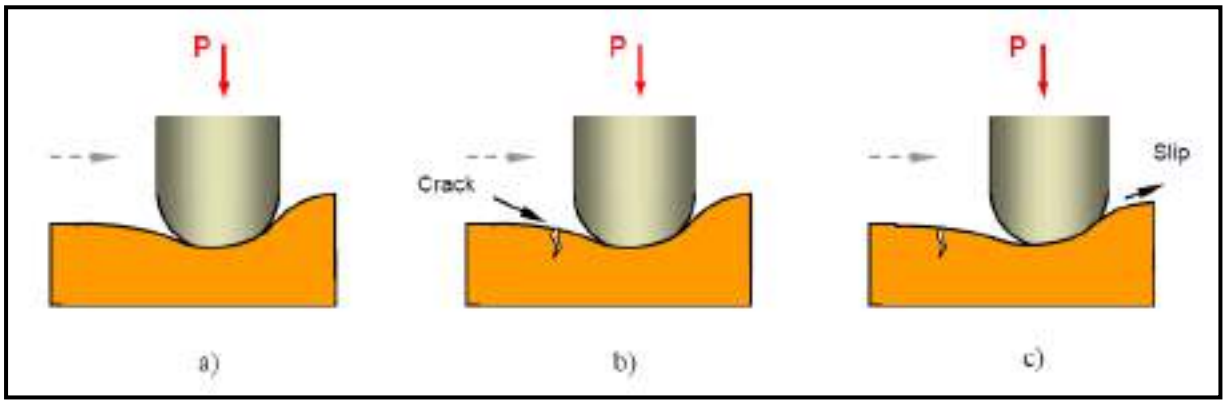

Figure (3-10) Formation mechanisms of parabolic crack pattern: (a) stick step, (b) formation of crack, and (c) slip step [95].

Chapter Four
Experimental Work

Chapter Four

Experimental Work

4.1 Introduction

This chapter is devoted for describing the parameters adopted in the current work, the techniques used for preparing pure and reinforced PMMA samples, and the devices used in mechanical, surface and thermal tests conducted on the samples to study the evolution of PMMA properties as well as the type and specifications of the solvents used and the SiO_2 nanoparticle specifications. Figure (4-1) shows the flow chart of experimental work in current study.

4.2 Parameters of the present study

The parameters affecting the PMMA properties studied in the current work can be illustrated as follows:

1. **Addition ratios of SiO_2 nanoparticles.**

   Two sets of SiO_2 ratios were used the first from 1wt% to 4wt% with an increase of 1wt% and the second from 0.1wt% to 0.5wt% with an increase of 0.1wt%.

2. **Preparation methods of specimens.**

   Three techniques were used for preparing pure and reinforced PMMA specimens were chemical dissolving, pressing and casting techniques.

3. **Applied normal load on the indenter.**

   The values of the normal load imposed on the indenter ranged from 1N to 70N in order to obtain the minimum load required for scratching.

4. **Sliding speed of the moving tip.**

   Various sliding speeds were used during the scratch test, which ranged from 10 mm/s to 35 mm/s.

5. Indenter geometry.

During the scratch test, two types of indenters were used the first a stainless steel indenter with a conical tip with a radius of 0.3 mm and apex angle of 60° and the second a spherical indenter from stainless steel with diameter of 1 mm.

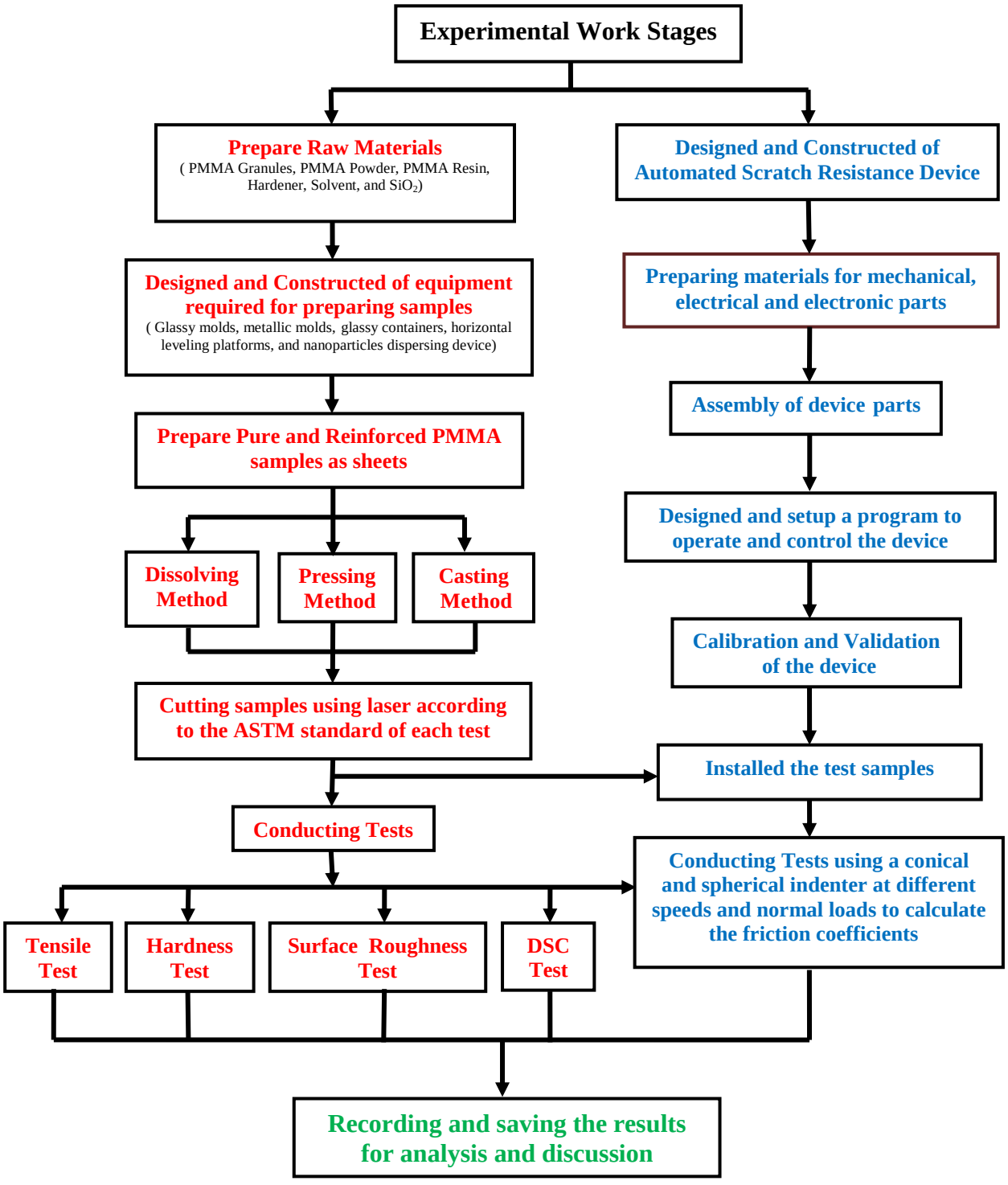

Figure (4-1) Block diagram of experimental work.

4.3 Specimens Preparation

In this section, methods for preparing PMMA specimens, types of solvents used, and filler specifications used in the reinforcement will be explained. The polymerization method, whether in addition or condensation, is the general method used in the production and preparation of PMMA industrially. Due to the difficulty of the polymerization process, the lack of necessary equipment, and shortage of time, pure and reinforced PMMA specimens were prepared in present study in three laboratory methods are:

a. Dissolving method: by dissolving the PMMA granules in solvents and then casting them into glassy molds.
b. Pressing method: by pressing the PMMA powder in metallic molds using hydraulic thermal press.
c. Casting method: by casting the PMMA resin and hardener into glassy molds.

Dissolving PMMA in organic solvents is an important process for several reasons including the ability of solvent to dissolve the PMMA, the dissolution rate, temperature, the evaporation rate of the solvent, and the formation of bubbles after the evaporation of the solvent. Three solvents were used to dissolve the PMMA granules, which were acetone, tetrahydrofuran (THF) and isopropanol, their specifications, are listed in table (4-1). During experiments in current work, it was established that isopropanol was unable to dissolve PMMA granules, unlike the other two solvents. It was also observed that tetrahydrofuran was faster than acetone in dissolving the PMMA granules, as well as the amount of bubbles present in the sample after the evaporation of tetrahydrofuran was less compared to acetone, this is completely identical to the result obtained by Evchuk et al. [100], as a result for that, tetrahydrofuran was adopted .The perfect amount of solvent used for dissolving the mixture of PMMA granules and filler was four times the weight of the mixture (i.e. for each 100 g of mixture, 400 g of solvent was used). Silicon oxide nanoparticles (SiO_2) have been used as

reinforcement filler. The most important reasons that led to the selection of this filler are abundance, cheapness, non-toxicity, high hardness, and high melting point, another important reason is that PMMA transparency is not significantly affected when adding small amounts of SiO_2.

Table (4-1) Specifications of THF, Acetone and Isopropanol [100].

Property	THF	Acetone	Isopropanol
Chemical Formula	C_4H_8O	C_3H_6O	C_3H_8O
Gas Number	109-99-9	67-64-1	67-63-0
Molecular Weight (g/mol)	72.11	58.08	60.1
Appearance	Colorless	Colorless	Colorless
Physical State	Liquid	Clear liquid	Liquid
Boiling Point (^{o} C)	66	56	82
Freezing Point (^{o} C)	-108	-96	-89
Autoignition Temp. (^{o} C)	230	465	235
Density (kg/l)	0.89	0.786	0.785
Vapor Pressure	19300	24700	4400
Purity %	99.7	99.5	99.5

4.3.1 Dissolving Method

PMMA material used in this method is a spherical granules with a diameter of 3 mm purchased from Xinxiang Chuangmei Technology Co., Ltd in China. The filler is a silicon oxide nanoparticles (SiO_2) treated with silane coupling agent and specifications are purity: 99%, average particle size: 10-30 nm, PH: 5.5-6, and square surface area: 400m^2/gm purchased from SkySpring Nanomaterials, Inc. Houston, TX. 77082. USA. The solvent used is (THF) tetrahydrofuran (C_4H_8O) with minimum assay (GC) 99.7% purchased from Central Drug House (P) Ltd - Company, New Delhi, India, as shown in figure (4-2). Casting molds are glassy molds with dimensions of 210 mm length, 140 mm wide and 20 mm high for first group and with dimensions of 140 mm length, 110 mm wide and 20 mm high for second group. These molds are placed on horizontal leveling platforms to ensure uniform thickness of the cast material.

The molds are covered by glassy containers to protect them from unwanted external factors such as dust and wind as well as to ensure a saturated perimeter around the casting mold, as in figure (4-3).

The technique used in this method to prepare the specimens and disperse nanoparticles is based on dissolving PMMA granules using a solvent placed inside a closed flask with adding filler and mixing the mixture using magnetic stirrer at room temperature for 2 hours and a speed of 1500 rpm. The amount of solvent used to dissolve 100 g of the PMMA and SiO_2 mixture is 400 g. Table (4-2) shows the ratios of mixing (SiO_2) nanoparticles with PMMA granules. The resulting solution is then poured into glassy molds placed on the leveling platform and covered with a glassy container and left to dry under the sun for 5 days to ensure complete evaporation of the solvent, as shown in figure (4-4). The specimens are then removed from the molds by placing them in a cold water tank for 30 minutes. The final stage of preparation is to place the samples in an electric thermal oven at 95 °C for 45 minutes and then compress the samples at a pressure of 0.5 MPa for two minutes using a hydraulic thermal press to ensure a smooth surface and free of bubbles, as shown in figure (4-5). The specimens required for each test are cut using a laser cutting device.

Table (4-2) The mixing ratios between PMMA granules and SiO_2

Specimen code	**PMMA** granules (wt %)	**SiO_2** ratio (wt %)
S0	100	0
S1	99	1
S2	98	2
S3	97	3
S4	96	4
G0	100	0
G1	99.9	0.1
G2	99.8	0.2
G3	99.7	0.3
G4	99.6	0.4
G5	99.5	0.5

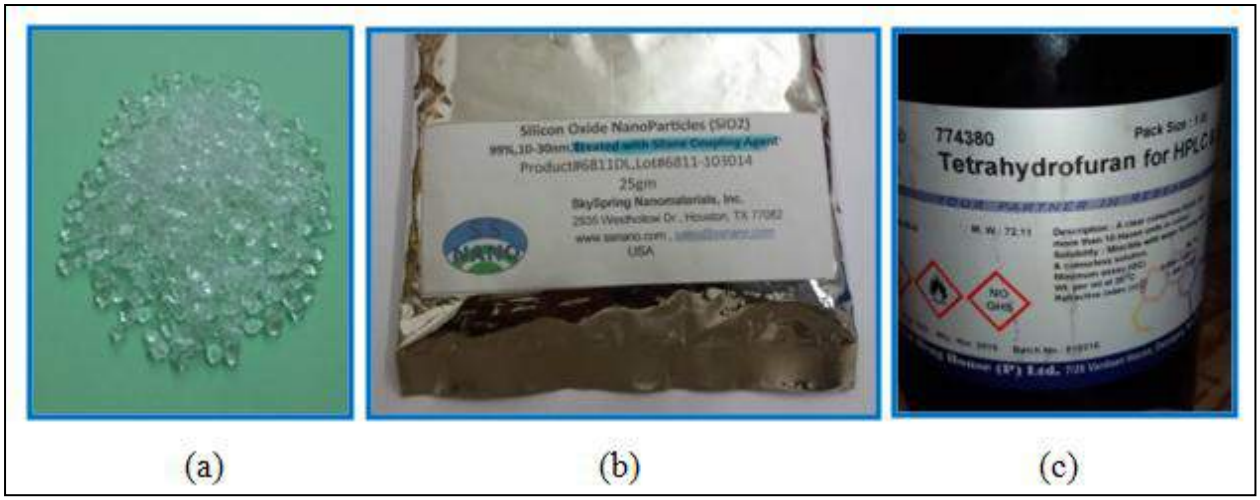

Figure (4-2) (a) PMMA granules, (b) Silicon oxide nanoparticles (SiO_2) and (c) Tetrahydrofuran solvent.

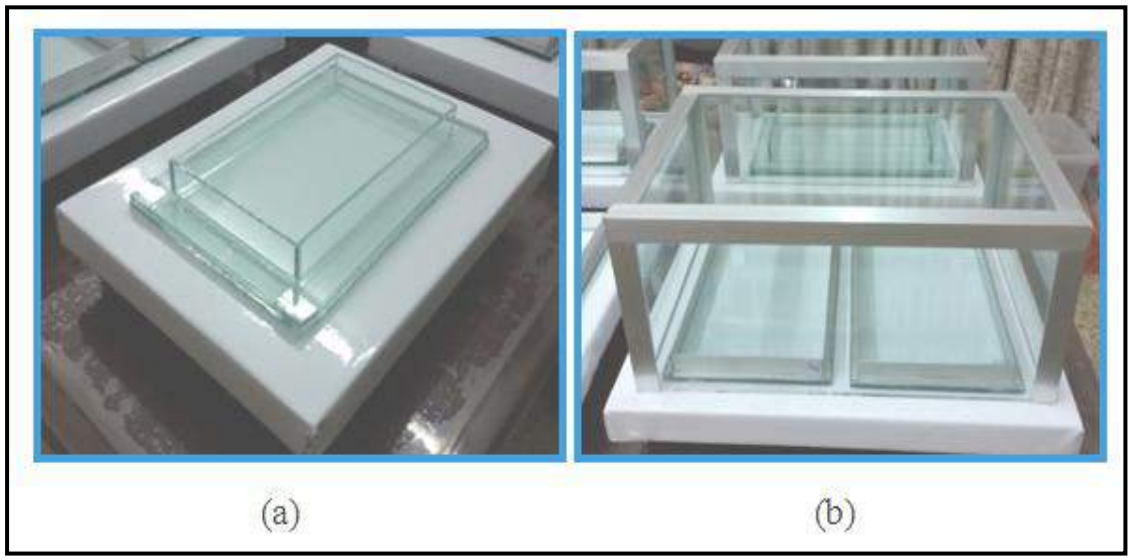

Figure (4-3) (a) Glassy molds and (b) Glassy containers and leveling platforms.

Figure (4-4) Preparation of PMMA/SiO_2 composites

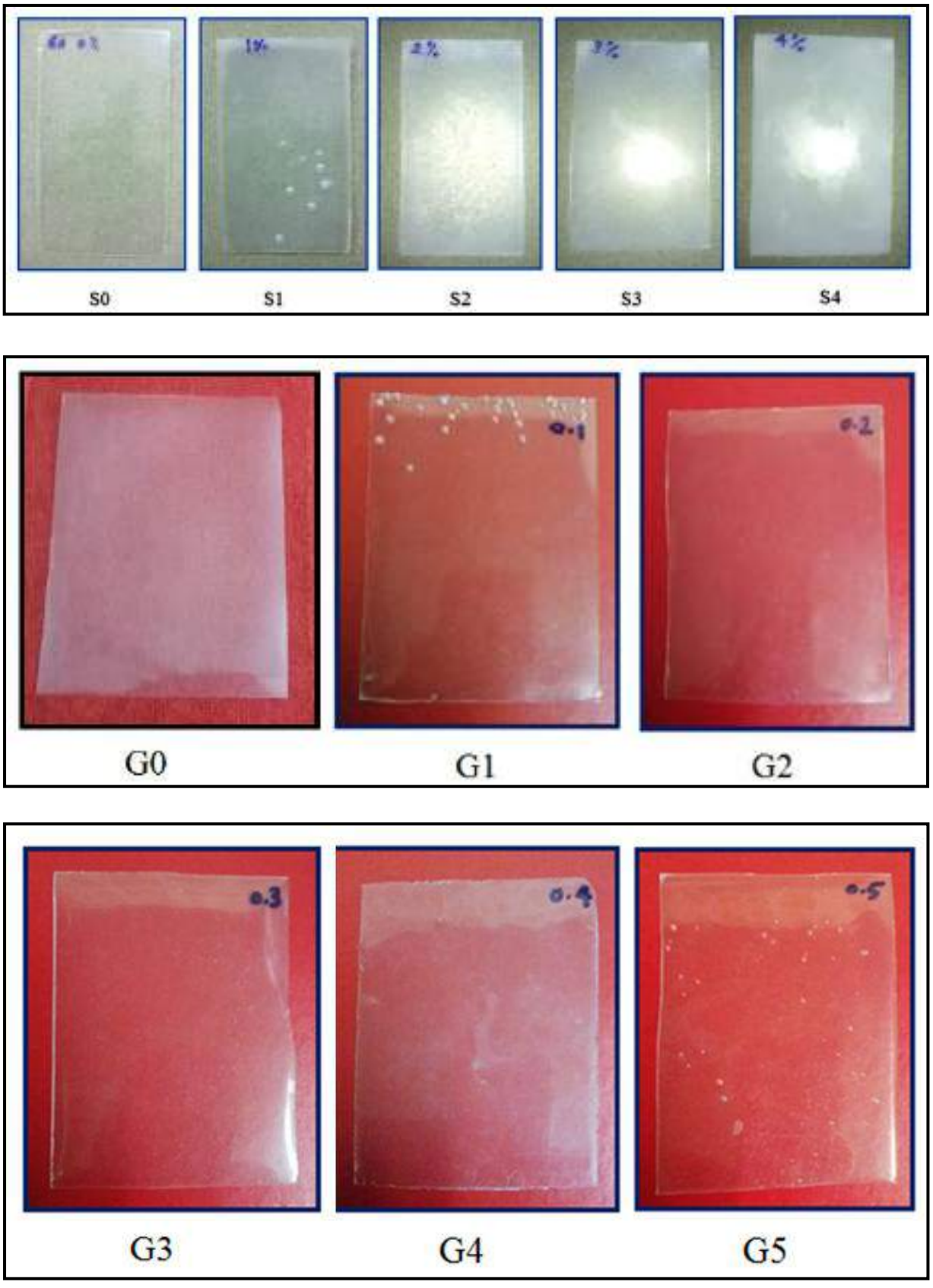

Figure (4-5) Specimens of PMMA/SiO_2 composites (Dissolving Method).

4.3.2 Pressing Method

Polymethyl methacrylate used is PMMA powder with specifications are appearance: white micro powder, composition: Acrylic PMMA powder, average particle size: about 5.5 to 80.5 μm, heating loss: 2.0% or less and PH: 5 to 7.5 purchased from Xinxiang Chuangmei Technology Co., Ltd in China. The filler is the same used in the first method, as shown in figure (4-6). The equipments used in this method are: (a) An iron mold consisting of three parts, the first is a rectangular plate with a thickness of 10 mm and dimensions of 200 mm ×140 mm and the second is a rectangular plate with a thickness of 6 mm and dimensions of 145 mm × 85 mm and the third is a ring with a thickness of 10 mm consisting of an outer rectangle with dimensions of 140 mm × 200 mm and an internal rectangle with dimensions of 90 mm × 150 mm. (b) Nanoparticles dispersing device which has three speeds of 750/600/450 rpm. (c) Electric thermal oven to melt the PMMA powder inside the mold. (d) Hydraulic thermal press to compress the molten powder inside the iron mold to the thickness required for the specimen. All of these equipments are offered in figure (4-7).

The steps for preparing samples using pressing method are as follows, the required amount of PMMA powder is placed for each sample with the ratio of SiO_2 nanoparticles inside a plastic container containing three metallic balls with a diameter of 5 mm, then the container is placed on the nanoparticles dispersing device that was manufactured in the current study for 6 hours with a rotational speed of 600 rpm. The mixture of powder and nanoparticles is then placed inside an iron mold and left in the thermal oven for 90 minutes at a temperature of (165 - 220° C). After the mixture is melted inside the mold, the mold is pressed using a hydraulic thermal press with a pressure of 5 MPa and a temperature of (165 - 220°C) for 2 minutes in order to expel bubbles and obtain the required thickness and for leveling the specimen surface. After the pressing process, the mold is left to cool down and then the specimen is extracted from the mold. Table (4-3) shows the ratios of mixing SiO_2 nanoparticles with PMMA powder and

temperature of electric thermal oven and hydraulic thermal press of this method, and figure (4-8) shown the resulting specimens.

Table (4-3) The mixing ratios between PMMA powder and SiO_2 and temperature of electric thermal oven and hydraulic thermal press

Specimen code	PMMA powder wt %	SiO_2 wt %	Temperature of oven & press ° C
P0	100	0	165
P1	99.9	0.1	176
P2	99.8	0.2	188
P3	99.7	0.3	197
P4	99.6	0.4	209
P5	99.5	0.5	220

Figure (4-6) (a) PMMA powder and (b) Silicon oxide nanoparticles (SiO_2)

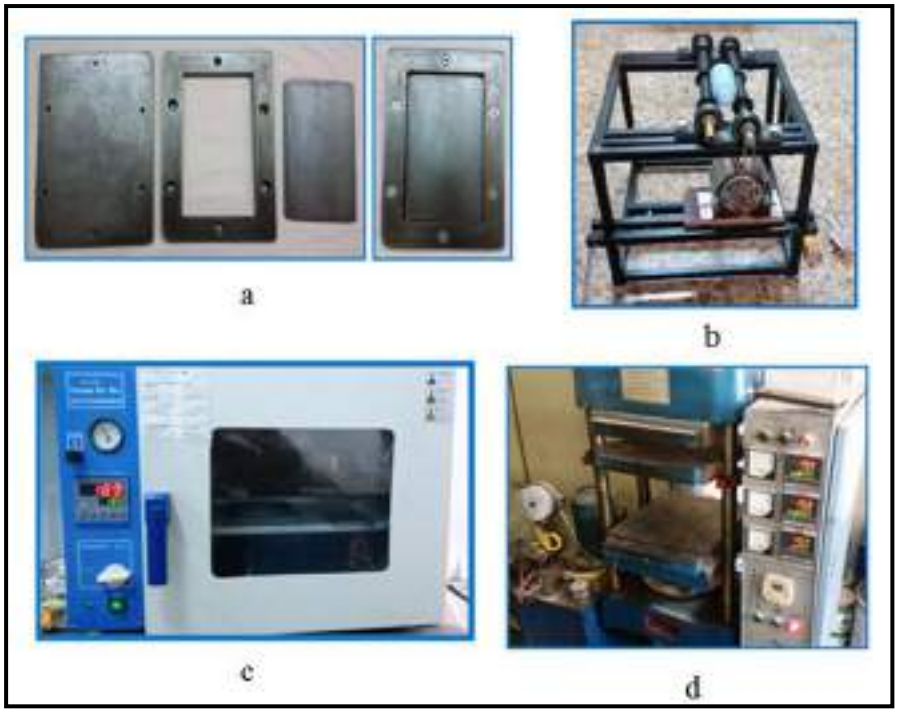

Figure (4-7) Equipments required for pressing method (a) Iron mold (b) Nanoparticles dispersing device (c) Electric thermal oven and (d) Hydraulic thermal press.

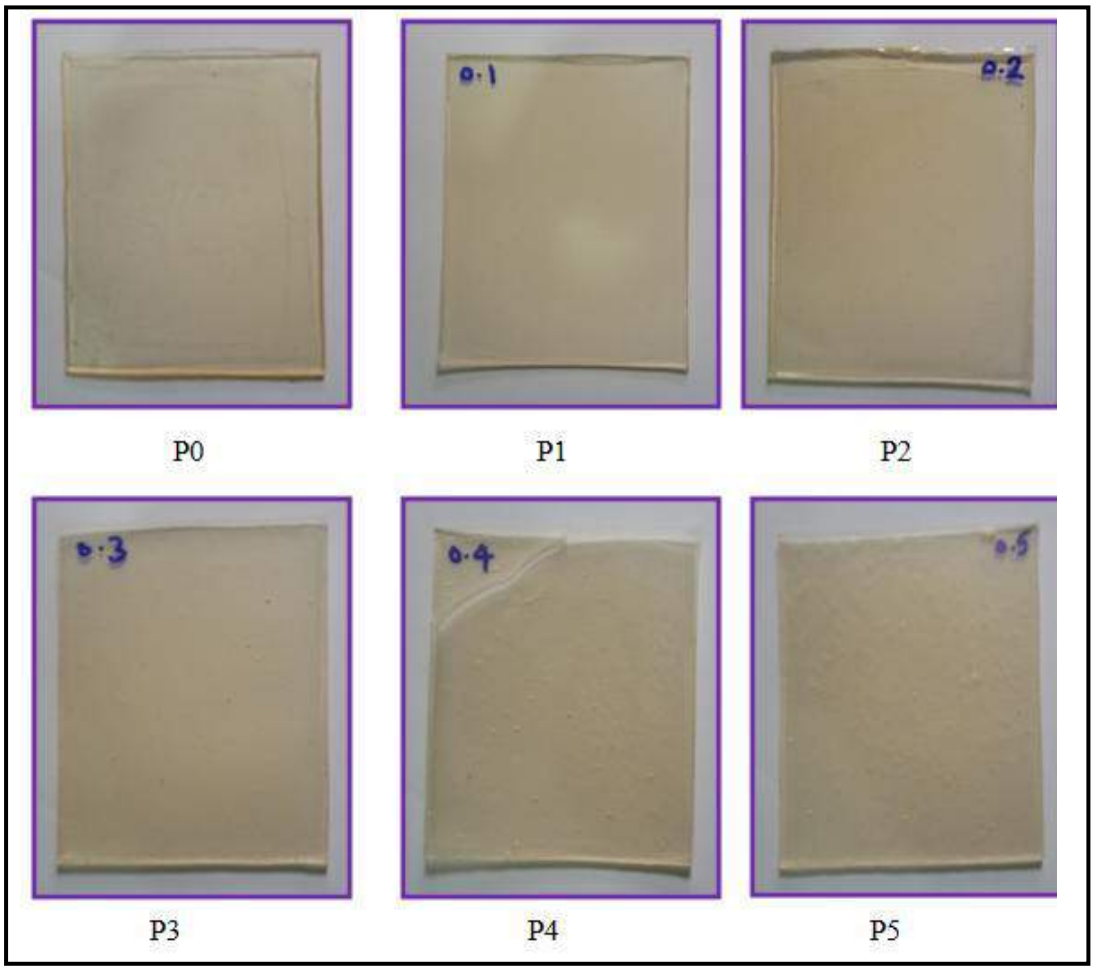

Figure (3-7) Specimens of PMMA/SiO_2 composites (Pressing Method).

4.3.3 Casting Method

Polymethyl methacrylate used is PMMA resins with specifications are Appearance: colorless transparent liquid, Viscosity at 25°C, 300-1500 Cps (1 Cps (Centipoise)) = 1 mPa s (Millipascal Second), PH: 8 - 9, Density 1.02-1.05 g/l, Size: 0.20-0.30 μm and T_g (glass transition temperature): 105 °C purchased from Xinxiang Chuangmei Technology Co., Ltd in China. The hardener used is Dibenzoyl Peroxide with specifications are Brand names: Luperox A75, Luperox A75FP, Luperox A75S, Luperox ANS50G, Chemical name (IUPAC): Diphenylperoxyanhydride, Molecular formula: $C_{14}H_{10}O_4$, Physical state: Solid at ambient temperature, Form: White powder, Density: 1.33 g/cm^3, Melting temperature:103-108°C and Molecular weight : 242.23 g/mol, purchased from Uniprox GmbH & Co. KG Company Insights, Heinrich-Heine-Street 4, Zeulenroda, Thuringia, 07937, Germany, as provided in figure (4-9). The equipments used in this method are: (a) Glassy casting molds with dimensions of 140 mm length, 110 mm wide and 20 mm high for first group and with dimensions of 210 mm length, 140 mm wide and 20 mm high for second group, (b) Horizontal leveling platforms to ensure uniform thickness for molded material inside the mold, (c) Ultrasonic probe machine for dispersing the SiO_2 nanoparticles with specifications are Frequency: 20 kHz, Power Rating: 2000 Watts, Timer of programmable: 10 Hours, Adjustable Pulses On/Off: 1 second to1minute, and Voltage: 230V, 50/60Hz. Figure (4-10) shows all of these equipments.

In this method of preparation, the required amount of PMMA resin is placed for each sample with the ratio of SiO_2 nanoparticles inside a glassy container. The nanoparticles are dispersed using an ultrasonic probe machine for 45 minutes after which the hardener is added to the mixture with 1 wt % and mixed well. Table (4-4) shows the ratios of mixing the SiO_2 nanoparticles with PMMA resin. Then the mixture is poured inside the glassy mold placed on the

horizontal leveling platform and leave until hardens. The next stage of preparation is to remove the sample from the mold by placing the mold inside a cold water tank for 30 minutes; the resulting specimens are shown in figure (4-11).

Table (4-4) Mixing ratios between PMMA resin and SiO_2 for casting method.

Specimen code	PMMA resin wt %	SiO_2 wt %
R0	100	0
R1	99.9	0.1
R2	99.8	0.2
R3	99.7	0.3
R4	99.6	0.4
R5	99.5	0.5

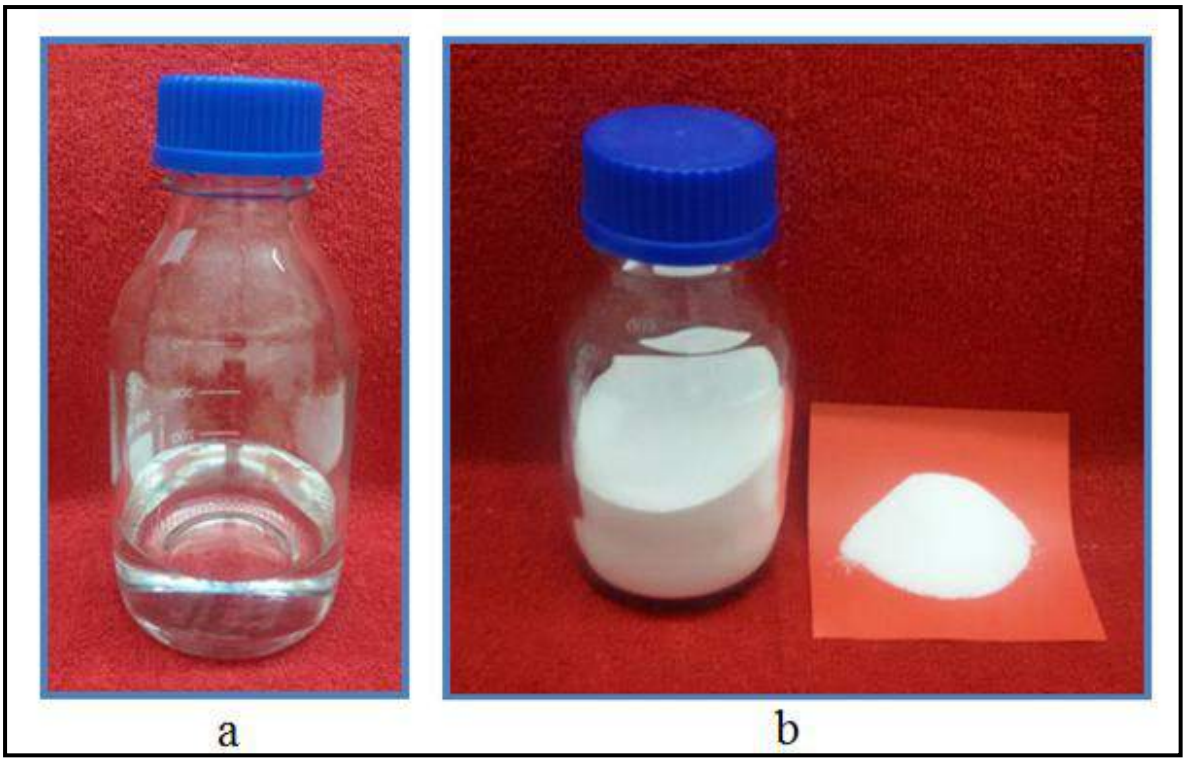

Figure (4-9) (a) PMMA resin and (b) Dibenzoyl peroxide ($C_{14}H_{10}O_4$).

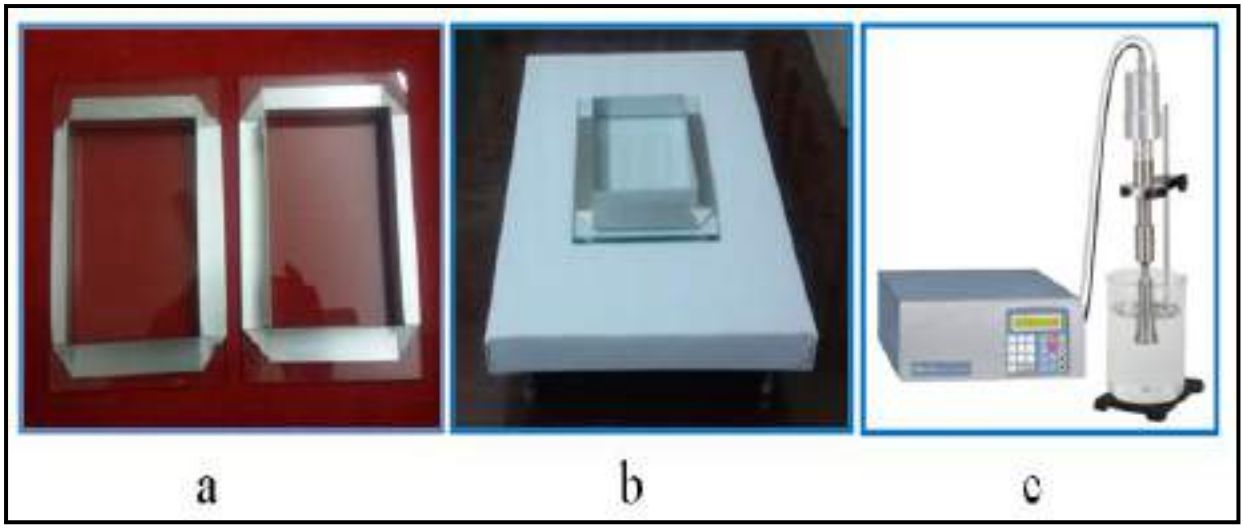

Figure (4-10) (a) Glassy molds (b) Horizontal leveling platforms and (c) Ultrasonic probe machine.

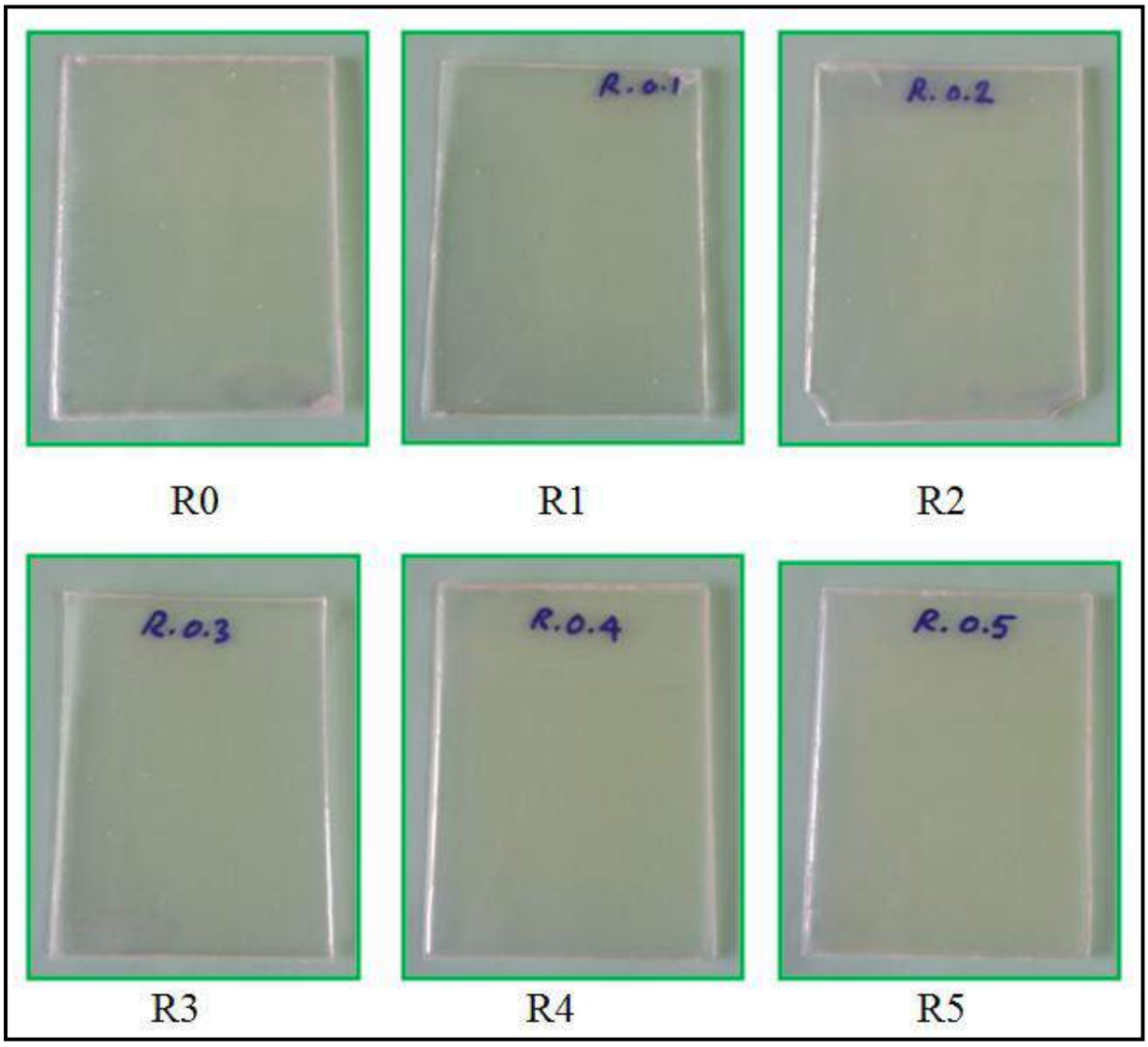

Figure (4-11) Specimens of PMMA/SiO_2 composites (Casting Method).

4.4 Differential Scanning Calorimetry (DSC) Test.

The temperatures of the melting (T_m) and glass transition (T_g) for the PMMA material can be obtained by means of the DSC test. The sample for this test should be in powder form and this test was conducted based on D3418-03 of ASTM standard and heat rate of 10 ^{o}C/min with the temperature range to 300 ^{o}C. To perform this test is brought a special crucible of the DSC device and placed on the scale and neglecting its weight then about 0.2 mg or 0.4 mg of the sample to be analyzed is weighted and then the crucible is completely closed with the sample by a special press of the device then the crucible is placed with its content inside the device next to the standard material and then is done closing the device on it to be in an atmosphere of nitrogen, and then conduct the analysis, figure (4-12) shows DSC test device.

Figure (4-12) DSC Test device.

4.5 Tensile Test

Samples used in the tensile test were cut according to (ASTM) D-638; the dimensions and shape of test sample are offered in figure (4-13). Tensile test was conducted at the temperature of room (23°C) with rate of displacement of 5 mm/min using a universal test device, as offered in figure (4-14). The tensile tests were conducted in laboratories of Materials Engineering College, Babylon University. The equations used to calculate stress and strain were listed in the appendix. The curve of stress and strain of the samples tested is plotted by the device itself on graph paper. The tensile test samples for the three methods of preparation before and after conducting the tensile tests are shown in figure (4-15).

ASTM D638-10 Type IV	Dimensions (mm)
W – Width of narrow section	6
L – Length of narrow section	33
WO – Width overall, min	19
LO – Length overall, min	115
G – Gage length	25
D – Distance between grips	65
R – Radius of fillet	14
RO – Outer radius	25
T – Thickness	4

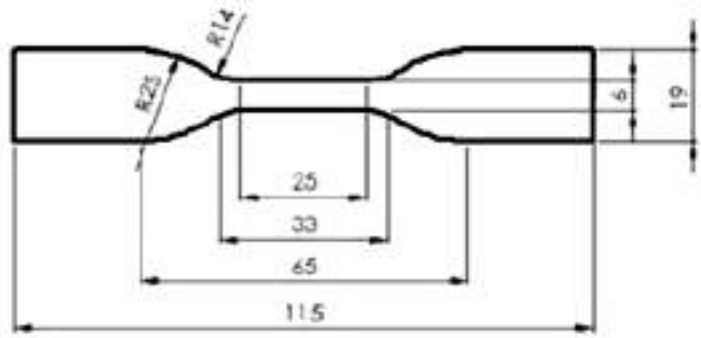

Figure (4-13) The dimensions and shape of the tensile test specimens.

Figure (4-14) Tensile test machine.

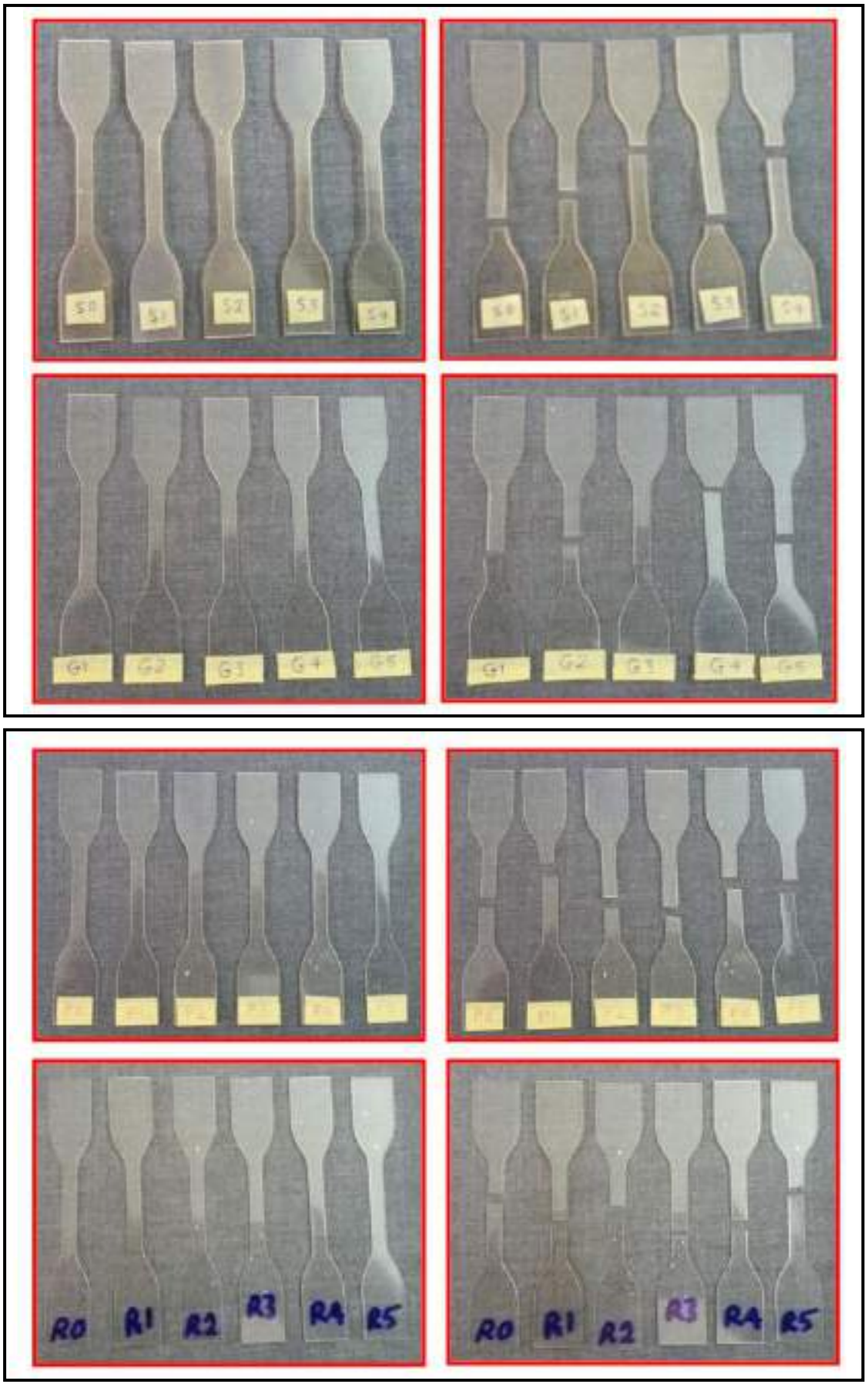

Figure (4-15) Specimens of tensile test for the three methods of preparation before and after conducting the tensile tests.

4.6 Shore-D Hardness Test

These tests were performed at room temperature (23°C) using Chinese hardness device (type TH-200) in laboratories of Materials Engineering College, Babylon University. Test samples were cut based on (ASTM) D-2240, the dimensions and shape of test sample and device used are shown in figure (4-16).

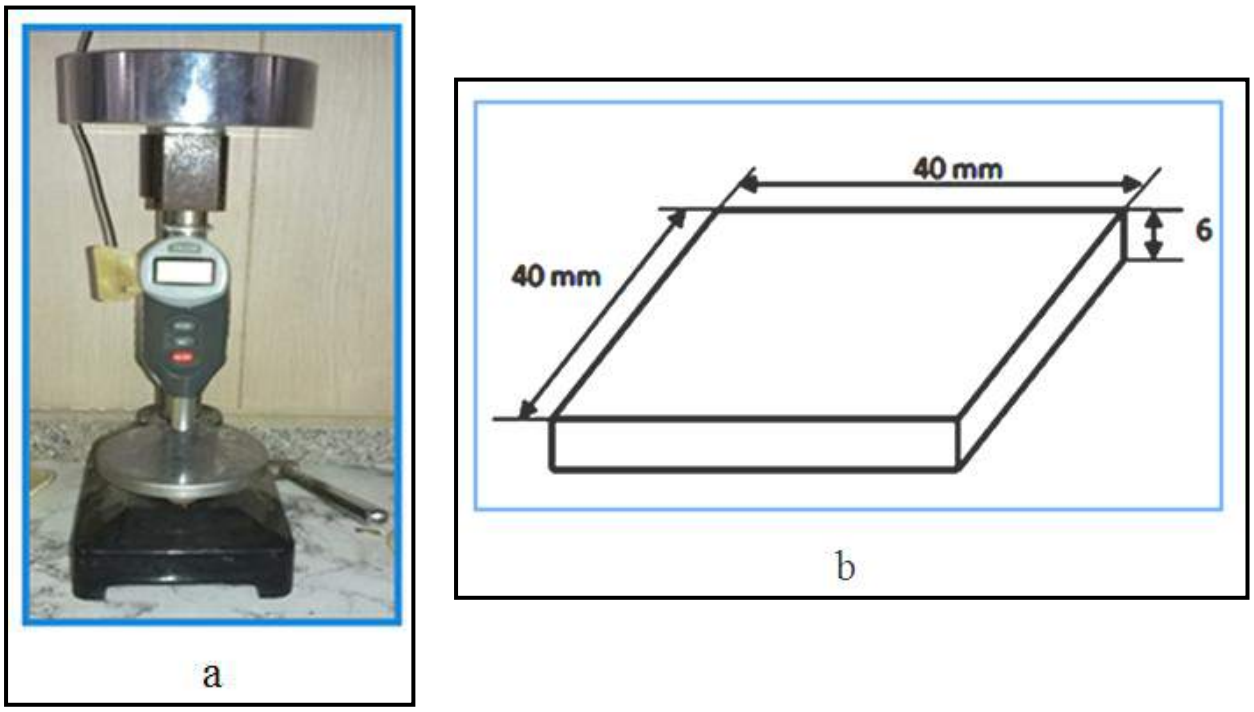

Figure (4-16) (a) Shore D hardness machine and (b) Dimensions and shape of the hardness test sample.

4.7 Surface Roughness Test

Roughness is defined as the irregularity or deviation from the ideal engineering shape of the manufacturer's surfaces and roughness is defined as vertical, horizontal, and irregular depth and which are integrated within the general surface curves. Roughness tester can measure several preset lengths. Shorter distances are used to measure fine surfaces, while the longest lines are used for more stringent surfaces. The most important parameter that expresses surface roughness is the surface roughnesses coefficient (Ra). Information about this parameter is processed by the processing unit and the information is

displayed in digital form on the display. Figure (4-17) shows the surface roughness measuring device used in this work.

Figure (4-17) Surface Roughness Test device.

4.8 Scratch Resistance Test

Scratch resistance tests were conducted with sliding velocity of 20 mm/s and the scratch path length of 100 mm to scratch all specimens at room temperature (23°C) using a new automated scratch device designed and constructed in this work. The test was conducted in two stages, the first using a stainless steel indenter with a conical tip with a radius of 0.3 mm and apex angle of 60^{o} and the applied normal load from 1 N to 30 N. The second using a spherical indenter from stainless steel with diameter of 1 mm and the applied normal load from 1 N to 70 N. The specimens used for the test were cut according to ASTM 7027-5 where the dimensions of the scratch test specimen were 60 mm for width, 140 mm for length and 4 mm for thickness which allow repeating the scratch test more than five times in several locations of the

specimen. Figure (4-18) shows the scratch device, the general description of the scratch device will be explained in chapter 5.

The scratch test for PMMA specimens is carried out by imposing a load on the indenter, this load is gradually increased to obtain the minimum load required to cause scratch on the surface of the specimen. The process of examining the remaining scratches on the surface of the sample after carrying out each load are made using the optical microscope with digital camera as shown in figure (4-19), and table (4-5) contains the specifications of the optical microscope used.

Figure (4-18) Scratch resistance device.

Table (4-5) Specifications of the optical microscope.

Specification	Value
Model	DM3
Resolution	1080P, 720P, VGA (DM3)
Magnification	1X - 1000X (Manually)
Focus Range	10-40mm
Object Distance	15mm-infinity
Display	4.3in LCD Display
Pixel	2.0 Mega Pixels
LED Quantity	8 pieces White LED
Brightness Control	Manual Adjustment
Power Supply	USB DC 5V
TF Card Slot	Support 8GB or 32GB
PC Operating System	Windows XP, Win7, Win8.1, Win10, Mac OS x 10.5
Battery	1 × 18650 Lithium Battery 3.7 V, 2000mA
Material	ABS Plastic + Aluminum

Figure (4-19) Optical microscope

Chapter Five
Scratch Device Construction

Chapter Five

Scratch Device Construction

5.1 Introduction

This chapter is dedicated for describing the scratch device that has been designed and constructed to perform scratch resistance tests for PMMA samples for current work. The equipments needed to prepare pure and reinforced PMMA samples have also been described such as glassy molds, metallic molds, glassy containers, horizontal leveling platforms, and the dispersion device used for dispersion SiO_2 nanoparticle in the PMMA powder.

5.2 General Description of Scratch Device

The scratch resistance test is considered one of the most important tests that are conducted on polymeric materials to determine their surface properties, so that researchers and manufacturers can then devise methods and treatments to improve these properties. Scratches on the PMMA surfaces, especially transparent ones, are defects that limit their use in many industries and engineering applications such as automotive, aircraft, solar cells, lenses, eyeglasses, dental industry, and many structural applications. The reason for increasing the use of PMMA in various industries and engineering applications is due to the specifications that these materials enjoy such as cheapness, abundance, good intensity, good durability, electrical insulation, moisture resistance, non-toxicity, and ease of formation and cutting them to the required shapes and sizes and the possibility of recycling, but the most important defects are weak scratch resistance.

The scratch resistance test of PMMA depends on indenter geometry, sliding speed and applied normal load. In order to conduct scratch test with wide ranges for sliding speed and applied load as well as the ability to test samples with various dimensions and sizes, to achieve all these requirements, an

automated device was designed and constructed, as shown in figure (5-1) to test the scratch resistance of the PMMA by measuring the force required to cause scratch on the surface of the PMMA, also to calculate the friction coefficient from the inputs and outputs of the device using equation $\mu_{sc} = F_t / F_n$

where μ_{sc} is the friction coefficient of the polymeric material, F_t is the measured tangential force necessary for occurrence the scratch (represents the output of the device), in Newton, F_n the normal load (represents the input of the device), in Newton. The device was made from materials available in the local market and some parts were manufactured in local mechanical workshops, the device consists of four main parts:-

• Mechanical parts.

• Scratch tool parts.

• Electrical and electronic parts.

• The operating and controlling program of the device.

Figure (5-1) Scratch device photographs.

5.2.1 Mechanical parts

Figure (5-2) shows the mechanical parts of the device which consist of :-

1. A metal box of iron sheets with a thickness of 3 mm, with dimensions of 260 mm in width, 420 mm in length and 260 mm in height, which is used to install the rest of the device components.
2. Two stainless steel sliding bars (rails) with a length of 400 mm and two sliders which is used to install the moving platform.
3. Four serrated pillars (legs) to adjust the position of the device horizontally.
4. Stepper motor to generate horizontal linear motion of the moving platform.
5. A stainless steel serrated shaft with length of 320 mm and diameter of 8 mm used to transfer the movement from the stepper motor to the moving platform, one end of it is connected to the stepper motor via the flexible disk coupling and the second end is connected to the load cell which is installed on moving platform via serrated flange.
6. A square iron plate (80 mm x 80 mm) and 8 mm thickness which represent the moving platform used to relate the sliders that move on the rails.
7. Iron plate with a length of 250 mm and a width of 220 mm and a thickness of 8 mm installed on the moving platform used to place the sample on its upper surface
8. Three iron hoops with a thickness of 6 mm in the form of a hollow rectangle, the first hoop with dimensions of (250 mm × 220 mm contains an empty rectangle with dimensions of 200 mm × 170 mm) while the second hoop (200 mm × 170 mm contains an empty rectangle with dimensions of 150 mm ×120 mm) and the third hoop (150 mm ×120 mm contains an empty rectangle with dimensions of 100 mm × 70 mm), these hoops are used to install large and medium sized specimens to the moving platform.
9. Six aluminum clamps used to install small samples on the moving platform.
10. Sets of iron discs with several diameters and thicknesses are used as dead weights which represent the applied normal loads.

11. A variety of screws of different diameters and lengths are used for fixing and connecting.

Figure (5-2) Mechanical parts of device.

5.2.2 Scratch tool parts

Figure (5-3) shows the parts of the scratch tool which consist of :-

1. Two iron pillars in L-shaped with a length of 430 mm, and a width of 50 mm, and a thickness of 8 mm, attached to one side of the iron box. Each one contains a 22 mm diameter hole in which a ball-bearing is placed.
2. A stainless steel bar of 200 mm in length and 12 mm in diameter which is installed to pillars at both ends via the ball-bearings.
3. A stainless steel bar with a length of 520 mm and a diameter of 12 mm serrated from one end used to install the counterweight and the second non-serrated end connects with the bar that contains the indenter holder.
4. A stainless steel bar of 300 mm in length and 10 mm in diameter installed on one end of the indenter holder, and is also used to stabilize dead weights.
5. Two pieces to connect the iron bars together, which are pieces of aluminum with dimensions (35 x 35 x 55) and (35 x 40 x 60) dimensions in millimeters, containing holes similar to the diameters of the bars that pass through them.

Figure (5-3) Scratch tool parts.

5.2.3 Electrical and Electronic parts

The components of the electrical circuit used to supply the device with electrical power are illustrated in figure (5-4) and the circuit of connecting the parts is shown in figure (5-6), which consists of:-

1. Electrical cable (2 x 2.5mm).
2. An electrical transformer that converts voltages from 220 volts to 19.5 volts.
3. Switch on / off button.
4. Fuse
5. Lamp starting operating .
6. Plug to connect the cable into the device.

Figure (5-4) Electrical parts of device.

The components of the electronic circuit used to control the device via a computer are illustrated in figure (5-5), and the circuit of connecting the parts is shown in figure (5-6) which consists of:-

1. Lab Jack U3-HV.
2. Microstep Driver DC:9-42VDC.
3. Load cell.
4. Electric capacitors.
5. Integrated Circuit IC.
6. Electrical resistors.

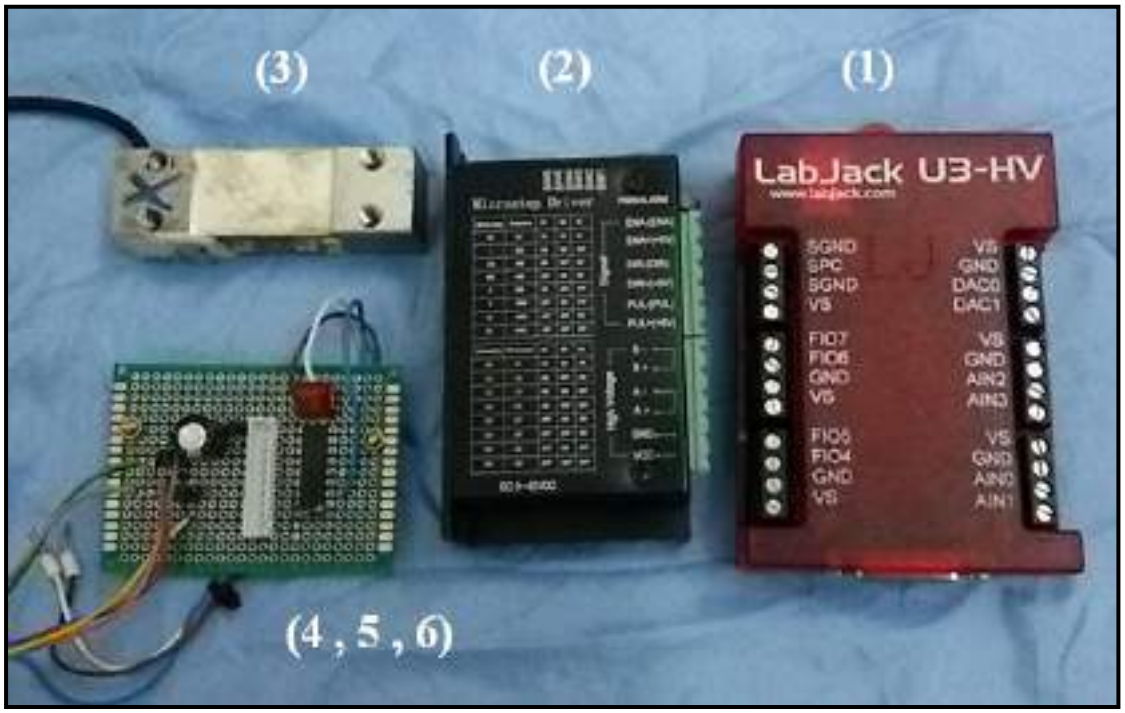

Figure (5-5) Electronic parts of device.

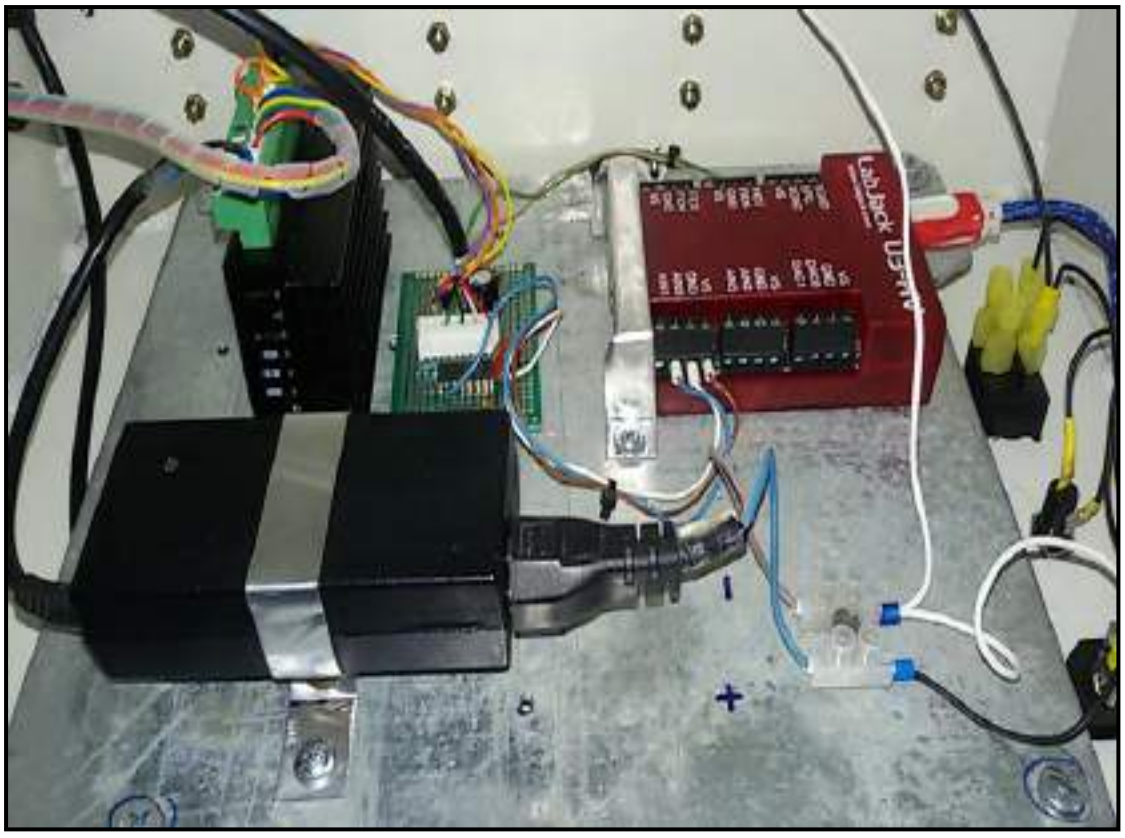

Figure (5-6) The electrical and electronic circuit of the device.

5.2.4 The operating and controlling program of the device

In this device, automation (control of the device by a computer program) was adopted to control the scratch mechanism, enter of variables and display results; the Visual Studio software was prepared using Visual Basic programming language (the program steps are mentioned in the appendix). The input data through the Visual Studio software are the sliding speed, required length of the scratch path, required time to take the readings, the distance between readings along scratch path and the direction of platform movement. While the outputs are the tangential force required to scratch the polymeric surface and graph of the relationship between tangential force and time or scratch path. When click on the program icon, the window shown in figure (5-7) will appear which contains the following options:-

1. Speed (mm / s) to specify the required speed.
2. Distant (mm) to determine the length of the required scratch path.
3. Scale (N / V) constant number obtained from load cell calibration.
4. Sliding ratio (mm / Rev) is a constant number obtained from the velocity calibration of the stepper motor, which represents the length of the linear distance traveled per revolution.

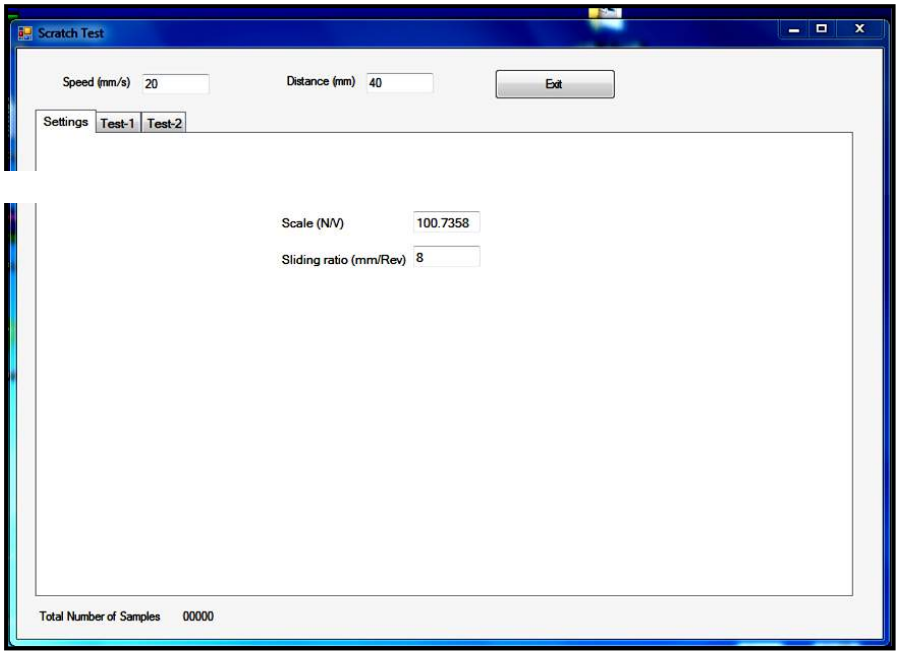

Figure (5-7) The main interface of the device software.

After selecting both the speed and the length of the path, and after click on the Test-1 button, a new window appears, as shown in figure (5-8). The upper section of this window shows the fields for determining the speed and the length of the path that were specified in the first window and the button of close program (Exit). while the lower section contains the following fields:-

1. Reading Time (sec) to specify the time required to take readings.
2. Direction : to determine the movement direction of the moving platform (Forward) or (Backward).
3. Sampling distant (mm): determines the distance between consecutive readings along the scratch path.
4. Start motion: to start the movement of the moving platform.
5. Stop: to stop the movement of the moving platform.
6. Read: to record the readings against time and display them as a table.
7. Set as Zero: through which the resulting reading can be made as a zero reading and this feature is used at the beginning of the test and without load so that the force resulting from the friction of the device parts is not included in the subsequent readings when placing loads, i.e. it is the process of zeroing the device.
8. Save Data: to store the recorded readings as a table in a file inside the computer.
9. Maximum & Minimum: to determine the largest and lowest value of the vertical coordinate in the diagram that depicts the relationship between the tangential forces and the time that appears on the right side of the window.

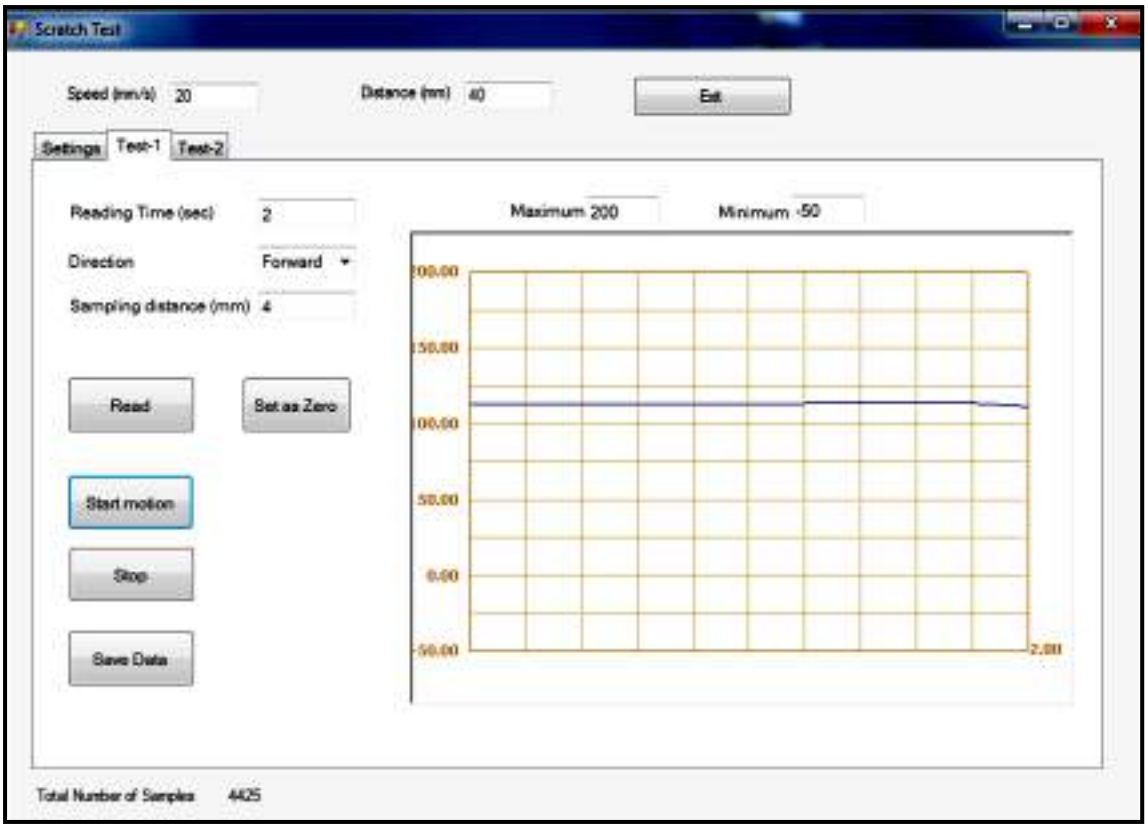

Figure (5-8) Device driver settings interface.

5.3 Device Operating Procedures

The following points illustrate the method to perform the scratch test using the device, and figure (5-9) shows the flow chart of scratch resistance test.

1. Installing the specimen to be tested on the moving platform and installing the scratch tool (indenter) in the holder and balancing the scratch mechanism by rotating the counterweight.
2. Connecting the device to a power source and a computer.
3. Specify the speed, the length of the scratch path and the number of points on the path in the driver interface.
4. Running of the device without load and inserting the reading in the program as a zero reading.
5. Beginning the test using small loads and observe the sample surface.

6. When the indenter reaches the end of the path, it can be brought back to the starting point as well as its lateral position change.
7. Increase loads gradually until a scratch occurs on the sample surface.
8. When scratch occurs, the load is reduced slightly and the test is performed to obtain the lowest load required for scratch.
9. The test is performed five times using the lowest load required to scratch and the readings are used for comparison and to calculate average.
10. The readings obtained from the device are the tangential force (F_t) required for scratch and represent the friction force.
11. The device reads the tangential force at each specific point on the path, and reads the tangential force of the path as a whole by taking the average for readings in all the points.
12. The friction coefficient μ_{sc} of each sample can be calculated from the division of the measured tangential force (F_t) which represents output of the device on the applied normal load (F_n) which represents input of the device.
13. Exiting from the program by clicking the button (Exit) and turn off both the device and the computer after completing the test, then the sample can be lifted from the device and examined using the microscopes such as (AFM) or (SEM) to study the behavior and properties of the remaining scratch on PMMA surface.

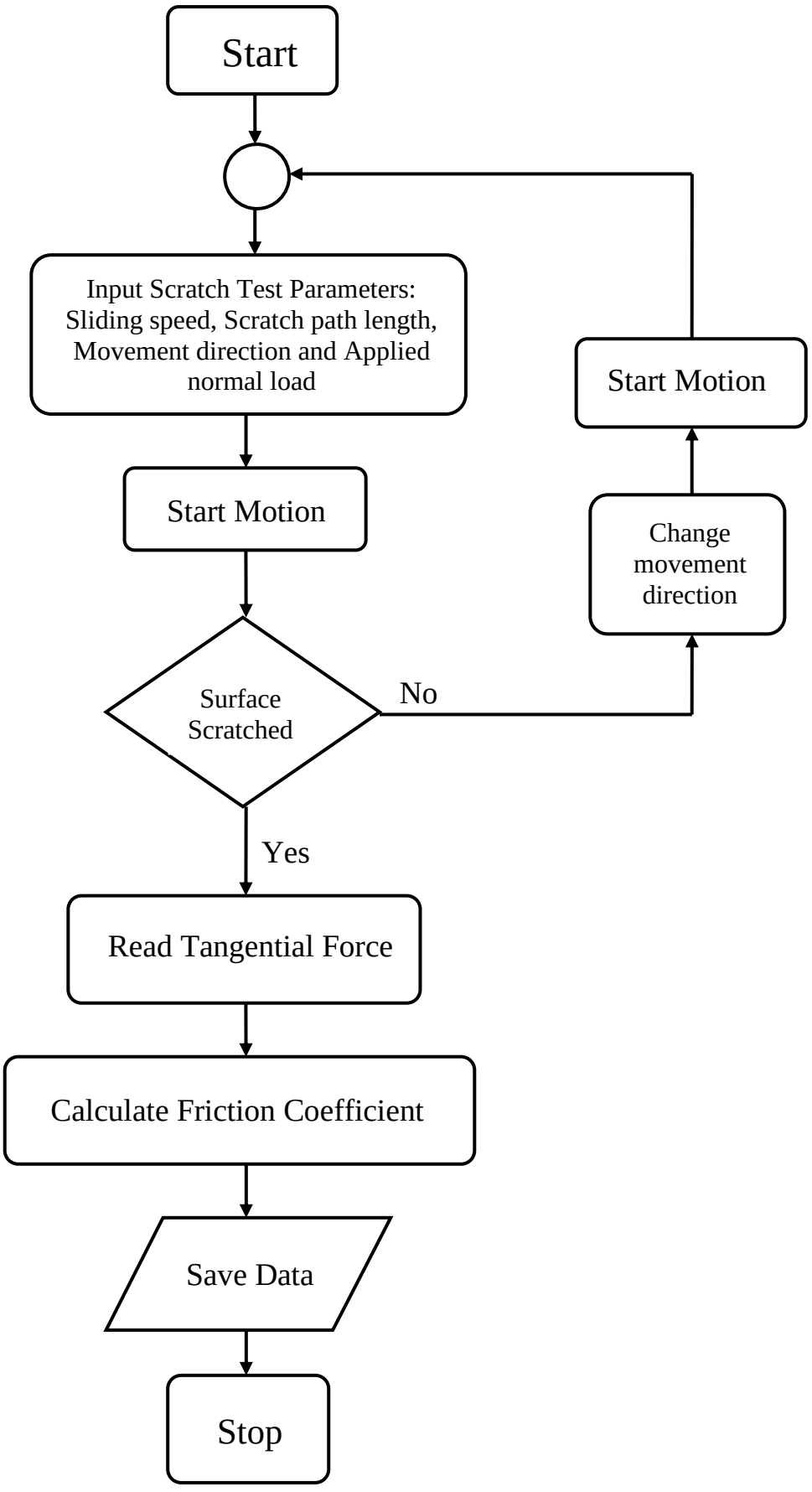

Figure (5-9) Flow chart of scratch resistance test.

5.4 Device Features

In the literature, the scratch test in all researches related to the study of scratch resistance of PMMA was performed using various devices with different specifications. For example, Ezio Amerio et al. used a CSM scratch device (Micro-Combi Tester) with specifications: normal load (0.05N-30N), sliding speed (0.4- 600 mm/min) and maximum scratch length of 120 mm [101]. A new device based on the moving head of tensile machine (Instron 4502) with specifications: normal load (0.05N - 5N) and sliding speed (1 µm/s to104 µm/s) was used by C. Gauthier and R. Schirrer [48]. Christopher M. et al. used a CSM nano-scratch tester with specifications: normal load (10µN-1N), sliding speed (0.4 - 600 mm/min), tangential force measured by load cell (6 µN - 1 N) and dimensions of the sample (20mm × 120mm) [102]. C. Fond et al. used a micro-visioscratch device with specifications: normal load (0.05N - 35N), sliding speed (1 µm/s - 104 µm/s) and temperature range (-70^{o}C to+120 ^{o}C) [103]. Scratch apparatus with specifications such as sliding speed (1 µm/s - 15 mm/s), normal load (0.05 N - 5N) and temperature range (-70 ^{o}C to +120 ^{o}C) was used by S. Lafaye et al. [25]. M. Manshaa et al. used a micro- visio- scratch device with specifications: normal load (0.05 N-35 N) and sliding speed (10^{-3}mm/s -15 mm/s) [21]. N.L. Surampadi et al. used a device with specifications: normal load (0.5 N-10 N), maximum sliding speed of 10 mm/s and three indenters (loop, needle and Hoffman) [53].

The specifications of the device designed in the present study can be summarized in the following points:-

1. Range of linear speed of the moving platform (1 mm/s - 35 mm/s).
2. Range of applied normal load (0.1 N - 325 N) or (10 gm - 33000 gm).
3. The tangential force measured by the load cell ranges (from 0.1 N to 294 N).
4. The length of the scratch path ranges (from 5 mm to 195 mm).
5. The height of the indenter ranges (from 0.25 mm to 50 mm).

6. The dimensions of the samples that can be tested are: Length ranges (from 10 mm to 195 mm), width ranges (from 10 mm to 125 mm), and thickness ranges (0.25 mm to 50 mm).
7. Ability to change the speed of the moving platform and the applied normal load in a single scratch path.
8. Ability to measure the force required for scratching directly and easily through which the coefficient of friction can be calculated directly.
9. Ability to measure the scratch force required for the path as a whole and for specific points on the path.
10. The possibility of lifting the scratch mechanism to the comfort position allowing the user to install and remove samples and indenter in an easy and safe way.
11. The method of installing and removing both sample and indenter is simple and fast.
12. Used to test the plastic and elastic materials.
13. The space occupied by the device in the laboratory is small due to the small size of the device.
14. The method of device operation is simple and easy does not require the user a lot of experience or time to learn.
15. The user of the device does not need many safety requirements.

5.5 Calibration of the stepper motor and load cell

The stepper motor speed calibration was performed using the digital tachometer, as shown in figure (5-10), also the linear distance traveled for the moving platform was calculated per revolution where was equal to 8 mm / rev. Calibration of the load cell used to measure the tangential force was performed by applying normal loads on the load cell and recording the load cell readings as shown in the table (5-1), figure (5-11) offers the relationship between applied normal loads and the corresponding readings of the load cell. Calibration of stepper motor and load cell was performed in the laboratories of the Mechanical Engineering Department, Engineering College in Basrah University.

Table (5-1) Values of applied normal loads and load cell readings

Applied Normal Load (Kg)	**Load Cell Reading (Kg)**
0	0
0.891	0.89
1.881	1.88
2.992	2.99
3.832	3.83
4.763	4.76
5.774	5.77
6.774	6.77
7.735	7.73
8.686	8.68
9.755	9.75
10.617	10.61
11.618	11.61
12.709	12.7
13.579	13.57
14.521	14.51
15.491	15.48
16.592	16.58
17.632	17.62
19.234	19.22
20.575	20.56
21.495	21.48
22.786	22.77
24.397	24.38
26.179	26.16
27.107	27.09
27.149	27.13

Figure (5-10) Digital Tachometer

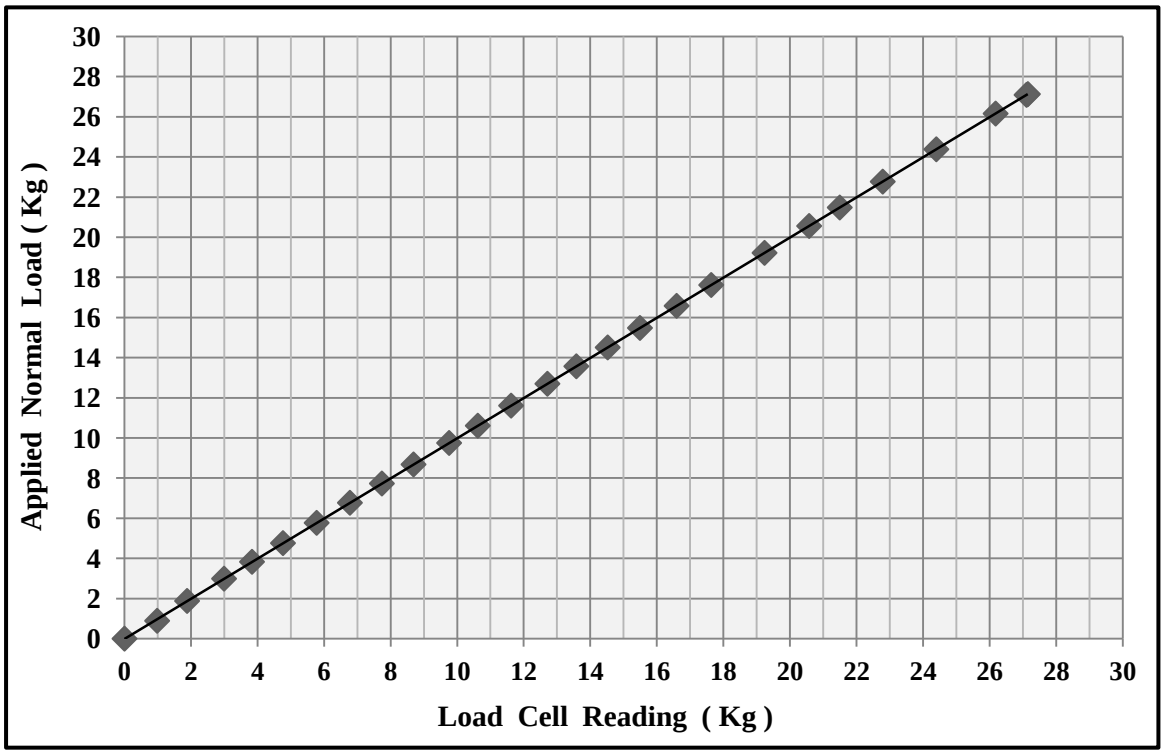

Figure (5-11) The relationship between the normal loads and the corresponding readings of load cell.

The slope value in the relationship between the normal load and load cell reading represents the value of (Scale) used in the main interface of operating program, and calculated as follows

$$\text{Slope (Scale)} = \frac{\sum \text{Applied normal loads}}{\sum \text{Load cell readings}}$$

$$\text{Scale} = \frac{354.7808}{354.52} = \mathbf{1.0007356}$$

5.6 Device validation

In order to validate the results of the device, the tangential force measured by the device during the scratch resistance test of polymethyl methacrylate (PMMA) and polycarbonate (PC) was used to calculate friction coefficient of both materials. A comparison was made with the values of the friction coefficient mentioned by the manufacturer in material data sheet, the results showed an excellent convergence as shown in figure (5-12).

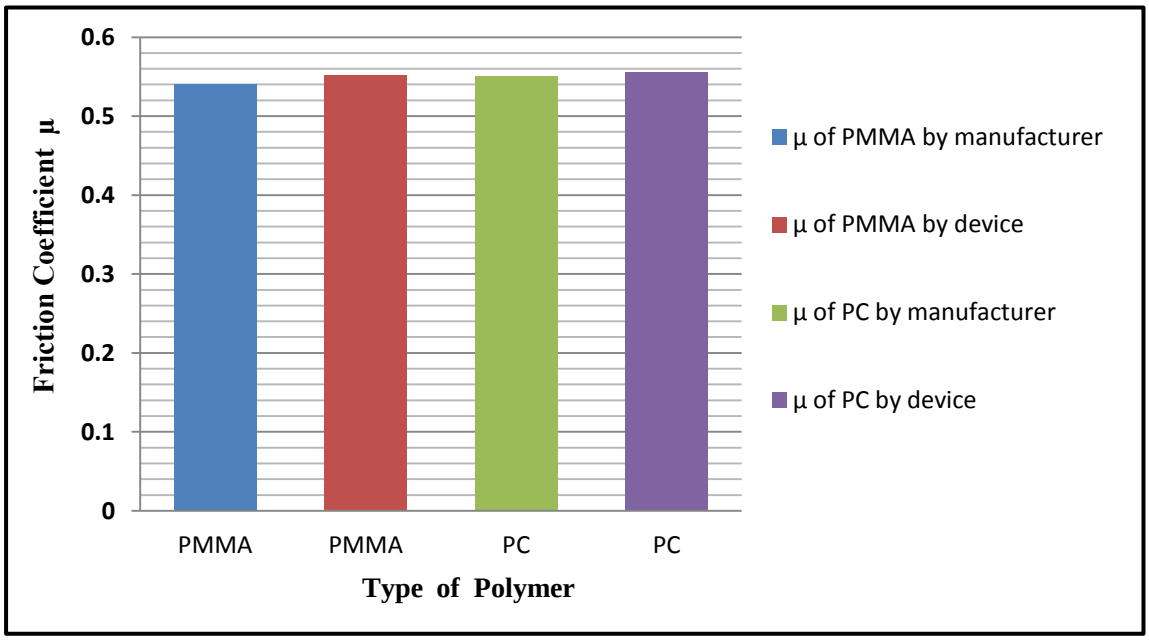

Figure (5-12) Comparison of friction coefficient values of PMMA and PC.

5.7 Device Equipments Specifications

The equipments specifications used in the scratch resistance device that will be mentioned in this part are the stepper motor, load cell, LapJak and Microstep Driver.

5.7.1 Lab Jack

Dealing with various input data between the parts of the device such as sliding speed, scratch path length , the distance between points on the scratch path, motion direction of the moving platform and the readings time, in addition to obtaining the output data such as tangential force, all this was done using the LabJack U3-HV that was installed on the control panel as shown in figure (5-6). Lab Jack is interface equipment between the scratch resistance device and the laptop that contains the driver and device control. The technical specifications of Lab Jack are:-

- 12 input/output may be used as input digital, output digital, or input analog.
- 12 inputs analog with resolution of 12 bits and voltage ranges from 0 to 3.6 V.
- 4 allocated to HV analog-inputs with voltage of -10 to +20V.
- 16 digital input/output I/O, with voltage of 3.3V-logic.
- 2 counters or 2 timers with 32-bits each.
- 2 allocated to analog-outputs with 10-bits, 0-5V.
- Temperature range -40 to 85°C.
- 2 PWM (Pulse-Width-Modulated), quadrature, pulse width.
- Times for command and response are less than 1ms.
- Input for the stream rate 50 kHz (based on resolution).

5.7.2 Load Cell

The tangential force required to scratch the surface of the PMMA specimen resulting from the applied normal load was measured using the load cell, it installed in the bottom surface of the moving platform and connected to the serrated bar of the movement by the serrated flange, as shown in figure (5-13). Table (5-2) represents the load cell specifications.

Table (5-2) Load cell specifications.

Specification	Value
Model	AB130
Type	Parallel beam type (single point load cell)
Material	Aluminum alloy
Rated Load	30 kg (294.3 N)
Zero Balance	0±0.1 mV/V
Rated Output	2.0±10% mV/V
Input Resistance	400±30 Ω
Output Resistance	350±3.5 Ω

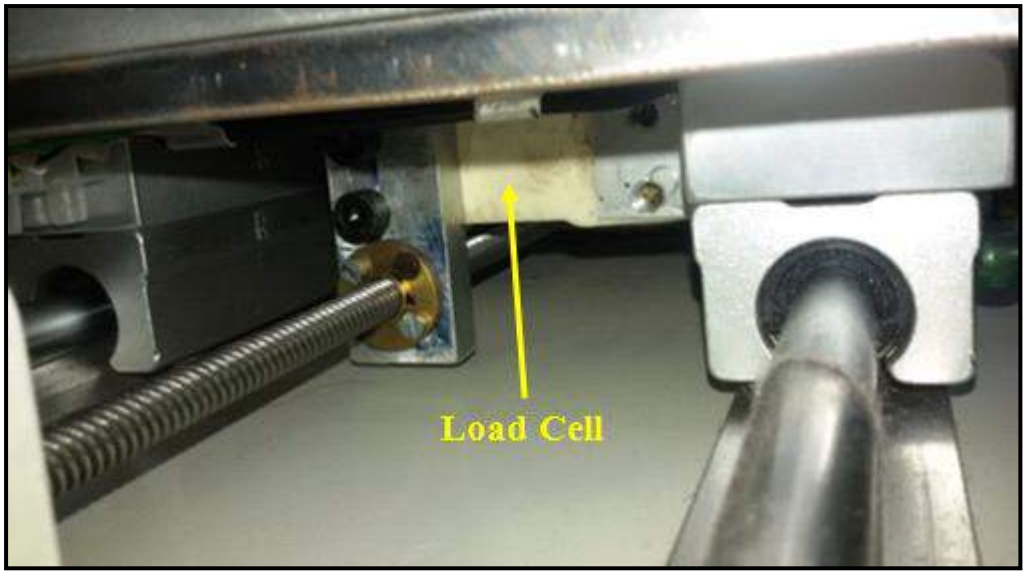

Figure (5-13) Load cell location.

5.7.3 Stepper Motor and Microstep Driver

The linear movement of the moving platform was obtained by using the stepper motor, where the rotational movement is converted to linear movement using serrated bar that is connected to the stepper motor by flexible disk coupling while the second end of serrated bar is connected to the moving platform by the serrated flange installed on the load cell. The rotation direction of the stepper motor was controlled by the Microstep Driver installed in the control panel. The specifications of stepper motor listed in table (5-3) and table (5-4) represents the specifications of Microstep Driver.

Table (5-3) Stepper motor specifications

Specification	Value
Model	57HS112-4004A08-A21
Step angle	1.8 degree
Rated current	3 A/Phase
Rated voltage	4.8 V
Resistance	1.6 Ω/Phase
Inductance	6.8 mH/Phase
Holding torque	2.8 N.m
Detent torque	12 N.cm
Rotor inertia	800 $g.cm^2$
Motor length	112 mm
Lead wire	4 NO.
Net weight	1.4 kg

Table (5-4) Microstep Driver specifications

Specification	Value or Description
DC power supply	9V-42V
Output current	4 A
Rated output	3.5 A
Power supply	Single
Reset	Enable pin
Rotation	Forward and reverse
Provide energy	Semi-automatic

5.8 Specimens Preparation Equipments

The equipment required for preparing the specimens of pure PMMA and SiO_2/PMMA composites in sheet-form are glassy molds, metallic molds, glassy containers, horizontal leveling platforms, and a dispersion device used to disperse SiO_2 nanoparticles in the PMMA powder will be described in this section.

5.8.1 Glassy Molds

Two sets of glassy molds were made using 6 mm thickness glass sheets, adhesion material, and L-shaped aluminum corners of 20 x 20 mm. The number of molds in the first group is 10, which are used to obtain samples with dimensions of 4 mm thickness, 100 mm width, and 130mm length. The number of molds in the second group is also 10, which are used to obtain samples with dimensions of 4 mm thickness, 130 mm width , and 200 mm length, as shown in figure (5-14). These molds were used in the first and third preparation methods which used for preparing pure and reinforced PMMA samples.

5.8.2 Metallic Molds

Two iron molds were made each one consisting of three parts, the first part is a rectangular plate with dimensions of 200 mm ×140 mm × 10 mm and the second part is a rectangular plate with dimensions of 145 mm × 85 mm × 6 mm and the third part is a ring with a thickness of 10 mm consisting of an outer rectangle with dimensions of 140 mm × 200 mm and an internal rectangle with dimensions of 150 mm × 90 mm, as shown in figure (5-15). The first part is installed with the third part by 6 screws with a diameter of 6 mm and a length of 16 mm; fixing screws are low by 2 mm from the surface of the two parts. The space resulting from the difference between the dimensions of the second and third parts allows exiting the surplus molten during pressing process. While the difference between the thicknesses of the same two parts allows obtaining the required thickness of the specimen which is 4 mm.

5.8.3 Glassy Containers

Ten glassy containers with dimensions of 250 mm length, 160 mm width and 100 mm height were made using 6 mm thickness glass sheets, adhesion material, and L- shaped aluminum corners of 20 x 20 mm, as shown in figure (5-16). These containers were used to cover sample molds prepared using the first and third sample preparation methods. The containers were designed with dimensions that allow placing either one large glassy mold or two small glassy molds within a single container. The glassy containers are used for two objectives, first to protect the samples from dust and impurities during the solvent evaporation process and the solidification of samples. The second objective is to provide a space saturated with solvent steam that prevents the top layer of the sample surface from solidifying for as long as possible during the evaporation process, which reduces the formation of bubbles.

5.8.4 Horizontal leveling platforms

Ten horizontal leveling platforms were made with dimensions of 270 mm length and 180 mm width using wooden boards with a thickness of 18 mm. Each platform is provided with four legs adjustable up and down in order to level the platform horizontally to ensure that one thickness of PMMA samples is obtained. The surface of the platforms was covered with a layer of chemical-resistant leather, as shown in figure (5-17). The platforms are designed with dimensions that allow one glassy container to be placed on their surface.

5.8.5 Nanoparticles Dispersing Device

Nanoparticles dispersing device consisting of an iron box-shaped structure with dimensions of 400 mm × 350 mm × 450 mm installed on its upper surface a pair of steel bars coated with a layer of rubber to prevent the plastic container that contains a mixture of PMMA powder and nanoparticles SiO_2 from slipping during the rotation of the bars which installed on the surface of the box by ball bearing pillow blocks. A pulley is attached to the end of one

of the bars with a belt to transmit the movement from the electric motor that fixed in the middle of the box, which has three speeds of 750/600/450 rpm, as shown in figure(5-18). Table (5-5) represents the specifications of motor used.

Table (5-5) Specifications of motor used in nanoparticles dispersing device.

Specification	Value
Model	YDK-100-6
Type	A.C. Fan Motor
Frequency	50-60 Hz
AC Voltage	220-240 V
Current	1.12 A
Power	100 W
Phase	Single- Phase
Rotate Speed	750/600/450 RPM
Capacitance	8.0 µF/450 V

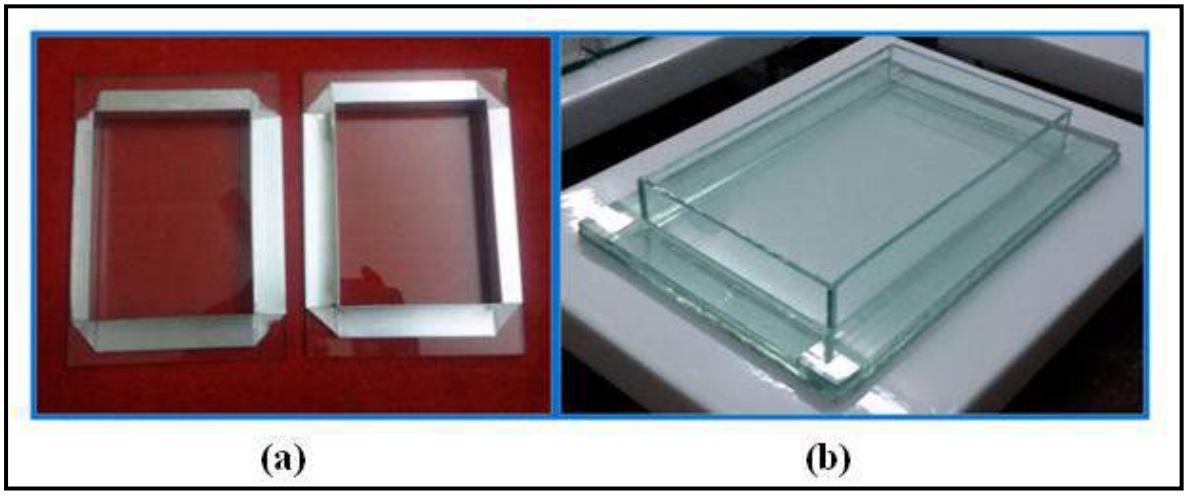

Figure (5-14) (a) Small glassy mold, (b) Large glassy mold.

Figure (5-15) Metallic molds

Figure (5-16) Glassy container.

Figure (5-17) Horizontal leveling platform.

Figure (5-18) Nanoparticles dispersing device.

Chapter Six
Results
and
Discussions

Capter Six

Results and Discussion

6.1 Introduction

The experimental tests results for pure PMMA and PMMA/SiO_2 composite specimens will be discussed in this chapter. The tested specimens were divided into three groups according to the method of preparation; also, the first group was divided into two sets according to the added SiO_2 ratio as illustrated in table (6-1). The properties studied and discussed for all samples in this chapter were temperature of glass transition (T_g), ultimate tensile strength and elongation, surface hardness, surface roughness, and tangential force required for scratching as well as friction coefficient using DSC test, tensile test, shore D hardness test, surface roughness test, and scratch resistance test, respectively.

Table (6-1) Specimens groups

Group Name	Preparation Method	Specimen Code	SiO_2 ratio (wt %)
First group	**Dissolving** method	Set A : S0, S1, S2, S3, and S4 Set B : G0, G1, G2, G3, G4, and G5	Set A: 0, 1, 2, 3, and 4wt% Set B : 0, 0.1, 0.2, 0.3, 0.4, and 0.5 wt%
Second group	**Pressing** method	P0, P1, P2, P3, P4, and P5	0, 0.1, 0.2, 0.3, 0.4, and 0.5 wt%
Third group	**Casting** method	R0, R1, R2, R3, R4, and R5	0, 0.1, 0.2, 0.3, 0.4, and 0.5 wt%

6.2 Results and discussion of Glass Transition Temperatures (T_g).

The temperatures of the glass transition (T_g) of the PMMA specimens can be obtained by means of the DSC test. This test was conducted based on D3418-03 of ASTM standard and heat rate of 10^{o}C/min and the temperature range to 300^{o}C. Figures (6-1 and 6-2) show the DSC curves of pure PMMA specimens and PMMA/SiO_2 composite S and P specimens, it can be seen from the curves that the glass transition temperature (T_g) of the PMMA/SiO_2 composite specimens was higher than that of the pure specimens, also, it can be observed

that the glass transition temperature for the PMMA/SiO_2 composite specimens increases with increasing ratio of SiO_2 nanoparticles. The melting temperature of silicon oxide nanoparticles (SiO_2) about 1600^{o}C which much higher than that of the PMMA material (about 165^{o}C), therefore, adding them to the PMMA increases the temperature of the glass transition and this temperature increases with increasing ratio of added nanoparticles. Table (6-2) contains the temperature of glass transition (T_g) for both S and P specimens, while for G and R specimens were listed in table (6-7).

From the values of glass transition temperature listed in table (6-8), can be concluded that T_g in the PMMA/SiO_2 composite specimens increases with an increase in SiO_2 content compared to pure specimens. Also, it can be observed that the highest values of T_g were for specimens containing SiO_2 ratios ranging from 1wt% to 4wt% which was prepared by dissolving method. Whereas in the case of PMMA/SiO_2 composite specimens containing SiO_2 ratios range (0.1wt% - 0.5wt %), the best values for the increase in T_g were for the specimens prepared by pressing method.

Table (6-2) Glass transition temperatures (T_g) for S and P specimens.

Specimen code	**SiO_2 Ratio (wt %)**	**Glass transition temperature T_g (^{o}C)**
S0	**0**	**108.67**
S1	**1**	**141.79**
S2	**2**	**149.02**
S3	**3**	**154.53**
S4	**4**	**159.71**
P1	**0.1**	**115.58**
P2	**0.2**	**120.37**
P3	**0.3**	**124.99**
P4	**0.4**	**130.84**
P5	**0.5**	**135.56**

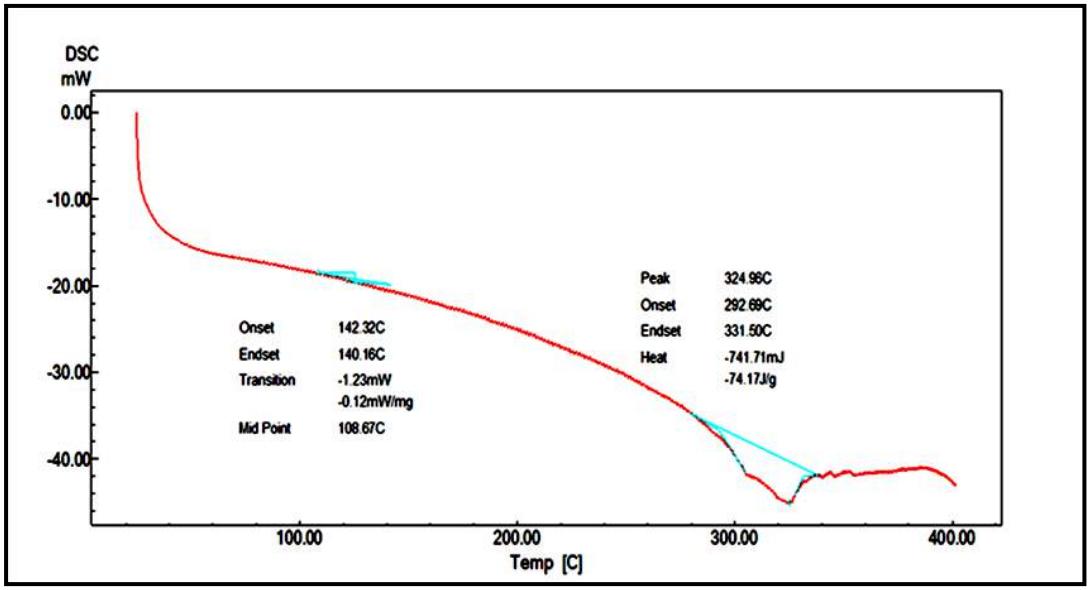

(a) S0 specimen

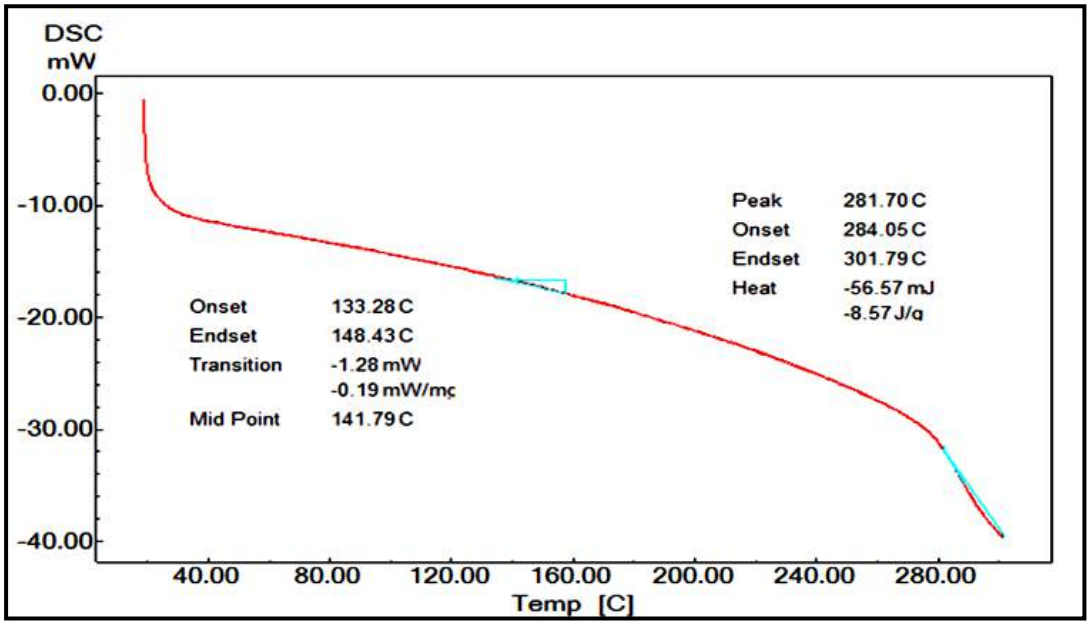

(b) S1 specimen

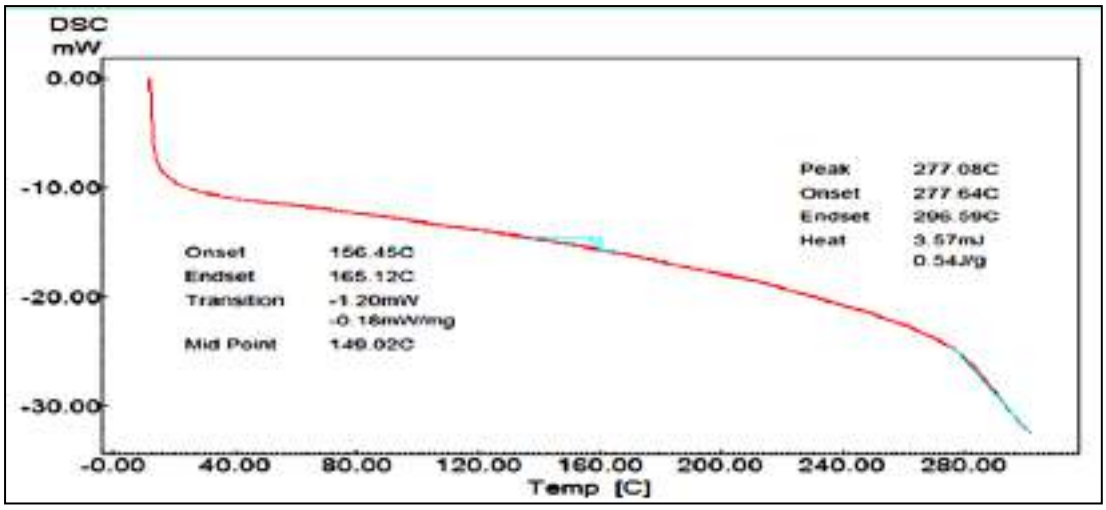

(c) S2 specimen

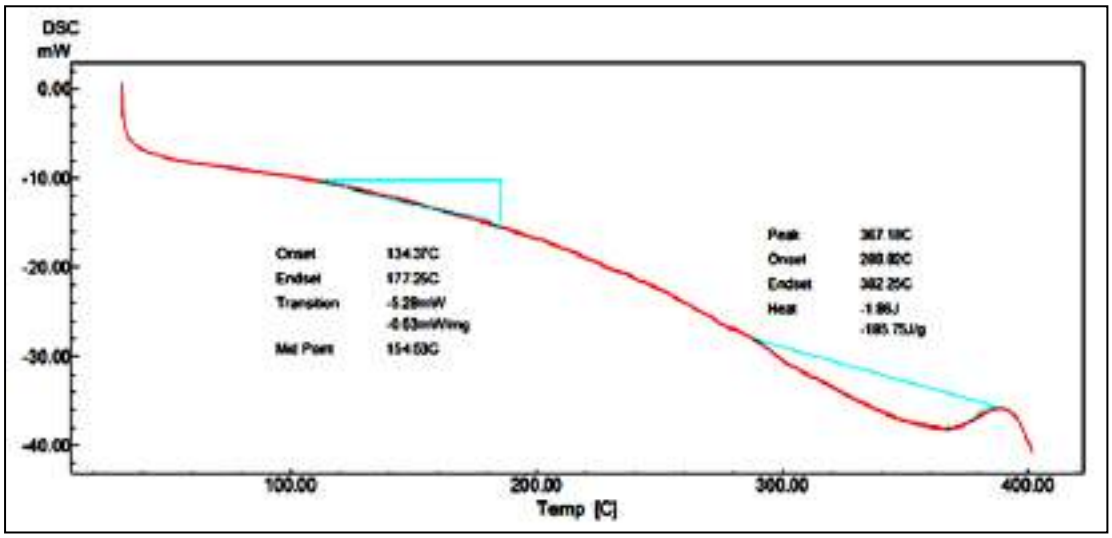

(d) S3 specimen

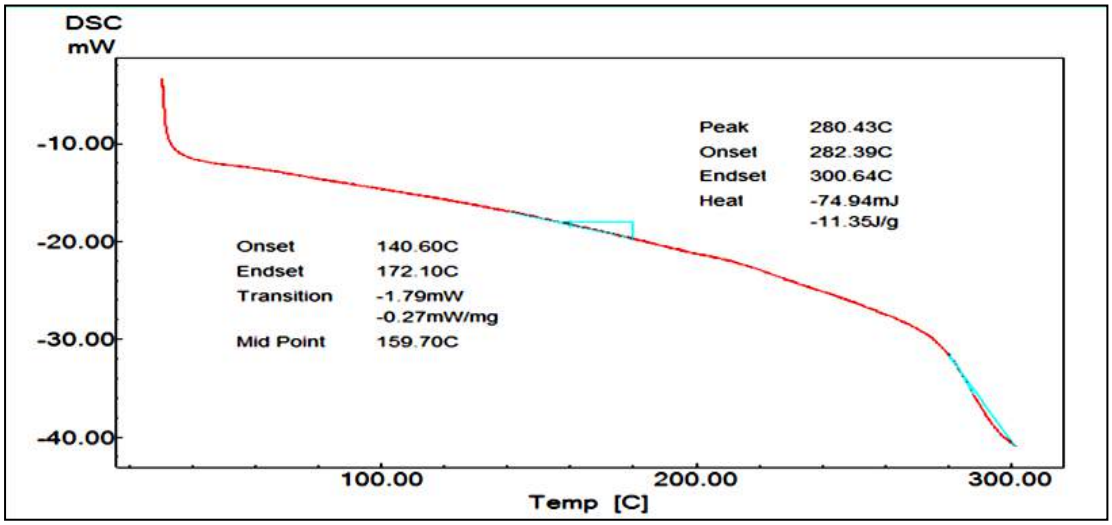

(e) S4 specimen

Figure (6-1) DSC curves for S specimens.

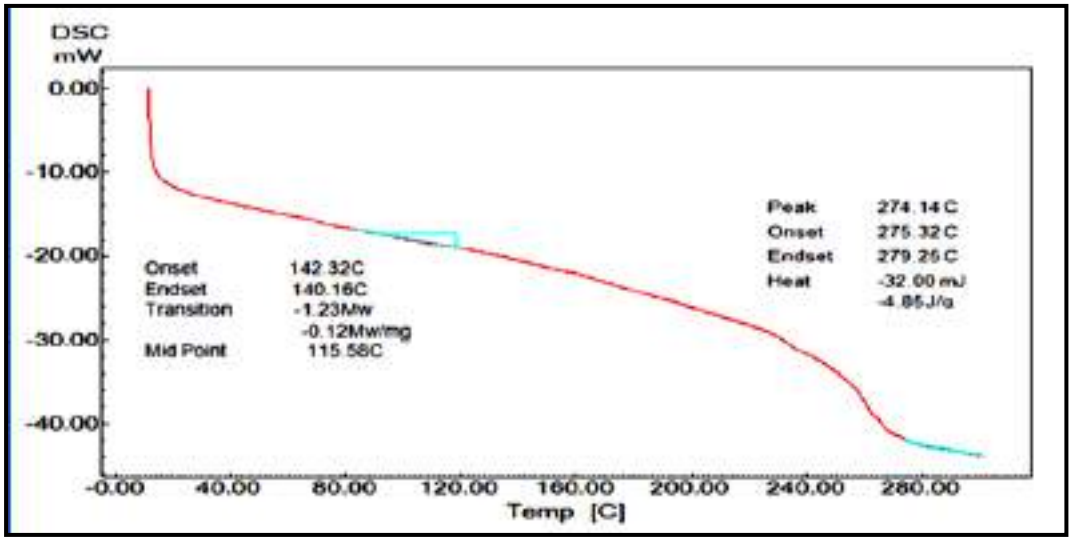

(a) P1 specimen

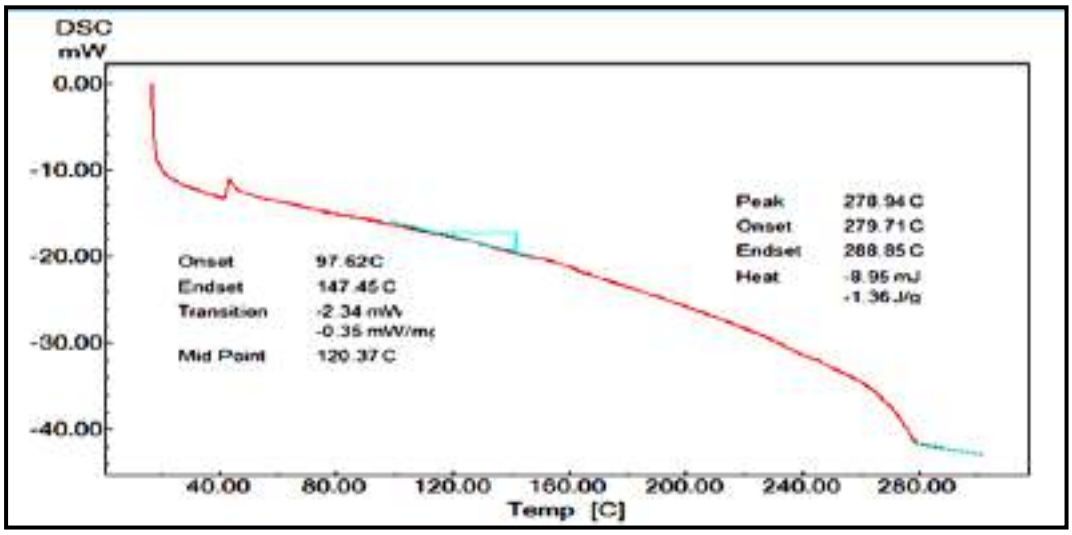

(b) P2 specimen

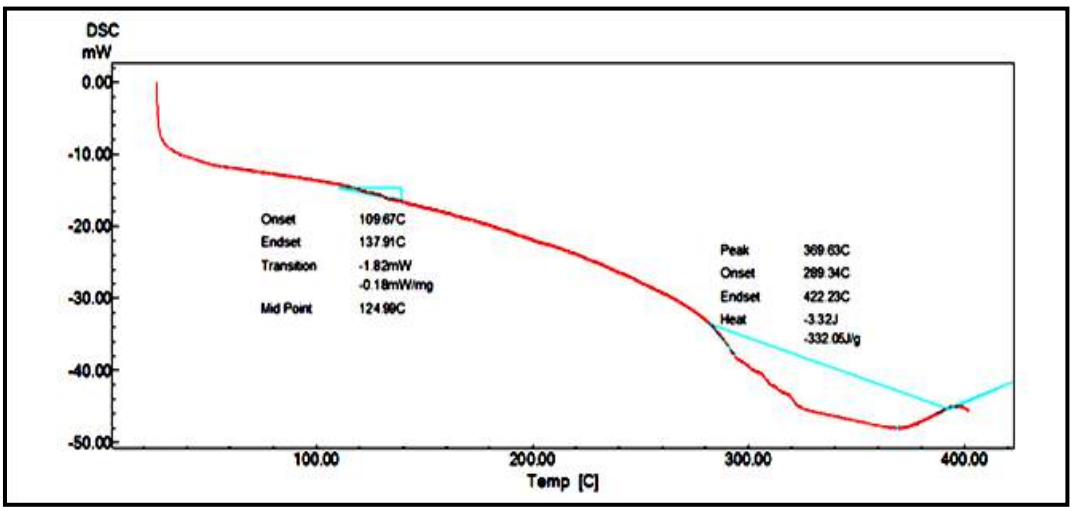

(c) P3 specimen

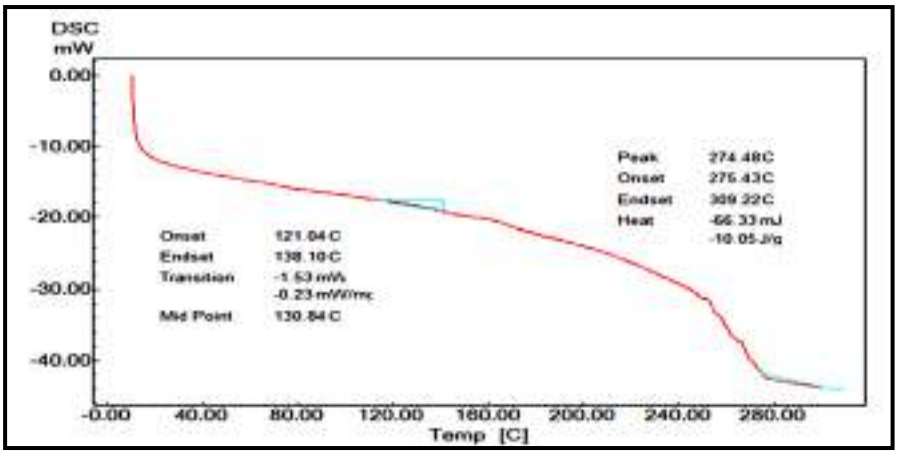

(d) P4 specimen

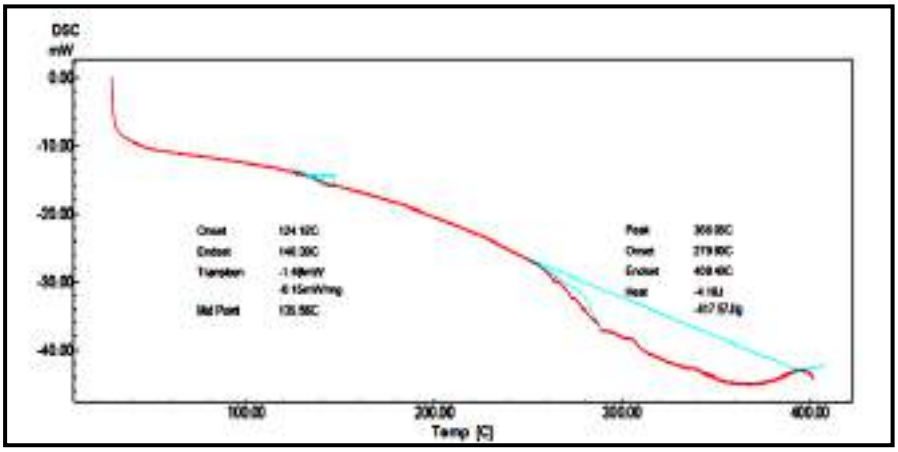

(e) P5 specimen

Figure (6-2) DSC curves for P specimens.

6.3 Results and discussion of Tensile Strength

The samples used in the tensile tests were cut according to (ASTM) D-638; dimensions and shape of the test sample were presented in figure (4-13) in chapter four. Tensile tests were obtained at the room temperature (23°C) and rate of displacement of 5 mm/min using a universal test apparatus, all tests were conducted in laboratories of Materials Engineering College, University of Babylon. The curve of stress and strain of the samples tested was plotted by the device itself on graph paper.

Figures (6-3 to 6-7) represent the tensile test behavior of specimens (S0, S1, S2, S3, and S4) set A from first group. The results showed an improvement of the tensile strength for PMMA/SiO_2 composites (S1, S2, and S3 specimens) while a decrease in tensile strength was observed for the S4 specimen compared

to pure PMMA (S0 specimen).This behavior was caused by the effect of nanoparticles scattered between free spaces within the chain on restricting the movement of molecular chains in the PMMA matrix. A significant increase in ultimate tensile strength can be observed for PMMA/SiO_2 composite by 1wt% compared with the other ratios of SiO_2. Any other increase in SiO_2 nanoparticles content above 1wt% imposes an adverse effect by reducing the ultimate tensile strength as shown in figure (6-8). The reason for this behavior was that the increase in SiO_2 leads to the nanoparticles agglomerate with each other, the same behavior has been observed in the work of Saeed Shirkavand and Elnaz Moslehifard [43]. Aggregated nanoparticles act as centers of stress concentration within PMMA and impose a negative effect by reducing the ultimate tensile strength. Figure (6-9) represents the elongation of specimens (S0, S1, S2, S3, and S4) set A from first group as a function of SiO_2 nanoparticles ratio, the results showed a decrease in elongation for PMMA/SiO_2 composites compared to pure PMMA this behavior is due to the distribution of stress on both the base material and the reinforcement filler, while an increase in elongation was observed for PMMA/SiO_2 composites by 2 wt%, 3wt%, and 4wt% ratios compared to 1wt% ratio, the reason is that at a certain stress, the interface between the base material and the reinforcement filler fails, causing its withdrawal and make it act as gaps and areas to focus the stresses.

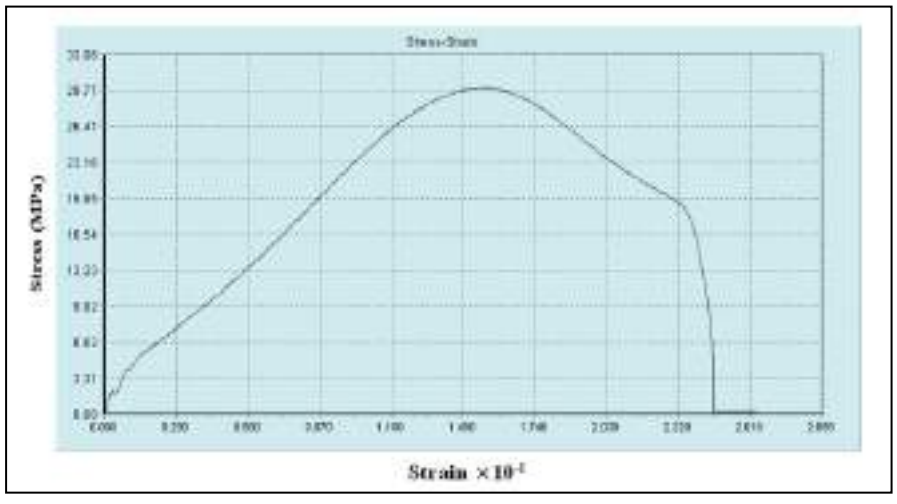

Figure (6-3) Diagram of stress against strain for S0 specimen (pure PMMA).

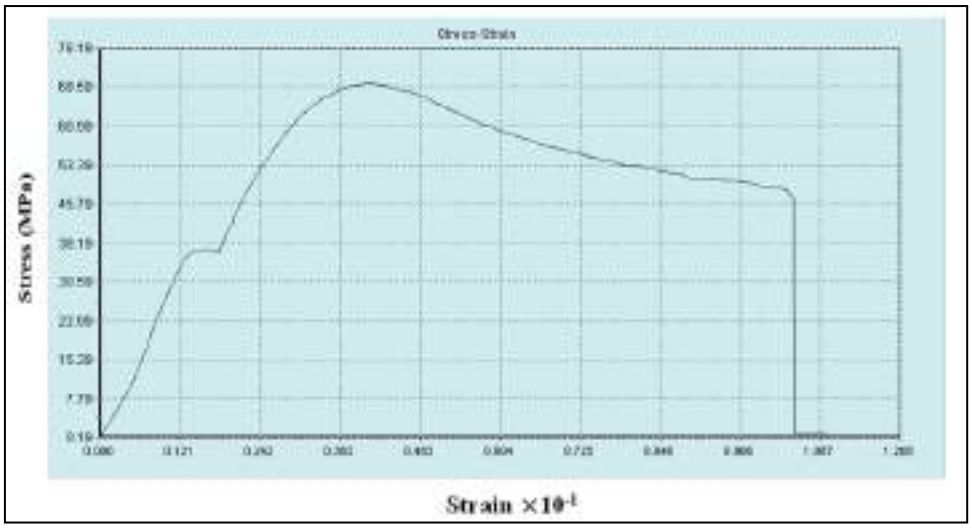

Figure (6-4) Diagram of stress against strain for S1 specimen (1wt% SiO_2).

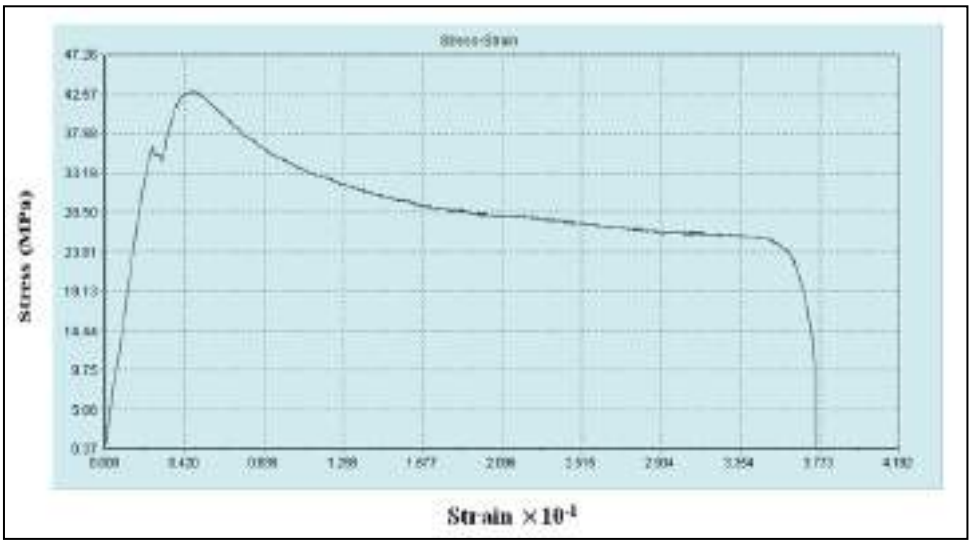

Figure (6-5) Diagram of stress against strain for S2 specimen (2wt% SiO_2).

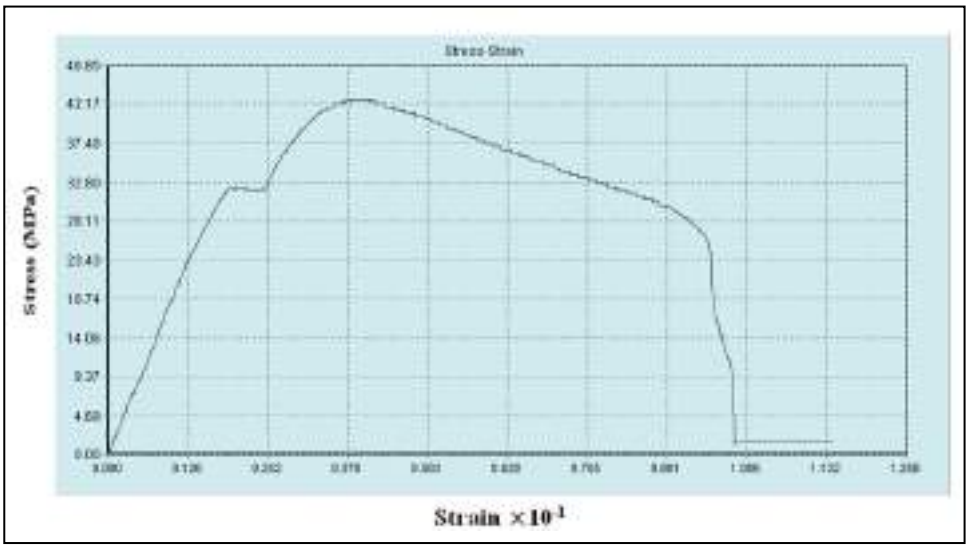

Figure (6-6) Diagram of stress against strain for S3 specimen (3wt% SiO_2).

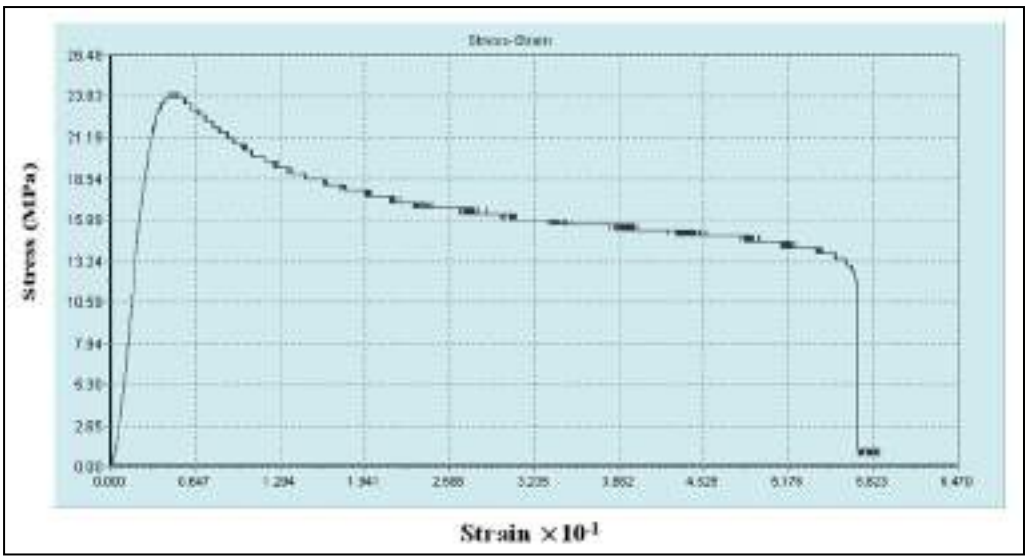

Figure (6-7) Diagram of stress against strain for S4 specimen (4wt% SiO_2).

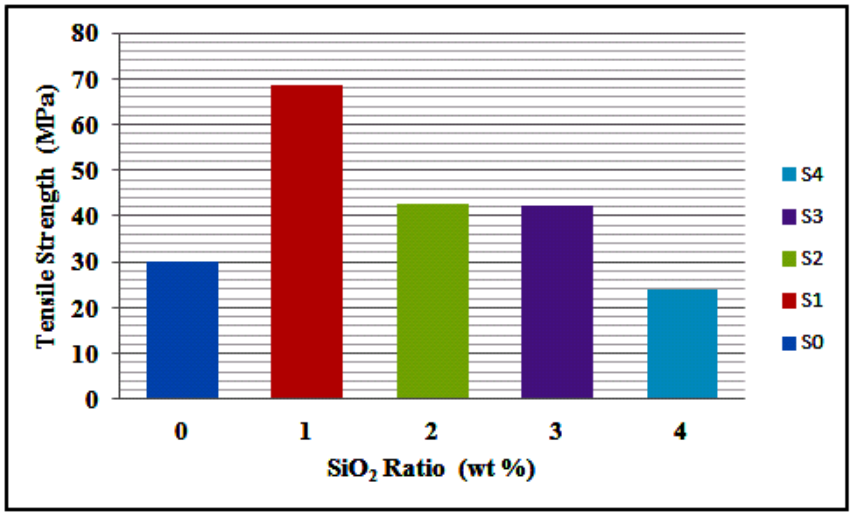

Figure (6-8) Ultimate tensile strength for specimens (S0, S1, S2, S3, and S4) set A from first group as a function of SiO_2 nanoparticles ratio.

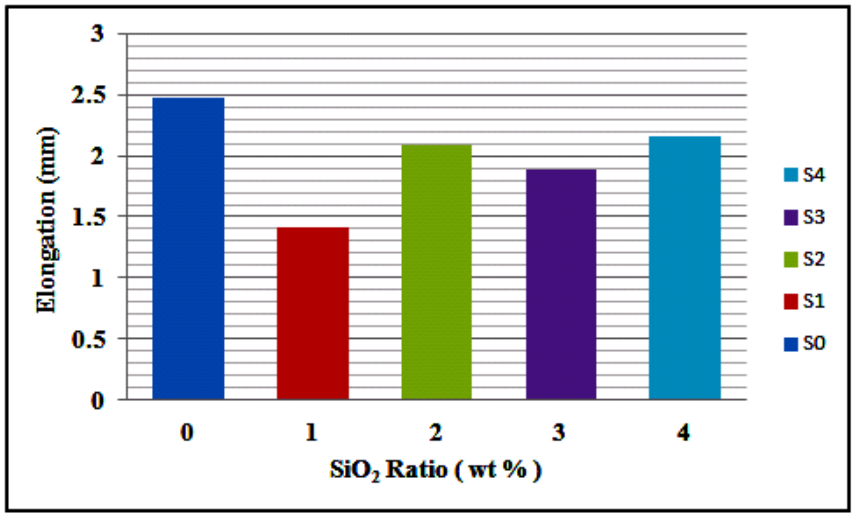

Figure (6-9) Elongation of specimens (S0, S1, S2, S3, and S4) set A from first group as a function of SiO_2 nanoparticles ratio.

It was clear from the results of the tensile test of the specimens S1, S2, S3, and S4 that the best ratio for adding SiO_2 nanoparticles was 1wt % compared to other ratios. Accordingly, the ratio of SiO_2 nanoparticles in the set B of the first group, as well as for the specimens of the second and third groups, was reduced to become from 0.1wt% to 0.5 wt% at an increase rate of about 0.1 wt%. This is due to the desire not to influence the transparency advantage of PMMA and for the current study to be of economic benefit.

Figures (6-10 to 6-16) represent the tensile test behavior of specimens (G0, G1, G2, G3, G4, and G5) set B from first group. The results showed an improvement of the tensile strength for PMMA/SiO_2 composite specimens compared to pure PMMA (G0 specimen). Also, it can be noted that for PMMA/SiO_2 composites that the ultimate tensile strength increases with increasing SiO_2 nanoparticles ratio. This behavior was due to the increased effect of nanoparticles scattered between the free spaces within the chain on restricting the movement of molecular chains in the PMMA matrix as a result of the increase in the ratio of SiO_2 nanoparticles, as shown in the figure (6-16).

Figure (6-17) represents the elongation of specimens (G0, G1, G2, G3, G4, and G5) set B from first group as a function of SiO_2 nanoparticles ratio, the results showed a decrease in elongation for PMMA/SiO_2 composites specimens compared with pure PMMA (G0 specimen), this behavior was due to the distribution of stress on both the base material and the reinforcement filler, also, a decrease in elongation was observed for PMMA/SiO_2 composites with increase the SiO_2 ratio, this was due to the increase in resistance of PMMA/SiO_2 composites to the applied tensile force, the decrease in elongation was an indication of the increase in resistance.

Figure (6-10) Diagram of stress against strain for G0 specimen (pure PMMA).

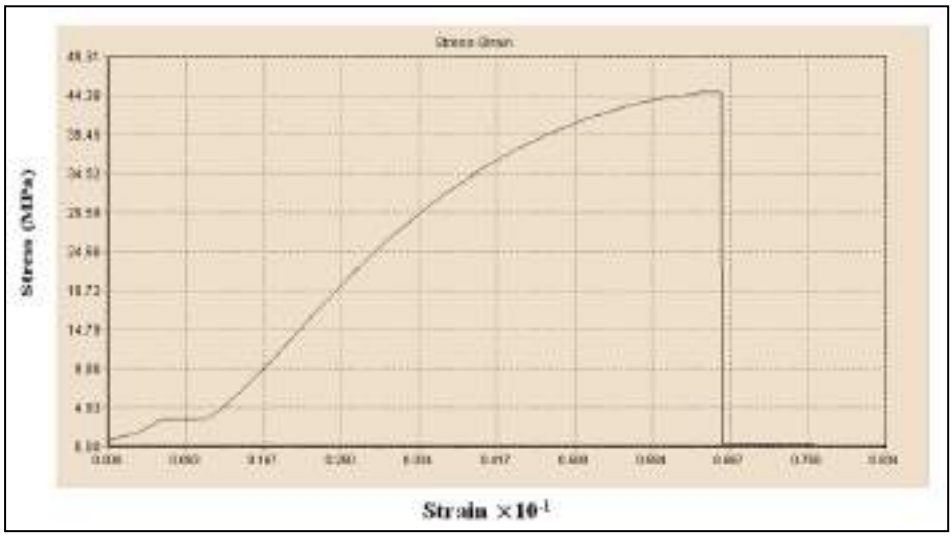

Figure (6-11) Diagram of stress against strain for G1 specimen (0.1% SiO_2).

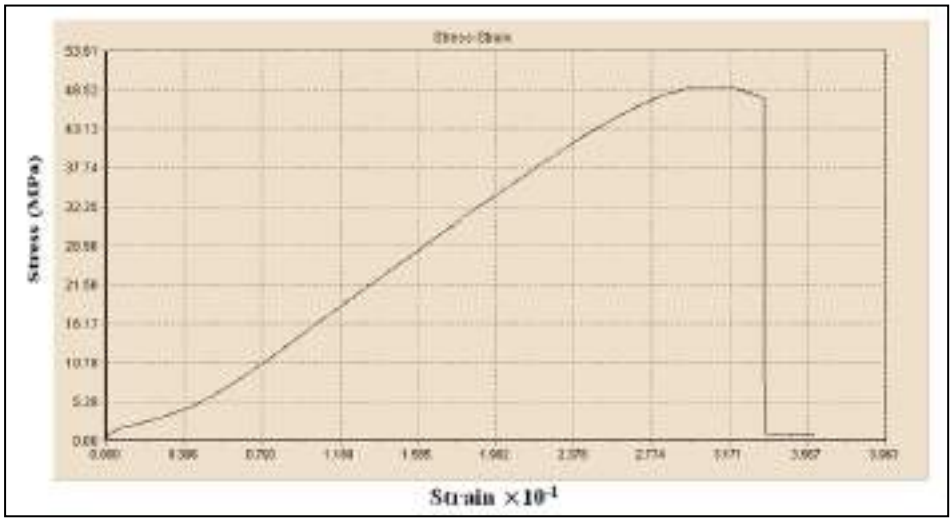

Figure (6-12) Diagram of stress against strain for G2 specimen (0.2% SiO_2).

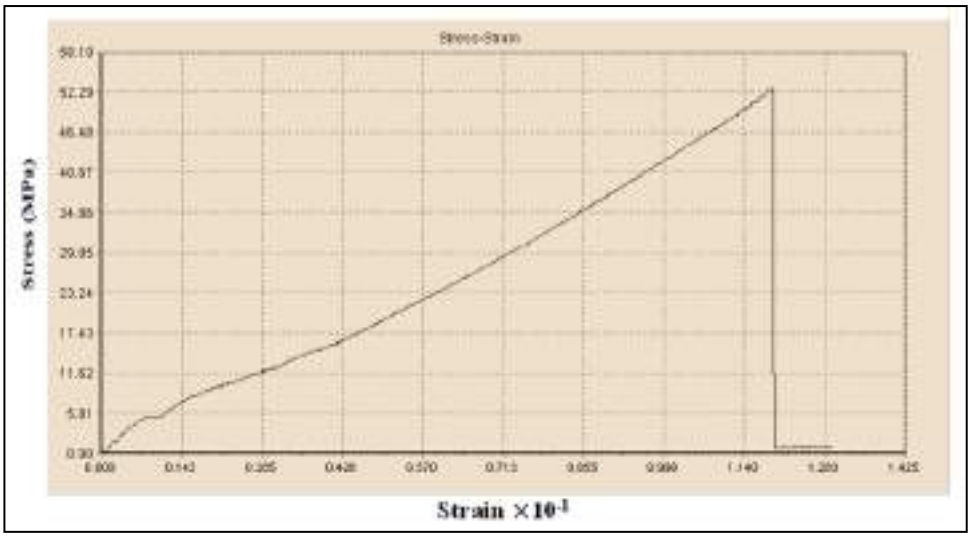

Figure (6-13) Diagram of stress against strain for G3 specimen (0.3% SiO_2).

Figure (6-14) Diagram of stress against strain for G4 specimen (0.4% SiO_2).

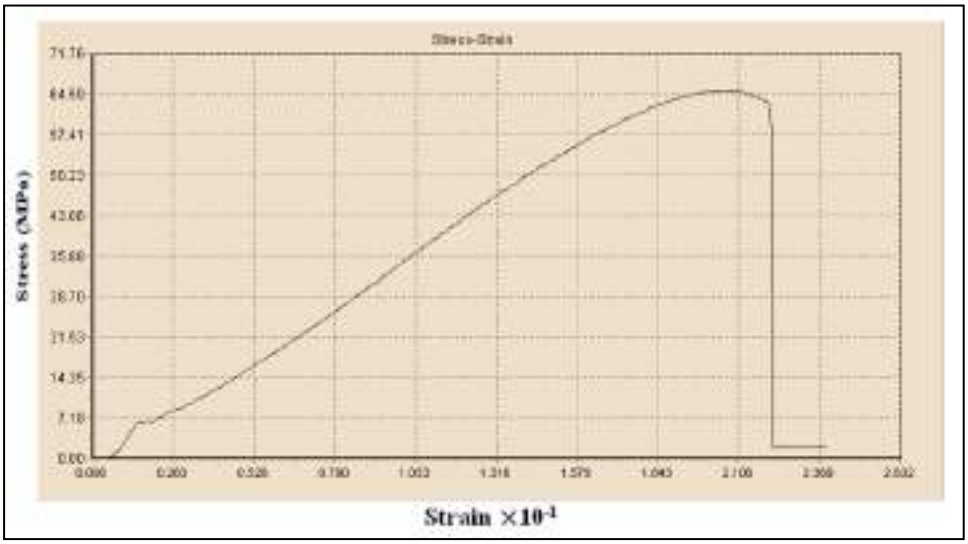

Figure (6-15) Diagram of stress against strain for G5 specimen (0.5% SiO_2).

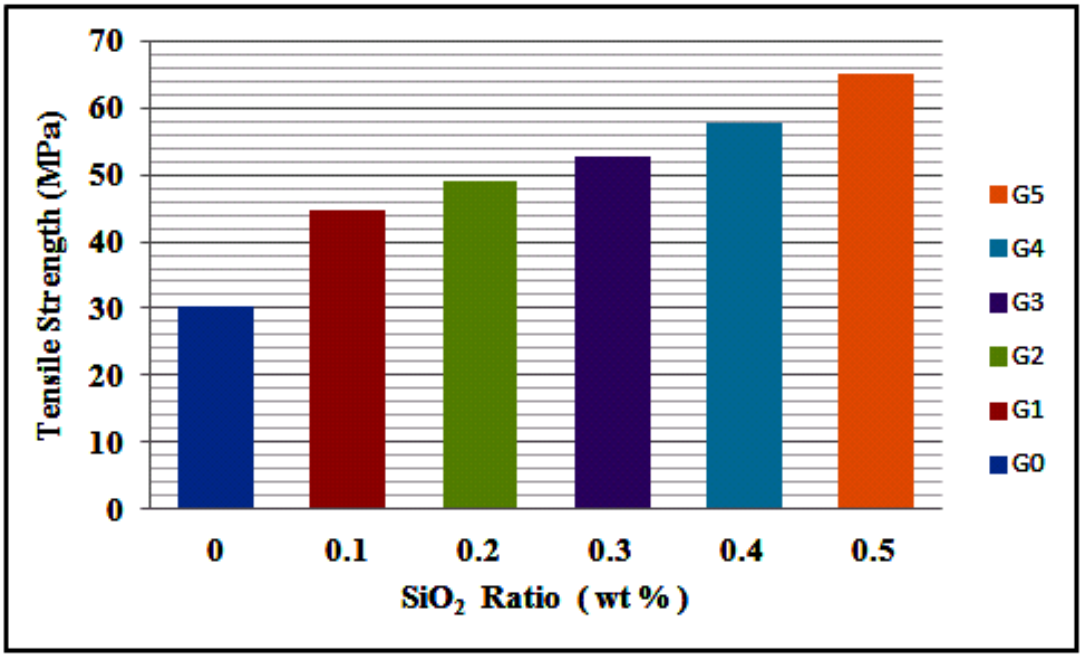

Figure (6-16) Ultimate tensile strength of specimens (G0, G1, G2, G3, G4, and G5) set B from first group as a function of SiO_2 nanoparticles ratio.

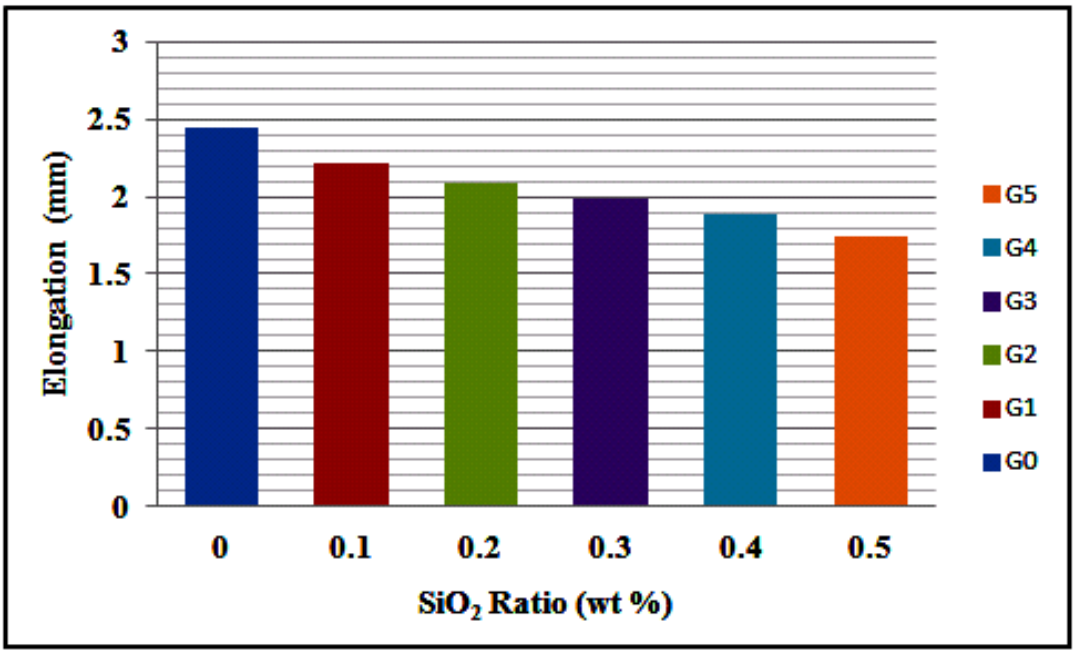

Figure (6-17) Elongation of specimens (G0, G1, G2, G3, G4, and G5) set B from first group as a function of SiO_2 nanoparticles ratio.

Figures (6-18 to 6-23) represent the tensile test behavior of specimens (P0, P1, P2, P3, P4, and P5) for second group and figures (6-24 to 6-29) represent the tensile test behavior of specimens (R0, R1, R2, R3, R4, and R5) for third group. The results for both groups showed an improvement of the tensile strength for PMMA/SiO_2 composites specimens compared to pure PMMA (P0 and R0 specimens). It can be noted that for PMMA/SiO_2 composites that the ultimate tensile strength for both groups increases with increasing SiO_2 nanoparticles ratio. This behavior was due to the increased effect of nanoparticles scattered between the free spaces within the chain on restricting the movement of molecular chains in the PMMA matrix as a result of the increase in the ratio of SiO_2 nanoparticles, as offer in figures (6-30) and (6-31).

Figure (6-32) represents a elongation of specimens (P0, P1, P2, P3, P4, and 5) for second group as a function of SiO_2 nanoparticles ratio, and figure (6-33) represents the elongation of specimens (R0, R1, R2, R3, R4, and R5) for third group as a function of SiO_2 nanoparticles ratio, the results for both groups showed a decrease in elongation for PMMA/SiO_2 composites specimens compared with pure PMMA (P0 and R0 specimens), this behavior was due to the distribution of stress on both the base material and the reinforcement filler, also, a decrease in elongation was observed for PMMA/SiO_2 composites with increase the SiO_2 ratio for both groups, this was due to the increase in resistance of PMMA/SiO_2 composites to the applied tensile force, the decrease in elongation was an indication of the increase in resistance.

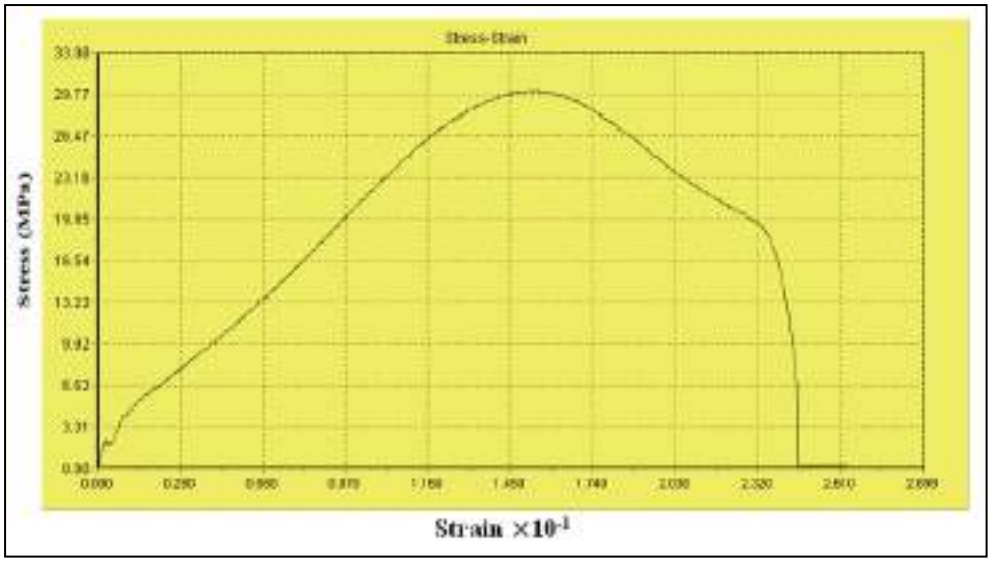

Figure (6-18) Diagram of stress against strain for P0 specimen (pure PMMA)

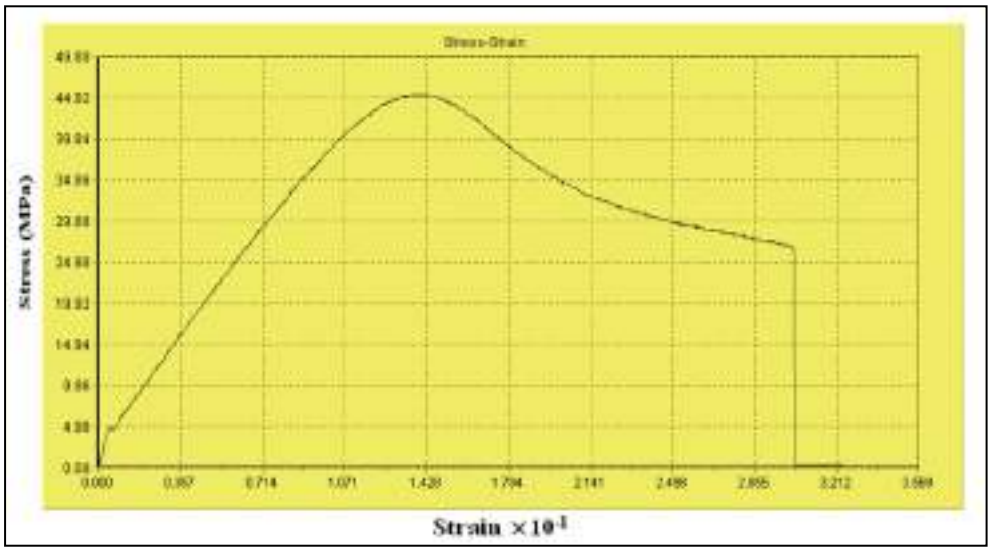

Figure (6-19) Diagram of stress against strain for P1 specimen (0.1% SiO_2).

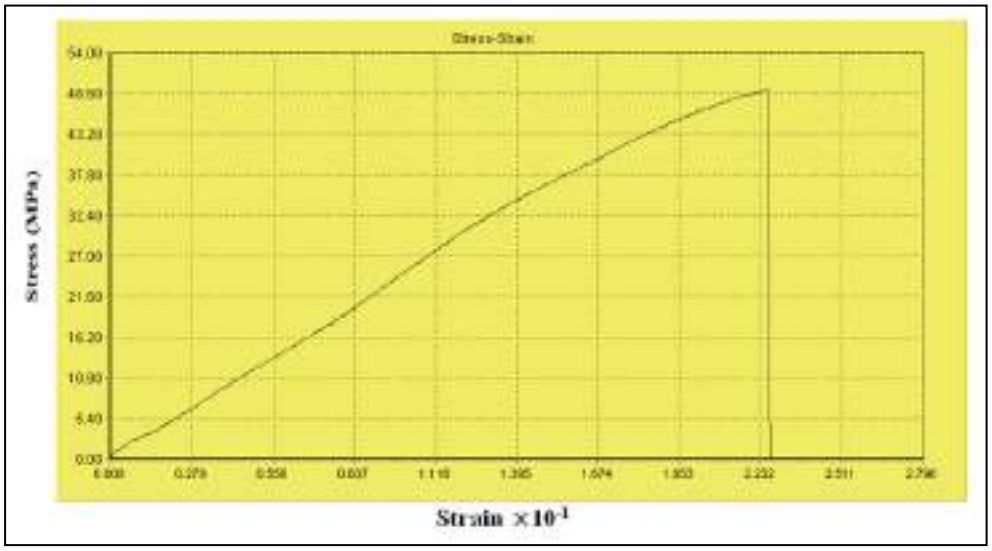

Figure (6-20) Diagram of stress against strain for P2 specimen (0.2% SiO_2).

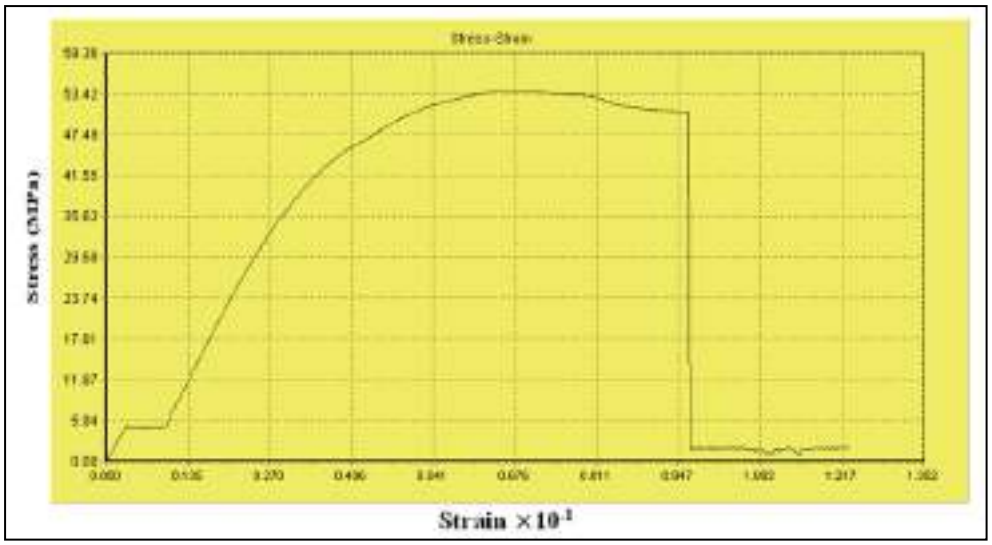

Figure (6-21) Diagram of stress against strain for P3 specimen (0.3% SiO_2).

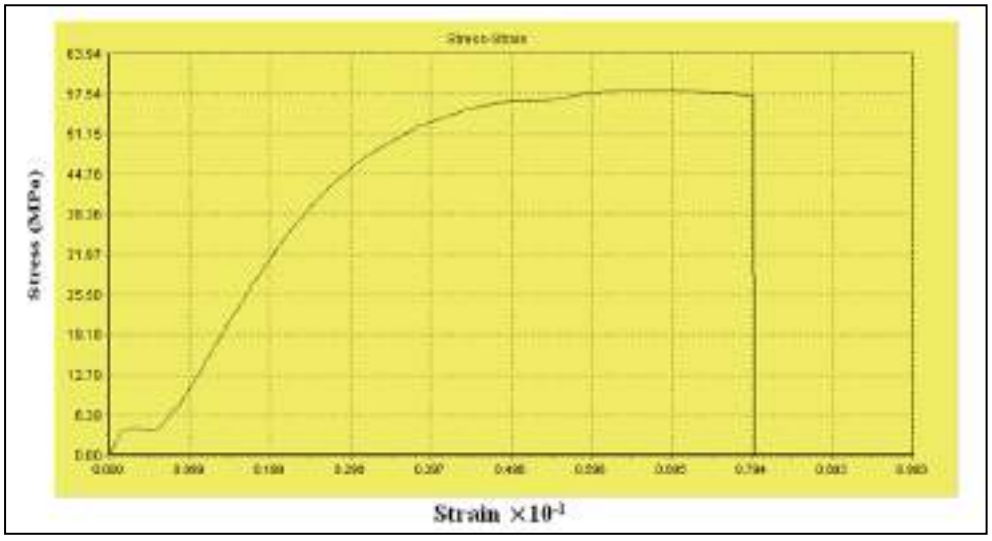

Figure (6-22) Diagram of stress against strain for P4 specimen (0.4% SiO_2).

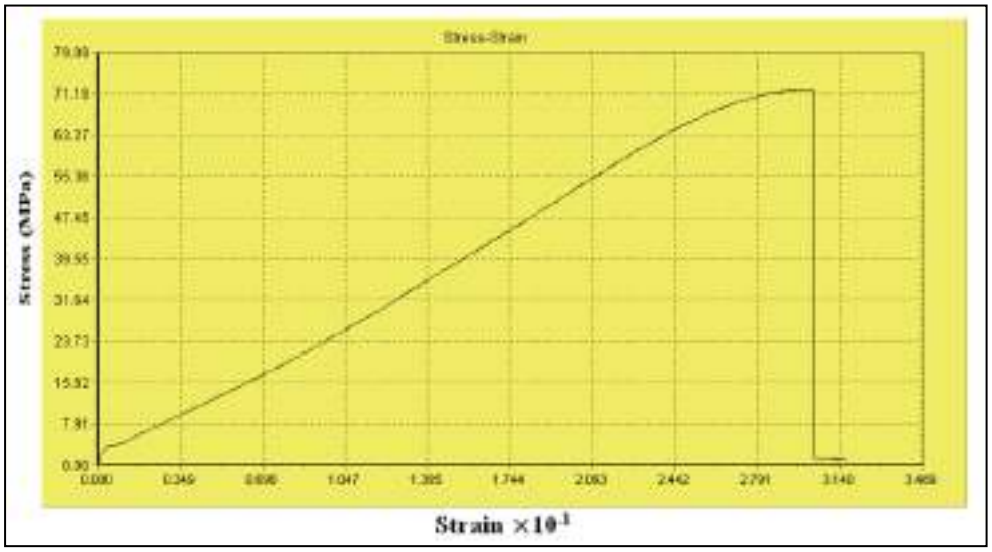

Figure (6-23) Diagram of stress against strain for P5 specimen (0.5% SiO_2).

Figure (6-24) Diagram of stress against strain for R0 specimen (pure PMMA).

Figure (6-25) Diagram of stress against strain for R1 specimen (0.1% SiO_2).

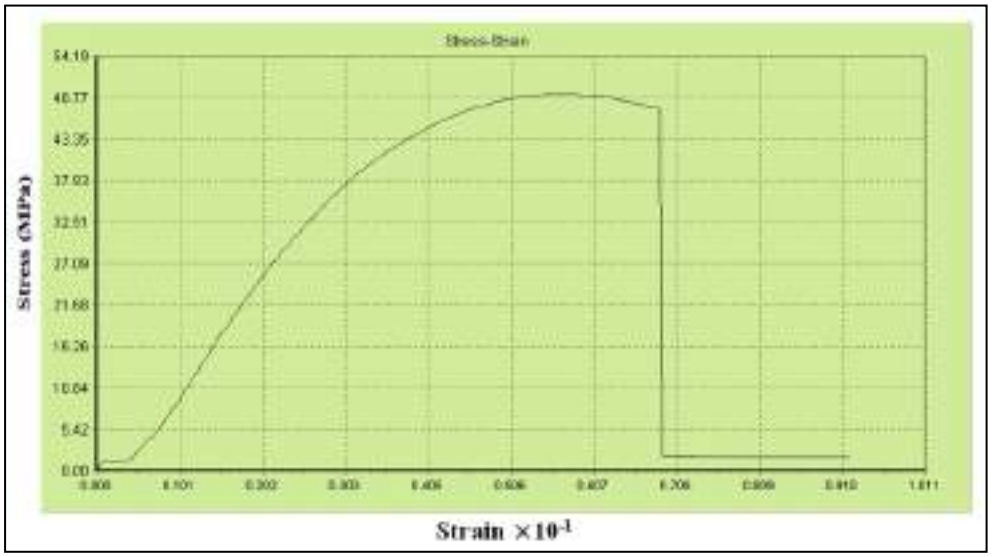

Figure (6-26) Diagram of stress against strain for R2 specimen (0.2% SiO_2).

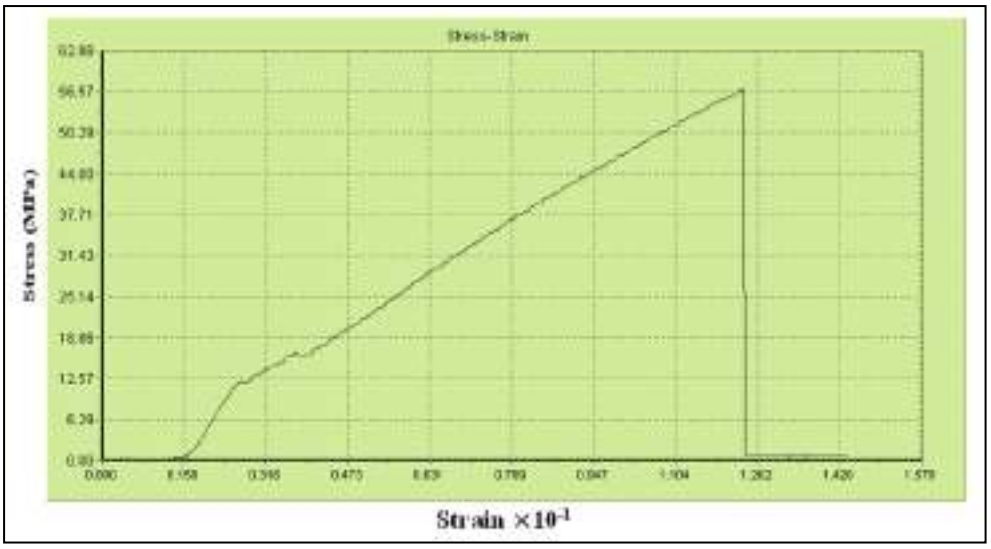

Figure (6-27) Diagram of stress against strain for R3 specimen (0.3% SiO_2).

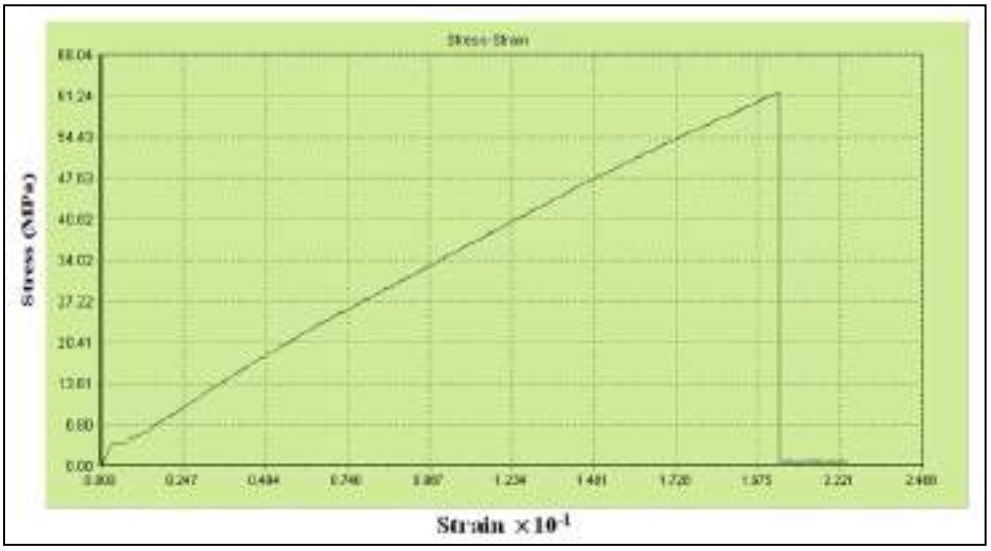

Figure (6-28) Diagram of stress against strain for R4 specimen (0.4% SiO_2).

Figure (6-29) Diagram of stress against strain for R5 specimen (0.5% SiO_2).

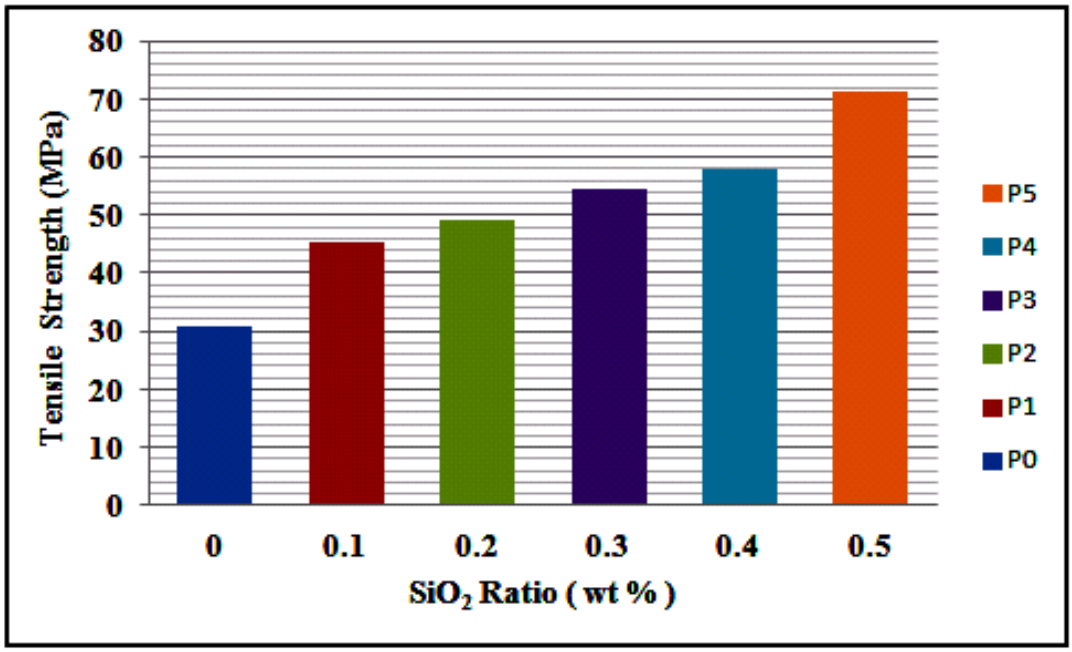

Figure (6-30) Ultimate tensile strength of specimens (P0, P1, P2, P3, P4, and P5) for second group as a function of SiO_2 nanoparticles ratio.

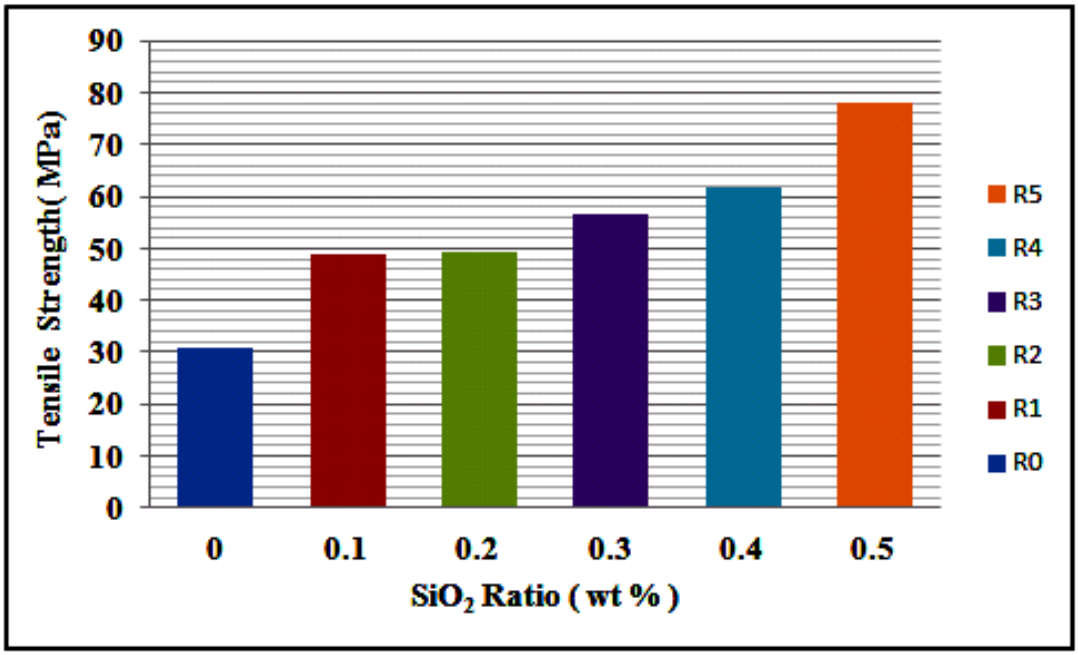

Figure (6-31) Ultimate tensile strength of specimens (R0, R1, R2, R3, R4, and R5) for third group as a function of SiO_2 nanoparticles ratio.

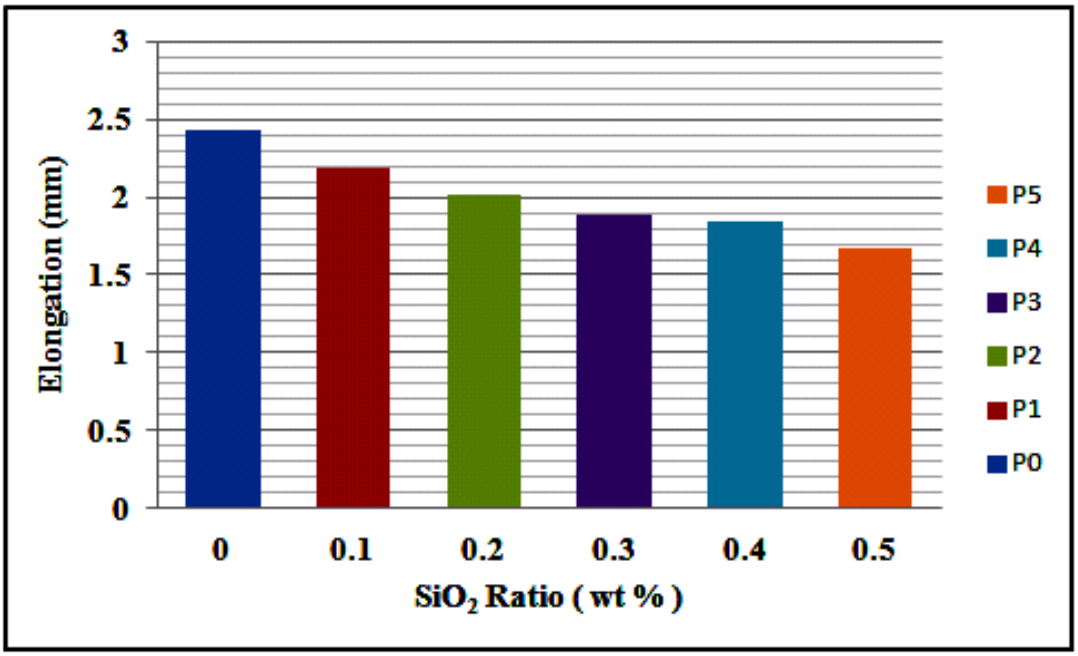

Figure (6-32) Elongation of specimens (P0, P1, P2, P3, P4, and P5) for second group as a function of SiO_2 nanoparticles ratio.

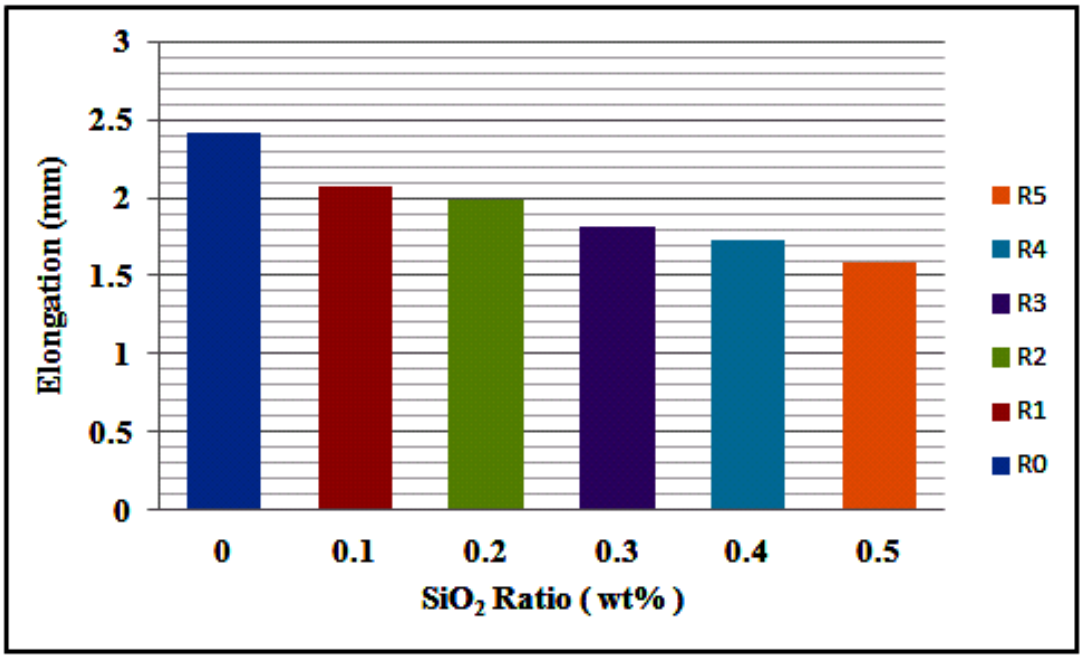

Figure (6-33) Elongation of specimens (R0, R1, R2, R3, R4, and R5) for third group as a function of SiO_2 nanoparticles ratio.

Figure (6-34) shows a comparison of the ultimate tensile strength against the ratio of SiO_2 nanoparticles between the three groups. The comparison results showed that the highest values of ultimate tensile strength occurred for the third group specimens (R specimens), where specimens were prepared using a PMMA resin and hardener, the nanoparticles were dispersed using an ultrasonic probe machine. Followed by the second group (P specimens), in which the specimens were prepared using the thermal pressing of the PMMA powder and the nanoparticles were dispersed using the nanoparticles dispersing device that designed in present study. The tensile strength values of the set B from the first group (G specimens) came in the last rank, where the specimens were prepared using PMMA granules and solvent, the nanoparticles were dispersed using magnetic stirrer.

Also, a comparison of the elongation against the ratio of SiO_2 nanoparticles was performed between the three groups, as shown in figure (6-35). It can be observed that the largest elongations occurred for the set B from the first group (G specimens) followed by the second group (P specimens), and that the smallest elongations occurred for the third group (R specimens).

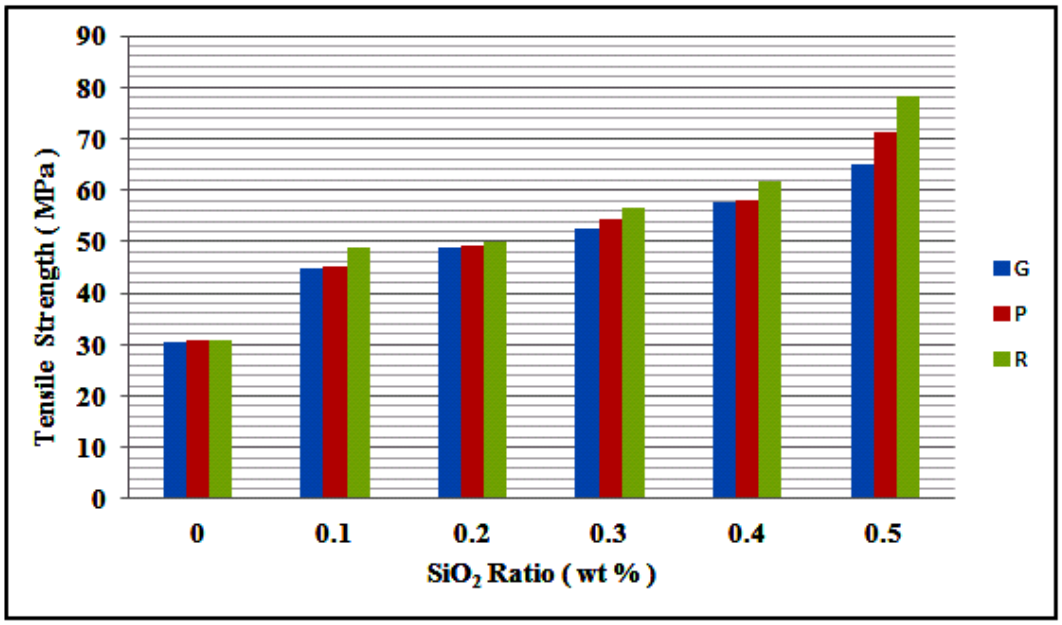

Figure (6-34) Comparison of the ultimate tensile strength against the ratio of SiO_2 nanoparticles between the three groups.

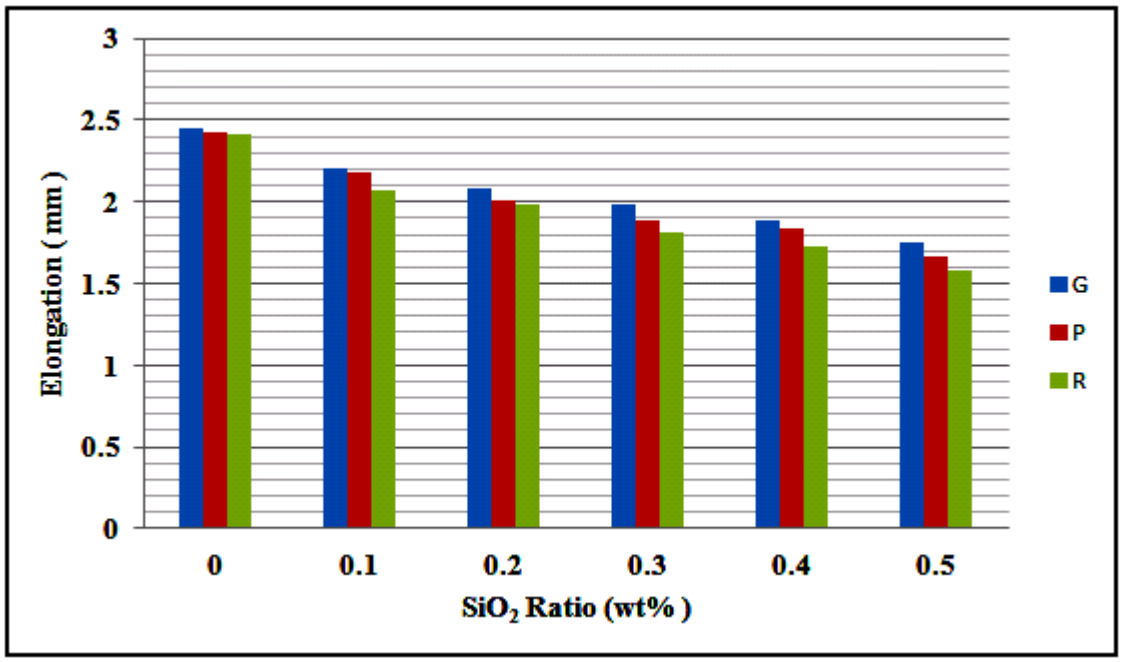

Figure (6-35) Comparison of elongation against the ratio of SiO_2 nanoparticles between the three groups.

From the results of the tensile test, for the samples containing SiO_2 ratios ranging from 1wt% to 4wt% it can be concluded that the highest value of the ultimate tensile strength and the lowest value of elongation were obtained for the sample with 1wt% SiO_2. For the samples containing SiO_2 ratios ranging from 0.1wt% to 0.5wt% it can be concluded that the value of the ultimate tensile strength increases with increasing of SiO_2 ratio and the value of elongation decreases with increasing of SiO_2, also, the best values for the ultimate tensile strength and elongation were for the samples prepared by casting method.

6.4 Results and discussion of Surface Hardness

Shore D hardness tests were performed at room temperature (23°C) using Chinese hardness device (type TH-200) in laboratories of Materials Engineering College, Babylon University. Test samples were cut based on (ASTM) D-2240, the dimensions and shape of test sample and device used were shown in figure (4-16) in chapter four. Figures (6-36 to 6-39) represent the hardness of PMMA as a function of SiO_2 nanoparticles ratio for all groups. It can be seen an improvement of the hardness for PMMA/SiO_2 composites specimens compared with pure PMMA specimens in all groups. It can also be observed that the hardness of PMMA/SiO_2 composites increases with increasing the SiO_2 nanoparticles ratio, this behavior was due to the effect of silicon oxide nanoparticles (SiO_2) where this material was characterized by high hardness and their diffusion between the molecular chains of PMMA improved the penetration resistance and thus improved the hardness. The interphase region, which is the area between the SiO_2 inorganic filler and PMMA organic polymer, mainly affects the improvement of the properties of the resulting PMMA / SiO_2 composite, it depends on the type of coupling agent used. The silane coupling agent acts like a bonding agent to enhancement the adhesion between PMMA and SiO_2. Many desired changes can be obtained as a result of modification of the interphase region such as improve the SiO_2 distracting in PMMA, reduce viscosity and improve hardness and scratch resistance by formation of overlapping polymer networks. Hasanen A. and Mohammed M. explained the effect of adding SiO_2 nanoparticles on the PMMA resin hardness, their results showed a significant increase in hardness at the SiO_2 nanoparticles ratios of (3, 5, and 7 wt %) [104].

Figure (6-40) represents the comparison of the hardness as a function of SiO_2 nanoparticles ratio between the three groups. It can be observed that the largest values of the hardness occurred for the specimens of the second group (P specimens) and this was due to the use of pressure (hydraulic thermal press)

in the preparation of this group of specimens, where the pressure leads to reduce the interfaces between PMMA chains and makes them more close, and therefore increases of the hardness, then followed by the specimens of the third group (R specimens), and that the smallest values of the hardness occurred for the specimens of set B from the first group (G specimens). Table (6-3) shows the percentages of increase in hardness for the G, P, and R specimens compared to the S specimens.

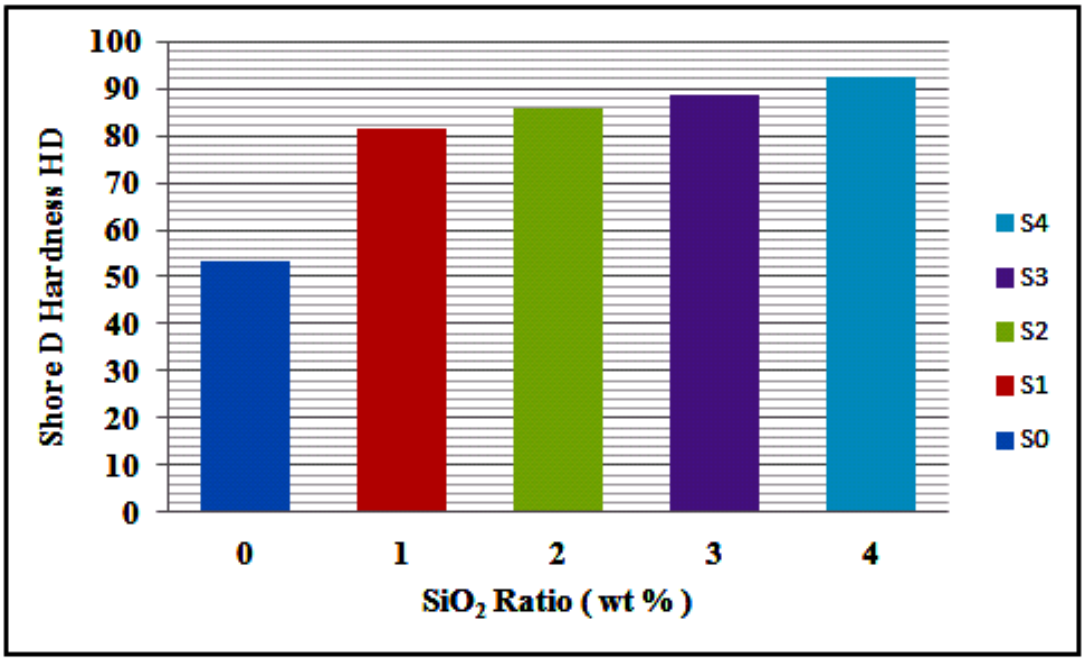

Figure (6-36) Hardness of the S specimens (set A from first group) against the ratio of SiO_2 nanoparticles.

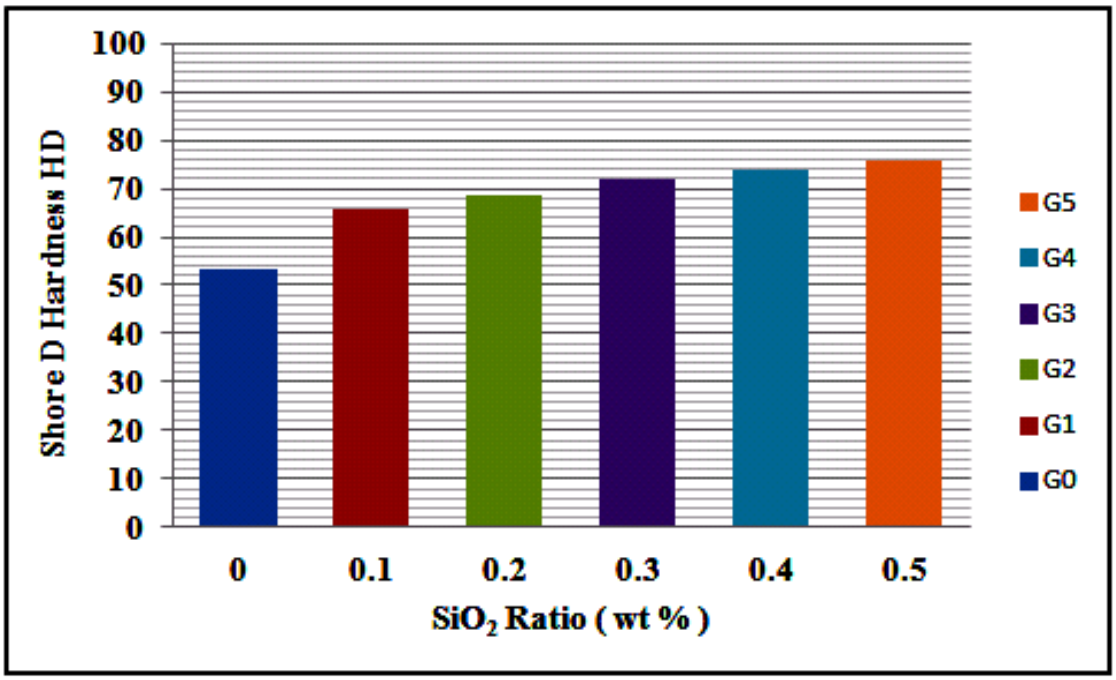

Figure (6-37) Hardness of the G specimens (set B from first group) against the ratio of SiO_2 nanoparticles.

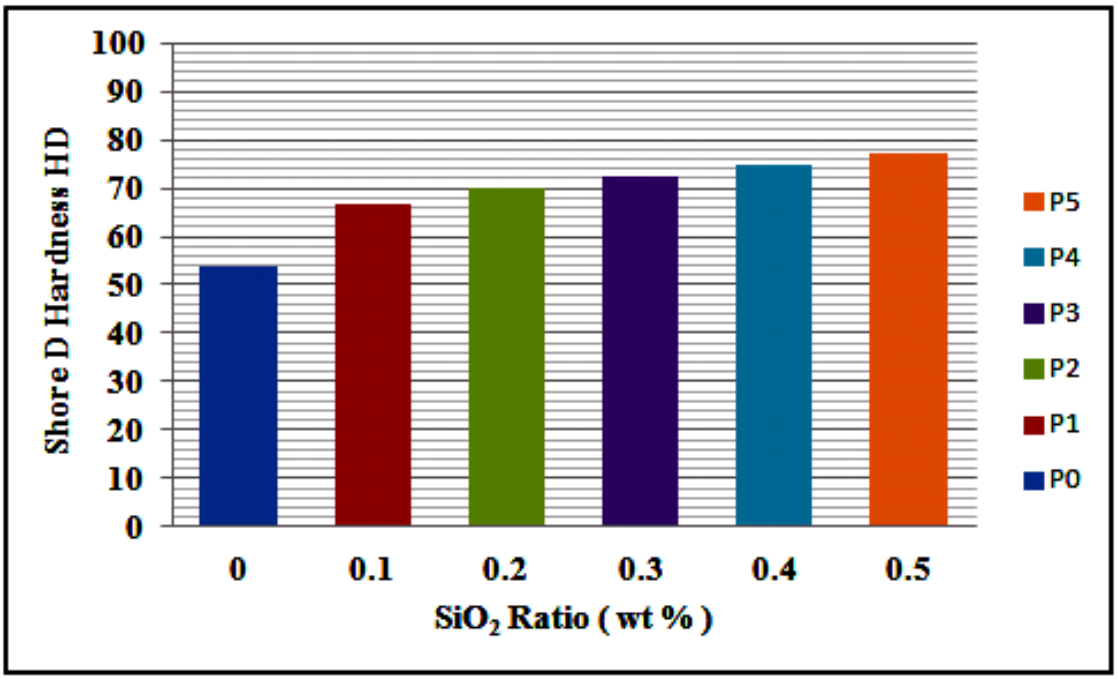

Figure (6-38) Hardness of the P specimens (second group) against the ratio of SiO_2 nanoparticles.

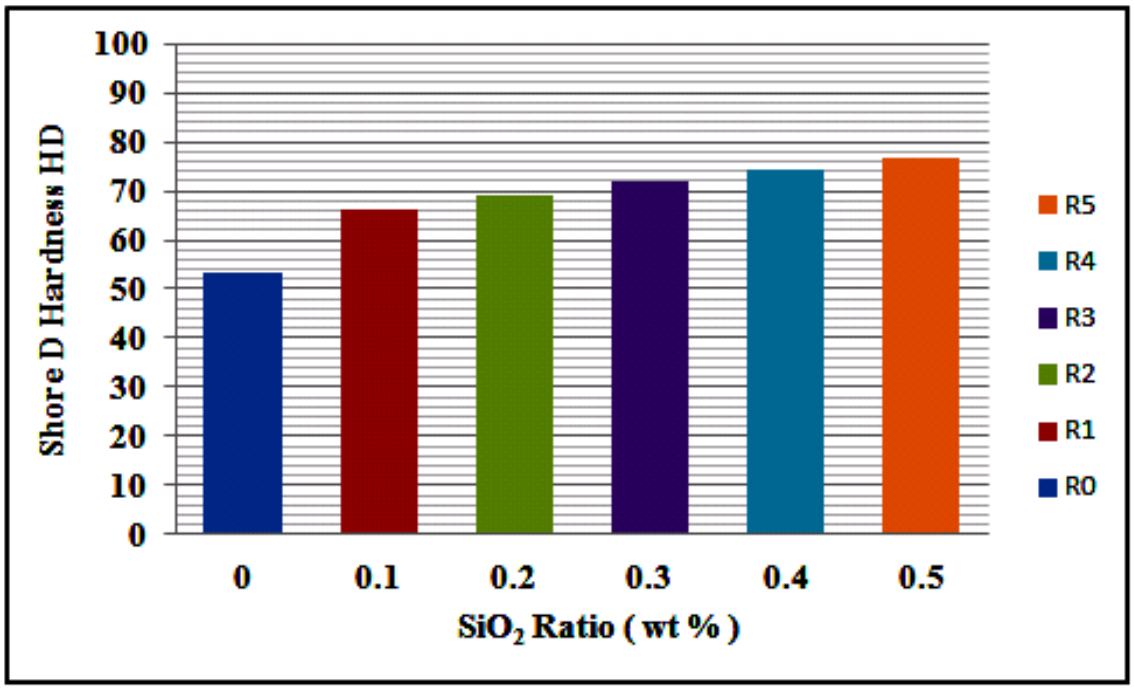

Figure (6-39) Hardness of the R specimens (third group) against the ratio of SiO_2 nanoparticles.

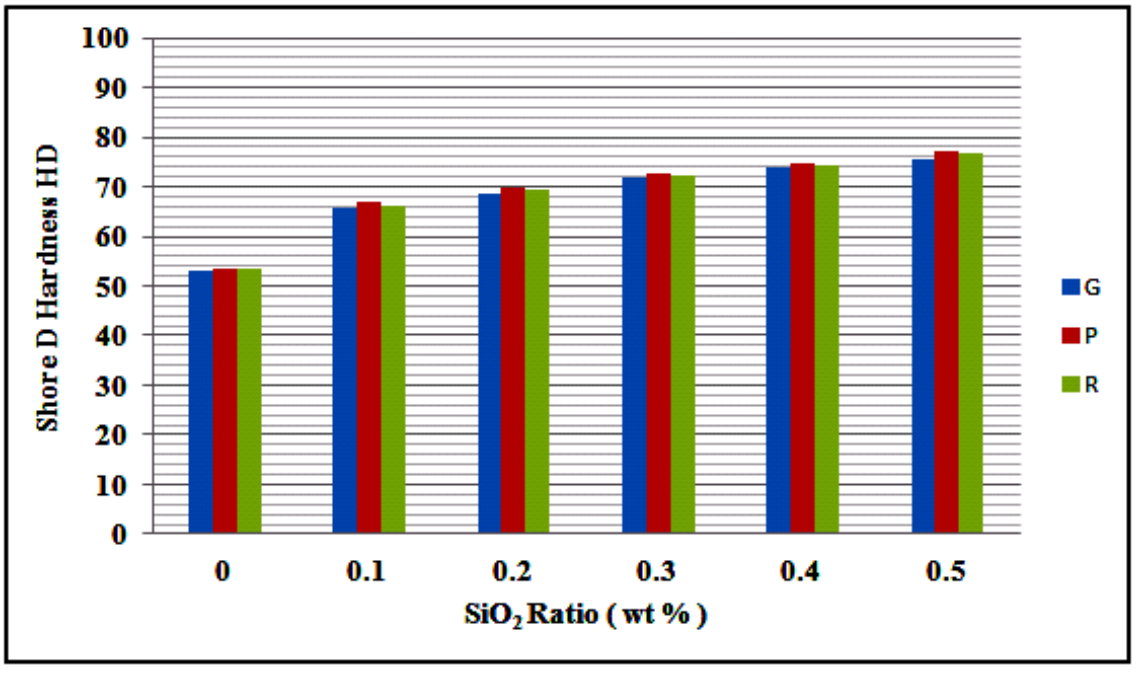

Figure (6-40) Comparison of hardness against the ratio of SiO_2 nanoparticles between the three groups.

Table (6-3) The percentages of increase in hardness for the G, P, and R specimens compared to the S specimens.

Specimen code	SiO_2 Ratio (wt %)	Surface Hardness (HD)	Increase in Hardness (%)
S0	**0**	**53.4**	**-----**
S1	**1**	**81.3**	**52.25 %**
S2	**2**	**85.5**	**60.11 %**
S3	**3**	**88.6**	**65.91 %**
S4	**4**	**92.3**	**72.85 %**
G0	**0**	**53.2**	**-----**
G1	**0.1**	**65.7**	**23.49 %**
G2	**0.2**	**68.5**	**28.76 %**
G3	**0.3**	**71.7**	**34.77 %**
G4	**0.4**	**73.8**	**38.72 %**
G5	**0.5**	**75.6**	**42.11 %**
P0	**0**	**53.6**	**-----**
P1	**0.1**	**66.8**	**24.63 %**
P2	**0.2**	**69.8**	**30.22 %**
P3	**0.3**	**72.6**	**35.45 %**
P4	**0.4**	**74.9**	**39.74 %**
P5	**0.5**	**77.3**	**44.22 %**
R0	**0**	**53.3**	**-----**
R1	**0.1**	**66.1**	**24.02 %**
R2	**0.2**	**69.2**	**29.83 %**
R3	**0.3**	**72.1**	**35.27 %**
R4	**0.4**	**74.2**	**39.21 %**
R5	**0.5**	**76.8**	**44.09 %**

From the results of the hardness test, it can be concluded that the magnitude of increase in the hardness for the samples containing 0.5wt% of SiO_2 does not change much from the magnitude of increase in the hardness for the sample that contains 1 wt% of SiO_2, this is indicates the correctness of the decision to reduce the SiO_2 ratios in order to maintain the transmittance of PMMA. For samples with SiO_2 ratios ranging from 0.1wt% to 0.5 wt%, it can be concluded that the best hardness values obtained for the samples prepared by pressing method.

6.5 Results and discussion of Surface Roughness.

Surface Roughness tests were performed at room temperature (23 °C) using the surface roughness test device type HSR210. The dimensions of the specimens used in the test were (40×20×3) length, width, and thickness, respectively all in mm. Tests were conducted in the laboratories of Materials Engineering College at Babylon University. Figures (6-41 to 6-44) represent the surface roughness against the SiO_2 nanoparticles ratio for the three groups. It can be observed that the surface roughness of pure PMMA specimens and PMMA/SiO_2 composite specimens in the same group was approximately equal; the reason for this was due to the approved preparation method for each group of specimens as well as to surface finishing processes and there was no effect of SiO_2 nanoparticles on the surface smoothness. Figure (6-45) represents a comparison of surface roughness against the SiO_2 nanoparticles ratio between the three groups. It can be noted that the best surface smoothness obtained for the specimens of the P specimens (second group), the reason for this was due to that the specimens of this group were prepared using heat and pressure, which gives it another factor of smoothness in addition to factor of the casting in molds, then followed by the R specimens (third group), and the specimens of set B from the first group (G specimens) came in the last rank.

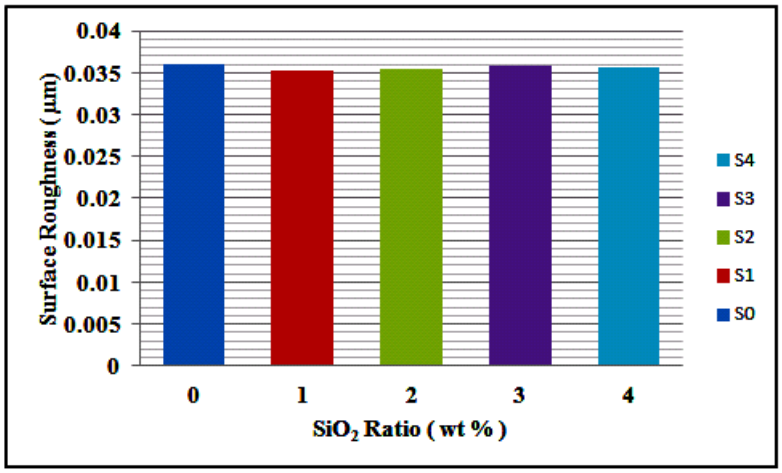

Figure (6-41) Surface roughness of the S specimens (set A from first group) against the SiO_2 nanoparticles ratio.

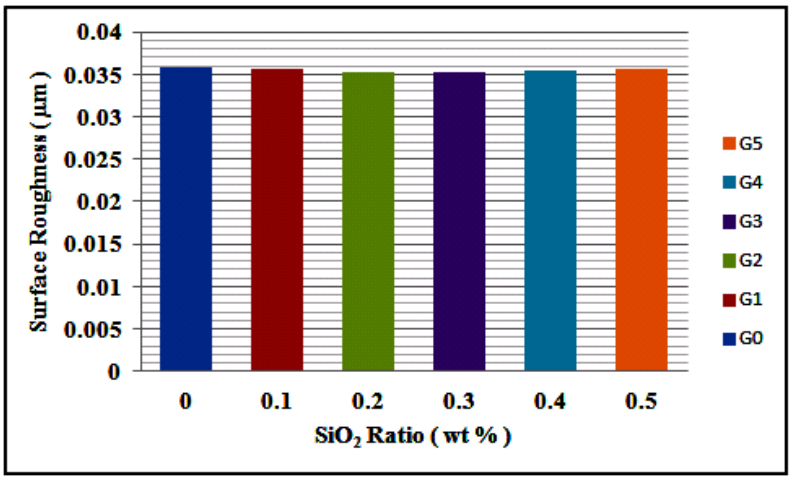

Figure (6-42) Surface roughness of the G specimens (set B from first group) against the SiO_2 nanoparticles ratio.

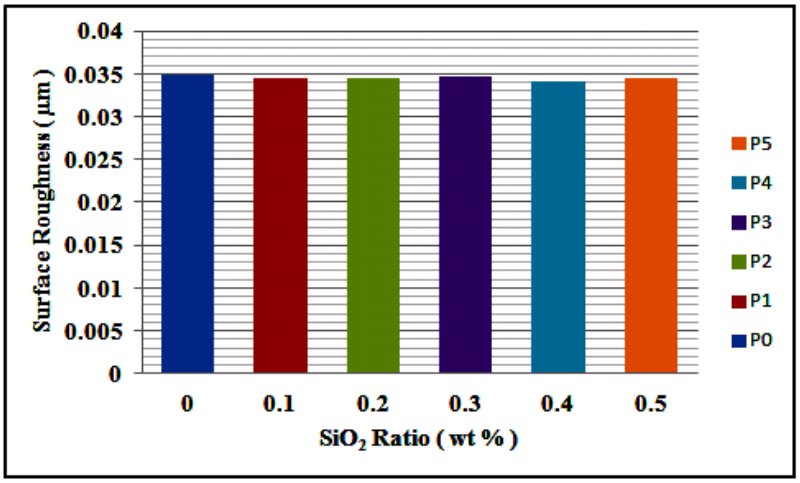

Figure (6-43) Surface roughness of the P specimens (second group) against the SiO_2 nanoparticles ratio.

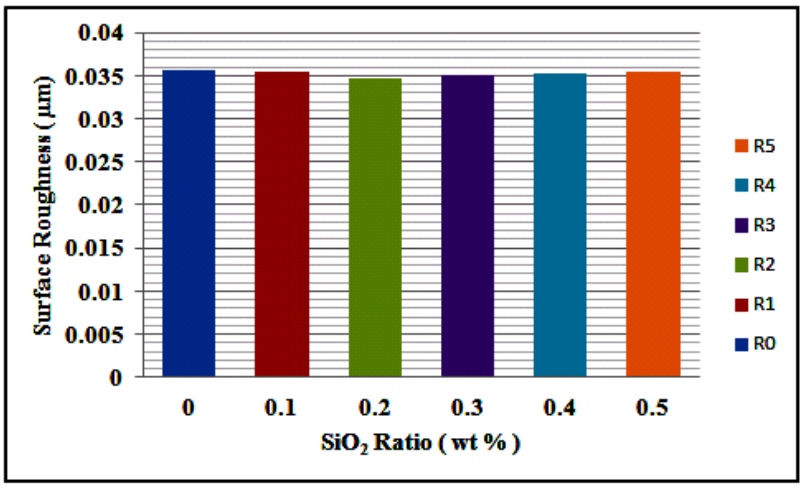

Figure (6-44) Surface roughness of the P specimens (second group) against the SiO_2 nanoparticles ratio.

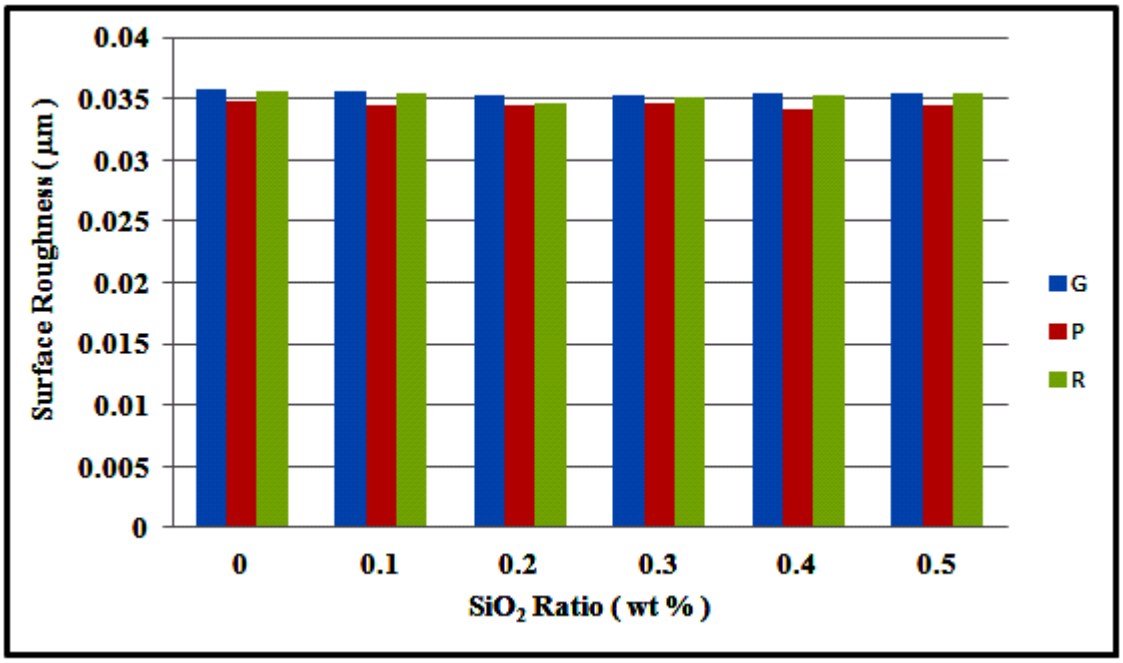

Figure (6-45) Comparison of surface roughness against the SiO_2 nanoparticles ratio between the three groups.

6.6 Results and discussion of Scratch Resistance.

Scratch resistance tests were conducted with sliding velocity of 20 mm/s and the scratch path length of 100 mm to scratch all specimens at room temperature (23°C) using the automated scratch device designed in this work. The test was conducted in two stages, the first using a stainless steel indenter with a conical tip with a radius of 0.3 mm and apex angle of 60^{o} and the applied normal load from 1 N to 30 N. The second using a spherical indenter from stainless steel with diameter of 1 mm and the applied normal load from 1 N to 70 N. The specimens used for the test were cut according to ASTM 7027-5 where the dimensions of the scratch test specimen were 60 mm for width, 140 mm for length and 4 mm for thickness. The normal load applied to start the scratch, measured tangential force, and friction coefficient for both stages were recorded in tables (6-4) and (6-5) respectively. The applied normal load required to start the scratch for each specimen was obtained using small dead weights and increased gradually during the scratch test until the minimum load required to start the scratch was reached, figures (6-46 and 6-47) show images of scratching during applying the normal load to obtain the minimum normal load required for scratching using conical and spherical indenters, pictures were taken using a digital microscope.

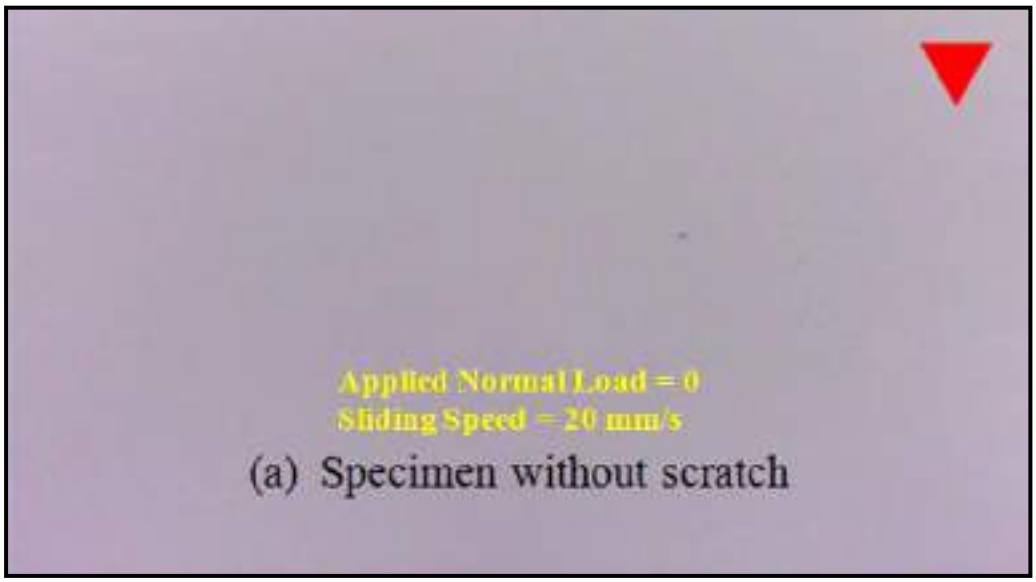
Applied Normal Load = 0
Sliding Speed = 20 mm/s
(a) Specimen without scratch

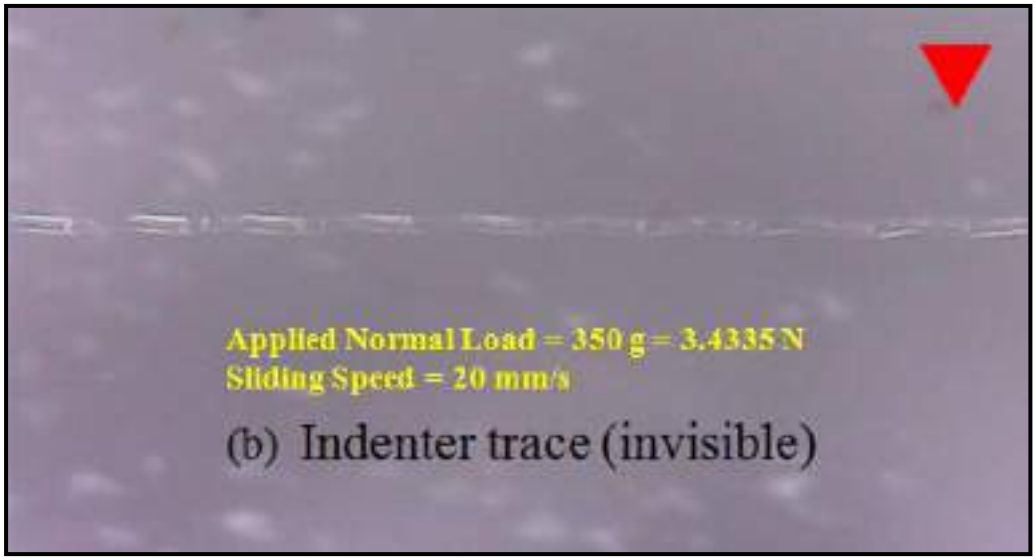
Applied Normal Load = 350 g = 3.4335 N
Sliding Speed = 20 mm/s
(b) Indenter trace (invisible)

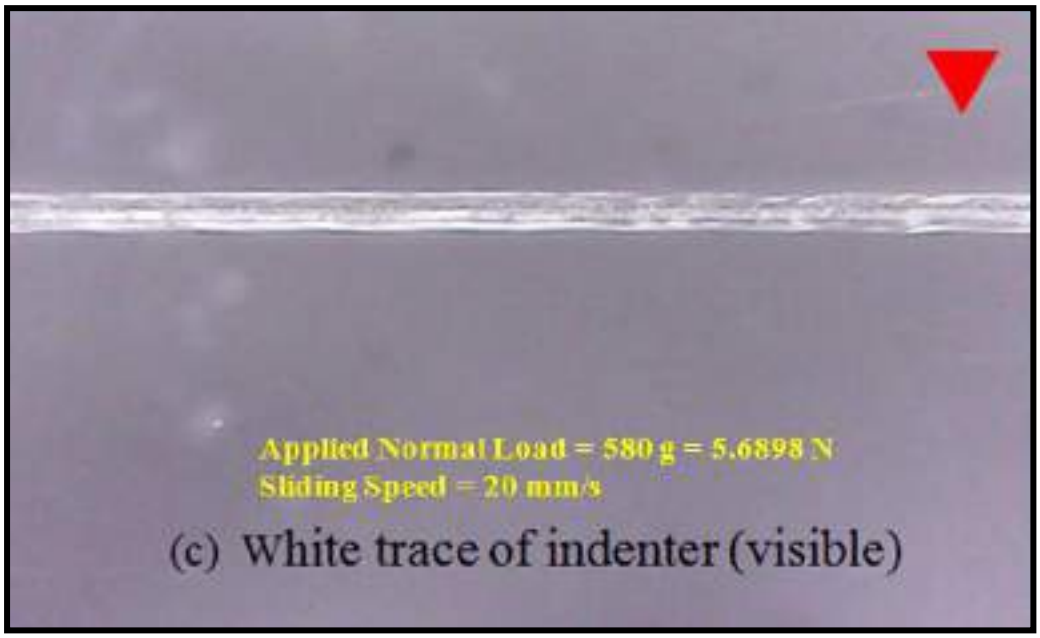
Applied Normal Load = 580 g = 5.6898 N
Sliding Speed = 20 mm/s
(c) White trace of indenter (visible)

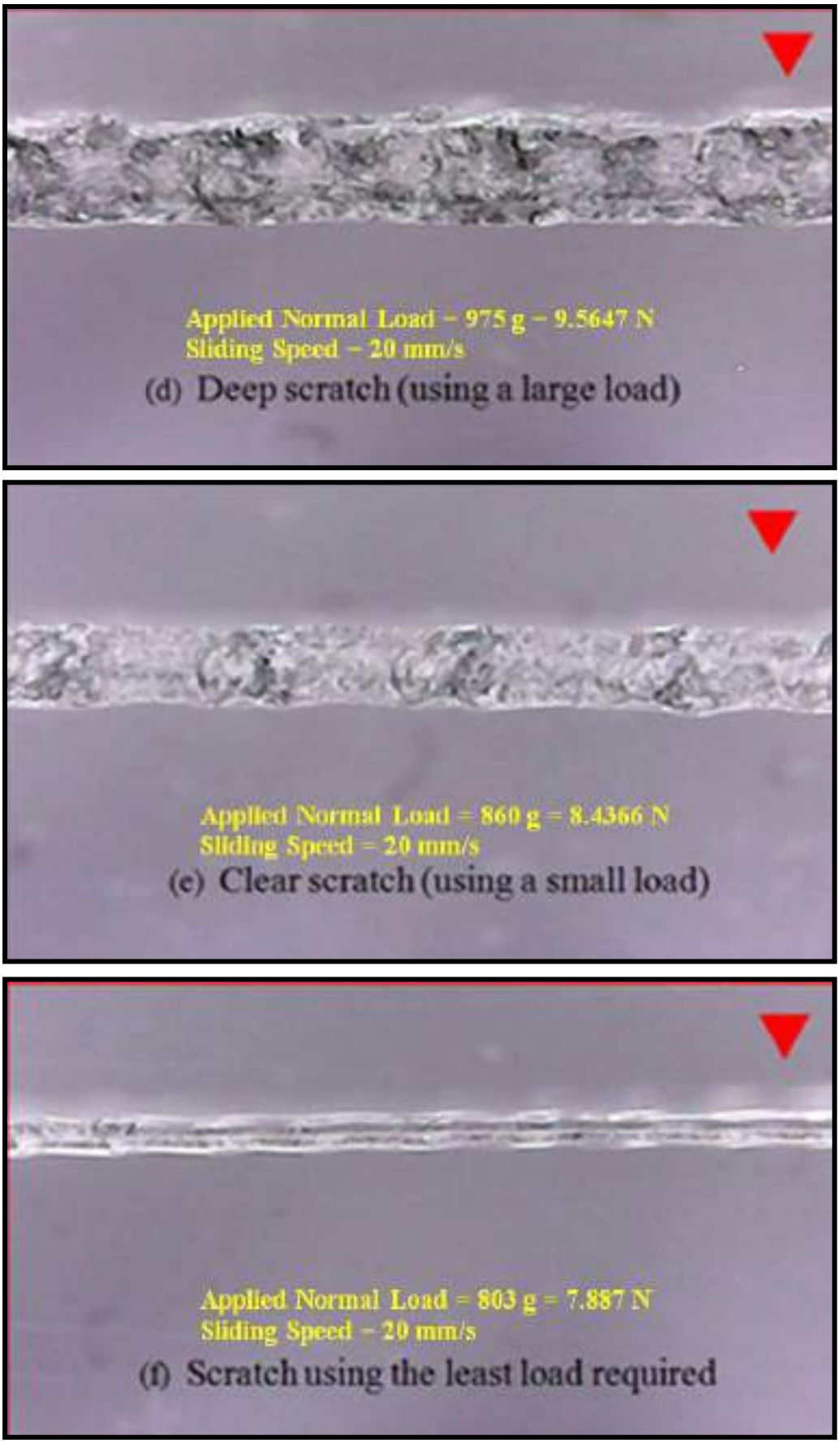

Figure (6-46) Scratch stages of the R0 specimen using a conical indenter.

(a) Specimen without scratch

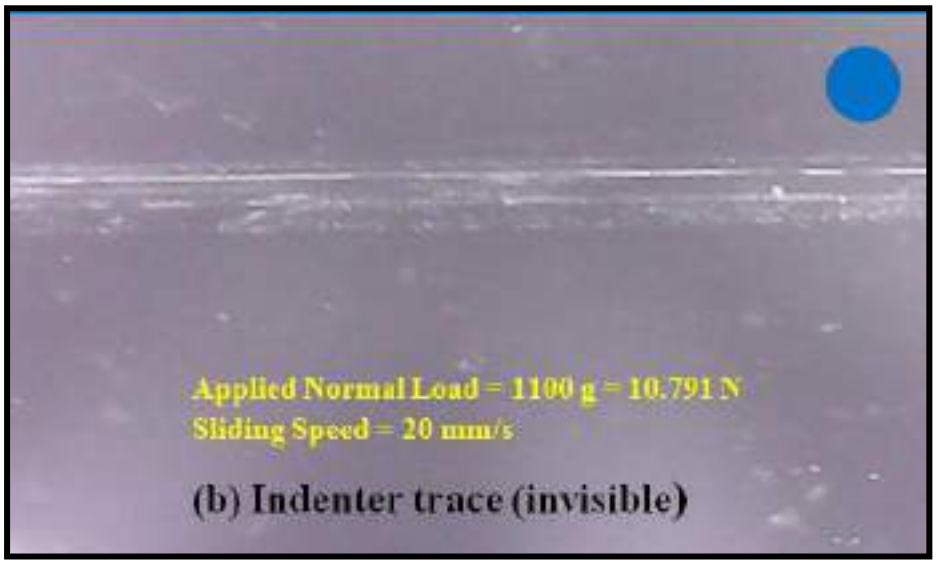

(b) Indenter trace (invisible)

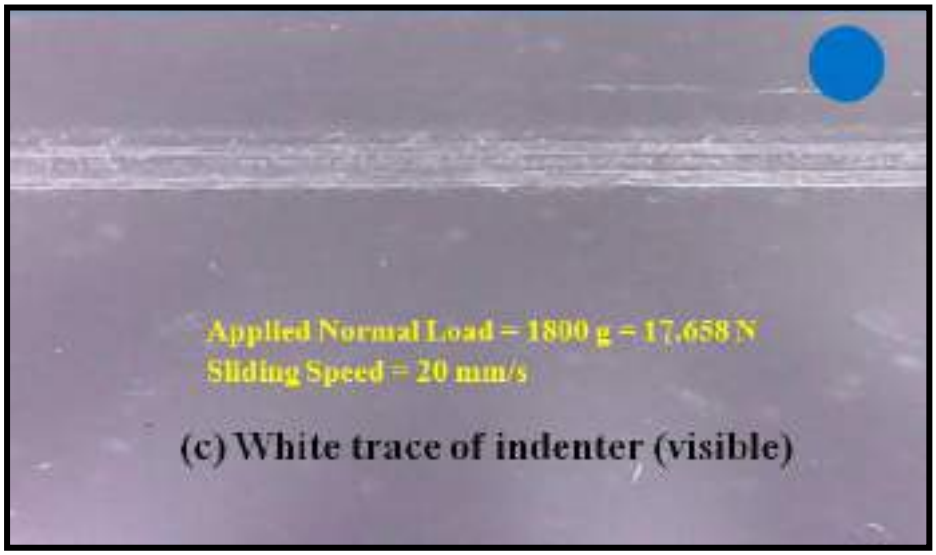

(c) White trace of indenter (visible)

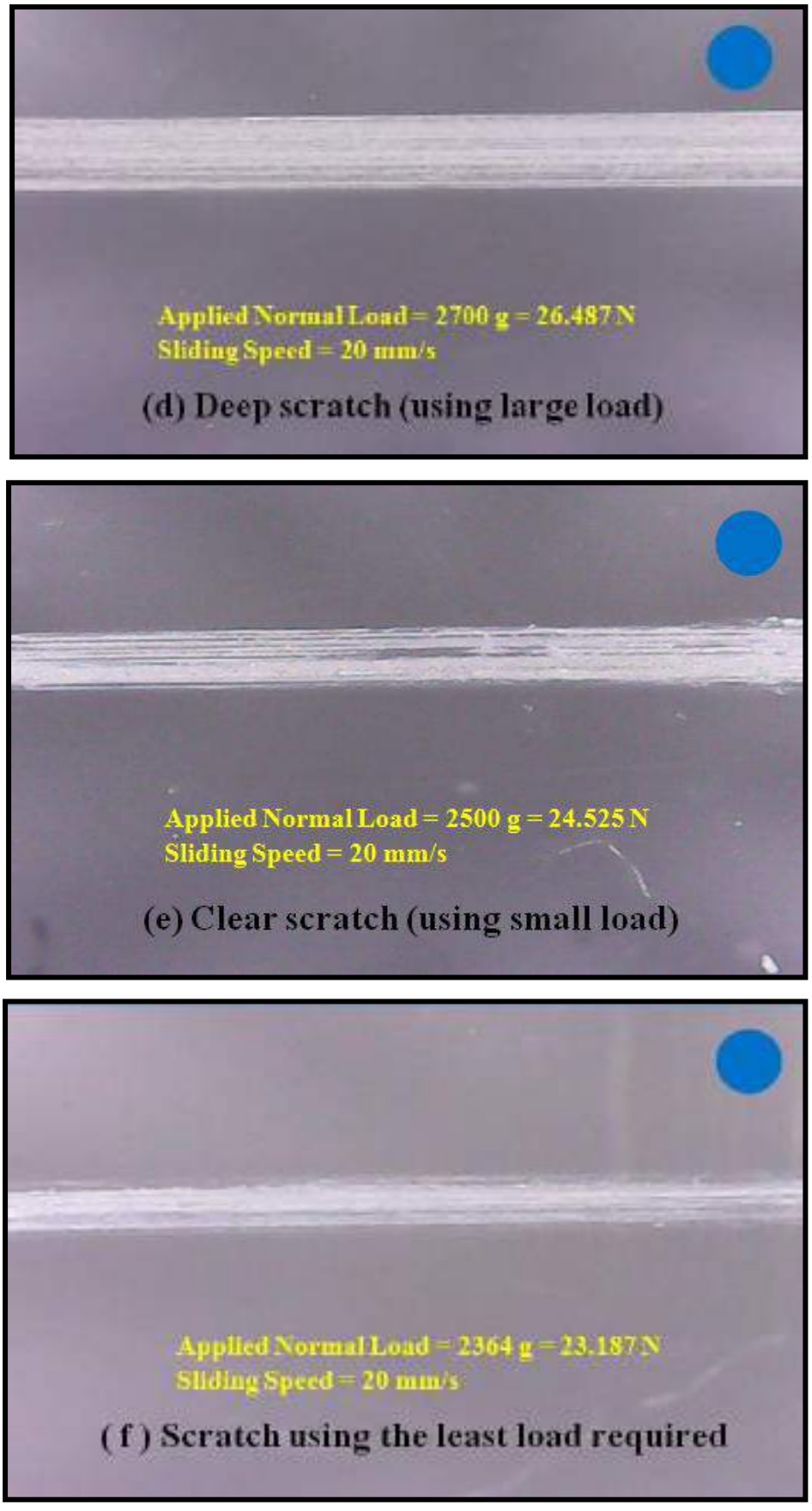

Figure (6-47) Scratch stages of the R0 specimen using a spherical indenter.

Figures (6-48 to 6-51) display the distribution of tangential force (F_t) against the scratch path length (100 mm) for each specimen of the PMMA by using the conical and spherical indenter. It can be noted that the values of tangential force (F_t) were approximately equal at all points along the scratch path of each specimen and this was good evidence of the uniform distribution of SiO_2 nanoparticles within the PMMA matrix. It can also be observed that the tangential force of the PMMA/SiO_2 composites was greater than the tangential force of pure PMMA; it was also observed that the tangential force of the PMMA/SiO_2 composites increases when the ratio of SiO_2 nanoparticles increases. The reason was that with the increase of nanoparticles, the scratch resistance increases due to the increasing of the surface hardness.

Figures (6-52 to 6-55) represent the applied normal load (F_n) required to starting the scratch for each group of the PMMA specimens against the SiO_2 nanoparticles ratio by using the conical and spherical indenter. The results show that the applied load for PMMA/SiO_2 composites was greater than that for the pure PMMA, and the applied load for PMMA/SiO_2 composites increases with increasing of SiO_2 nanoparticles ratio when using both types of indenters, due to increasing of scratch resistance as a result of increasing in the surface hardness because the addition of nanoparticles which were characterized by high hardness and the ability to form overlapping PMMA networks. The results also showed that the applied loads required to start scratching using the spherical indenter were greater than that the applied loads required to start scratching using the conical indenter, these results clearly show the effect of indenter geometry on scratch resistance in PMMA. The value of applied normal load required to start scratch on the surface of the polymeric material is greatly influenced by the geometry of the indenter, this value does not mean anything without accurate

description of the tip used [19]. Ezio Amerio et al. [101] carried out a comparison of scratch resistant behavior between PMMA coating films obtained through double-processing with those of PMMA coating films containing pre-formed Nano SiO_2 Particles. The pre-formed nano SiO_2 particles (Aerosil TT600 silica nanoparticles) at the ratios of 5 wt% and 10 wt% were dispersed by ultrasonication device for 30 minutes. Their results showed high scratch resistance for coatings obtained by double-processing while low scratch resistance for coatings obtained by dissipating the pre-formed nano-silica within the PMMA resin.

The friction coefficient μ for each PMMA specimen can be calculated by dividing the measured tangential force (F_t) which represents device output on the applied normal load (F_n) which represents device input. Figures (6-56 to 6-59) show the friction coefficients of pure PMMA and PMMA/SiO_2 composites against the SiO_2 nanoparticles ratio along length of the scratch path of 100 mm, it can be noted that the friction coefficients of the PMMA/SiO_2 composites were lower compared to pure PMMA. A decrease in the friction coefficient of PMMA/SiO_2 composites was also observed when the ratio of nanoparticles increases. Decreasing in friction coefficient refers to increase in the hardness and scratch resistance of the PMMA due to the addition of high hardness SiO_2 nanoparticles.

Figure (6-60) represents a comparison of applied normal load against the SiO_2 nanoparticles ratio between the three groups by using the conical and spherical indenter. It can be noted that the largest applied load obtained for the specimens of the second group (P specimens), this was due to the use of pressure (hydraulic thermal press) in the preparation of this group of specimens, where the pressure leads to reduce the interfaces between PMMA chains and

makes them closer, and therefore increases of the hardness which leads to increasing scratch resistance, then followed by the specimens of the third group (R specimens), and the specimens of set B from the first group (G specimens) came in the last rank.

Figure (6-61) represents a comparison of friction coefficient against the SiO_2 nanoparticles ratio between the three groups by using the conical and spherical indenter. It can be observed that the lowest friction coefficients occurred for the P specimens as a result of increase scratch resistance then followed by the specimens of the third group (R specimens), and then specimens of set B from the first group (G specimens).

It was clear from the results of the friction coefficients of the S specimens in figure (6-56) that the best ratio of adding the SiO_2 nanoparticles was 4wt % compared to other ratios when using the conical and spherical indenter. The ratio of SiO_2 nanoparticles in the rest groups (G, P and R specimens, respectively), was reduced to become from 0.1wt% to 0.5 wt% at an increase rate of about 0.1 wt% as mentioned previously, this was due to the desire not to influence the transmittance advantage of PMMA and for there to be economic benefit for the current study. Figure (6-62) illustrates the comparison of friction coefficients against the SiO_2 nanoparticle ratio between the G5, P5 and R5 specimens (0.5 wt% of SiO_2 for each one) with the friction coefficient of the S4 specimen (4wt% SiO_2) when using two types of indenter. The comparison results showed that although SiO_2 ratios of G5, P5, and R5 specimens were reduced by 87.5% from SiO_2 ratio of S4 specimen, the friction coefficients of these specimens were not significantly affected as shown in table (6-6). Also, these results reinforced the decision correctness to reduce nanoparticles ratios in order to there will be an economic benefit for current study.

Finally, it is necessary to explain the effect of changing the sliding speed on the scratch resistance behavior of pure PMMA and PMMA/SiO_2 composites. It was observed through experimental work that the indenter's behavior in removing matter during high-speed motion was in the form of removing small pieces (shrapnel) for both types of the indenters, this behavior was different than behavior in slow- speed motion. This was caused by the change in the strain rate due to a change in the sliding speed, where the strain rate was equal to the tip speed divided by the width of the scratch groove ($\dot{\epsilon} = V_{tip} / w$), also, by increasing the sliding speed , the brittleness of the PMMA material increases, and thus leads to an early fracture. This behavior was not illustrated in photographs due to the unavailability of an instantaneous microscopic imaging device.

Table (6-4) Applied normal loads (F_n) required for scratching, measured tangential forces (F_t) and friction coefficients (μ) for all specimens using conical indenter.

Specimen code	SiO_2 Ratio (wt %)	Normal Load required for scratching F_n (N)	Measured Tangential Force F_t (N)	Friction Coefficient $\mu = F_t / F_n$
S0	**0**	**7.835**	**4.356**	**0.556**
S1	**1**	**18.032**	**6.185**	**0.343**
S2	**2**	**19.838**	**6.368**	**0.321**
S3	**3**	**20.723**	**6.528**	**0.315**
S4	**4**	**24.037**	**7.115**	**0.296**
G0	**0**	**7.782**	**4.319**	**0.555**
G1	**0.1**	**8.924**	**4.498**	**0.504**
G2	**0.2**	**9.443**	**4.551**	**0.482**
G3	**0.3**	**10.175**	**4.702**	**0.462**
G4	**0.4**	**11.092**	**4.782**	**0.431**
G5	**0.5**	**12.625**	**4.821**	**0.382**
P0	**0**	**8.105**	**4.482**	**0.553**
P1	**0.1**	**9.721**	**4.792**	**0.493**
P2	**0.2**	**10.942**	**4.935**	**0.451**
P3	**0.3**	**11.724**	**5.018**	**0.428**
P4	**0.4**	**12.917**	**5.102**	**0.395**
P5	**0.5**	**14.083**	**5.225**	**0.371**
R0	**0**	**7.887**	**4.371**	**0.554**
R1	**0.1**	**9.155**	**4.587**	**0.501**
R2	**0.2**	**9.981**	**4.621**	**0.463**
R3	**0.3**	**10.875**	**4.763**	**0.438**
R4	**0.4**	**11.573**	**4.803**	**0.415**
R5	**0.5**	**13.341**	**5.003**	**0.375**

Table (6-5) Applied normal loads (F_n) required for scratching, measured tangential forces (F_t) and friction coefficients (μ) for all specimens using spherical indenter.

Specimen code	SiO_2 Ratio (wt %)	Normal Load required for scratching F_n (N)	Measured Tangential Force F_t (N)	Friction Coefficient $\mu = F_t / F_n$
S0	0	21.154	11.741	0.555
S1	1	50.489	17.418	0.345
S2	2	56.935	18.561	0.326
S3	3	59.682	19.158	0.321
S4	4	64.899	19.534	0.304
G0	0	21.789	12.071	0.554
G1	0.1	25.879	12.965	0.501
G2	0.2	27.573	13.207	0.479
G3	0.3	29.405	13.467	0.458
G4	0.4	32.611	13.859	0.425
G5	0.5	37.622	14.334	0.381
P0	0	23.828	13.153	0.552
P1	0.1	28.774	14.128	0.491
P2	0.2	31.841	14.265	0.448
P3	0.3	34.586	14.629	0.423
P4	0.4	38.492	15.051	0.391
P5	0.5	41.685	15.341	0.368
R0	0	23.187	12.822	0.553
R1	0.1	26.732	13.339	0.499
R2	0.2	29.244	13.481	0.461
R3	0.3	31.755	13.813	0.435
R4	0.4	34.603	14.222	0.411
R5	0.5	39.489	14.691	0.372

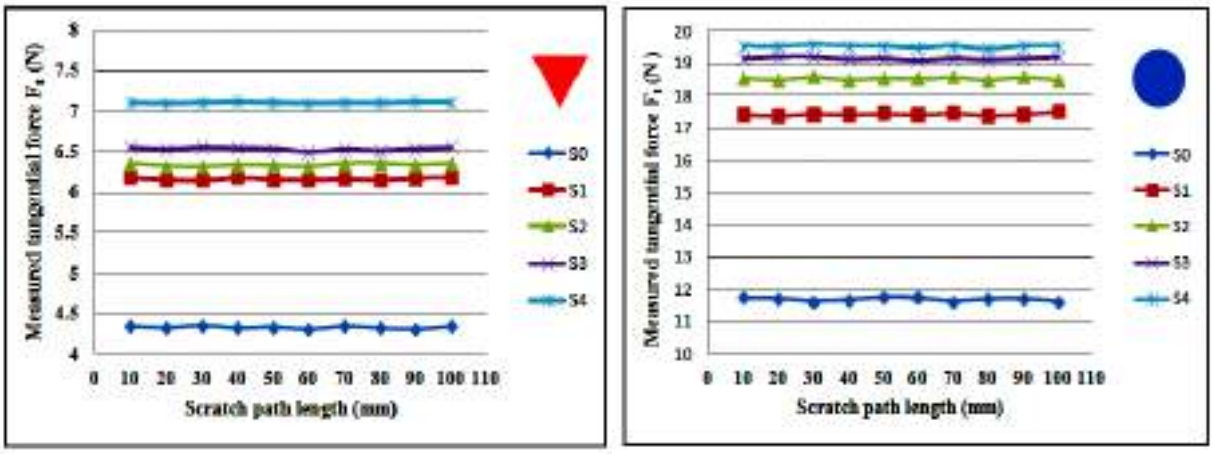

(a) (b)

Figure (6-48) Measured tangential force F_t of the S specimens (set A from first group) against scratch path length, using indenter (a) conical and (b) spherical.

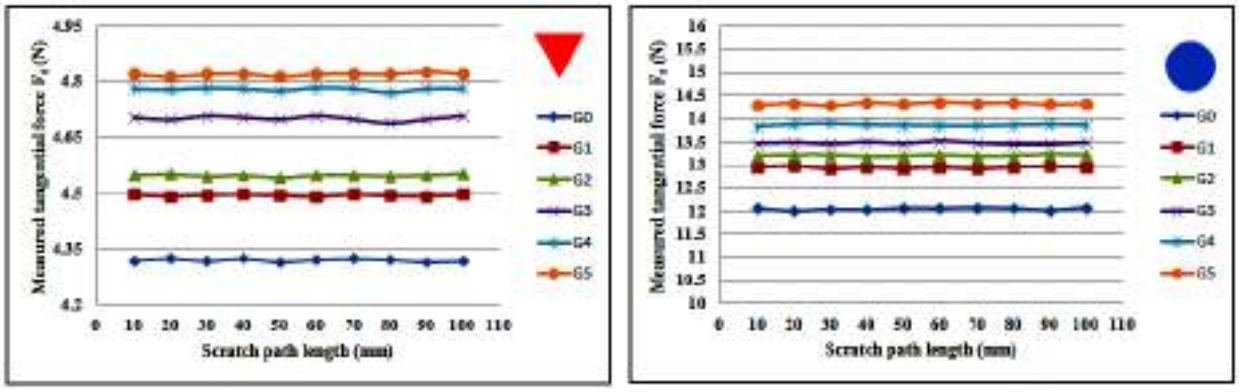

(a) (b)

Figure (6-49) Measured tangential force F_t of the G specimens (set B from first group) against scratch path length, using indenter (a) conical and (b) spherical.

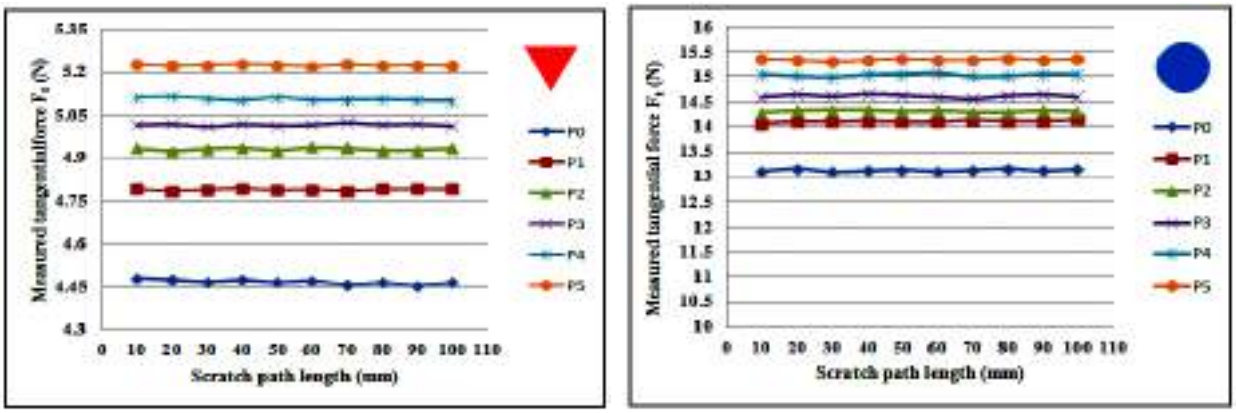

(a) (b)

Figure (6-50) Measured tangential force F_t of the P specimens (second group) against scratch path length, using indenter (a) conical and (b) spherical.

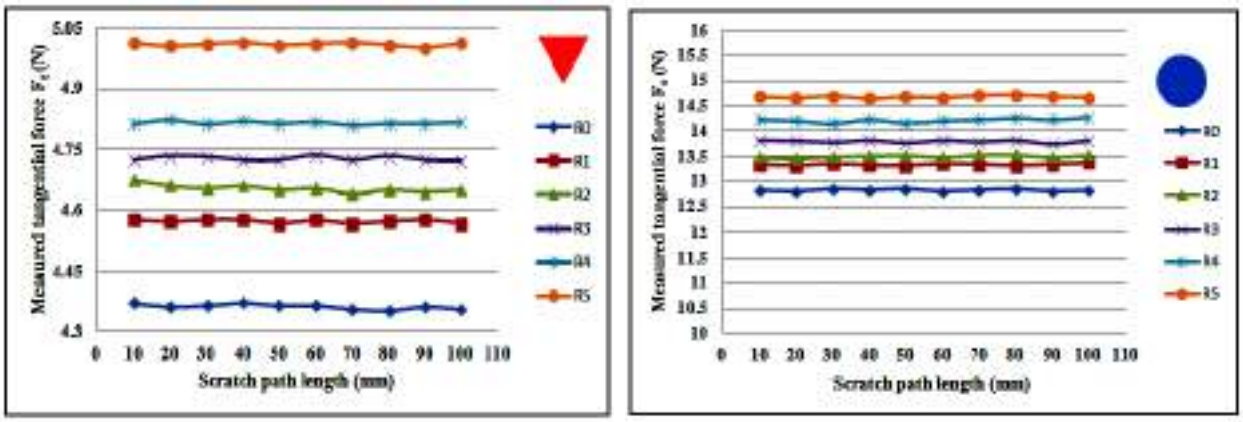

(a) (b)

Figure (6-51) Measured tangential force F_t of the R specimens (third group) against scratch path length, using indenter (a) conical and (b) spherical.

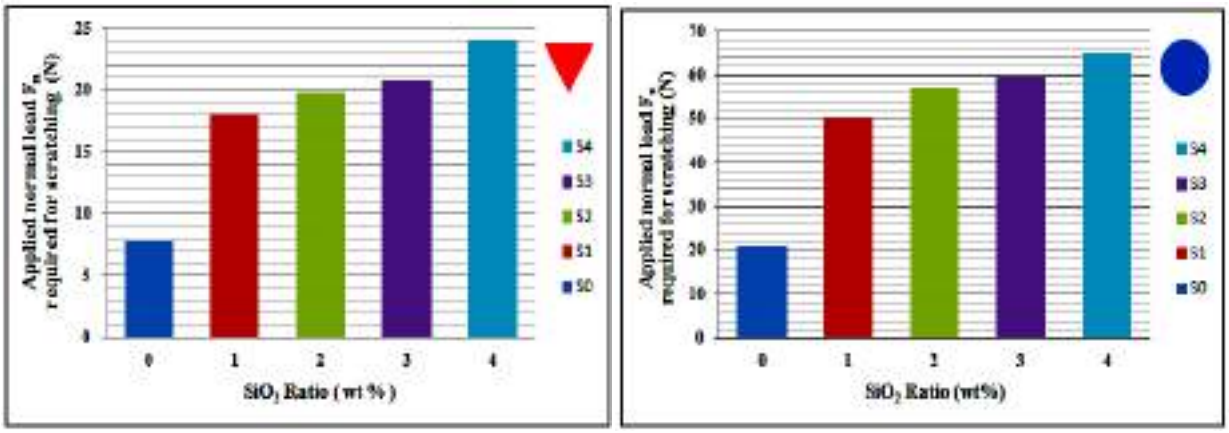

(a) (b)

Fig. (6-52) Applied normal load F_n of the S specimens (set A from first group) against SiO_2 nanoparticles ratio, using indenter (a) conical and (b) spherical.s

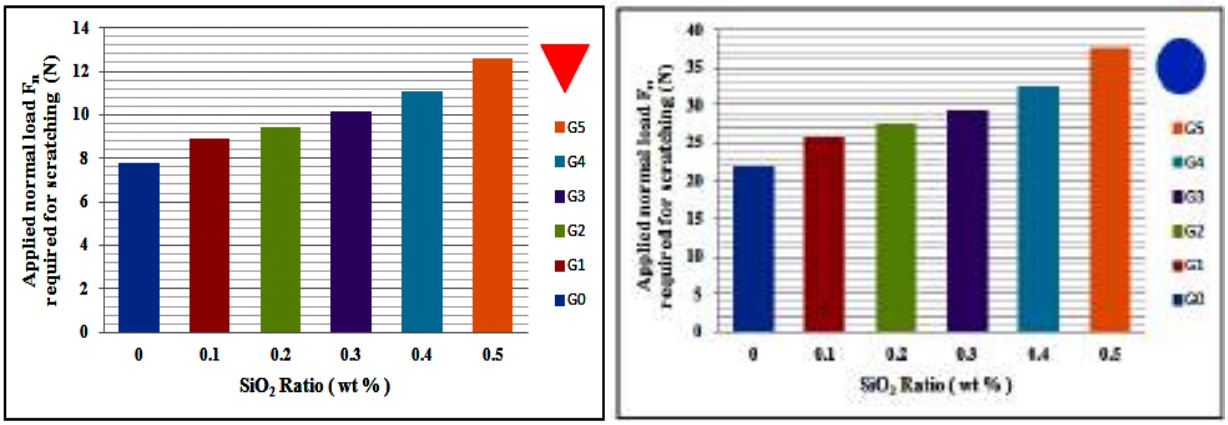

(a) (b)

Fig. (6-53) Applied normal load F_n of the G specimens (set B from first group) against SiO_2 nanoparticles ratio, using indenter (a) conical and (b) spherical.

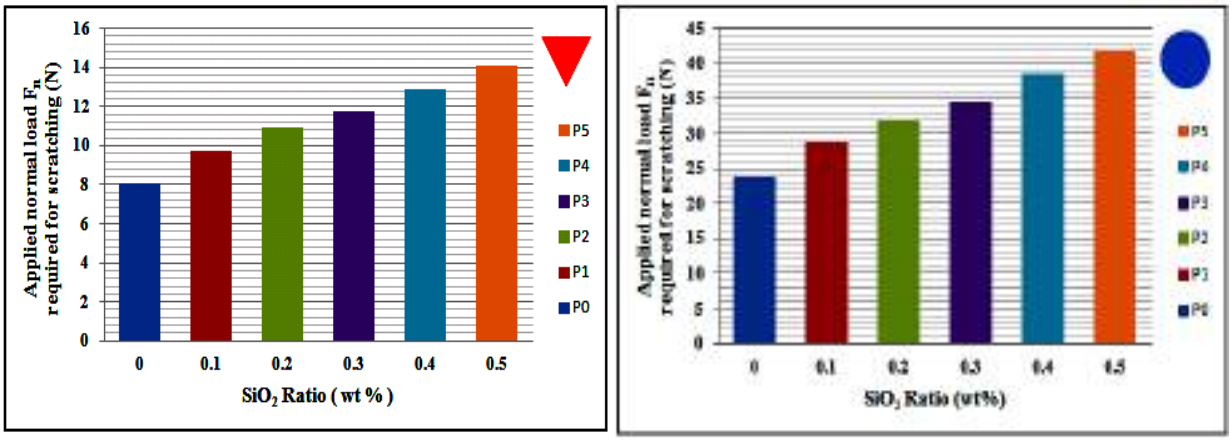

(a) (b)

Fig. (6-54) Applied normal load F_n of the P specimens (second group) against SiO_2 nanoparticles ratio, using indenter (a) conical and (b) spherical.

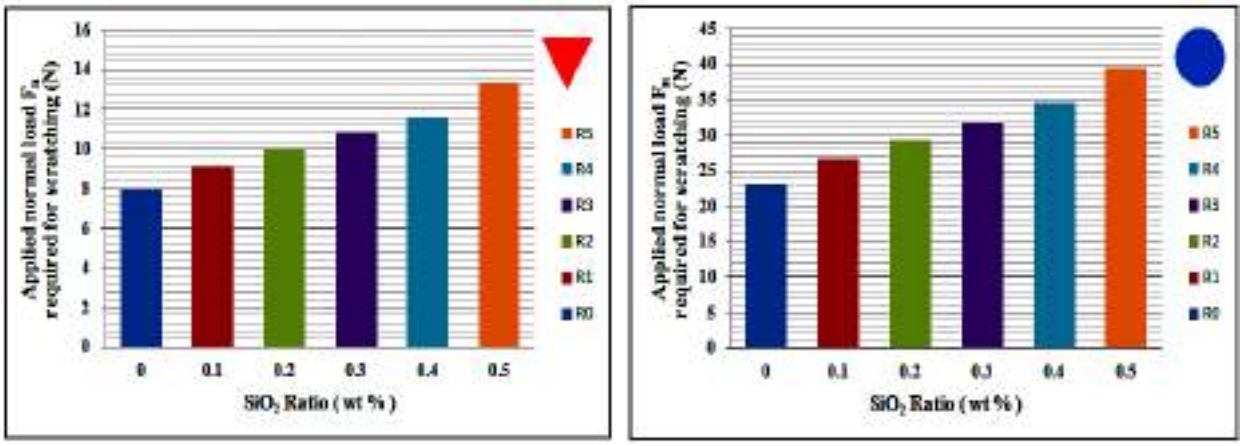

(a) (b)

Fig. (6-55) Applied normal load F_n of the R specimens (third group) against SiO_2 nanoparticles ratio, using indenter (a) conical and (b) spherical.

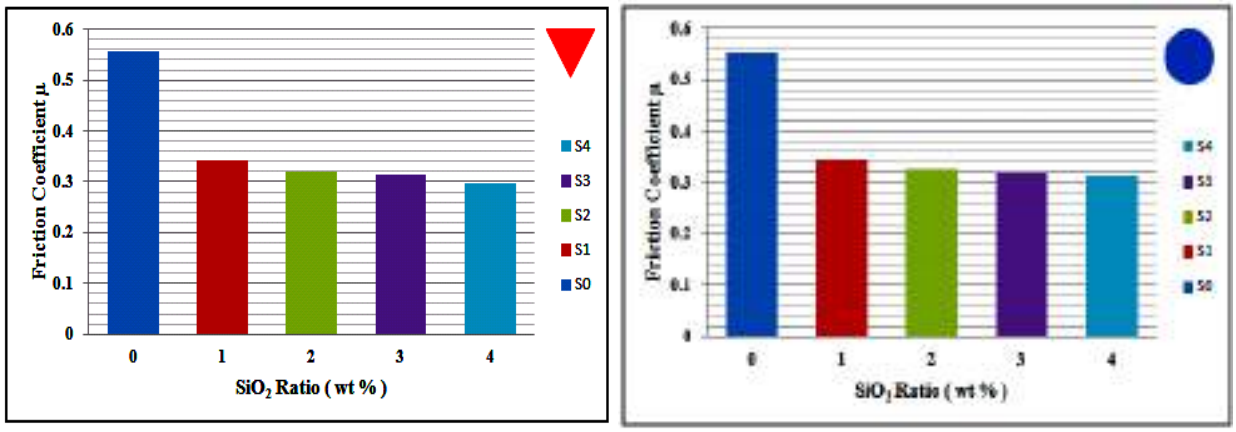

(a) (b)

Fig. (6-56) Friction coefficient μ of the S specimens (set A from first group) against SiO_2 nanoparticles ratio, using indenter (a) conical and (b) spherical.

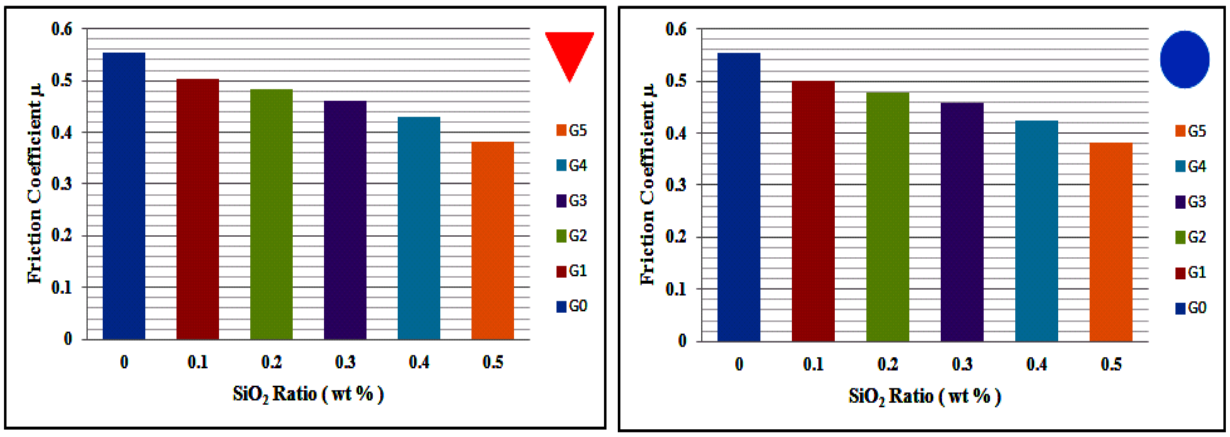

(a) (b)

Fig. (6-57) Friction coefficient μ of the G specimens (set B from first group) against SiO_2 nanoparticles ratio, using indenter (a) conical and (b) spherical.

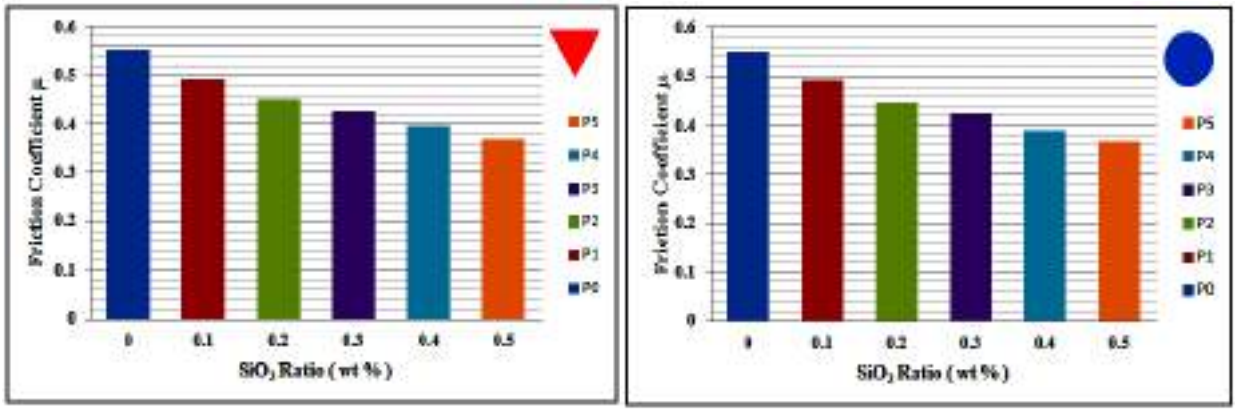

(a) (b)

Fig. (6-58) Friction coefficient μ of the P specimens (second group) against SiO_2 nanoparticles ratio, using indenter (a) conical and (b) spherical.

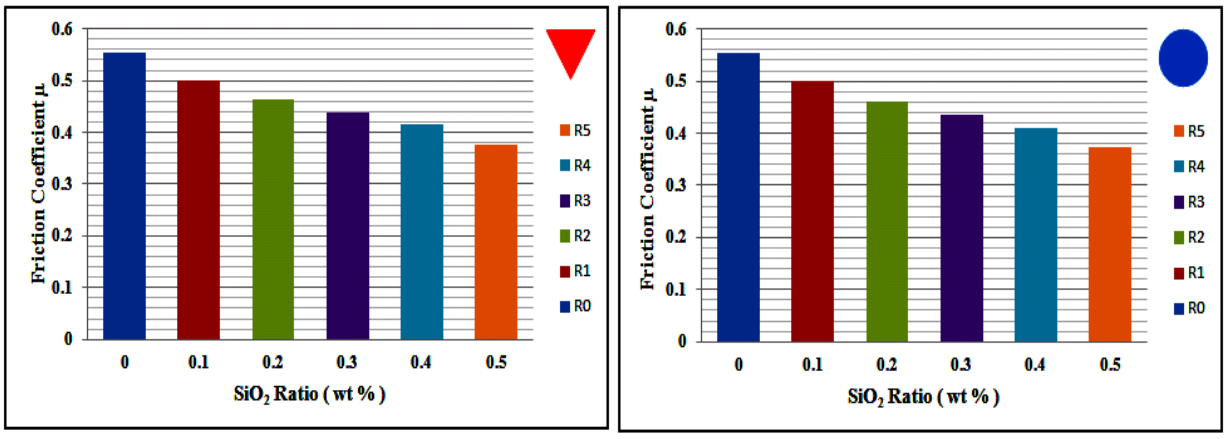

(a) (b)

Fig. (6-59) Friction coefficient μ of the R specimens (third group) against SiO_2 nanoparticles ratio, using indenter (a) conical and (b) spherical.

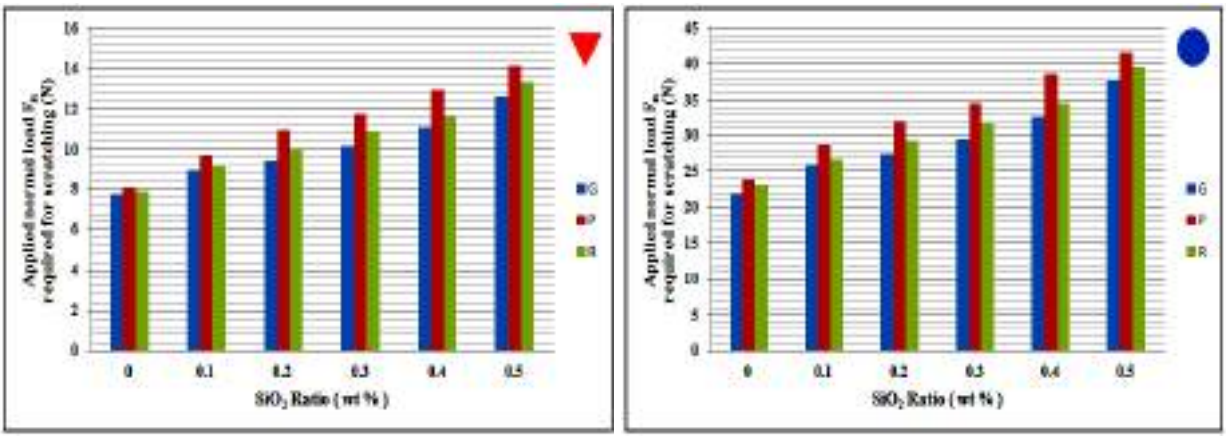

(a) (b)

Fig. (6-60) Comparison of applied load F_n required for scratching against the SiO_2 nanoparticles ratio between the three groups, using indenter (a) conical and (b) spherical.

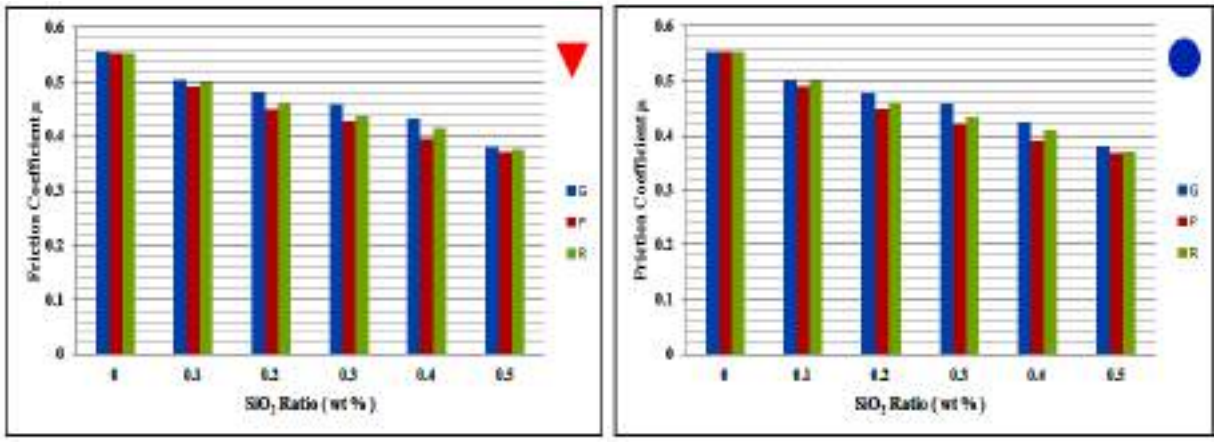

(a) (b)

Fig. (6-61) Comparison of friction coefficient μ against SiO_2 ratio between the three groups, using (a) conical indenter and (b) spherical indenter.

(a)

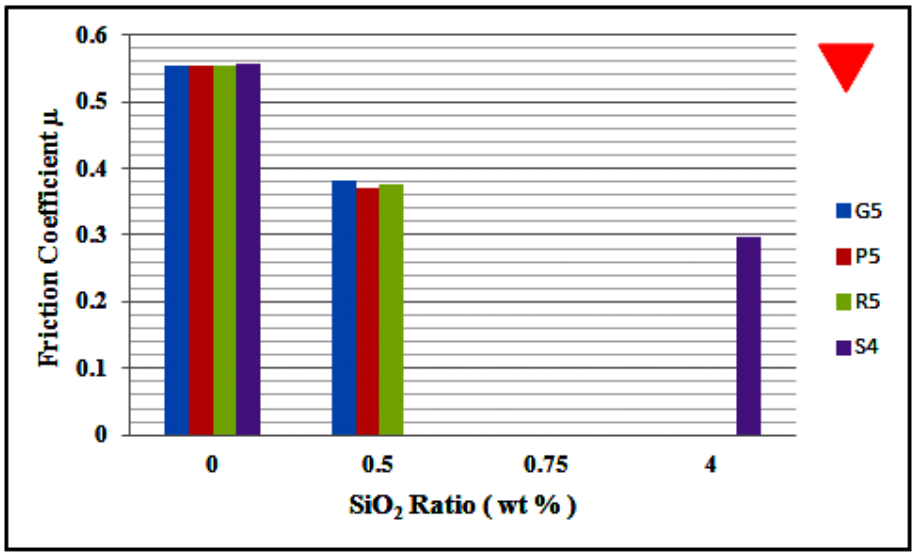

(b)

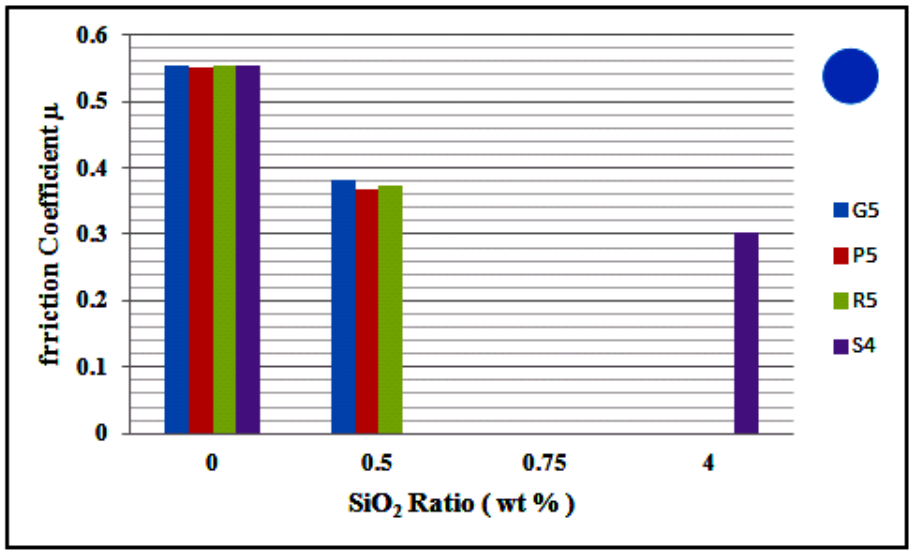

Fig. (6-62) Comparison of friction coefficient μ against SiO_2 ratio between S4, G5, P5, and R5 specimens using (a) conical indenter and (b) spherical indenter.

Table (6-6) Percentages of the friction coefficient improvement for the S4, G5, P5 and R5 specimens relative to the S0 specimen for three groups using two types of indenters.

Indenter Type	Specimen Code	SiO_2 Ratio (wt %)	Friction Coefficient μ	Improvement Percentages %)
Conical indenter	S0	0	0.556	------
	S4	4	0.296	46.76 %
	G5	0.5	0.382	31.29 %
	P5	0.5	0.371	33.27 %
	R5	0.5	0.375	32.55 %
Spherical indenter	S0	0	0.555	------
	S4	4	0.304	45.22 %
	G5	0.5	0.381	31.35 %
	P5	0.5	0.368	33.69 %
	R5	0.5	0.372	32.97 %

From the results above and using the two types of indenters it can be concluded that the normal load required for scratching and tangential force increases with an increase in the SiO_2 ratio, the friction coefficient decreases with an increase in the SiO_2 ratio and that the best friction coefficient values for specimens containing SiO_2 range from 0.1wt to 0.5wt obtained for specimens prepared using the pressing method. It can also be concluded that PMMA / SiO_2 composites behave as brittle material and early fracture occurs at high sliding speeds.

6.7 Summary

All the results of the tests conducted on the PMMA specimens were listed in table (6-7) to provide data sheet for the PMMA material where it's mechanical and tribological properties were improved in this study, also to make the comparison process between the specimens groups more easy and useful.

Table (6-7) The tests results of PMMA specimens.

Specimen code	SiO_2 Ratio (wt %)	Tensile Test		Shore D Hardness Test	Surface Roughness Test	DSC Test	Scratch Resistance Test					
							Using Conical indenter			Using Spherical indenter		
		Ultimate tensile strength (MPa)	Elongation (mm)	Surface Hardness (HD)	Surface Roughness (µm)	T_g (°C)	F_n (N)	F_t (N)	μ	F_n (N)	F_t (N)	μ
S0	0	30.1	2.47	53.4	0.037	108.67	7.835	4.356	0.556	21.154	11.741	0.555
S1	1	68.59	1.41	81.3	0.035	141.79	18.032	6.185	0.343	50.489	17.418	0.345
S2	2	42.57	2.091	85.5	0.034	149.02	19.838	6.368	0.321	56.935	18.561	0.326
S3	3	42.17	1.88	88.6	0.033	154.53	20.723	6.528	0.315	59.682	19.158	0.321
S4	4	23.83	2.164	92.3	0.036	159.71	24.037	7.115	0.296	64.899	19.534	0.304
G0	0	30.4	2.45	53.2	0.037	106.45	7.782	4.319	0.555	21.789	12.071	0.554
G1	0.1	44.828	2.21	65.7	0.035	113.73	8.924	4.498	0.504	25.879	12.965	0.501
G2	0.2	48.92	2.08	68.5	0.034	118.36	9.443	4.551	0.482	27.573	13.207	0.479
G3	0.3	52.564	1.99	71.7	0.036	123.42	10.175	4.702	0.462	29.405	13.467	0.458
G4	0.4	57.559	1.88	73.8	0.032	128.63	11.092	4.782	0.431	32.611	13.859	0.425
G5	0.5	65.1	1.75	75.6	0.033	133.87	12.625	4.821	0.382	37.622	14.334	0.381
P0	0	30.7	2.43	53.6	0.037	107.31	8.105	4.482	0.553	23.828	13.153	0.552
P1	0.1	45.2	2.18	66.8	0.031	115.58	9.721	4.792	0.493	28.774	14.128	0.491
P2	0.2	49.01	2.01	69.8	0.029	120.37	10.942	4.935	0.451	31.841	14.265	0.448
P3	0.3	54.36	1.89	72.6	0.028	124.99	11.724	5.018	0.428	34.586	14.629	0.423
P4	0.4	57.94	1.84	74.9	0.027	130.84	12.917	5.102	0.395	38.492	15.051	0.391
P5	0.5	71.2	1.67	77.3	0.028	135.56	14.083	5.225	0.371	41.685	15.341	0.368
R0	0	30.9	2.41	53.3	0.037	106.95	7.887	4.371	0.554	23.187	12.822	0.553
R1	0.1	48.77	2.07	66.1	0.035	114.62	9.155	4.587	0.501	26.732	13.339	0.499
R2	0.2	49.5	1.98	69.2	0.033	119.73	9.981	4.621	0.463	29.244	13.481	0.461
R3	0.3	56.746	1.81	72.1	0.032	123.85	10.875	4.763	0.438	31.755	13.813	0.435
R4	0.4	61.856	1.73	74.2	0.034	129.32	11.573	4.803	0.415	34.603	14.222	0.411
R5	0.5	78.241	1.58	76.8	0.033	134.15	13.341	5.003	0.375	39.489	14.691	0.372

Chapter Seven
Conclusions
and
Recommendations

Chapter Seven
Conclusions and Recommendations

7.1 Conclusions

The conclusions obtained in the current study can be summarized according to the tests conducted on the PMMA by the following points:

1. The glass transition temperature (T_g) for the PMMA/SiO_2 composites was higher than that for pure PMMA and increases with increasing ratio of SiO_2 nanoparticles.

2. Increase in tensile strength and decrease in elongation for PMMA/SiO_2 composites compared to pure PMMA, the best results were obtained for samples contains SiO_2 ratio of 1 wt%, also, increase in hardness for PMMA/SiO_2 composites compared to pure PMMA, the hardness increases with increasing the SiO_2 nanoparticles ratio.

3. The surface roughness of pure PMMA and PMMA/SiO_2 composites in the same group was approximately equal, but the best surface smoothness obtained for the P specimens, then followed by the R specimens then G specimens in the last rank.

4. Both the applied normal load required to start scratching and tangential force for PMMA/SiO_2 composites were greater than that for the pure PMMA, and both increase with increasing the SiO_2 nanoparticles ratio, also, the applied loads used with the spherical indenter were greater than those used with a conical indenter.

5. Friction coefficient for PMMA/SiO_2 composites was lower compared to pure PMMA and decreases when the ratio of nanoparticles increases.

6. The study proved the ability of the designed device to measure the tangential force required for scratching accurately and quickly and in simple steps as well as the possibility of calculating the friction coefficient directly from the inputs and outputs of the device, the study also demonstrated the effectiveness of the program designed to control the device in terms of ease of entering variables and the accuracy of outputs.

7.2 Recommendations

The recommendations proposed for future studies can be summarized in the following points:

1. Conducting a theoretical study and using simulation to obtain theoretical results for the purpose of comparing them with the experimental results obtained in the current study.
2. Using other types of nanoparticles separately or mix them with nanoparticles used in the current study.
3. Using other types of indenters, whether by changing the metal or the tip shape or the tip diameter.
4. Preparing the pure PMMA and PMMA/SiO_2 composites specimens using polymerization and compare the tests results with the preparing methods used in the present study.
5. Using the PMMA/SiO_2 composites substance obtained by the present study in the coating form and conducting tests.

References

References

[1] L.H. Sperling, Introduction to Physical Polymer Science, Wiley, 4th Edition, ISBN: 9788126542369, (2019).

[2] Gennady E. Zaikov, Oleg V. Stoyanov and Elena I. Kulish, Progress in Polymer Materials Science: Research, Development and Applications, 1st Edition, CRC Press-Apple Academic Press, ISBN: 9781926895413 - CAT# N10835, (2013).

[3] J.M.G. Cowie and Valeria Arrighi, Polymers: Chemistry and Physics of Modern Materials, CRC Press-Taylor and Francis Group, 3rd Edition, ISBN: 9780849398131-CAT#9813, (2007).

[4] Charles E. Carraher, Jr., Polymer Chemistry, Marcel Dekker, Inc., 6th Edition, ISBN: 0–8247–0806–7, (2003).

[5]Aluko Miriam, ″ Self assembly of star shaped amphiphiles -Opportunities for drug delivery″, Thesis for Department of Pharmaceutics, The School of Pharmacy, University of London, (2010).

[6] Christopher S. Brazel and Stephen L. Rosen, Fundamental Principles of Polymeric Materials, John Wiley & Sons, Inc., 3rd Edition, ISBN: 978-0-470-50542-7, (2012).

[7] Manas Chanda and Salil K. Roy, Plastics Fundamentals, Properties, and Testing, CRC Press-Taylor and Francis Group, 1st Edition, ISBN: 9781420080605 - CAT# 80601, (2008).

[8] George Odian, Principles of Polymerization, John Wiley & Sons, Inc., 4th Edition, ISBN: 978-0-471-27400-1, (2004).

[9] Umar Ali, Khairil Juhanni Bt. Abd Karim and Nor Aziah Buang, ″A Review of the Properties and Applications of Poly (Methyl Methacrylate) (PMMA), Polymer Reviews″, Vol. 55(4), pp. 678-705, (2015).

[10] Klaus Friedrich and Alois Schlarb, Tribology of Polymeric Nanocomposites, Elsevier Science, 1st Edition, ISBN: 9780080559087, (2008).

[11] Lim G.T., ″ Scratch behavior of polymers ″, Dissertation in Mechanical Engineering, Texas A&M University: College Station, Texas, (2005).

[12] A.M.S. Hamouda,″ The influence of humidity on the deformation and fracture behavior of PMMA″, Journal of Materials Processing technology, Vol. 124 (1-2), pp. 238–243, (2002).

[13] S. Kitova, M. Minchev, G. Danev, ″ Soft plasma treatment of polymer surfaces″, Journal of Optoelectronics and Advanced Materials, Vol. 7 (1), pp. 249-252, (2005).

[14] International Organization for Standardization, "ISO 19252-1: 2008- Determination of scratch properties –part 1: Method for determining the scratch properties of plastics under defined conditions, " ISO Standards, 83.080.01, (2008).

[15] G. Subhash, W. Zhang, ″ Investigation of the overall friction coefficient in single pass scratch test″, Elsevier Journal- Wear, Vol. 252 , pp. 123-134, (2002).

[16] E.T. Kopesky, G.H. McKinley, R.E. Cohen, ″ Toughened poly(methyl methacrylate) nanocomposites by incorporating polyhedral oligomeric silsesquioxanes″, Elsevier Journal - Polymer, Vol. 47, pp. 299-309, (2006).

[17] Vincent Jardret and Pierre Morel, ″ Viscoelastic effects on the scratch resistance of polymers: relationship between mechanical properties and scratch properties at various temperatures″, Elsevier Journal - Progress in Organic Coatings, Vol. 48, pp.322-331, (2003).

[18] Michael J. Adams, Alexander Allan, Brian J. Briscoe, Peter J. Doyle, David M. Gorman, Simon A. Johnson, ″An experimental study of the nano-scratch behavior of poly(methyl methacrylate) ″, Elsevier Journal-Wear, Vol. 251, pp.1579-1583, (2001).

[19] Vincentd D. Jardret and Warren C. Oliver, ″ On the robustness of scratch testing for thin films: the issue of tip geometry for critical load measurement″, Materials Research Society Symposium Proceedings, Vol. 594, pp.395-400, (2000).

[20] Ernest Rabinowicz, Friction and Wear of Materials, John Wiley & Sons, Inc. 2nd Edition, ISBN: 978-0-471-83084-9, (2013).

[21] M. Manshaa, C. Gauthiera, P. Gerardb and R. Schirrera, ″ The effect of plasticization by fatty acid amides on the scratch resistance of PMMA″, Elsevier Journal - Wear, Vol. 271, pp.671- 679, (2011).

[22] B.J. Briscoe, S.K. Sinha, ″ Scratch resistance and localized damage characteristics of polymer surfaces – a review″, Materialwissenschaft and Werkstofftechnik, Vol. 34, pp. 989 –1002, (2003).

[23] V. Jardret a.h, H. Zahouani, J.L. Loubet and T.G. Mathia, ″Understanding and quantification of elastic and plastic deformation during a scratch test″, Elsevier Journal- Wear, Vol. 218, pp. 8-14, (1998).

[24] S. Lafaye, C. Gauthier and R. Schirrer, ″A surface flow line model of a scratching tip: apparent and true local friction coefficients″, Elsevier Journal - Tribology International, Vol. 38, pp. 113-127, (2005).

[25] R. Schirrer, S. Lafaye and C. Gauthier, ″ Analysis of the apparent friction of polymeric surfaces″, Journal of Materials Science, Vol. 41, pp. 6441-6452, (2006).

[26] H Pelletier, C Gauthier, and R Schirrer, ″ Experimental and finite-element analysis of scratches on amorphous polymeric surfaces″, Journal of Engineering Tribology, Vol.222, pp.221-230, (2008).

[27] Mitsuru Tanahashi, ″Development of Fabrication Methods of Filler/Polymer Nanocomposites: With Focus on Simple Melt-Compounding- Based Approach without Surface Modification of Nanofillers″, Materials, Vol. 3, pp. 1593-1619, (2010).

[28] P.M. Ajayan, L.S. Schadler, P.V. Braun, Nanocomposite Science and Technology, Wiley-VCH, 1st Edition, ISBN: 978-3527303595, (2003).

[29] A. Fudala, I. Pálinkó, and I. Kiricsi, ″ Preparation and Characterization of Hybrid Organic-Inorganic Composite Materials Using the Amphoteric Property of Amino Acids: Amino Acid Intercalated Layered Double Hydroxide and Montmorillonite″, Inorganic Chemistry, Vol. 38, pp. 4653-4658, (1999).

[30] Ray S.S., Okamoto M., ″ Polymer/layered silicate nanocomposites: A review from preparation to processing″, Elsevier Journal –Progress in Polymer Science, Vol. 28, pp. 1539–1641, (2003).

[31] E. J. A. Pope, M. Asami, and J. D. Mackenzie, ″ Transparent silica gel-PMMA composites″, Journal of Materials Research, Vol. 4, pp. 1018-1026, (1989).

[32] Chujo Y. and Tamaki R. , ″ New preparation methods for organic-inorganic polymer hybrids″, MRS Bulletin Journal, Vol. 26, pp. 389-392, (2001).

[33] Yang F. and Nelson G.L., ″ Polymer/silica nanocomposites prepared via extrusion″, Polymers for Advance Technology, Vol. 17, pp.320-326, (2006).

[34] Jankong S. and Srikulkit K., ″ Preparation of Polypropylene/Hydrophobic Silica Nanocomposites″, Journal of Metals, Materials and Minerals, Vol.18, pp.143-146, (2008).

[35] Preghenella M., Pegoretti A., Migliaresi C., ″ Thermo - mechanical characterization of fumed silica-epoxy nanocomposites″, Elsevier Journal-Polymer, Vol. 46, pp. 12065–12072, (2005).

[36] Anoop Anand K, U.S. Agarwal, Anuya Nisal, Rani Joseph, ″ PET-SWNT nanocomposites through ultrasound assisted dissolution-evaporation″, European Polymer Journal, Vol. 43, pp. 2279–2285, (2007).

[37] M. Balzano and K. Ravi-Chandar, ″ Temperature effects on quasi-static fracture of PMMA″, Journal of Materials Science, Vol. 26, pp.1387- 1390, (1991).

[38] Maurizio Avella, Maria Emanuela Errico, and Ezio Martuscelli, ″ Novel PMMA/$CaCO_3$ Nanocomposites Abrasion Resistant Prepared by a in Situ Polymerization Process″, American Chemical Society publications- Nano Letters, Vol. 1(4), pp. 213-217, (2001).

[39] Hesham Afifi and Ebtisam Hasan, ″Annealing Effect on Microhardness and Elastic Constants of PMMA″, Polymer-Plastics Technology and Engineering, Vol. 42(4), pp. 543-554, (2003).

[40] Min Chen, Limin Wu, Shuxue Zhou, and Bo You, ″ Synthesis of Raspberry-like PMMA/SiO_2 Nanocomposite Particles via a Surfactant-Free Method″, American Chemical Society publications- Macromolecules, Vol. 37(25), pp.9613-9619, (2004).

[41] Jyothi Atla, Prakash Manne, A. Gopinadh, Anche Sampath, Suresh Babu Muvva, Krishna Kishore, Chiramana Sandeep and Harika Chittamsetty, ″ The Effect of Al_2O_3 Addition on the Thermal Diffusivity of Heat Activated Acrylic Resin″, Journal of Clinical and Diagnostic Research, Vol.7(8), p.p1797-1798, (2013).

[42] Onur Coban, ″ Heat treatment effect on erosion behavior of poly (methylmethacrylate) for optical transmittance efficiency″, Elsevier Journal- Applied Surface Science, Vol. 317, pp.405-413, (2014).

[43] Saeed Shirkavand and Elnaz Moslehifard, ″ Effect of TiO_2 Nanoparticles on Tensile Strength of Dental Acrylic Resins″, Journal of Dental Research, Dental Clinics, Dental Prospects, Vol. 8(4), pp. 197-203, (2014).

[44] Vipul Asopa, S. Suresh, Meenakshi Khandelwal, Vivek Sharma, Shivalika S. Asopa and Laxman Singh Kaira, ″ A comparative evaluation of properties of zirconia reinforced high impact acrylic resin with that of high

impact acrylic resin″, The Saudi Journal for Dental Research, Vol. 6, pp. 146-151, (2015).

[45] A. O. Alhareb, H. M. Akil, and Z. A. Ahmad, ″ Influence of Al_2O_3 / Y-TSZ mixture as filler loading on the radiopacity of PMMA denture base composites″, Elsevier Journal- Procedia Chemistry, Vol. 19, pp.646-650, (2016).

[46] Ahmed Omran Alhareb, Hazizan Md Akil, Zainal Arifin Ahmad, ″Impact strength, fracture toughness and hardness improvement of PMMA denture base through addition of nitrile rubber/ceramic fillers″, The Saudi Journal for Dental Research, Vol.8, pp.26-34, (2017).

[47] Z Hasratiningsih, V Takarini, A Cahyanto, Y Faza, L A T W Asri, and B S Purwasasmita, ″ Hardness evaluation of PMMA reinforced with two different calcinations temperatures of ZrO_2-Al_2O_3-SiO_2 filler system″, Journal of Materials Science and Engineering, Vol. 172, pp.899- 907, (2017).

[48] C. Gauthier and R. Schirrer, ″ Time and temperature dependence of the scratch properties of poly (methylmethacrylate) surfaces″, Journal of Materials Science, Vol. 35, pp.2121- 2130, (2000).

[49] C. Gauthier, S. Lafaye and R. Schirrer, ″ Elastic recovery of a scratch in a polymeric surface: experiments and analysis″, Elsevier Journal - Tribology International, Vol. 34, pp.469-479, (2001).

[50] R.D.K. Misra, R. Hadal, and S.J. Duncan, ″ Surface damage behavior during scratch deformation of mineral reinforced polymer composites″, Elsevier Journal - Acta Materialia, Vol. 52, pp.4363- 4376, (2004).

[51] J. L. Bucaille, E. Felder and G. Hochstetter, ″ Experimental and Three-Dimensional Finite Element Study of Scratch Test of Polymers at Large Deformations″, Journal of Tribology, Vol. 126(2), pp.372-379, (2004).

[52] M. Bonne, B.J. Briscoe, C.J. Lawrence, S. Manimaaran, D. Parsonage and A. Allan, ″ Nano-indentation of scratched poly (methyl methacrylate)

surfaces″, Springer Journal - Tribology Letters, Vol. 18(2), pp.125-133, (2005).

[53] N.L. Surampadi, T.C. Pesacreta and R.D.K. Misra, ″ The determining role of scratch indenter radius on surface deformation high density polyethylene and calcium carbonate-reinforced composite″, Elsevier Journal - Materials Science and Engineering, Vol. 456, pp.218-229, (2007).

[54] Herve Pelletier, Anne-Lise Durier, Christian Gauthier and Robert Schirrer, ″ Viscoelastic and elastic– plastic behaviors of amorphous polymeric surfaces during scratch″, Elsevier Journal - Tribology International, Vol. 41, pp. 975-984, (2008).

[55] N. Aleksy, G. Kermouche, J.M. Bergheau, J.L. Loubet, and S. Pavan , ″Mechanical investigation of the healing phenomenon of the PMMA″, International Journal of Material Forming, Vol. 3, pp.575-578, (2010).

[56] Ehsan Moghbelli, ReidBanyay and Hung-JueSue, ″ Effect of moisture exposure on scratch resistance of PMMA″, Elsevier Journal - Tribology International, Vol. 69, pp. 46-51, (2014).

[57] Ehsan Moghbelli, ″ Scratch behavior of multiphase styrenic copolymers and the influence of environmental conditioning ″, Dissertation in Materials Science and Engineering, Texas A&M University: College Station, Texas, (2014).

[58] MIN HAO WONG, ″ The development of scratch test methodology and characterization of surface damage of polypropylene″, Thesis Submitted to the Office of Graduate Studies of Mechanical Engineering, Texas A&M University, (2003).

[59] International Organization for Standardization, ″ ISO 12137-1:1997 - Determination of mar resistance - Part 1: Method using a curved stylus″, ISO Standards, 87.040, (1997).

[60] International Organization for Standardization, ″ ISO 12137-2:1997 -

Determination of mar resistance - Part 2: Method using a pointed stylus″, ISO Standards, 87.040, (1997).

[61] ASTM International, ″ ASTM G 171-03: Standard test method for scratch hardness of materials Using a Diamond Stylus″, Annual Book of ASTM Standards, Vol. 3, (2003).

[62] Lim G. T., Wong M. , Reddy J. N., and Sue, H.-J., ″An integrated approach towards the study of scratch damage of polymer, ″ Journal of Coatings Technology and Research, Vol. 2(5), pp. 361-369, (2005).

[63] I.M. Hutchings, Tribology - Friction and Wear of Engineering Materials, Butterworth-Heinemann, 1st Edition, ISBN: 978-0340561843, (1992).

[64] B.N.J. Persson, Sliding Friction - Physical Principles and Applications, 2nd Edition, Springer-Verlag Berlin Heidelberg, ISBN: 978-3-662-04283-0, (2000).

[65] F. P. Bowden and D. Tabor, ″ Friction, lubrication and wear: a survey of work during the last decade″, British Journal of Applied Physics, Vol. 17, pp. 1521-1544, (1966).

[66] B. J. Briscoe and D. Tabor, ″ The effect of pressure on the frictional properties of polymers″, Elsevier Journal - Wear, Vol. 34, pp. 29-38, (1975).

[67] J.L. Bucaille, E. Felder, G. Hochstetter, ″ Mechanical analysis of the scratch test on elastic and perfectly plastic materials with the three-dimensional finite element modeling ″, Elsevier Journal - Wear, Vol. 249, pp. 422-432, (2001).

[68] N. Tayebi, T.F. Conry, A.A. Polycarpou, ″Determination of hardness from nanoscratch experiments: correction for interfacial shear stress and elastic recovery″, Journal of Materials Research, Vol. 18, pp. 2150–2162, (2003).

[69] J. Goddard and H. Wilman, ″ A theory of friction and wear during the abrasion of metals″, Elsevier Journal - Wear, Vol. 5, pp. 114-135, (1962).

[70] ASTM International, ″ASTM D7027-05: Standard test method for evaluation of scratch resistance of polymeric coatings and plastics using an instrumented scratch machine″, Annual Book of ASTM Standards, Vol. 5, (2005).

[71] Browning R., Sue H.-J., Minkwitz R., ″ Effects of Acrylonitrile Content and Molecular Weight on the Scratch Behavior of Styrene-Acrylonitrile Random Copolymers″, Polymer Engineering and Science, Vol. 51, pp. 2282-2294, (2011).

[72] Liang Y. –L., Sue H. -J., Minkwitz R., ″ Rubber Content Effect on Scratch Behavior in Acrylonitrile-Styrene-Acrylate Copolymers″, Journal of Applied Polymer Science, Vol. 126, pp. 1088-1096, (2012).

[73] D. Tabor, ″ The physical meaning of indentation and scratch hardness″, British Journal of Applied Physics, Vol. 7, pp.159-166, (1956).

[74] P.R. Guevin, ″ State-of-the-art instruments to measure coating hardness ″, Journal of coating technology, Vol. 67, pp. 61-65, (1995).

[75] Kody R.S. and Martin D.C., ″Quantitative Characterization of Surface Deformation in Polymer Composites Using Digital Image Analysis ″, Polymer Engineering and Science, Vol.36, pp. 298-304, (1996).

[76] Chu J., Rumao L., Coleman B., ″ Scratch and Mar Resistance of Filled Polypropylene Materials″, Polymer Engineering and Science, Vol. 38, pp. 1906-1914, (1998).

[77] Krupicka A., Johnansson M., Hult A., ″ Use and interpretation of scratch tests on ductile polymer coatings″, Elsevier Journal- Progress in Organic Coatings, Vol. 46, pp. 32-40, (2003).

[78] Wong M., Lim G. T.,, Moyse A., Reddy J. N., Sue H. -J., ″ A new test methodology for evaluating scratch resistance of polymers″, Elsevier Journal- Wear, Vol. 256, pp. 1214-1227, (2004).

[79] ASTM International, ″ASTM D7027-05: Standard test method for evaluation of scratch resistance of polymeric coatings and plastics using an

instrumented scratch machine″, Annual Book of ASTM Standards, Vol. 5, (2005).

[80] Browning R., Lim G. T., Moyse A., Sue H.-J., Chen H., Earls J. D., ″ Quantitative evaluation of scratch resistance of polymeric coatings based on a standardized progressive load scratch test ″, Elsevier Journal - Surface and Coatings Technology , Vol. 201, pp. 2970-2976, (2006).

[81] Jiang H., Lim G. T., Reddy J. N. , Whitcomb J., Sue H. -J., ″ Finite Element Method Parametric Study on Scratch Behavior of Polymers″, Journal of Polymer Science: Part B: Polymer Physics, Vol. 45, pp. 1435-1447, (2007).

[82] Jiang H., Browning R.L., Sue H.-J., ″ Understanding of scratch-induced damage mechanisms in polymers ″, Elsevier Journal - Polymer , Vol. 50, pp. 4056-4065, (2009).

[83] Hossain M. M., Browning R. L., Minkwitz R., Sue H.-J., ″ Effect of Asymmetric Constitutive Behavior on Scratch-Induced Deformation of Polymers″, Tribology Letters, Vol. 47, pp. 113-122, (2012).

[84]] Hossain M. M., Jiang H., Sue H.-J., ″ Effect of constitutive behavior on scratch visibility resistance of polymers-A finite element method parametric study″, Elsevier Journal – Wear, Vol. 270, pp. 751-759, (2011).

[85] Hossain M. M., Minkwitz R., Sue H.-J., ″ Minimization of Surface Friction Effect on Scratch-Induced Deformation in Polymers″, Polymer Engineering and Science, Vol. 53, pp. 1405-1413, (2013).

[86] T. Triplett, ″ Two-component: the magic's in the mix″, Ind. Paint Powder, Vol. 72 (4), pp. 34-37, (1996).

[87] D. Tabor, The Hardness of Metals, Oxford University Press, 4th Edition, ISBN: 9780198507765, (2020).

[88] F.P Bowden, D. Tabor, The Friction and Lubrication of Solids Part II, 1st Edition, Oxford University Press, ISBN: 978-0198507772, (1964).

[89] A. Chanda, D. Basu, A. Dasgupta, S. Chattopadhyay, A.K. Mukhopadhyay, ″A new parameter for measuring wear of materials″, Journal of Materials Science Letters, Vol. 16(20), pp. 1647-1651, (1997).

[90] Chu J., Xiang C., Sue H.-J., Hollis R.D.,″ Scratch resistance of mineral-filled polypropylene materials″, Polymer Engineering and Science, Vol. 40(4), pp. 944-955, (2000).

[91] B.J. Briscoe, A. Delfino, E. Pelillo, ″ Single-pass pendulum scratching of poly(styrene) and poly(methylmethacrylate) ″, Elsevier Journal - Wear, Vol. 225 (1), pp. 319-328, (1999).

[92] O. Vingsbo, S. Hogmark, ″ Single-pass pendulum grooving- a technique for abrasive testing″, Elsevier Journal - Wear, Vol. 100, pp. 489-502, (1984).

[93] Y.N. Liang, S.Z. Li, D.F. Li, S. Li, ″ Some developments for single-pass pendulum scratching″, Elsevier Journal - Wear, Vol. 199, pp. 66-73, (1996).

[94] Jiang H., Browning R., Fincher J., Gasbarro A., Jones S., Sue H.-J., ″ Influence of surface roughness and contact load on friction coefficient and scratch behavior of thermoplastic olefins″, Elsevier Journal - Applied Surface Science, Vol. 254, pp. 4494-4499, (2008).

[95] HAN JIANG, ″ Experimental and numerical study of polymer scratch behavior ″, Dissertation in Mechanical Engineering, Texas A&M University: College Station, Texas, (2009).

[96] K. Li, B.Y. Ni and J.C.M. Li, ″ Stick-slip in the scratching of styrene-acrylonitrile copolymer″, Journal of Materials Research, Vol. 11, pp. 1574-1580, (1996).

[97] K. Li, Y. Shapiro and J. C. M. Li, ″ Scratch test of soda-lime glass″, Acta Materialia, Vol. 46, pp. 5569-5578, (1998).

[98] R. Smith, D. Mulliah, S.D. Kenny, E. McGee, A. Richter and M. Gruner, ″ Stick slip and wear on metal surfaces ″, Elsevier Journal - Wear, Vol. 259, pp. 459-466, (2005).

[99] S.L. Zhang and J.C.M. Li, ″ Slip process of stick-slip motion in the scratching of a polymer″, Elsevier Journal - Materials Science and Engineering, Vol. 344, pp. 182-189, (2003).

[100] I. Yu. Evchuk, R. I. Musii, R. G. Makitra, and R. E. Pristanskii, ″ Solubility of Polymethyl Methacrylate in Organic Solvents″, Russian Journal of Applied Chemistry, Vol. 78, pp. 1576-1580, (2005).

[101] Ezio Amerio, Paola Fabbri, Giulio Malucelli, Massimo Messori, Marco Sangermano, Rosa Taurino, ″ Scratch resistance of nano-silica reinforced acrylic coatings″, Elsevier Journal- Progress in Organic Coatings, Vol. 62, pp. 129-133, (2008).

[102] Christopher M. Seubert, Mark E. Nichols, ″ Scaling behavior in the scratching of automotive clearcoats ″, Journal of Coating Technology and Research, Vol.4 (1), pp. 21-30, (2007).

[103] C. Gauthier, A. L. Durier, C. Fond, R. Schirrer, ″ Scratching of a coated polymer and mechanical analysis of a scratch resistance solution″, Elsevier Journal - Tribology International, Vol. 39, pp. 88-98, (2006).

[104] Alnamel H.A and Mudhaffer M.M, ″ The effect of Silicon dioxide Nano-Fillers Reinforcement on Some Properties of Heat Cure Polymethyl Methacrylate Denture Base Material ″ Journal of Baghdad College Dentistry, Vol. 26, pp. 32-36, (2014).

List of Publications

List of Publications

[1] Mushtaq Abdul Kareem Hussein, Abdul Kareem F. Hassan, Najim Abdul Ameer Saad, "Design and Construction of a New Automated Device for Testing the Scratch Resistance of Polymeric Materials", Basrah Journal for Engineering Sciences, Vol. 20, No. 1, pp. 30-36, 2020.

[2] Mushtaq Abdul Kareem Hussein, Abdul Kareem F. Hassan, Najim Abdul Ameer Saad, “Effect of silicon oxide nanoparticles (SiO_2) on mechanical and tribological properties of polymethyl methacrylate (PMMA**)** ", Test Engineering and Management, Vol. 83, pp. 14965-14981, 2020.

Basrah Journal for Engineering Sciences, Vol. 20, No. 1, (2020), 30-36

Basrah Journal for Engineering Sciences

Journal homepage: www.bjes.edu.iq
ISSN (Online): 23118385, ISSN (Print): 18146120

OPEN ACCESS

Design and Construction of a New Automated Device for Testing the Scratch Resistance of Polymeric Materials

Mushtaq Abdul Kareem Hussein [1,*], Abdul Kareem F. Hassan [2], Najim Abdul Ameer Saad [1]

[1] Department of Mechanical Engineering, College of Engineering, University of Basrah, Basrah, Iraq
[2] Department of Materials Engineering, College of Engineering, University of Babylon, Babylon, Iraq
E-mail address: mushtaqkareem777@gmail.com , karem_f_h@yahoo.com , Jasim_916@yahoo.com
Received: 26 November 2019; Accepted: 16 December 2019; Published: 2 February 2020

Abstract

This paper aims to design and construct of an automated device for testing the scratch resistance of the polymeric materials by measuring the force required to cause a scratch on the surface of polymeric materials as well as calculating the friction coefficient from the input and output of the device. The device was made of materials available in the local market and some parts were manufactured in local mechanical workshops. The device consists of four main parts were mechanical parts, scratching mechanism parts, electrical and electronic parts and the device operating program. The device designed in this work has the following specifications: normal load (0.1 N - 325 N), sliding speed (1 mm/s - 35 mm/s), tangential force measured by the load cell (0.1 N to 294 N), the samples dimensions (length: 10 - 195 mm, width: 10 - 125 mm, and thickness: 0.25 - 50 mm), maximum scratch length of 195 mm, and the height of the indenter from the platform surface (0.25 mm to 50 mm). Scratch test and calculation of the friction coefficient were performed for samples of pure and reinforced PMMA by Silicon Oxide nanoparticles (SiO_2). The results showed an increase in scratch resistance and a decrease in the friction coefficient with increasing the weight ratio of SiO_2. Also, the ability of the designed device to measure the tangential force required for scratching accurately and quickly and in simple steps.

Keywords: Scratch device, Polymer, Scratch resistance, Friction.

1. Introduction

The scratch resistance test is one of the most important tests conducted on polymeric materials to determine its surface properties so that researchers and manufacturers can then devise methods and treatments to improve these properties. Scratch resistance test for polymers depends on many parameters such as indenter geometry, applied normal load and sliding speed. Indenter geometry includes the indenter type (conical or spherical), radius and apex angle of the tip and attack angle of the indenter. The strain hardening and height of the polymeric material accumulated on both sides of the scratch groove increases as the attack angle of the indenter increases [1]. The value of applied normal load required to start scratching on the surface of the polymeric material is greatly influenced by the geometry of the indenter, this value does not mean anything without accurate description of the tip used [2]. When the scratching begins to occur on the surface of the polymeric material, tensile and compressive stresses are generated behind and in front of the indenter respectively, which associated mainly with the indenter geometry. The polymeric material begins fracturing at the bottom of scratch groove when the tensile stress value reaches the value of ultimate tensile strength [3]. The wear volume resulting from the scratching is proportional to the applied normal load [1, 4]. An increase in sliding speed lead to decreases the true contact radius and increases the mean strain in the contact region [5].

In the literature, the scratch test in all researches related to the study of scratch resistance of polymeric materials was performed using various devices with different specifications. For example, Amerio et al. used a CSM scratch device (Micro-Combi Tester) with specifications: normal load (0.05N-30N), sliding speed (0.4-600 mm/min) and maximum scratch length of 120 mm [6]. A new device based on the moving head of tensile machine (Instron 4502) with specifications: normal load (0.05 N - 5 N) and sliding speed (1 µm/s to104 µm/s) was used by Gauthier and Schirrer [7]. Christopher et al. used a CSM Nano-scratch tester with specifications: normal load (10 µN - 1 N), sliding speed (0.4 - 600 mm/min), tangential force measured by load cell (6 µN - 1 N) and dimensions of the sample (20 mm × 120 mm) [8]. Fond et al. used a micro-visioscratch device with specifications: normal load (0.05 N - 35 N), sliding speed (1 µm/s - 104 µm/s) and temperature range (- 70 °C to + 120 °C) [9]. Scratch apparatus with specifications such as sliding speed (1 µm/s - 15 mm/s), normal load (0.05 N - 5 N) and temperature range (- 70 °C to + 120 °C) was used by Lafaye et al. [10]. Mashaa et al. used a micro-visioscratch device with specifications: normal load (0.05 N - 35 N) and sliding speed (10^{-5} mm/s -15 mm/s) [5]. Surampadi et al. used a device with specifications: normal load (0.5 N - 10 N), maximum sliding speed of 10 mm/s and three indenters (loop, needle and Hoffman) [11].

Scratching occurs as a result of friction between the surface of the polymeric material and the body that causes the scratch, hence the importance of determining the friction coefficient of the polymeric material to improve its resistance to scratching. The ratio between the tangential force that causes the movement of the scratching tip and the vertical

TEST Engineering & Management

March-April 2020
ISSN: 0193-4120 Page No. 14965 – 14981

Effect of Silicon Oxide Nan Particles (SIO2) on Mechanical and Tribological Properties of Polymethyl Methacrylate (PMMA)

Mushtaq Abdul Kareem Hussein[1], Najim Abdul Ameer Saad [2], Abdul Kareem F. Hassan[3]
[1]Mechanical Engineering Department, Basrah University, Basrah, Iraq
[2]Materials Engineering College, Babylon University, Babylon, Iraq
[3]Mechanical Engineering Department, Basrah University, Basrah, Iraq

Article Info
Volume 83
Page Number: 14965 – 14981
Publication Issue:
March - April 2020

Abstract:
The urban planning policy that has been applied in the city of Constantine has contributed to the creation of an urban dynamic towards its periphery and satellite cities. The policy sought to solve the problem of urban growth, in the face of concern about the preservation of agricultural land and the spread of areas of natural hazards such as landslides and floods. In this context, satellite cities appear as a strategic option to solve this problem according to the direction of successive urban development plans. Satellite cities are supposed to contain urban growth; in Constantine, this is achieved through the redirection of surplus population and the provision of extensive land for urbanization. These opportunities offer significant possibilities for extension and the realization of different residential and equipment projects. The aim of this paper is to highlight the variety of relationships as well as their intensity with the mother city, without forgetting to appreciate the degree of dependence on Constantine.This paper studies the effect of adding silicon oxide nanoparticles (SiO_2) with ratios (1wt%, 2wt%, 3wt%, and 4wt %) and an average particle size of 10-30 nm on the mechanical and tribological properties of polymethyl methacrylate. The dissolving and casting method in glass molds was used to prepare samples of neat and reinforced PMMA. The influence of the addition of silicon oxide nanoparticles on hardness and ultimate tensile strength of polymethyl methacrylate was studied using shore D hardness test and tensile test, respectively. The behavior of scratch resistance and friction coefficient of neat and reinforced polymethyl methacrylatewas studied using scratch test was performed by a new automated scratch device designed in this work. The results show that the ultimate tensile strength of reinforced polymethyl methacrylate is improved compared with neat polymethyl methacrylate. The hardness of polymethyl methacrylate increases with increasing the nanoparticles ratio. The scratch resistance of reinforced PMMA improved significantly compared to neat PMMA and increases with increasing nanoparticles ratio. The friction coefficient of the reinforced polymethyl methacrylate is lower than of neat polymethyl methacrylate and decreases with increasing SiO_2 ratio. The friction coefficient values calculated from the input and output of the device for all samples against filler ratio are 0.554 for neat PMMA, 0.488 for 1wt %, 0.436 for 2 wt%, 0.385 for 3 wt% and 0.3401 for 4 wt% of SiO_2.

Article History
ArticleReceived: 24 July 2019
Revised: 12 September 2019
Accepted: 15 February 2020
Publication: 15 April 2020

Keywords:Urban growth, urban planning, urbanization, mother city, satellite city, city of Constantine, Algeria ,PMMA/SiO_2, tensile strength, hardness, scratch resistance, friction.

Appendix

Appendix

1. The equations used to calculate stress and strain

$$\sigma = F/A$$

$$\varepsilon = L\text{-}\, L_0 / L_0$$

$$\varepsilon = \Delta L / L_0$$

2. The equation used to calculate the strain rate

$$\dot{\varepsilon} = V_{tip} / w$$

3. Software of scratch device

```
'------------------------------------------------------------------------
-
'
'  Scratch Test
'
'------------------------------------------------------------------------
'
Option Explicit On
Imports System.Threading.Thread
Imports System.Runtime.InteropServices
Imports System.Diagnostics
Imports LabJack.LabJackUD
Public Class Form1

    Dim NUM_SCANS As Double = 1000   'SCAN_RATE * (READ_INTERVAL/1000)
    Dim SCAN_RATE As Long = 500
    Dim READ_INTERVAL As Long = 500  'millisecond interval to read stream
dat

    Dim ioType As LJUD.IO = 0
    Dim channel As LJUD.CHANNEL = 0
```

```
    Dim dblValue As Double = 0
    Dim dblCommBacklog As Double = 0
    Dim dblUDBacklog As Double = 0
    Dim numScansRequested As Double
    Dim Ai(9000) As Double   ' size= SCAN_RATE*No. of Ch. *
(READ_INTERVAL/1000)
    Dim AB(4, 256000) As Single
    Dim u3 As U3
    Dim dummyDouble As Double = 0
    Dim dummyInt As Integer = 0
    Dim dummyDoubleArray(1) As Double
    Dim ZeroRead(4), VAvg(4), MaxRead(4), MinRead(4) As Single
    Dim SFactor(4) As Single, Spath As String
    Dim TotalScans As Double
    Dim WTimer As New Stopwatch
    Dim count As Integer = 0
    Dim divVal As Integer = 0 'timer divider post value
    Dim NumSensors As Integer = 1
    Dim DCounter, idr As Integer
    Dim x0, y0, x1, y1, xr, yr, MaxA, MinA As Single
    Dim t(8) As Single
    Dim MaxX As Single

    Sub showErrorMessage(ByVal err As LabJackUDException)
        MsgBox("Function returned LabJackUD Error #" & _
            Str$(err.LJUDError) & _
            "  " & _
            err.ToString)
    End Sub

    Private Sub StopStream()
        Try

            'Stop the stream
            LJUD.eGet(u3.ljhandle, LJUD.IO.STOP_STREAM, 0, dummyDouble,
dummyDoubleArray)
        Catch ex As Exception
            showErrorMessage(ex)
        End Try

    End Sub
```

```
    Private Sub Button1_Click(ByVal sender As System.Object, ByVal e As
System.EventArgs) Handles Button1.Click
        'Button1.Enabled = False
        MaxX = Val(TextBox1.Text)
        SFactor(0) = Val(TextBox3.Text)
        READ_INTERVAL = 1000 * Val(TextBox1.Text)
        Timer1.Interval = 100  'additional 0.5 sec for adequate data
        PreparePic(Pic1)
        ' StartStream()
        Try
            'Start the stream.
            LJUD.eGet(u3.ljhandle, LJUD.IO.START_STREAM, 0, dblValue, 0)
        Catch ex As LabJackUDException
            showErrorMessage(ex)
        End Try
        TotalScans = 0
        DCounter = 0
        Timer1.Enabled = True
    End Sub

    Private Sub StartStream()
        ' Open U3
        Try
            u3 = New U3(LJUD.CONNECTION.USB, "0", True)
        Catch ex As LabJackUDException
            showErrorMessage(ex)
        End Try

        Try
            'Start by using the pin_configuration_reset IOType so that all
            'pin assignments are in the factory default condition.
            LJUD.ePut(u3.ljhandle, LJUD.IO.PIN_CONFIGURATION_RESET, 0, 0,
0)

            'Configure FIO0 and FIO1 as analog, all else as digital.  (No
need for U3-HV since a0-3 are set to AI by default)
            'That means we will start from channel 0 and update all 16
flexible bits.  We will
            'pass a value of b0000000000001111 or 15.
```

```
            LJUD.ePut(u3.ljhandle, LJUD.IO.PUT_ANALOG_ENABLE_PORT, 0, 15,
16)

            'Configure the stream:
            'a nonzero value will cause Stream scans overlapped
            'LJUD.AddRequest(u3.ljhandle, LJUD.IO.PUT_CONFIG,
LJUD.CHANNEL.AIN_RESOLUTION, 12, 0, 0)
            LJUD.AddRequest(u3.ljhandle, LJUD.IO.PUT_CONFIG,
LJUD.CHANNEL.AIN_RESOLUTION, 0, 0, 0)



            'Set the scan rate.
            LJUD.AddRequest(u3.ljhandle, LJUD.IO.PUT_CONFIG,
LJUD.CHANNEL.STREAM_SCAN_FREQUENCY, SCAN_RATE, 0, 0)

            'Give the driver a 8 second buffer (scanRate * 4 channels * 8
seconds).
            LJUD.AddRequest(u3.ljhandle, LJUD.IO.PUT_CONFIG,
LJUD.CHANNEL.STREAM_BUFFER_SIZE, SCAN_RATE * 4 * 8, 0, 0)

            'Configure reads to retrieve whatever data is available without
waiting (wait mode LJUD.STREAMWAITMODES.NONE).
            'See comments below to change this program to use
LJUD.STREAMWAITMODES.SLEEP mode.
            ' LJUD.AddRequest(u3.ljhandle, LJUD.IO.PUT_CONFIG,
LJUD.CHANNEL.STREAM_WAIT_MODE, LJUD.STREAMWAITMODES.SLEEP, 0, 0)

            'Configure reads to retrieve whatever data is available without
waiting (wait mode LJUD.STREAMWAITMODES.NONE).
            'See comments below to change this program to use
LJUD.STREAMWAITMODES.SLEEP mode.
            LJUD.AddRequest(u3.ljhandle, LJUD.IO.PUT_CONFIG,
LJUD.CHANNEL.STREAM_WAIT_MODE, LJUD.STREAMWAITMODES.NONE, 0, 0)

            'Define the scan list as AIN0 then FIOEIO.
            LJUD.AddRequest(u3.ljhandle, LJUD.IO.CLEAR_STREAM_CHANNELS, 0,
0, 0, 0)
            LJUD.AddRequest(u3.ljhandle, LJUD.IO.ADD_STREAM_CHANNEL, 0, 0,
0, 0)
```

```
            ' LJUD.AddRequest(u3.ljhandle, LJUD.IO.ADD_STREAM_CHANNEL, 1,
0, 0, 0)
            ' LJUD.AddRequest(u3.ljhandle, LJUD.IO.ADD_STREAM_CHANNEL, 2,
0, 0, 0)
            ' LJUD.AddRequest(u3.ljhandle, LJUD.IO.ADD_STREAM_CHANNEL, 3,
0, 0, 0)

            LJUD.AddRequest(u3.ljhandle, LJUD.IO.PUT_CONFIG,
LJUD.CHANNEL.TIMER_COUNTER_PIN_OFFSET, 4, 0, 0)

            'Use the 48 MHz timer clock base with divider.  Since we are
using clock with divisor
            'support, Counter0 is not available.
            LJUD.AddRequest(u3.ljhandle, LJUD.IO.PUT_CONFIG,
LJUD.CHANNEL.TIMER_CLOCK_BASE, LJUD.TIMERCLOCKS.MHZ1_DIV, 0, 0)
            'we don't need timers when using counters.

            'Set the divisor to 4 so the actual timer clock is
LJUD.TIMERCLOCKS.MHZ1_DIV/divisor
            LJUD.AddRequest(u3.ljhandle, LJUD.IO.PUT_CONFIG,
LJUD.CHANNEL.TIMER_CLOCK_DIVISOR, 128, 0, 0)

            'Enable 1 timer.  It will use FIO4.
            LJUD.AddRequest(u3.ljhandle, LJUD.IO.PUT_CONFIG,
LJUD.CHANNEL.NUMBER_TIMERS_ENABLED, 1, 0, 0)

            'PWM Configure Timer0 as 8-bit PWM.  Frequency will be 1M/256 =
3906 Hz.
            'LJUD.AddRequest(u3.ljhandle, LJUD.IO.PUT_TIMER_MODE, 0,
LJUD.TIMERMODE.PWM8, 0, 0)
            'Set the PWM duty cycle to 50%.
            'LJUD.AddRequest(u3.ljhandle, LJUD.IO.PUT_TIMER_VALUE, 0,
32768, 0, 0)

            ' Counters. Timer 0 will use FIO4 as Frequency Output , post
divider value, where 0 gives divisor of 256,
            'output freq= LJUD.TIMERCLOCKS.MHZ4_DIV /
LJUD.CHANNEL.TIMER_CLOCK_DIVISOR / (2*Value)

            'LJUD.AddRequest(u3.ljhandle, LJUD.IO.PUT_TIMER_MODE, 0,
LJUD.TIMERMODE.FREQOUT, divVal, 0)
```

```
            LJUD.AddRequest(u3.ljhandle, LJUD.IO.PUT_DIGITAL_BIT, 6, 1, 0,
0)
            LJUD.AddRequest(u3.ljhandle, LJUD.IO.PUT_DIGITAL_BIT, 7, 1, 0,
0)
            'Execute the list of requests.
            LJUD.GoOne(u3.ljhandle)

        Catch ex As LabJackUDException
            showErrorMessage(ex)
        End Try

        ' Get results until there is no more data available for error
checking
        Dim isFinished As Boolean
        isFinished = False
        While Not isFinished
            Try
                LJUD.GetNextResult(u3.ljhandle, ioType, channel,
dummyDouble, dummyInt, dummyDouble)
            Catch ex As LabJackUDException
                ' If we get an error, report it.  If the error is
NO_MORE_DATA_AVAILABLE we are done
                If (ex.LJUDError = u3.LJUDERROR.NO_MORE_DATA_AVAILABLE)
Then
                    isFinished = True
                Else
                    showErrorMessage(ex)
                End If
            End Try
        End While


    End Sub
    Private Sub writeDigital(ByVal digCh As Integer, ByVal value As Double)
        'Set the state of FIO6
        LJUD.ePut(u3.ljhandle, LJUD.IO.PUT_DIGITAL_BIT, digCh, value, 1)
    End Sub

    Private Sub Form1_FormClosing(ByVal sender As Object, ByVal e As
System.Windows.Forms.FormClosingEventArgs) Handles Me.FormClosing
```

```
        StopLabJack()
    End Sub
    Private Sub Form1_Load(ByVal sender As System.Object, ByVal e As
System.EventArgs) Handles MyBase.Load
        ComboBox1.SelectedIndex = 0
        Timer1.Enabled = False
        Timer2.Enabled = False
        NUM_SCANS = 2000   'requested number of scans in each reading
process
        'each scan has a number of channels, so if we have 4 active
channels,
        ' each scan has 4 samples (ch1, ch2, ch3, ch4) so the total samples
= Num_Scan * No. of Ch
        SCAN_RATE = 2000    'sample rate per channel
        READ_INTERVAL = 5500  'mil
        For i As Integer = 0 To 4
            ZeroRead(i) = 0
            SFactor(i) = 1
        Next
        Spath = My.Application.Info.DirectoryPath
        StartStream()
    End Sub

    Private Sub Timer1_Tick(ByVal sender As System.Object, ByVal e As
System.EventArgs) Handles Timer1.Tick
        Dim j As Integer

        Dim Avg(4) As Single
        numScansRequested = 2 * SCAN_RATE * (Timer1.Interval / 1000.0)

        Try
            'Read the data.  The special functions AddReqest_ByRef or
eGet_ByRef
            'must be used since we are retrieving an array.
            'By passing the first element of the array, we are giving the
            'LabJackUD DLL a pointer to the array.  Since each sample uses
8 bytes, you
            'should probably keep the array to 8000 samples or less to stay
under 64k in size in RAM.
```

```
            ' the data is read sequentially, so if we have total number of
scans of 5000, we can read them 1000 by 1000
            ' sequentially by issuing the following command



            LJUD.eGet(u3.ljhandle, LJUD.IO.GET_STREAM_DATA,
LJUD.CHANNEL.ALL_CHANNELS, numScansRequested, Ai)
            ' Debug.Print("actual scans=" + numScansRequested.ToString)


            For j = 0 To NumSensors - 1
                Avg(j) = 0
                For k = 0 To numScansRequested - 1

                    VAvg(j) += Ai(k * NumSensors + j)  'voltage average
                    Avg(j) += (Ai(k * NumSensors + j) - ZeroRead(j)) *
SFactor(j) 'scale the reading and subtract zero voltage
                Next
                Avg(j) = Avg(j) / numScansRequested
                AB(j, DCounter) = Avg(j)
            Next
            UpdateShape(Pic1, 0, DCounter)
            DCounter += 1

            'UpdateShape(Pic2, 1, TotalScans, numScansRequested)
            ' UpdateShape(Pic3, 2, TotalScans, numScansRequested)
            ' UpdateShape(Pic4, 3, TotalScans, numScansRequested)
            ' UpdateShape(Pic5, 4, TotalScans, numScansRequested)
            ' UpdateShape(Pic6, 5, TotalScans, numScansRequested)
            'UpdateShape(Pic7, 6, TotalScans, numScansRequested)
            TotalScans += numScansRequested

            If (TotalScans / SCAN_RATE) > MaxX Then
                For j = 0 To NumSensors - 1
                    VAvg(j) = VAvg(j) / TotalScans
                Next
                Finish()
            End If

            AcquiredScans.Text = Str(TotalScans)
```

```
            'number of samples= number of scans * number of channels
            'firstScanDisplay.Text = Str(adblData(0 + numScansRequested)) +
", " + Str(adblData(1))


        Catch ex As Exception
            'showErrorMessage(ex)
            Finish()
            MsgBox(ex.Message)
        End Try

    End Sub
    Private Sub PreparePic(ByVal Pic As PictureBox)
        Dim Fstr As String

        Dim c1 As New System.Drawing.Pen(System.Drawing.Color.Blue)
        Dim Pname, UntStr As String
        Dim Gr1 As System.Drawing.Graphics



        Pname = "Overall"
        UntStr = "kg"
        'Dim Font1 As New Font("Tahoma", 9, FontStyle.Bold)
        Dim Brush1 As New SolidBrush(Color.DarkSlateGray)
        Dim Font2 As New Font("Tahoma", 8, FontStyle.Bold)
        Dim Brush2 As New SolidBrush(Color.Black)
        Dim TxtSize, TxtSize2 As New System.Drawing.SizeF
        'spectrum draw start here
        Dim TPen3 As New
System.Drawing.Pen(System.Drawing.Color.DarkGoldenrod, 1)
        Dim LPen1 As New
System.Drawing.Pen(System.Drawing.Color.DarkGoldenrod)
        Dim SBrush4 As New
System.Drawing.SolidBrush(System.Drawing.Color.WhiteSmoke)
        x0 = 0.085 * Pic.Width : y0 = Pic.Height * 0.88 : xr = 0.84 *
Pic.Width : yr = 0.8 * Pic.Height
        If Pic.Image IsNot Nothing Then Pic.Image.Dispose()
        Pic.Image = New Bitmap(Pic.Width, Pic.Height)
        Gr1 = Graphics.FromImage(Pic.Image)  'grap graphics object from
Pic1.image
```

```
        MaxA = Val(MaxTxt1.Text)
        MinA = Val(MinTxt1.Text)
        Gr1.Clear(System.Drawing.Color.White)
        Gr1.TextRenderingHint =
Drawing.Text.TextRenderingHint.AntiAliasGridFit
        ' Gr1.DrawString("Source: " + Pname, Font1, Brush1, x0 + 100, 10)
        'Gr1.DrawString(UntStr, Font1, Brush1, 30, 10)
        Gr1.FillRectangle(SBrush4, x0, y0 - yr, xr, yr)
        Gr1.DrawRectangle(TPen3, x0, y0 - yr, xr, yr)
        LPen1.DashStyle = Drawing2D.DashStyle.Dot
        Fstr = " sec"
        Dim Brush3 As New SolidBrush(Color.DarkGoldenrod)
        For j = 0 To 10
            x1 = x0 + j * xr / 10
            Gr1.DrawLine(LPen1, x1, y0 - yr, x1, y0)

            y1 = y0 - j * yr / 10
            Gr1.DrawLine(LPen1, x0, y1, x0 + xr, y1)
            TxtSize = Gr1.MeasureString(Format(MinA + (MaxA - MinA) * j /
10, "0.00"), Font2)

            If j = 10 Then
                TxtSize2 = Gr1.MeasureString(Format(MaxX * j / 10, "0.00"),
Font2)
                Gr1.DrawString(Format(MaxX * j / 10, "0.00"), Font2,
Brush3, x1 + 1, y0 - 8)

                'Gr1.DrawString(Format(MinA + (MaxA - MinA) * j / 10,
"0.00"), Font2, Brush3, x0 - TxtSize.Width - 5, y1 - TxtSize.Height / 2)
            End If
            If j Mod 2 = 0 Then
                Gr1.DrawString(Format(MinA + (MaxA - MinA) * j / 10,
"0.00"), Font2, Brush3, x0 - TxtSize.Width - 5, y1 - TxtSize.Height / 2)
            End If

        Next
        Brush1.Dispose()
        Brush2.Dispose()
        Font2.Dispose()
        Pic.Refresh()
    End Sub
```

```
    Private Sub UpdateShape(ByVal pic As PictureBox, ByVal ChIndex As
Integer, ByVal Stp As Integer)
        Dim x2, y2 As Single
        Dim c1 As New System.Drawing.Pen(System.Drawing.Color.Blue)
        Dim Gr1 As System.Drawing.Graphics
        Gr1 = pic.CreateGraphics
        Dim j As Integer

        x0 = 0.085 * pic.Width : y0 = pic.Height * 0.88 : xr = 0.84 *
pic.Width : yr = 0.8 * pic.Height
        Select Case ChIndex
            Case 0
                c1.Color = Color.DarkBlue
            Case 1
                c1.Color = Color.Green
            Case 2
                c1.Color = Color.DarkKhaki
            Case 3
                c1.Color = Color.DarkRed
            Case 4
                c1.Color = Color.DarkSlateBlue

        End Select
        c1.Width = 1
        If Stp > 0 Then
            For j = Stp - 1 To Stp
                x2 = x0 + j * (Timer1.Interval / 1000.0) * xr / (MaxX)

                y2 = y0 - yr * (AB(ChIndex, j) - MinA) / (MaxA - MinA)
                If j >= Stp Then Gr1.DrawLine(c1, x1, y1, x2, y2)
                x1 = x2
                y1 = y2
            Next
        End If
        ' Debug.Print("j=" + j.ToString)
    End Sub
    Private Sub Finish()
        Timer1.Enabled = False
        'Stop the stream
```

```
        LJUD.eGet(u3.ljhandle, LJUD.IO.STOP_STREAM, 0, dummyDouble,
dummyDoubleArray)
        Button1.Enabled = True

    End Sub

    Private Sub DrawShape(ByVal Gr1 As Graphics, ByVal GWidth As Integer,
ByVal GHeight As Integer, ByVal ChIndex As Integer, ByVal NPoints As
Integer, ByVal Pname As String, ByVal UntStr As String)
        Dim x0, y0, x1, y1, xr, yr, x2, y2 As Single
        Dim MaxA, MinA As Single
        Dim Fstr As String
        Dim MaxX As Single
        Dim c1 As New System.Drawing.Pen(System.Drawing.Color.Blue)

        Dim Font1 As New Font("Tahoma", 9, FontStyle.Bold)
        Dim Brush1 As New SolidBrush(Color.DarkSlateGray)

        x0 = 0.12 * GWidth : y0 = GHeight * 0.8 : xr = 0.78 * GWidth : yr =
0.7 * GHeight
        Gr1.TextRenderingHint =
Drawing.Text.TextRenderingHint.AntiAliasGridFit
        Gr1.DrawString("Source: " + Pname, Font1, Brush1, x0, y0 + 2)
        Gr1.DrawString(UntStr, Font1, Brush1, 2, y0 - yr + 16)

        Dim Font2 As New Font("Tahoma", 8, FontStyle.Bold)
        Dim Brush2 As New SolidBrush(Color.Black)
        Dim TxtSize As New System.Drawing.SizeF
        'spectrum draw start here

        Dim SBrush4 As New
System.Drawing.SolidBrush(System.Drawing.Color.WhiteSmoke)
        Gr1.FillRectangle(SBrush4, x0, y0 - yr, xr, yr)
        Dim TPen3 As New
System.Drawing.Pen(System.Drawing.Color.DarkGoldenrod, 2)
        Gr1.DrawRectangle(TPen3, x0, y0 - yr, xr, yr)
        Dim LPen1 As New
System.Drawing.Pen(System.Drawing.Color.DarkGoldenrod)
        LPen1.DashStyle = Drawing2D.DashStyle.Dot
        MaxA = MaxRead(ChIndex)
        MinA = MinRead(ChIndex)
```

```
        For j As Integer = 0 To 10
            x1 = x0 + j * xr / 10
            Gr1.DrawLine(LPen1, x1, y0 - yr, x1, y0)
            y1 = y0 - j * yr / 10
            Gr1.DrawLine(LPen1, x0, y1, x0 + xr, y1)
        Next

        TxtSize = Gr1.MeasureString(Format(MaxA, "0.00"), Font2)
        Dim Brush3 As New SolidBrush(Color.DarkGoldenrod)
        Gr1.DrawString(Format(MaxA, "0.00"), Font2, Brush3, x0 -
TxtSize.Width - 5, y0 - yr - 5)
        TxtSize = Gr1.MeasureString(Format(MinA, "0.00"), Font2)
        Gr1.DrawString(Format(MinA, "0.00"), Font2, Brush3, x0 -
TxtSize.Width - 5, y0 - 10)

        Fstr = " sec"
        MaxX = NPoints / SCAN_RATE
        TxtSize = Gr1.MeasureString(Format(MaxX, "0.0") + Fstr, Font2)
        Gr1.DrawString(Format(MaxX, "0.0") + Fstr, Font2, Brush3, x0 + xr -
TxtSize.Width / 2, y0 + 2)

        Select Case ChIndex
            Case 0
                c1.Color = Color.DarkBlue
            Case 1
                c1.Color = Color.Green
            Case 2
                c1.Color = Color.DarkKhaki
            Case 3
                c1.Color = Color.DarkRed
            Case 4
                c1.Color = Color.DarkSlateBlue

        End Select
        For j = 0 To NPoints - 1
            x2 = x0 + j * xr / NPoints

            y2 = y0 - yr * (AB(ChIndex, j) - MinA) / (MaxA - MinA)
            If j > 0 Then Gr1.DrawLine(c1, x1, y1, x2, y2)
            x1 = x2 : y1 = y2
```

```
        Next
    End Sub

    Private Sub StopLabJack()
        Try
            'Reset all pin assignments to factory default condition.
            LJUD.ePut(u3.ljhandle, LJUD.IO.PIN_CONFIGURATION_RESET, 0, 0,
0)
            'The PWM output sets FIO4 to output, so we do a read here to
set
            'it to input.
            'LJUD.eGet(u3.ljhandle, LJUD.IO.GET_DIGITAL_BIT, 4, dblValue,
dummyDoubleArray)
            'FileClose(4)

            'number of samples= number of scans * number of channels
            'firstScanDisplay.Text = Str(adblData(0 + numScansRequested)) +
", " + Str(adblData(1))
            LJUD.eGet(u3.ljhandle, LJUD.IO.GET_CONFIG,
LJUD.CHANNEL.STREAM_BACKLOG_COMM, dblValue, 0)
            'commBacklogDisplay.Text = Str(dblValue)
            LJUD.eGet(u3.ljhandle, LJUD.IO.GET_CONFIG,
LJUD.CHANNEL.STREAM_BACKLOG_UD, dblValue, 0)
            'udBacklogDisplay.Text = Str(dblValue)

            'Stop the stream
            '   LJUD.eGet(u3.ljhandle, LJUD.IO.STOP_STREAM, 0, dummyDouble,
dummyDoubleArray)

        Catch ex As LabJackUDException
            showErrorMessage(ex)
        End Try
    End Sub

    Private Sub Button2_Click(ByVal sender As System.Object, ByVal e As
System.EventArgs) Handles Button2.Click
        Application.Exit()
    End Sub

    Private Sub Button3_Click(ByVal sender As System.Object, ByVal e As
System.EventArgs) Handles Button3.Click
```

```
        For i As Integer = 0 To 3
            ZeroRead(i) = VAvg(i)
        Next

    End Sub

    Private Sub Button4_Click(ByVal sender As System.Object, ByVal e As
System.EventArgs) Handles Button4.Click
        Dim curDateStr As String
        Dim curTime, S, S1 As String
        Dim j, i As Integer
        Dim FileName As String
        SaveFileDialog1.InitialDirectory =
Environment.GetFolderPath(Environment.SpecialFolder.MyDocuments)
        SaveFileDialog1.Filter = "text file |*.txt"
        Dim res As DialogResult = SaveFileDialog1.ShowDialog
        If res = Windows.Forms.DialogResult.Cancel Then Exit Sub
        FileName = SaveFileDialog1.FileName
        If DCounter <= 0 Then Exit Sub
        curTime = TimeString
        curDateStr = DateString
        Dim sum As Single
        Try
            FileOpen(4, FileName, OpenMode.Append)
            PrintLine(4, curTime)
            PrintLine(4, " Time (sec)     Ch1  ")
            PrintLine(4, " ======================")
            sum = 0
            For i = 0 To DCounter - 1
                S = AdjStr(Format(i * (Timer1.Interval / 1000.0), "0.000"),
15)

                For j = 0 To 0
                    S1 = AdjStr(Format(AB(j, i), "0.000"), 11)
                    S = S + S1
                    sum += AB(j, i)
                Next
                PrintLine(4, S)
            Next
            sum = sum / DCounter
            S1 = "Average=" + AdjStr(Format(sum, "0.000"), 11)
```

```
            PrintLine(4, S1)
            FileClose(4)
        Catch ex As Exception
            FileClose(4)
        End Try
    End Sub

    Public Function AdjStr(ByVal Instr As String, ByVal Length As Integer)
As String
        If Instr.Length > Length Then
            Instr = Mid(Instr, 0, Length)
        Else
            While Instr.Length < Length
                Instr = Instr + " "
            End While
        End If
        AdjStr = Instr
    End Function

    Private Sub Button5_Click(ByVal sender As System.Object, ByVal e As
System.EventArgs) Handles Button5.Click
        Dim dis, slideratio, spd, rps, Clk, t, t1, SampDis As Single
        dis = Val(DistanceTxt.Text) 'total distance required
        slideratio = Val(SlidingRatioTxt.Text) 'mm/Rev
        spd = Val(ReqSpeedTxt.Text) 'mm/s
        rps = spd / slideratio
        Clk = rps * 200
        divVal = Math.Round((1000000.0 / 128) / Clk / 2)
        Debug.Print("RPS, CLK, DivVAL: " + rps.ToString + ", " +
Clk.ToString + ", " + divVal.ToString)
        If divVal > 255 Then divVal = 255
        If divVal < 1 Then divVal = 1
        t = dis / spd
        SampDis = Val(SamDistanceTxt.Text)
        t1 = SampDis / spd
        Timer1.Interval = t1 * 1000
        Debug.Print("time, interval: " + t.ToString + ", " +
Timer1.Interval.ToString)

        Timer2.Interval = t * 1000
```

```
        'start stream and motion
        MaxX = t
        SFactor(0) = Val(TextBox3.Text)
        READ_INTERVAL = 1000 * t

        PreparePic(Pic1)
        ' StartStream()
        Try
            'Start the stream.
            LJUD.eGet(u3.ljhandle, LJUD.IO.START_STREAM, 0, dblValue, 0)
        Catch ex As LabJackUDException
            showErrorMessage(ex)
        End Try
        TotalScans = 0
        DCounter = 0
        Timer1.Enabled = True
        Timer2.Enabled = True

        writeDigital(7, ComboBox1.SelectedIndex)
        LJUD.ePut(u3.ljhandle, LJUD.IO.PUT_TIMER_MODE, 0,
LJUD.TIMERMODE.FREQOUT, 0)
        LJUD.ePut(u3.ljhandle, LJUD.IO.PUT_TIMER_VALUE, 0, divVal, 0)
    End Sub


    Private Sub Timer2_Tick(ByVal sender As System.Object, ByVal e As
System.EventArgs) Handles Timer2.Tick
        Timer2.Enabled = False
        LJUD.ePut(u3.ljhandle, LJUD.IO.PUT_TIMER_MODE, 0,
LJUD.TIMERMODE.DUTYCYCLE, 0)
    End Sub

    Private Sub Button7_Click(ByVal sender As System.Object, ByVal e As
System.EventArgs) Handles Button7.Click
        'set timer 0 as dutycycle input measurement to disable Freq Out
        LJUD.ePut(u3.ljhandle, LJUD.IO.PUT_TIMER_MODE, 0,
LJUD.TIMERMODE.DUTYCYCLE, 0)
        'Reset all pin assignments to factory default condition.
        ' LJUD.ePut(u3.ljhandle, LJUD.IO.PIN_CONFIGURATION_RESET, 0, 0, 0)
    End Sub
```

```
    Private Sub Button8_Click(ByVal sender As System.Object, ByVal e As
System.EventArgs) Handles Button8.Click
        Dim dis, slideratio, spd, rps, Clk, t As Single
        dis = Val(DistanceTxt.Text) 'total distance required
        slideratio = Val(SlidingRatioTxt.Text) 'mm/Rev
        spd = Val(ReqSpeedTxt.Text) 'mm/s
        rps = spd / slideratio
        Clk = rps * 200
        divVal = Math.Round((1000000.0 / 128) / Clk / 2)
        Debug.Print("RPS, CLK, DivVAL: " + rps.ToString + ", " +
Clk.ToString + ", " + divVal.ToString)
        If divVal > 255 Then divVal = 255
        If divVal < 1 Then divVal = 1
        t = dis / spd



        Debug.Print("time, interval: " + t.ToString)

        Timer3.Interval = t * 1000



        DCounter = 0

        Timer3.Enabled = True
        idr = 0
        writeDigital(7, idr Mod 2)
        LJUD.ePut(u3.ljhandle, LJUD.IO.PUT_TIMER_MODE, 0,
LJUD.TIMERMODE.FREQOUT, 0)
        LJUD.ePut(u3.ljhandle, LJUD.IO.PUT_TIMER_VALUE, 0, divVal, 0)
    End Sub

    Private Sub Timer3_Tick(ByVal sender As System.Object, ByVal e As
System.EventArgs) Handles Timer3.Tick
        idr += 1
        writeDigital(7, idr Mod 2)
        If idr >= Val(NCyclesTxt.Text) Then
            LJUD.ePut(u3.ljhandle, LJUD.IO.PUT_TIMER_MODE, 0,
LJUD.TIMERMODE.DUTYCYCLE, 0)
            Timer3.Enabled = False
```

```
            Debug.Print("Done")
        End If
    End Sub

    Private Sub Button6_Click(ByVal sender As System.Object, ByVal e As
System.EventArgs) Handles Button6.Click
        LJUD.ePut(u3.ljhandle, LJUD.IO.PUT_TIMER_MODE, 0,
LJUD.TIMERMODE.DUTYCYCLE, 0)
    End Sub
End Class
```

الملخص

تُستخدم مادة PMMA في العديد من الصناعات والتطبيقات الهندسية مثل السيارات والطائرات وإشارات المرور والإعلانات الضوئية والعدسات والنظارات والخلايا الشمسية وصناعة الأسنان والعديد من الأجهزة الكهربائية وتطبيقات البناء مثل الديكورات وعارضات السلع واحواض السباحة الرياضية و ملاعب الجولف وكذلك في العديد من المجالات الزراعية. تتميز مادة PMMA بالوفرة و رخص الثمن و الكثافة المنخفضة و المتانة النسبية الجيدة و سهولة التشكيل والتقطيع حسب الأحجام والأشكال المطلوبة وعدم السمية والعزل الكهربائي والمقاومة الكيميائية ، لكن مقاومتها للخدش ضعيفة.

أصبح الحصول على أسطح عالية الجودة من مادة PMMA أولوية لكل من الشركات المصنعة والباحثين على حد سواء لسببين ، أحدهما وظيفي والآخر جمالي ، لأن الخدوش على سطح مادة PMMA تقلل من استخدامها في الصناعة البصرية والعديد من التطبيقات الهندسية، حيث أن وجود الخدوش يؤدي إلى زيادة الاجهاد أثناء تحميل الشد والصدم والكلل الذي يقوض عمرمادة PMMA أثناء فترة الاستخدام. في الدراسة الحالية ، تمت إضافة جسيمات نانوية من أوكسيد السيليكا (SiO_2) الى مادة PMMA في مجموعتين من النسب ، الأولى (1، 2، 3 و 4 wt%) والثانية (0.1 ، 0.2 ، 0.3 ، 0.4 و 0.5 wt%) من أجل دراسة تأثيرها على مقاومة الخدش والخواص الاخرى لمادة PMMA.

تم تحضير عينات مادة PMMA النقية والمقواة بثلاث طرق في العمل الحالي ، وهي طريقة الإذابة والضغط والصب. تم تصميم وبناء جهاز خدش مؤتمت لإجراء اختبارات الخدش في الدراسة الحالية. يتكون الجهاز من ثلاثة أجزاء هي الأجزاء الميكانيكية وآلية الخدش والأجزاء الكهربائية والإلكترونية ، بالإضافة إلى برنامج تشغيل الجهاز والتحكم فيه.

النتائج التي تم الحصول عليها من الاختبارات التي أجريت على مادة PMMA النقية والمقواة في الدراسة الحالية كانت تحسن قوة الشد لمركبات $PMMA/SiO_2$ مقارنة بمادة PMMA النقية ، أفضل تحسن حدث للعينات ذات نسبة 1wt% من الجسيمات النانوية مقارنة بالنسب الأخرى. انخفاض في استطالة مركبات $PMMA/SiO_2$ مقارنة بمادة PMMA النقية ، وتحدث أقل استطالة للعينات ذات نسبة 1wt% من الجسيمات النانوية. تحسن الصلابة لمادة PMMA المقواة مقارنة مع PMMA النقية ، وأن الصلابة تزداد مع زيادة نسبة الجسيمات النانوية (SiO_2). وأظهرت النتائج أيضًا تحسن في مقاومة الخدش حيث كان الحمل العمودي

المطبق المطلوب لخدش مادة PMMA المقواة أكبر من الحمل العمودي المطلوب لخدش PMMA النقية ، ويزداد مع زيادة نسبة الجسيمات النانوية ، كما كانت الأحمال المطبقة المستخدمة مع قلم الخدش ذو النهاية الكروية أكبر من الاحمال المطبقة المستخدمة مع قلم الخدش ذو النهاية المخروطية. معامل الاحتكاك لمادة PMMA المقواة كان أقل مقارنة بـ PMMA النقية وينخفض عندما تزداد نسبة الجسيمات النانوية. درجة حرارة التحول الزجاجي (T_g) للعينات المقواة كانت أعلى من درجة حرارة التحول الزجاجي للعينات النقية وتزداد مع زيادة نسبة الجسيمات النانوية (SiO_2).

وأخيرًا ، أثبتت الدراسة قدرة الجهاز المصمم على قياس القوة العرضية المطلوبة للخدش بدقة وبسرعة وبخطوات بسيطة بالإضافة إلى إمكانية حساب معامل الاحتكاك مباشرة من مدخلات ومخرجات الجهاز ، كما أظهرت فعالية البرنامج المصمم للتحكم في الجهاز من حيث سهولة إدخال المتغيرات ودقة المخرجات.

تحسين مقاومة الخدش لمادة البولي مثيل ميثا اكريليت بالتقوية بجسيمات ثاني اوكسيد السيليكا النانوية

رسالة مقدمة الى

كلية الهندسة – جامعة البصرة

كجزء من متطلبات نيل درجة دكتوراه فلسفة

في الهندسة الميكانيكية

(ميكانيك تطبيقي)

تقدم بها

مشـتاق عبـد الكـريم حسـين البحـراني

ماجستير في علوم الهندسة الميكانيكية

ايلول 2020